IMPERIAL COLLEGE OF SCIENCE AND TECHNOLOGY

MECHANICAL ENGINEERING DEPARTMENT

DYNAMICS SECTION

THEORY AND PRACTICE OF MODAL IDENTIFICATION

by

JACOB KIRSHENBOIM

B.Sc (Eng.), M.Sc (Mechanics) TECHNION, ISRAEL

Thesis presented for the degree of Ph.D

of the University of London

LONDON SEPTEMBER 1981

ACKNOLEDGEMENT

The author wishes to express his thanks to Dr D J Ewins for his advice and support during the course of this project.

Thanks are also extended to Mr D R Gaukroger, Mr J C Copley and Mr C W Skingle of the Royal Aircraft Establishment, Farnborough, for their active interest and invaluable advice and for providing access to their multi-point excitation system (MAMA).

Special thanks are due to Mr R D Gunn for his willing help in the Dynamics Section laboratory.

Thanks are also extended to the Ministry of Defence (Procurement Executive) for sponsoring this project and for the bursary awarded to the author.

SUMMARY

This thesis is concerned with the development and refinement of some aspects of the 'modal testing method'

The basis of the research is a definitive theoretical description of the two most common models of damped linear systems (i.e viscous and hysteretic damping). The normal mode shapes of such systems are generally expressed in complex terms and experimental observations using the single-point excitation method tend to confirm this. On the other hand, the normal modes used in finite element calculations and those derived by the traditional multi-point excitation method are the real undamped modes.

The exact relationship between the complex normal modes and the real undamped modes is established and a theoretical study investigates the relationship between the level of the 'complexity' of the normal modes and the closeness of the natural frequencies showing that for well-separated natural frequencies the 'complexity' of the normal modes is very small. Experimental results from real structures, however, have so far produced larger values of 'complexity'. It is shown that this is caused by the nonlinear behaviour of the measured structure and measuring procedures which give emphasis to this part of the structures response. A numerical study of some simple theoretical systems shows the influence of small nonlinearities on the linearly-derived modal parameters and an experimental study on a real structure serves as a vehicle on which the methods developed in this research to tackle nonlinearities are demonstrated.

Although it is theoretically possible to derive the complete matrix of the normal modes from measurement of one column of the mobility matrix, it is usually found that measurement of more columns is needed. As a result, several different estimates for the modal parameters are derived, the quality of each of those sets is then quantified by a 'quality factor'.

A 'best' consistent set of modal parameters is derived by an optimization algorithm which makes use of the quality factor and thus a large amount of measured data is reduced to a set of parameters which can be used in any further theoretical calculations.

Finally, an experimental study of a typical air frame structure demonstrates the single-point excitation identification methods developed in this research and a comparison is made with the experimental results obtained by the traditional multi-point excitation method .

NOTATION

$_rA_{ij}$	modal constant of mode r of receptance α_{ij}
[A]	matrix defined by (2-60)
[B]	matrix defined by (2-100)
[C]	viscous damping matrix
E	error function
{F}	complex vector of force amplitudes
$\{_rG_k\}$	defined by (2-129)
[H]	hysteretic damping matrix
[I]	unit matrix
J	nonlinearity factor
J_n	nonproportionality factor
[K]	stiffness matrix
$[\overline{K}]$	diagonal modal stiffness matrix
[M]	mass matrix
$[\overline{M}]$	diagonal modal mass matrix
P	excitation force amplitude
{P}	forcing vector defined by (2-107)
R	constant dry friction force
$\{_rR_k\}$	defined by (2-131)
$\{_rS_k\}$	defined by (2-132)
$_rS_{ij}$	quality factor of mode r in mobility Y_{ij}
U	constant linear error defined by (5-1)
V	constant logarithmic error defined by (5-1)
{X}	complex vector of harmonic displacement amplitudes
Y_{ij}	mobility (excitation of point j and response at i)
{Y}	vector defined by (2-109)

{Z} real vector of harmonic displacement amplitudes

a 'slightly varying' amplitude of nonlinear system

a k_2+k_1 defined by (3-33)

a_r 'modal mass' as defined by (2-104)

b cubic stiffness coefficient defined by (5-22)

b_r 'modal stiffness' as defined by (2-105)

c quadratic viscous damping coefficient defined by (5-22)

e base of natural logarithm

{f} complex vector of harmonic forces

$_rg_{ij}$ weighting factor for mode r of mobility Y_{ij}

h_{ij} element in the hysteretic damping matrix [H]

h linear viscous damping coefficient

i counter

j counter

k stiffness or counter

k_r modal stiffness

l counter

m mass

m_r modal mass

n counter

p counter

{q} complex vector of generalized displacement

r counter

s_r eigenvalue in eigenproblem (2-102)

t time

u	real part of λ_r^2
v	imaginary part of λ_r^2
x	displacement
{y}	vector defined by (2-97)

α_{ij}	receptance (response of point i to input at j)
$\bar{\alpha}$	phase angle defined by (3-45)
α	proportionality factor
β	proportionality factor
λ_r^2	eigenvalue for mode r
$\bar{\lambda}_r^2$	eigenvector of a proportionally-damped system
ω	frequency
ω_r	natural frequency of mode r
$\bar{\omega}_r$	natural frequency of a proportionally-damped system
η_r	loss factor of mode r
$\bar{\eta}_r$	phase angle defined by (3-45)
$\bar{\eta}$	generalized loss factor
η_M	M loss factor defined by (4-19)
η_K	K loss factor defined by (4-18)
γ_r	eigenvalue of eigenproblem (3-65)
ρ_r	phase angle
θ	phase angle
$\{\kappa\}_r$	eigenvector of the charateristic phase lag (2-55)
ξ_r	ratio of critical damping
μ	additional damping defined by Fig. 3-5

$\{\Psi\}_r$ complex eigenvector of hysteretically-damped system

$\{\Pi\}_r$ real eigenvector of undamped system

$\{\Phi\}_r$ mass-normalized eigenvector of hysteretically-damped system

$({}_r\Phi_k)$ k'th element in the r'th eigenvector $\{\Phi\}$

$\{\psi\}$ complex eigenvector of viscously-damped system

Ω_r modulus of eigenvalue of mode r of a viscously-damped system

$\{\Theta\}_r$ eigenvector in eigenproblem (2-1Ø2)

CONTENTS

1. INTRODUCTION.

Measurement of the vibration properties of an aerospace structure is an essential and integral part of its development programme. Originally, such tests were made in order to learn what the vibration characteristics were; later, they were sought to guide the development of the mathematical analysis and currently, they are required to check theoretical predictions made using finite elements or other advanced computational techniques. However, the rapid strides made in recent years by such prediction methods have not served to eliminate the need for experimental measurement of vibration properties; rather, they have tended to increase the demands made on such measurements by requiring greater accuracy and detail from the results. In addition, structures of this type are being designed with ever-increasing precision in the interest of efficiency and economy and this trend places particularly high demands on the dynamicist, requiring of him the prediction of vibration properties to much greater accuracy then hitherto. Thus, as theoretical prediction techniques improve, so also must the corresponding experimental methods in order to meet increased demands.

Traditionally, the vibration modes of aerospace structures have been measured by the multi-point excitation method in which the structure is forced simultaneously at several points in such a way that it can only respond by vibrating in a single mode (undamped normal mode). Once

identified, each such normal mode can then be compared with its theoretically-predicted counterpart. This type of test, although extensively developed, is a slow and costly procedure. However, once the structure is made to vibrate in this single mode the modal properties are directly measured and no further analysis is needed.

The modes identified by this method are the hypothetical undamped normal modes and not the actual normal modes of the structure. Usually, it is assumed that the damping matrix does not couple the equations of motion and, therefore, the hypothetical undamped modes and the normal modes of the structure are regarded as identical. Although these identified modes (specifically, the natural frequencies and mode shapes) provide a basis for comparison between theory and practice, they are quite often not the vibration chracteristics which are of greatest interest to the dynamicist. In helicopters, for example, it is the steady forced vibration levels at various critical positions resulting from the inevitable forcing generated by the power unit which are of greatest interest and there are several stages of analysis between knowledge of (some of) the vibration modes and predicting the forced vibration characteristics of the structure.

Coupled with these observations are recent developments in those vibration measurement techniques often referred to as 'impedence' or 'mobility testing'. The essential feature of this approach (which differentiates it from the

aforementioned 'multi-point' or 'pure mode excitation' method) is that it involves the excitation of the test structure with just a single input and then extricates the contributions of the various modes from the total response which results by suitable analysis of the measured data. In effect, the central problem - that of determining the vibration modes of a structure from test data - is tackled in this approach by placing greater emphasis on the analysis of the measured data and less on the complexities of the experimental procedure than is the case for a multi-point excitation approach; a change of emphasis with significant effect on the economics of time and money.

This shift of emphasis has resulted directly from marked improvements in the precision obtainable from vibration measurement equipment plus the availability of fast and inexpensive digital computers directly accessible to the measured data.

The great interest in this field of modal identification is reflected in the growing number of technical papers published each year. The concept is not particularly recent and one of the earliest papers was that of Kennedy and Pancu (1947) [42] which showed how mobility measurements could be used to identify vibration chracteristics of complex structures. Since then many papers on all aspects of this subject have been published; to mention some of the latest ones: Hamma et. al (1976) [1], Walegrave et. al (1978) [2], Snoeys et. al (1979) [3], Kortum et. al (1980) [4], Ewins

et. al (1980) [5] and even a paper by Flannelly [6] to explain the problem of modal analysis to the layman. Comprehensive lists of references were compiled by Ewins [7] and Rades [8,9]. The only book to summarize the methods of modal identification and their application is, unfortunately, not yet available in English (Rades [10]).

The work described in this thesis is mainly concerned with development and refinement of some aspects of the 'mobility testing method'. In addition, a testing procedure is developed which is applicable to perform the routine modal testing of helicopters and other similar structures and also to obtain simultaneously the additional forced vibration data needed for a full dynamic analysis of the structure.

The basis of this research is a definitive theoretical description of linear systems (chapter 2) with different models of damping (i.e hysteretic and viscous). The different mathematical expressions which describe the behaviour of a system subjected to several forms of external harmonic excitation are developed and the main differences between the two models of damping are pointed out. Because it seemed that there was no clear definition to the basic term 'mode of vibration' it is defined precisely and some of its special forms are described.

The normal mode shapes of a real system are generally described in complex terms. On the other hand, the mode shapes used in finite elements calculations and those

derived by multi-point excitation testing are the hypothetical real undamped normal modes. Practically it is assumed that the system under test is proportionally-damped and, therefore, that its normal modes are real and identical to the undamped normal modes. Experimental observations, however, do not always justify this assumption and in many cases it is simply not valid . In order to find the relationship between the (real) undamped modes and the (complex) normal modes of a system, a theoretical and numerical study is made in chapter 3. The main results of this study are that for most cases encountered in practice, where the 'complexity' of the experimentally-derived modes is small, these modes can be used as equal to the real undamped modes in any further calculation. When the modes are close, they tend to be more complex and then the error incurred by this assumption might be greater.

In the course of this study, two new useful parameters are defined; the 'nonproportionality factor' which quantifies the degree by which the damping matrix couples the equations of motion and the 'generalized loss factor' which gives an overall measure of the damping present in the system.

The next step in this work is the development of the necessary measurement and analysis techniques for derivation of the modal parameters (chapter 4). In this research, we are mainly interested in the single-point excitation method and two analysis programs have been developed to handle the

data produced by this method. The first is based on the well known Kennedy and Pancu method of treating each mode as a single degree of freedom mode (POLAR5) and the second is a more sophisticated program which analyses a complete measurement of several modes simultaneously (SIM2). The inherent limitations of both the experimental and subsequent analytical procedures are evaluated and demonstrated by studying a synthesised numerical case.

The main assumption made so far is that the system under consideration is linear and, subsequently, the modal identification programs have been developed accordingly. Real systems, however, do not always behave according to this convenient mathematical model; quite often they exhibit nonlinear behaviour which, unless noticed, may lead to an erroneous identification of the system.

The first part of chapter 5 studies a few theoretical cases of one-degree-of-freedom nonlinear systems and shows, in each case, how the presence of the nonlinearity can be detected by proper examination of the measured data. A sensitivity study to check the influence of the nonlinearity on the linearly-identified modal parameters proved that if not taken into account, it may lead to serious errors in the final identification of the system.

Because there is an infinite number of theoretical models to describe nonlinear systems, none of them adequately, it was decided that the best approach to deal with nonlinearity in practice is to establish its existence

and then to try to minimize its effect, rather than to identify its form in detail.

The second part of chapter 5 is an experimental study to demonstrate the behaviour of a real structure and the way to derive its linear modal parameters in the presence of a nonlinear response. In the course of this study a powerful parameter was devised - the 'nonlinearity factor'. No real structure is, even under the most favourable testing conditions, completely linear, and this parameter gives a measure of the degree of the nonlinearity and serves as a useful tool in checking the linearity of measured data under different excitation conditions.

In chapter 6, a systematic method for performance of a modal survey is outlined, in which the data are checked for nonlinearity and noise pollution before the analysis stage and once they are analysed, the quality of the identification of each set of modal parameters is quantified by a newly-defined 'quality factor'.

Although it is theoretically possible to derive the complete matrix of the normal mode shapes from the measurement of one column of the mobility matrix, it is usually found that measurement of more columns is necessary because some modes are not adequately excited and a change of excitation point improves their response and thus the subsequent identification.

Once these data are measured and analysed we obtain several estimates for many of the modal properties of the

structure which should, theoretically, be identical. Simple averaging has been used [76] to derive a single set of consistent parameters but this will not result in the best estimate because all the identified parameters are taken equally into account, good and poor alike.

In order to derive a 'best' estimate of the modal parameters, an overall weighted optimization of all the experimentally-derived modal parameters is made where the 'quality factor' is used as the weighting factor. By this method poorly identified modal parameters have less influence on the final derived results and the large amount of data collected is reduced to one consistent set of modal parameters which describes the system 'best'.

Finally, a comprehensive experimental study to demonstrate the methods developed so far was made (chapter 7). A typical test structure - a helicopter tailcone - was used as a vehicle on which the appropriate techniques were evaluated. A full modal test programme using the mobility approach was made and the measured data were analysed by three different identification programs; the simple POLAR5, the more advanced SIM2 and a third which assumes a viscous damping model (PAPA). In addition the tailcone was tested using the traditional multi-point excitation method thus providing a direct comparison between the two approaches. The difference between the final results obtained by each program is negligible although when checked with synthesised data there was a marked improvement of the sophisticated

SIM2 over the simple POLAR5.

The conclusion to draw from this result is that there is, therefore, little point in trying to improve the analysis algorithm by developing more accurate linear algorithms but rather, effort should be directed to improve the measuring techniques to reduce the amount of noise and nonlinear influence on the data.

However, lightly-damped structures, of which the fuselage of a helicopter is an example, can be identified satisfactorily by the single-point excitation method using the relatively simple polar analysis algorithm and the identified modal parameters can be used as the undamped modal parameters in any further theoretical calculation.

2. MATHEMATICAL MODELLING OF A DAMPED LINEAR SYSTEM

2.1 BASIC CONCEPTS.

The traditional route for constructing a mathematical model of a real system is paved with assumptions of all kinds; some of these are often well justified while others may be quite inappropriate in real life.

A related aspect is the problem of terminology. Some basic phenomena are given different definitions by different authors and are sometimes used very loosely and quite often, the same term is used by different investigators to describe different properties. Perhaps the most overworked term is 'mode of vibration': one can find in the current literature a large array of 'modes' such as 'principal', 'classical', 'normal', 'pure', 'natural', 'undamped', 'damped', 'complex', 'damped forced', etc. This situation is a confusing one and sometimes may lead to misunderstanding [11]. Accordingly, it is proposed to introduce a strict definition of this term and to use it throughout this work in a consistent manner as follows:

Mode of vibration.

A mode of vibration is a characteristic dynamic response in which the motion of every point on the system is a harmonic function of time with the same (complex) frequency.

Mode shape.

A mode shape is the time-invariant form of distortion

the system assumes in a certain mode of vibration.

Normal mode of vibration.

A normal mode is a mode of vibration that can exist independently of (uncoupled from) other modes of vibration when the system vibrates freely.

Two closely related terms are the 'natural frequency' and the 'resonance' which are defined as follows:

Natural frequency.

A natural frequency is a frequency at which the system vibrates in a normal mode of vibration.

Resonance.

A harmonically forced system is said to be in resonance when any change, however small, in the excitation frequency causes a decrease in the response of the system.

Resonance frequency.

A frequency at which a resonance exists.

The basic assumption concerning the system under consideration is that it is linear and that its fundamental properties are time-invariant.

By 'linearity' two basic characteristics are assumed, namely that (i) the response of the system is additive and that (ii) it is homogeneous.

The first of these assumptions implies that the response (output) of the system to the sum of several excitations (inputs) is equal to the sum of the system responses (outputs) obtained when each excitation is applied individually. If the input to the system is denoted by X_i and the output by Y_i (Fig.2-1a) then this property is illustrated by Fig. 2-1b.

The second assumption means that the response of the system to the product of some constant and the excitation is equal to the product of this same constant and the response generated by the excitation alone (Fig. 2-1c)

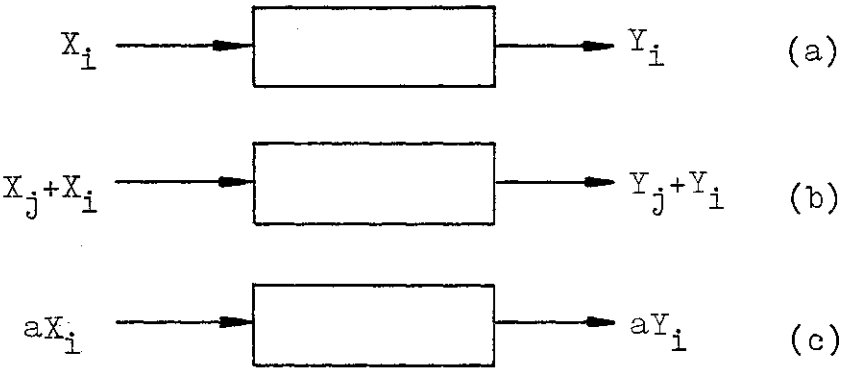

Fig. 2-1 Definition of linearity.

By time-invariant it is meant that the system's physical parameters are constants. In general, a system which is not time-invariant is assumed to have components whose mass, stiffness or damping are dependent on factors which are not included in the model, such as temperature, frequency, etc.

The assumption of linearity is well justified according to much experimental experience as well as theoretical investigation provided that the amplitude of the response is

small. In practice, the amplitude is regarded as 'small' as long as the measured results satisfy some external criterion for linearity.

The assumption of time-invariance, which must go together with that of linearity assumption, is usually justified when performing ground tests, or in many other practical cases where the investigator has some control over factors which may violate this assumption (temperature, for example).

In the following analysis we assume that a continuous system can be described by discrete elements such as masses, springs and dampers. Under this simplifying assumption the masses are rigid and have no compliance (the ability to deform under load); the springs are massless and have only the compliance property and the dampers are massless, dissipative elements. These assumptions permit us to represent a continuous system as consisting of n discrete masses and thus to describe it by an n-degree of freedom model resulting in a set of n coupled ordinary differential equations which describe the motion of the masses.

Practically, there are many cases in which it is impossible to identify discrete masses and springs and there may not be any valid reason to assume that the masses cannot deform and the springs have no mass. Furthermore, in many cases it is not justifiable to describe a continuous system by a small number of discrete elements and the information obtained then is far from accurate. In general, a discrete

system can be solved with more ease then a continuous one. However, the information obtained by using a discrete model may not be as accurate as the information obtained by representing the system by a continuous model. If the discrete model is made finer and finer, by increasing the the number of degrees of freedom and reducing the size of the masses, one obtains, in the limit, a continuous system.

There are many mathematical models used to represent damping, the most widely of which is the linear viscous dashpot. Another widely used model is structural or hysteretic damping. However, the assumption that any of these models accurately describes the actual physical mechanism in which energy is dissipated in a vibrating system is only a mathematical convenience, or to put it in more appropriate words 'Damping is in its very nature an uncertain and vague phenomenon and such a concept as a damping matrix should not be taken too seriously.' [11]

The equation of motion of a multi-degree of freedom damped linear system subjected to a harmonic excitation is:

$$[M]\{\ddot{q}\}+[K]\{q\}+i[H]\{q\}+[C]\{\dot{q}\}=\{f\} \qquad (2\text{-}1)$$

where,

[M] - mass matrix.

[K] - stiffness matrix.

[H] - hysteretic damping matrix.

[C] - viscous damping matrix.

These four matrices are of order nxn and are real and

symmetric. [M] and [K] are positive definite , [H] and [C] are at least semi-positive definite [14].

{q} - complex vector of generalized displacements.

{f} - complex vector of harmonic forces.

In this equation the two most common models of damping are included, namely hysteretic and viscous. The theoretical solution of this equation is well established. It is considered, however, necessary to present a definitive statement of this problem, both for hysteretic and viscous damping, to describe some special forms of damping and forcing and to point out the differences between the solutions for each type of damping. For each type of damping the homogeneous equation of free vibrations is considered followed by the special case of 'proportional damping'.

For the case of harmonic forced vibrations the force {f} is expressed as:

$$\{f\}=\{F\}e^{i\omega t} \qquad (2-2)$$

where ω is the frequency of harmonic excitation and {F} is, generally, a complex vector of harmonic amplitudes.

Apart from the general case of constant harmonic excitation where {F} is complex, two particular cases of harmonic excitation which are of great practical importance are described: excitation by a mono-phased harmonic force where {F} is a real vector and excitation by a single harmonic force F_k.

2.2 HYSTERETIC DAMPING

The equation of motion for the hysteretically-damped system subjected to a constant harmonic forcing is:

$$[M]\{\ddot{q}\}+[K]\{q\}+i[H]\{q\}=\{F\}e^{i\omega t} \qquad (2-3)$$

This model of hysteretic damping was introduced to describe a steady-state harmonic motion only and is not necessarily valid for the solution for any other type of excitation [13].

In order to solve equation (2-3) a harmonic solution of the following form is assumed,

$$\{q\}=\{X\}e^{i\omega t} \qquad (2-4)$$

where $\{X\}$ is a complex vector of harmonic amplitudes.
Insert (2-4) into (2-3) to give

$$(-\omega^2[M]+[K]+i[H])\{X\}=\{F\} \qquad (2-5)$$

2.2.1 FREE VIBRATION

First, the homogeneous eigenproblem is considered where ω^2 is replaced by λ_r^2, giving

$$(-\lambda_r^2[M]+[K]+i[H])\{\Psi\}_r=\emptyset \qquad (2-6)$$

This is an eigenproblem where the eigenvalues λ_r^2 and the associated eigenvectors $\{\Psi\}_r$ are generally complex.
If we write,

$$\lambda_r^2=\omega_r^2(1+i\,\eta_r) \qquad (2-7)$$

we may define ω_r as the 'natural frequency' and η_r as the 'modal loss factor' for the r'th mode.

Insert into (2-6) and we obtain

$$(-\omega_r^2(1+i\eta_r)\ [M]+[K]+i[H])\{\Psi\}_r=\emptyset \qquad (2-8)$$

There exists a non-trivial eigenvector $\{\Psi\}_r$ which satisfies (2-8) if the left-hand side matrix is singular, and hence the characteristic equation is:

$$|[I]\omega_r^2(1+i\eta_r)-[M]^{-1}([K]+i[H])|=\emptyset \qquad (2-9)$$

This eigenvector is unscaled and is determined within a multiplicative arbitrary constant.

If we pre-multiply (2-6) by $\{\Psi\}_s^T$, then

$$\{\Psi\}_s^T(-\lambda_r^2[M]+[K]+i[H])\{\Psi\}_r=\emptyset \qquad (2-10)$$

Assume now another eigenvalue, λ_s $(\lambda_s\neq\lambda_r)$, then

$$(-\lambda_s^2[M]+[K]+i[H])\{\Psi\}_s=\emptyset \qquad (2-11)$$

The transpose of (2-11) is

$$\{\Psi\}_s^T(-\lambda_s^2[M]^T+[K]^T+i[H]^T)=\emptyset \qquad (2-12)$$

and since [M], [K] and [H] are symmetric matrices then

$$\{\Psi\}_s^T(-\lambda_s^2[M]+[K]+i[H])=\emptyset \qquad (2-13)$$

Post-multiply (2-13) by $\{\Psi\}_r$ and subtract from (2-10)

$$(\lambda_s^2-\lambda_r^2)\{\Psi\}_s^T[M]\{\Psi\}_r=\emptyset \qquad (2-14)$$

Since $\lambda_s\neq\lambda_r$ then

$$\{\Psi\}_s^T[M]\{\Psi\}_r=\emptyset \qquad (2-15)$$

inserting (2-15) into (2-10) gives

$$\{\Psi\}_s^T([K]+i[H])\{\Psi\}_r=\emptyset \qquad (2-16)$$

Relationships (2-15) and (2-16) are referred to as the 'orthogonality conditions'.

Consider now the matrix product

$$[\overline{M}]=[\Psi]^T[M][\Psi] \qquad (2-17)$$

where $[\Psi]$ is the matrix of the eigenvectors $\{\Psi\}_r$.

Any element which is not on the diagonal of $[\bar{M}]$ is equal to

$$\{\Psi\}_s^T[M]\{\Psi\}_r \qquad (2\text{-}18)$$

and it has been shown (2-15) to be equal to zero. Only the diagonal elements

$$\{\Psi\}_r^T[M]\{\Psi\}_r \qquad (2\text{-}19)$$

are non-zero (because [M] is a positive definite matrix [12]) and so it follows that the matrix $[\bar{M}]$ is a complex diagonal matrix

$$[\bar{M}]=[\sim m_r \sim] \qquad (2\text{-}20)$$

and is referred to as the 'modal mass matrix', with the term m_r referred to as the 'modal mass' of the r'th mode.

The same reasoning applies to $[K]+i[H]$ where

$$[\bar{K}]=[\Psi]^T([K]+i[H])[\Psi] \qquad (2\text{-}21)$$

$[\bar{K}]$ is a complex diagonal matrix referred to as the 'modal stiffness matrix'

$$[\bar{K}]=[\sim k_r \sim] \qquad (2\text{-}22)$$

and k_r is referred to as the 'modal stiffness' of the r 'th mode.

(Because the eigenvectors are determined only to within arbitrary scalar multipliers the diagonal matrices $[\bar{K}]$ and $[\bar{M}]$ are determined in the same manner and are thus not unique for any given system.)

The characteristic equation can be expressed in the terms of the modal matrices, i.e

$$|-\lambda_r^2[\bar{M}]+[\bar{K}]|=0 \qquad (2\text{-}23)$$

It is clearly seen that the eigenvector $\{\Psi\}_r$ uncouples the general characteristic equation and that

$$\lambda_r^2=\frac{k_r}{m_r} \tag{2-24}$$

$\{\Psi\}_r$ is defined therefore, as a 'normal mode shape' of the system.

However, it should be appreciated that although $[\overline{K}]$ is a diagonal matrix neither $[\Psi]^T[K][\Psi]$ nor $[\Psi]^T[H][\Psi]$ is necessarily diagonal, since

$$\{\Psi\}_s^T[K]\{\Psi\}_r\neq\emptyset \tag{2-25}$$

$$\{\Psi\}_s^T[H]\{\Psi\}_r\neq\emptyset \tag{2-26}$$

because $\{\Psi\}_r$ in (2-16) is complex.

2.2.2 THE UNDAMPED SYSTEM

Of particular theoretical interest is the case where the damping is assumed to be removed from the system. The characteristic equation is then reduced to

$$|-\lambda_r^2[M]+[K]|=\emptyset \tag{2-27}$$

For this case the eigenvectors $\{\Pi\}_r$ are all real and the associated eigenvalues λ_r^2 are all real and positive [14]. The real mode shape $\{\Pi\}_r$ is referred to as the 'undamped normal mode'. The orthogonality conditions are also satisfied and the diagonal modal mass and modal stiffness matrices are both real.

2.2.3 PROPORTIONALLY DAMPED SYSTEM.

The eigenvectors derived for a damped system are, in general, complex. However, it may be shown that when the damping matrix can be expressed as a linear combination of the mass and stiffness matrices i.e

$$[H]=\alpha[K]+\beta[M] \tag{2-28}$$

the eigenvectors are real. Relation (2-28) is referred to as 'proportional damping' and the system is 'proportionally damped'.

Substituting (2-28) into the characteristic equation (2-9) leads to

$$|[I]\omega_r^2(1+i\eta_r)-(1+i\alpha)[M]^{-1}[K]-i[I]\beta|=\emptyset \tag{2-29}$$

and separating this into real and imaginary parts, we obtain a pair of characteristic equations which must be satisfied simultaneously:

$$|\omega_r^2[I]-[M]^{-1}[K]|=\emptyset \tag{2-30}$$

$$|\omega_r^2[I](\eta_r-\frac{\beta}{\omega_r^2})-[M]^{-1}[K]|=\emptyset \tag{2-31}$$

This set is satisfied by

$$\eta_r=\alpha+\frac{\beta}{\omega_r^2} \tag{2-32}$$

The eigenvalues of (2-29) are then given by

$$\lambda_r^2=\omega_r^2[1+i(\alpha+\frac{\beta}{\omega_r^2})] \tag{2-33}$$

Substituting into equation (2-6) yields

$$([I]\omega_r^2-[M]^{-1}[K])\{\Psi\}_r=\emptyset \tag{2-34}$$

which is the eigenproblem of the undamped system with real eigenvectors $\{\Pi\}_r$.

Because the eigenvectors are real, it follows from

(2-21) that

$$\{\Pi\}_S^T [K] \{\Pi\}_r = \emptyset \qquad (2\text{-}35)$$

$$\{\Pi\}_S^T [H] \{\Pi\}_r = \emptyset \qquad (2\text{-}36)$$

The real part of each eigenvalue is the natural frequency of one mode of the proportionally-damped system; the imaginary part determines the associated modal damping. The eigenvectors and the real part of the eigenvalues are independent of the values of the damping matrix [H] or the proportionality factors α or β.

Equation (2-34) is the equation of the theoretically-undamped system. The normal mode shapes $\{\Pi\}_r$ and the natural frequencies of a proportionally-damped system ω_r are, therefore, identical to those of the theoretically-undamped system. These modes are referred to as the ' proportional normal modes'.

When the damping matrix is proportional to the stiffness matrix only (i.e $\beta = \emptyset$) the eigenvectors are still real but then

$$\eta_r = \alpha \qquad (2\text{-}37)$$

which means that the modal loss factor is identical for all the modes.

This special form of damping which permits the uncoupling of the equation of motion by the undamped normal modes is not unique to the case of proportional damping.

It was shown by Caughey et.al.[15] that there is a general condition which is necessary and sufficient to uncouple the equation of motion by the undamped normal

modes. This condition states that the matrix product $[M]^{-1}[K]$ and $[M]^{-1}[H]$ must commute, i.e

$$([M]^{-1}[K])([M]^{-1}[H])=([M]^{-1}[H])([M]^{-1}[K]) \qquad (2-38)$$

The proportional case where $[H]=\alpha[K]+\beta[M]$ clearly satisfies this condition.

2.2.4 EXCITATION BY A GENERAL FORCE VECTOR

In order to solve equation (2-3) for the general case where $\{F\}$ is a complex vector, the vector $\{X\}$ is expressed as a linear combination of another set of independent vectors such as the eigenvectors, $\{\Psi\}_r$.

$$\{X\}=\sum_{r=1}^{n} \gamma_r\{\Psi\}_r \qquad (2-39)$$

Substitute into (2-5) and we obtain

$$(-\omega^2[M]+[K]+i[H])\sum_{r=1}^{n} \gamma_r\{\Psi\}_r=\{F\} \qquad (2-40)$$

Pre-multiply (2-40) by $\{\Psi\}_r^T$, to get

$$\{\Psi\}_r^T(-\omega^2[M]+[K]+i[H])\sum_{r=1}^{n} \gamma_r\{\Psi\}_r=\{\Psi\}_r^T\{F\} \qquad (2-41)$$

or

$$\gamma_r\{\Psi\}_r^T([K]+i[H])\{\Psi\}_r-\omega^2\gamma_r\{\Psi\}_r^T[M]\{\Psi\}_r=\{\Psi\}_r^T\{F\} \qquad (2-42)$$

Because of the orthogonality conditions (2-15 and 2-16), all the other terms in the summation of (2-41) are equal to zero.

Using the notation introduced in (2-20) and (2-22), we may write:

$$\gamma_r(k_r-\omega^2 m_r)=\{\Psi\}_r^T\{F\} \qquad (2-43)$$

and then

$$\gamma_r = \frac{\{\Psi\}_r^T \{F\}}{k_r - \omega^2 m_r} \tag{2-44}$$

substitute into (2-39)

$$\{X\} = \sum_{r=1}^{n} \frac{\{\Psi\}_r^T \{F\} \{\Psi\}_r}{k_r - \omega^2 m_r} \tag{2-45}$$

rearranging (2-45) using the relationship (2-24), namely

$$\lambda_r^2 = \frac{k_r}{m_r} = \omega_r^2 (1 + i\eta_r) \tag{2-46}$$

we obtain

$$\{X\} = \sum_{r=1}^{n} \frac{\{\Psi\}_r^T \{F\} \{\Psi\}_r}{m_r \omega_r^2 \left[1 - \left(\frac{\omega}{\omega_r}\right)^2 + i\eta_r\right]} \tag{2-47}$$

As the eigenvector $\{\Psi\}_r$ is unscaled we may introduce the 'mass-normalized' eigenvector $\{\Phi\}_r$ defined as

$$\{\Phi\}_r = \frac{1}{\sqrt{m_r}} \{\Psi\}_r \tag{2-48}$$

so that

$$\{X\} = \sum_{r=1}^{n} \frac{\{\Phi\}_r^T \{F\} \{\Phi\}_r}{\omega_r^2 \left[1 - \left(\frac{\omega}{\omega_r}\right)^2 + i\eta_r\right]} \tag{2-49}$$

Equation (2-49) is the steady-state response of a hysteretically-damped system subjected to harmonic inputs in terms of the (complex) mass-normalized normal modes.

2.2.5 EXCITATION BY MONO-PHASED FORCES

For the special case where the vector of force amplitudes {F} is real, we can seek a solution of equation (2-3) for which the response of the system is all in phase, although not necessarily in phase with the force, i.e.

$$\{q\}=\{Z\}e^{i(\omega t-\theta)} \qquad (2\text{-}5\emptyset)$$

where {Z} is a real vector of unknown amplitudes and θ is an unknown phase lag.

Substitute (2-5Ø) into (2-3)

$$(-\omega^2[M]+[K]+i[H])\{Z\}e^{i(\omega t-\theta)}=\{F\}e^{i\omega t} \qquad (2\text{-}51)$$

or

$$(-\omega^2[M]+[K]+i[H])\{Z\}e^{-i\theta}=\{F\} \qquad (2\text{-}52)$$

Separate equation (2-52) into real and imaginary components,

$$[(-\omega^2[M]+[K])\mathrm{Cos}\theta+[H]\mathrm{Sin}\theta]\{Z\}=\{F\} \qquad (2\text{-}53)$$

$$[(-\omega^2[M]+[K])\mathrm{Sin}\theta-[H]\mathrm{Cos}\theta]\{Z\}=\emptyset \qquad (2\text{-}54)$$

Equation (2-54) is a non-standard real homogeneous eigen-problem where the eigenvalues are θ_S for which there exist corresponding eigenvectors $\{\kappa\}_S$.

The corresponding force vector is obtained from equation (2-53):

$$[(-\omega^2[M]+[K])\mathrm{Cos}\theta_S+[H]\mathrm{Sin}\theta_S]\{\kappa\}_S=\{F\}_S \qquad (2\text{-}55)$$

It should be noted that the eigenvectors $\{\kappa\}_S$ and the phase lags θ_S are functions of the excitation frequency ω.

The harmonic forcing vector $\{F\}e^{i\omega t}$ may be 'tuned' so that $\theta_S=9\emptyset^\circ$ and then equation (2-54) reduces to

$$(-\omega^2[M]+[K])\{Z\}=\emptyset \qquad (2\text{-}56)$$

which is the equation of the theoretical case of an undamped

system having real eigenvectors $\{\Pi\}_s$ and natural frequencies ω_s . The forcing vector for this case is obtained from equation (2-55)

$$\{F\}_s=[H]\{\Pi\}_s \tag{2-57}$$

It is seen that by tuning the amplitudes of the exciting forces to produce a real vector (mono-phased) at a certain proportion to the damping and at a frequency equal to a natural frequency of the theoretically undamped system, the response of the system under consideration is mono-phased and in quadrature with the forcing vector. The real mode shape the system assumes $\{\kappa\}_s$ is then identical to the corresponding mode shape of the undamped system $\{\Pi\}_s$. This forced mode is not a normal mode of the system in the strict sense and is referred to as 'forced proportional mode'.

If the response of the system under this excitation is expressed in terms of its normal mode shapes $\{\Psi\}_r$, which are complex, then from equation (2-47) we obtain

$$\{X\}=\sum_{r=1}^{n}\frac{\{\Psi\}_r^T\{H\}\{\Pi\}_s}{m_r\omega_r^2\left[1-\left(\frac{\omega_s}{\omega_r}\right)^2+i\eta_r\right]}\{\Psi\}_r \tag{2-58}$$

It is of interest to examine the particular case of a proportionally-damped system where its proportional normal mode shapes $\{\Pi\}_r$ are real.

Equation (2-58) may then be written as

$$\{X\}=\sum_{r=1}^{n}\frac{\{\Pi\}_r^T(\alpha[K]+\beta[M])\{\Pi\}_s}{m_r\omega_r^2\left[1-\left(\frac{\omega}{\omega_r}\right)^2+i\eta_r\right]}\{\Pi\}_r \tag{2-59}$$

Because of the orthogonality conditions, all the terms in this summation where r≠s are equal to zero. Equation (2-59) may then be written as

$$\{X\} = \frac{\alpha k_s + \beta m_s}{m_s \omega_s^2 \left[1 - \left(\frac{\omega}{\omega_s}\right)^2 + i\eta_s\right]} \{\Pi\}_s = d_s \{\Pi\}_s \qquad (2\text{-}60)$$

which means that the system vibrates in one mono-phased mode only (its s'th proportional normal mode) and that the phase between the response and the excitation is a function of d_s (which is complex). This mono-phased response of the system is independent of the excitation frequency, so once the proper force vector $\{F\}_s$ is applied to the system, the response is in the s'th mono-phased mode at any frequency of excitation. The only parameters which change as the frequency is changed are the phase between response and excitation and the amplitude of the response.

(This discussion can be generalized for the ordinary case of the normal (complex) mode shapes $\{\Psi\}_s$. The excitation vector $\{F\}_s$ is then complex, which means that by proper tuning of the amplitudes and phases of the force distribution the system can be excited at one normal (complex) mode shape. The practical implementation of this is very complicated and only one reference to the use of this method was found in current literature [16]).

The results which have just been presented form the basis of the multi-point modal testing method. Once a properly tuned mono-phased force vector is applied to the

system, and the response is mono-phase and in quadrature with the applied force, the measured response gives the proportional normal mode shape of the system directly and is identical to the undamped normal mode of the system. The excitation frequency is then equal to the natural frequency of the undamped system.

Once the system is vibrating in this 'pure' mode, a check to establish whether the system is proportionally-damped can be carried out by changing the frequency of excitation and noting if there is a change in the measured shape of the response. A change indicates that the system is not proportionally-damped.

2.2.6 EXCITATION BY A SINGLE FORCE

From the general expression for the response of the system to a general harmonic (complex) force vector we can extract an expression for the system's response to a single harmonic force F_k. The vector of force amplitudes is then:

$$\{F\} = \begin{Bmatrix} \emptyset \\ F_k \\ \emptyset \end{Bmatrix} \tag{2-61}$$

Inserting into (2-49) produces

$$\{X\} = \sum_{r=1}^{n} \frac{({}_r\Phi_k)\ F_k \{\Phi\}_r}{\omega_r^2 \left[1 - \left(\frac{\omega}{\omega_r}\right)^2 + i\eta_r\right]} \tag{2-62}$$

where $({}_r\Phi_k)$ is the k'th element in the r'th eigenvector $\{\Phi\}_r$. From equation (2-62) we can extract the single

response x_j due to the single force F_k and derive an expression for the general receptance α_{jk} .

$$\alpha_{jk}=\frac{x_j}{F_k}=\sum_{r=1}^{n}\frac{({}_r\Phi_j)({}_r\Phi_k)}{\omega_r^2\left[1-\left(\frac{\omega}{\omega_r}\right)^2+i\eta_r\right]} \qquad (2\text{-}63)$$

The product $({}_r\Phi_j)({}_r\Phi_k)$ is denoted by ${}_rA_{jk}$

$${}_rA_{jk}=({}_r\Phi_j)({}_r\Phi_k) \qquad (2\text{-}64)$$

and is referred to as the 'r'th modal constant of receptance α_{jk}'. Equation (2-63) forms the basis of the single point modal identification method. From a measured set of individual receptance measurements the parameters of equation (2-63) can be identified.

2.3 VISCOUS DAMPING

A common type of damper which is widely used to model the damping mechanism in a vibrating system is the viscous dashpot. The equation of motion for a viscously damped system subjected to a constant harmonic excitation is:

$$[M]\{\ddot{q}\}+[C]\{\dot{q}\}+[K]\{q\}=\{F\}e^{i\omega t} \tag{2-65}$$

2.3.1 FREE VIBRATION

For the case of free vibrations where $\{F\}=\emptyset$, we assume a solution of the form:

$$\{q\}=\{X\}e^{st} \tag{2-66}$$

Inserting (2-66) into (2-65) we get

$$(s^2[M]+s[C]+[K])\{X\}=\emptyset \tag{2-67}$$

which is a complex eigenproblem where the eigenvalues are $\lambda_r=s$. There are in general 2n eigenvalues, λ_r , and associated eigenvectors, $\{\phi\}_r$, which satisfy the characteristic equation (2-67). Because they are in general complex, and [M], [K] and [C] are real, they occur in conjugate pairs [17] and satisfy the following equation,

$$(\lambda_r^2[M]+\lambda_r[C]+[K])\{\phi\}_r=\emptyset \tag{2-68}$$

The eigenvector $\{\phi\}_r$ is unscaled and is determined within a multiplicative constant (the order of this vector is n).

To demonstrate the orthogonality properties, pre-multiply (2-68) by $\{\phi\}_s^T$ then

$$\{\phi\}_s^T(\lambda_r^2[M]+\lambda_r[C]+[K])\{\phi\}_r=\emptyset \tag{2-69}$$

Assume now another eigenalue λ_s ($\lambda_s \neq \lambda_r$) then

$$(\lambda_s^2[M]+\lambda_s[C]+[K])\{\psi\}_s=\emptyset \tag{2-70}$$

The transpose of (2-70) is

$$\{\psi\}_s^T(\lambda_s^2[M]^T+\lambda_s[C]^T+[K]^T)=\emptyset \tag{2-71}$$

Since [M], [K] and [C] are symmetric matrices,

$$\{\psi\}_s^T(\lambda_s^2[M]+\lambda_s[C]+[K])=\emptyset \tag{2-72}$$

Post-multiply (2-72) by $\{\psi\}_r$ and subtract from (2-69)

$$(\lambda_r^2-\lambda_s^2)\{\psi\}_s^T[M]\{\psi\}_r+(\lambda_r-\lambda_s)\{\psi\}_s^T[C]\{\psi\}_r=\emptyset \tag{2-73}$$

since $\lambda_r \neq \lambda_s$ then

$$(\lambda_r+\lambda_s)\{\psi\}_s^T[M]\{\psi\}_r+\{\psi\}_s^T[C]\{\psi\}_r=\emptyset \tag{2-74}$$

Multiply equation (2-69) by λ_s and (2-71) by λ_r

$$\{\psi\}_s^T(\lambda_s\lambda_r^2[M]+\lambda_s\lambda_r[C]+\lambda_s[K])\{\psi\}_r=\emptyset \tag{2-75}$$

$$\{\psi\}_s^T(\lambda_r\lambda_s^2[M]+\lambda_r\lambda_s[C]+\lambda_r[K])\{\psi\}_r=\emptyset \tag{2-76}$$

then subtract equation (2-76) from (2-75)

$$\{\psi\}_s^T(\lambda_s\lambda_r(\lambda_r-\lambda_s)[M]+(\lambda_s-\lambda_r)[K])\{\psi\}_r=\emptyset \tag{2-77}$$

since $\lambda_r \neq \lambda_s$ then

$$\lambda_r\lambda_s\{\psi\}_s^T[M]\{\psi\}_r-\{\psi\}_s^T[K]\{\psi\}_r=\emptyset \tag{2-78}$$

Relationships (2-74) and (2-78) are the 'orthogonality conditions' for a viscously-damped system.

It is customary to display the eigenvalues λ_r in the form

$$\lambda_r=\Omega_r(-\xi_r+i\sqrt{1-\xi_r^2}) \tag{2-79}$$

where ξ_r is defined as the ratio of critical damping and Ω_r is the modulus of the eigenvalue. (Very often [17, 22, 24] Ω_r is referred to as the 'undamped natural frequency' which is a misleading definition. It is the undamped natural frequency only in the special cases of

proportional damping or a one-degree-of-fredom system.)

Consider the orthogonality relationship where λ_r and λ_s are conjugates. i.e.

$$\lambda_s=\Omega_r(-\xi_r-i\sqrt{1-\xi_r^2}) \tag{2-80}$$

and hence

$$\{\psi\}_s=\{\psi^*\}_r \tag{2-81}$$

Inserting (2-80) and (2-81) into (2-74) we get

$$-2\Omega_r\xi_r\{\psi^*\}_r^T[M]\{\psi\}_r+\{\psi^*\}_r^T[C]\{\psi\}_r=0 \tag{2-82}$$

from which

$$2\Omega_r\xi_r=\frac{\{\psi^*\}_r^T[C]\{\psi\}_r}{\{\psi^*\}_r^T[M]\{\psi\}_r} \tag{2-83}$$

Inserting (2-80) and (2-81) into (2-78) we get

$$\Omega_r^2\{\psi^*\}_r^T[M]\{\psi\}_r-\{\psi^*\}_r^T[K]\{\psi\}_r=0 \tag{2-84}$$

from which

$$\Omega_r^2=\frac{\{\psi^*\}_r^T[K]\{\psi\}_r}{\{\psi^*\}_r^T[M]\{\psi\}_r} \tag{2-85}$$

Equations (2-83) and (2-85) may be expressed as

$$2\Omega_r\xi_r=\frac{c_r}{m_r} \tag{2-86}$$

and

$$\Omega_r^2=\frac{k_r}{m_r} \tag{2-87}$$

where m_r, k_r and c_r are the modal mass, stiffness and damping respectively.

2.3.2 PROPORTIONALLY-DAMPED SYSTEM

When the system is proportionally-damped, i.e.

$$[C]=\alpha[K]+\beta[M] \tag{2-88}$$

the relationship between Ω_r and ξ_r may be derived from expression (2-83)

$$2\Omega_r\xi_r=\frac{\{\phi^*\}_r^T(\alpha[K]+\beta[M])\{\psi\}_r}{\{\phi^*\}_r^T[M]\{\psi\}_r} \tag{2-89}$$

or

$$2\Omega_r\xi_r=\alpha\Omega_r^2+\beta \tag{2-90}$$

from which

$$\xi_r=\frac{\alpha\Omega_r^2+\beta}{2\Omega_r} \tag{2-91}$$

Inserting expressions (2-8Ø) and (2-88) into equation (2-67) results in the following eigenproblem

$$(-\Omega_r^2[M]+[K])\{\psi\}_r=\emptyset \tag{2-92}$$

which is clearly the eigenproblem of the undamped system.

The mode shapes $\{\Pi\}_r$ of the proportionally-damped viscous system are, therefore, identical to those of the undamped system and satisfy the following orthogonality conditions, namely

$$[\Pi]^T[M][\Pi]=[\sim m_r \sim] \tag{2-93}$$

$$[\Pi]^T[K][\Pi]=[\sim k_r \sim] \tag{2-94}$$

$$[\Pi]^T[C][\Pi]=[\sim c_r \sim] \tag{2-95}$$

The natural frequency of the proportionally-damped viscous system is

$$\omega_r=\Omega_r\sqrt{1-\xi_r^2} \tag{2-96}$$

where Ω_r is equal to the natural frequency of the undamped

system.

As the proportional damping of the system is increased, the natural frequency is decreased according to equations (2-91) and (2-96). The modulus of the eigenvalue Ω_r is independent of the amount of damping and the proportionality factors α and β.

2.3.3 EXCITATION BY A GENERAL FORCE VECTOR.

The characteristic equation of a viscously-damped system (2-67) does not constitute a standard eigenvalue equation. In order to obtain a convenient solution for equation (2-65) we apply a different approach to the solution of the equation of motion for free vibrations by using the following transformation:

Define a new vector $\{y\}$ of order 2n

$$\{y\} = \begin{Bmatrix} q \\ - \\ \dot{q} \end{Bmatrix} \tag{2-97}$$

and substitute this into (2-65)

$$[C : M]\{\dot{y}\}+[K : \emptyset]\{y\}=\emptyset \tag{2-98}$$

As there are now n equations with 2n unknowns we add the dummy equation:

$$[M : \emptyset]\{\dot{y}\}+[O : -M]\{y\}=\emptyset \tag{2-99}$$

to give a set of 2n equations:

$$\left[\begin{array}{c:c} C & M \\ \hdashline M & \emptyset \end{array}\right]\{\dot{y}\}+\left[\begin{array}{c:c} K & \emptyset \\ \hdashline \emptyset & -M \end{array}\right]\{y\}=\emptyset \tag{2-100}$$

or

$$[A]\{\dot{y}\}+[B]\{y\}=\emptyset \qquad (2\text{-}101)$$

Consider now a trial solution of the form $\{y\}=\{Y\}e^{st}$ which yields a standard eigenproblem

$$(s[A]+[B])\{Y\}=\emptyset \qquad (2\text{-}102)$$

There are 2n eigenvalues, s_r, and associated eigenvectors, $\{\theta\}_r$, each satisfying the equation:

$$(s_r[A]+[B])\{\theta\}_r=o \qquad (2\text{-}103)$$

This equation is of similar form to that of the undamped system and possesses similar orthogonality properties:

$$[\theta]^T[A][\theta]=[-a_r-] \qquad (2\text{-}104)$$

$$[\theta]^T[B][\theta]=[-b_r-] \qquad (2\text{-}105)$$

and

$$s_r=\frac{-b_r}{a_r} \qquad (2\text{-}106)$$

These eigenvalues and eigenvectors are generally complex (for underdamped systems) and occur in conjugate pairs [18].

Consider now the harmonic forced vibrations where the amplitudes of the harmonic forcing vector $\{P\}$ are

$$\{P\}=\begin{Bmatrix} F \\ \cdots \\ \emptyset \end{Bmatrix}_{2n} \qquad (2\text{-}107)$$

and the equation of motion is

$$[A]\{\dot{Y}\}+[B]\{Y\}=\{P\} \qquad (2\text{-}108)$$

Assume a solution of the form

$$\{Y\}=\begin{Bmatrix} X \\ \cdots \\ i\omega X \end{Bmatrix} e^{i\omega t} \qquad (2\text{-}109)$$

and that the vector $\{Y\}$ may be expressed as a linear combination of the 2n linearly independent vectors $\{\theta\}_r$

hence

$$\{Y\}=\sum_{r=1}^{2n} Y_r\{\Theta\}_r \qquad (2\text{-}110)$$

where Y_r is an unknown coeffecient.

Substitute this into (2-108) and pre-multiply by $\{\Theta\}_s^T$, giving:

$$i\omega\{\Theta\}_s^T[A]\sum_{r=1}^{2n} Y_r\{\Theta\}_r+\{\Theta\}_s^T[B]\sum_{r=1}^{2n} Y_r\{\Theta\}_r=\{\Theta\}_s^T\{P\} \qquad (2\text{-}111)$$

Because of the orthogonality conditions, equation (2-111) reduces to

$$Y_r(i\omega\{\Theta\}_r^T[A]\{\Theta\}_r+\{\Theta\}_r^T[B]\{\Theta\}_r)=\{\Theta\}_r^T\{P\} \qquad (2\text{-}112)$$

or, using the notation introduced in (2-104) and (2-105), to

$$Y_r=\frac{\{\Theta\}_r^T\{P\}}{i\omega a_r+b_r}=\frac{\{\Theta\}_r^T\{P\}}{a_r(i\omega-s_r)} \qquad (2\text{-}113)$$

The solution of equation (2-108) can thus be written in the following manner:

$$\begin{Bmatrix} X \\ \cdots \\ i\omega X \end{Bmatrix}=\sum_{r=1}^{2n}\frac{\{\Theta\}_r^T\{P\}\{\Theta\}_r}{a_r(i\omega-s_r)} \qquad (2\text{-}114)$$

Because the eigenvalues and the eigenvectors occur in conjugate pairs equation (2-114) may be written as:

$$\begin{Bmatrix} X \\ \cdots \\ i\omega X \end{Bmatrix}=\sum_{r=1}^{n}\frac{\{\Theta\}_r^T\{P\}\{\Theta\}_r}{a_r(i\omega-s_r)}+\sum_{r=1}^{n}\frac{\{\Theta^*\}_r^T\{P\}\{\Theta^*\}_r}{a_r^*(i\omega-s_r^*)} \qquad (2\text{-}115)$$

This is the steady-state response of a viscously-damped system due to harmonic excitation in terms of the 2n modes $\{\Theta\}_r$.

It has been shown that when the system is proportionally-damped, the mode shapes are real. For this case expression (2-115) is much simpler; we may assume a solution of the form:

$$\{X\}=\sum_{r=1}^{n} Y_r\{\Pi\}_r \qquad (2\text{-}116)$$

Insert into equation (2-65) and pre-multiply by $\{\Pi\}_r^T$.

Due to the orthogonality conditions, we get

$$Y_r(-\omega^2\{\Pi\}_r^T[M]\{\Pi\}_r+i\omega\{\Pi\}_r^T[C]\{\Pi\}_r+\{\Pi\}_r^T[K]\{\Pi\}_r=\{\Pi\}_r^T\{F\} \qquad (2\text{-}117)$$

Because $\{\Pi\}_r$ is a real vector, we can use the notation introduced in expressions (2-79) and (2-87) to obtain:

$$Y_r=\frac{\{\Pi\}_r^T\{F\}}{m_r(-\omega^2+2i\omega\Omega_r\xi_r+\Omega_r^2)} \qquad (2\text{-}118)$$

Substitute into (2-116)

$$\{X\}=\sum_{r=1}^{n}\frac{\{\Pi\}_r^T\{F\}\{\Pi\}_r}{\Omega_r^2 m_r\left[1-\left(\frac{\omega}{\Omega_r}\right)^2+2i\left(\frac{\omega}{\Omega_r}\right)\xi_r\right]} \qquad (2\text{-}119)$$

Equation (2-119) is the steay-state response of a proportionally-damped viscous system due to harmonic excitation, described in terms of its proportional normal modes, $\{\Pi\}_r$.

2.3.4 EXCITATION BY MONO-PHASED FORCES

When the harmonic forcing vector {F} is real, we assume that the response of the system has the same frequency but with a certain phase lag θ relative to the force. i.e.

$$\{q\}=\{Z\}e^{i(\omega t-\theta)} \tag{2-120}$$

where $\{Z\}$ is a real vector of amplitudes.

Substituting (2-120) into equation (2-65)

$$(-\omega^2[M]+i\ [C]+[K])\{Z\}e^{-i\theta}=\{F\} \tag{2-121}$$

and separating into real and imaginary parts, we get

$$(-\omega^2[M]+[K])\{Z\}\text{Cos}\theta+\omega[C]\{Z\}\text{Sin}\theta=\{F\} \tag{2-122}$$

$$(-\omega^2[M]+[K])\{Z\}\text{Sin}\theta+\omega[C]\{Z\}\text{Cos}\theta=\emptyset \tag{2-123}$$

Equations (2-122) and (2-123) are similar to equations (2-53) and (2-54) for the hysteretically-damped system and may be analysed in the same way. The forcing vector needed, in this case, for the response to be in quadrature with the excitation is

$$\{F\}_S=\omega[C]\{\Pi\}_S \tag{2-124}$$

The 'forced proportional modes' of a viscously-damped system are identical to those obtained for the hysteretically-damped one. Actually, this result is independent of the model of damping chosen and is valid for the more general case of equation (2-1). The force distribution needed then is;

$$\{F\}_S=(\omega[C]+[H])\{\Pi\}_S \tag{2-125}$$

The analysis of the proportionally-damped viscous system is similar to that for the hysteretic case and all the conclusions drawn there apply for this case. The real response of the system is then,

$$\{Z\}_S=\frac{\alpha k_S+\beta c_S}{m_S\omega_S^2\left[1-\left(\frac{\omega}{\omega_S}\right)^2+2i\left(\frac{\omega}{\omega_S}\right)\zeta_S\right]} \tag{2-126}$$

This result which states that the system can be forced

to vibrate in a 'forced proportional mode' which is identical to the undamped normal mode of the system, regardless of the damping model assumed, is not fully recognized. Although it was proved by Fraeijs de Veubeke in 1948 [19] and later (1963) emphasised by Bishop and Gladwell [11] there are some more recent investigators who appear not to accept these results [20, 16]. (see appendix)

2.3.5 EXCITATION BY A SINGLE FORCE

The response of the system to a single harmonic force F_k can be extracted from the general expression (2-115) by setting $\{P\}$ as,

$$\{P\} = \begin{Bmatrix} \emptyset \\ F_k \\ \emptyset \\ \cdot \\ \emptyset \end{Bmatrix} \tag{2-127}$$

Using the notation introduced in (2-79), equation (2-115) for this case is

$$\begin{Bmatrix} X \\ \cdots \\ i\omega X \end{Bmatrix} = \sum_{r=1}^{n} \frac{({}_r\Theta_k)\{\Theta\}_r}{a_r\Omega_r\left[\xi_r + i\left(\frac{\omega}{\Omega_r} - \sqrt{1-\xi_r^2}\right)\right]} F_k + \sum_{r=1}^{n} \frac{({}_r\Theta_k^*)\{\Theta^*\}_r}{a_r^*\Omega_r\left[\xi_r + i\left(\frac{\omega}{\Omega_r} + \sqrt{1-\xi_r^2}\right)\right]} F_k \tag{2-128}$$

where $({}_r\Theta_k)$ is the k'th element in the r'th eigenvector $\{\Theta\}_r$.

Denote,

$$\{{}_rG_k\}=\frac{({}_r\Theta_k)}{a_r}\{\Theta\}_r \tag{2-129}$$

and the equation (2-128) can be written now as:

$$\begin{Bmatrix} X \\ \cdots \\ i\omega X \end{Bmatrix} = \sum_{r=1}^{n} \frac{\{{}_rR_k\}+i\left(\frac{\omega}{\Omega_r}\right)\{{}_rS_k\}}{\Omega_r^2\left[1-\left(\frac{\omega}{\Omega_r}\right)^2+2i\left(\frac{\omega}{\Omega_r}\right)\xi_r\right]}F_k \tag{2-130}$$

where

$$\{{}_rR_k\}=2\left(\xi_r \mathrm{Re}\{{}_rG_k\}-\mathrm{Im}\{{}_rG_k\}\sqrt{1-\xi_r^2}\right) \tag{2-131}$$

$$\{{}_rS_k\}=2\mathrm{Re}\{{}_rG_k\} \tag{2-132}$$

Equation (2-130) is the response of a viscously-damped system due to a single force excitation.

From this equation we can extract the single response x_j and derive the general receptance α_{jk}:

$$\alpha_{jk}=\frac{X_j}{F_k}=\sum_{r=1}^{n} \frac{({}_rR_{jk})+i\left(\frac{\omega}{\Omega_r}\right)({}_rS_{jk})}{\Omega_r^2\left[1-\left(\frac{\omega}{\Omega_r}\right)^2+2i\left(\frac{\omega}{\Omega_r}\right)\xi_r\right]} \tag{2-133}$$

where $({}_rR_{jk})$ and $({}_rS_{jk})$ are the j'th elements in their respective vectors.

2.4 CONCLUSIONS.

It appears that there exists no clear definition of one of the main terms used in modal analysis - the 'mode shape'. In this chapter, we have tried to define this term precisely and to point out some of its special forms.

The basic term is the 'normal mode shape' which is associated with the problem of free vibrations only. A system possesses n normal modes of vibration which are independent of each other: i.e. when it vibrates freely in one of its normal modes there is no transfer of energy to any other normal mode.

The exact nature of the normal modes revolves around the form of damping present in the system. For the theoretical case of an undamped system the normal mode shapes are real and orthogonal with respect to the system's matrices [M] and [K]; these are the 'undamped normal modes'.

When the damping has a special form whereby it is proportional to the stiffness and/or the mass distribution of the system, the modes are identical to the undamped normal modes and exhibit the same orthogonality conditions; these are the 'proportional normal modes'.

If the model assumed for the damping is the hysteretic one then the natural frequency associated with the proportional normal modes is equal to the natural frequency of the undamped normal mode. When the damping is assumed to be viscous, then the natural frequency is a function of the amount of damping present in the system.

For the general form of damping, the normal modes are complex and there is a marked difference between these properties depending on the model of damping used.

When the damping is hysteretic, the system posseses n complex normal modes which are orthogonal with respect to the system's matrices. For the viscous case, there are 2n complex mode shapes (actually, n conjugate pairs), each of order 2n. These mode shapes are orthogonal with respect to a special combination of the system's matrices and each one describes both a displacement and velocity 'shape' of the system.

Of considerable practical importance is the case where the system is excited by a set of mono-phased forces. It has been shown that regardless of the form or model assumed for damping, it is possible, by proper tuning of the amplitudes of the mono-phased forces, to excite the system into a mode which is identical to the (real) proportional normal mode; this is the 'forced proportional mode'. When the damping is of the more general form, this response is possible only at a frequency which is equal to the undamped natural frequency and then it is in quadrature with the excitation. When the damping is proportional, this response may be obtained at any frequency but then it is not in quadrature with the excitation.

There is no point in a comparison between the two models of damping just presented. A real system is neither hyster-

etically nor viscously-damped; these representations are just mathematical conveniences and the debate as to which one is 'better' may never end; each one of them has its own advantages and drawbacks depending on the particular case.

However, it seems that for the case of harmonic vibrations the hysteretic model is analytically simpler and, as will be seen later, it is more amenable to experimental analysis. As a matter of fact, this model is valid only for harmonic response. Nevertheless, it is found that the two models are used almost equally in the field of modal analysis by different investigators, and when used in experimental cases they are practically equal.

3. REAL AND COMPLEX NORMAL MODE SHAPES.

3.1 INTRODUCTION.

It has been shown that the nature of the normal mode shapes of a system revolves around the form of damping. For the particular case where the damping is proportional, the normal modes are real regardless of the amount of damping present in the system. The addition of nonproportional elements changes the real normal modes into complex normal modes. The favourable condition of proportional damping is not often encountered in practice and experiments suggest the need to assume complex-type modes rather than real ones.

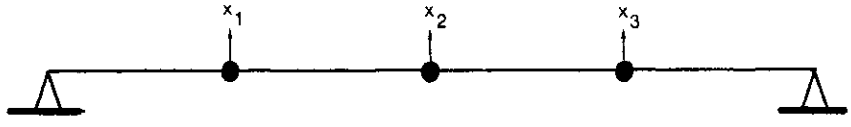

Fig. 3-1: Three degree of freedom model of a beam.

A physical interpretation of the concept of a 'complex normal mode' can be illustrated by the following simple example:

Consider the lumped-mass representation of a simply-supported beam (Fig. 3-1). The first normal mode shape of this beam may be described graphically (Fig 3-2a). However, in general not all the points in a normal mode shape necessarily reach their maximum or minimum position simultaneously. This 'phase lag' between the times when the

various points in a mode reach their extreme positions can be visualized by plotting the magnitude of the relative amplitude of each of the points in a mode as a rotating vector (Fig 3-2b). The reason that not all the points reach their extreme positions simultaneously is due to the fact that the damping forces are not distributed proportionally to the inertial and elastic forces in the system.

Mead [23] suggested that the physical interpretation of this phase difference is that there is an energy-carrying wave through the system transferring energy from points where there is an excess of energy input over energy dissipation, to areas where there is an excess of dissipation over energy input.

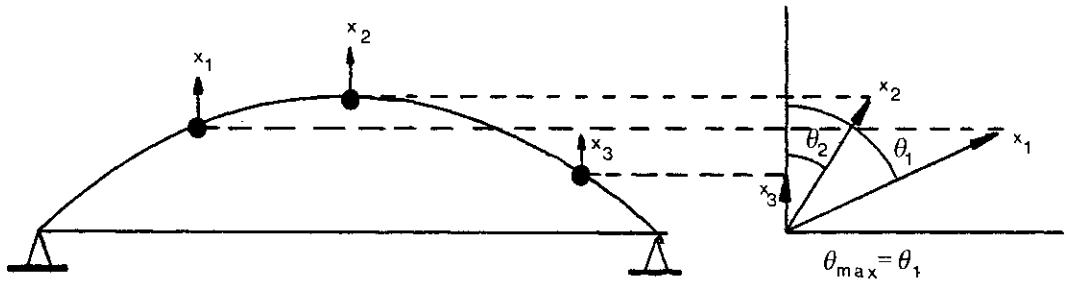

Fig.3-2: Vector representation of a complex normal mode shape.

The 'complexity' of a normal mode shape may be quantified by the maximum phase lag within the mode, θ_{max}. This is an arbitrary parameter which might enable us to decide which normal mode is more complex.

The level of 'complexity' of a normal mode is a function

of the nonproportionality between the damping matrix and the stiffness and/or the mass matrix. It is easily shown that the normal modes are real for proportional systems. However, for the nonproportional case, the relationship between the normal modes and the system matrices is only established by solving the complex eigenproblem (which is basically a solution of an n-degree complex polynomial) in order to derive the complex eigenvalues and a solution of a set of n-1 linear complex equations in order to derive the (complex) normal modes.

The final result of an experimental modal survey using the single-point excitation method is a set of complex, mass-normalized normal mode shapes $\{\Phi\}_r$. However, for comparison with theoretical studies by finite element calculations, or with results of a multi-point excitation test, the (real) proportional normal modes are required. Apparently, the most direct way to derive these modes is to calculate the system matrices from the orthogonality relationship, i.e

$$
\begin{aligned}
[M] &= [\Phi]^{T}[\Phi]^{-1} \\
[K] &= \mathrm{Re}\left([\Phi]^{T}[\lambda_r^2][\Phi]^{-1}\right) \\
[H] &= \mathrm{Im}\left([\Phi]^{T}[\lambda_r^2][\Phi]^{-1}\right)
\end{aligned}
\qquad (3\text{-}1)
$$

Once these matrices are calculated, the eigensolution for the undamped system can be obtained, using [M] and [K] only, and hence the required undamped normal modes can be determined [24,25].

Unfortunately, this simple method is impractical because

it requires the knowledge of all the (n) normal mode shapes of the system and, generally, experimentally-identified mode shapes constitute an incomplete set. Using such an incomplete set in the above scheme results in system matrices which are incomplete and which have, therefore, no physical meaning. (They might be called 'pseudo system matrices'). The inherent limitation of this approach may be demonstrated by this general example:

For the nxn complete system, there exists a matrix of mass-normalized eigenvectors $[\Phi_n]$. This matrix is orthogonal with respect to the mass matrix $[M_n]$, i.e

$$[\Phi_n]^T[M_n][\Phi_n]=[I] \qquad (3-2)$$

Next, the system may be modelled by p lumped masses $[M_p]$ where $p<n$, so that its normal mode shapes are identical to the first p normal modes of the complete (n) system. For this system there exists a matrix of mass-normalized eigenvectors $[\Phi_p]$. This matrix is also orthogonal but with respect to the corresponding mass matrix $[M_p]$, i.e

$$[\Phi_p]^T[M_p][\Phi_p]=[I] \qquad (3-3)$$

Now, if we truncate the $[\Phi_n]$ matrix by taking the first p eigenvectors and reducing the number of elements in each eigenvector from n to p, we can create a truncated (incomplete) square matrix of eigenvectors $[\Phi_t]$ which describes the normal mode shapes of the first p modes.

The truncated eigenvector matrix $[\Phi_t]$ is orthogonal with respect to the mass matrix $[M_p]$ but because its elements are mass-normalized with respect to the complete mass matrix

$[M_n]$, the orthogonality relationship is:

$$[\Phi_t]^T [M_p] [\Phi_t] = [\text{-} m_t \text{—}] \tag{3-4}$$

where $[\text{-} m_t \text{—}]$ is the truncated modal mass matrix. $[\Phi_t]$ is related to $[\Phi_p]$ by $[\text{-} m_t \text{—}]$ i.e

$$[\Phi_t] = [\Phi_p] [\text{-} m_t \text{—}]^{\frac{1}{2}} \tag{3-5}$$

It is clear that the knowledge of the truncated (incomplete) eigenvector matrix $[\Phi_t]$ does not enable us to derive the physical mass matrix $[M_p]$ because of the absence of the diagonal normalizing matrix $[\text{-} m_t \text{—}]$.

When a system is experimentally-identified, the derived eigenvectors $[\Phi_t]$ are normalized with respect to a mass matrix $[M_n]$; calculating the reduced mass matrix $[M_p]$ by assuming that $[\text{-} m_t \text{—}] = [I]$ produces a pseudo mass matrix which has no physical meaning.

Much attention has been devoted to this problem [25,28,29,31] and it is commonly agreed that there is no unique solution to it. Nevertheless, many investigators tried to 'solve' it by adding more constraints to the problem and thus limiting the number of solutions. Thoren [27] solved it by assuming that $[\text{-} m_t \text{—}] = [I]$ and was satisfied that the derived system matrices reproduced the original system response. Ross [26] showed that the system matrices need not necessarily have a physical meaning so long as they satisfy some energy constraints and reproduce the eigensolution. Imregun [30], who investigated the problem of reducing the size of the matrices representing a system, limited the mass matrix to be diagonal, and the sum of its elements to be

equal to the total mass of the system. Gleeson [40] checked the possibility of using the pseudo matrices for prediction of the effect of changes in the mass or stiffness of the system and found that, except for very simple synthesised cases, the pseudo-matrices do not provide satisfactory results.

Another branch of investigation uses the pseudo mass matrix as a means for improving theoretical or intuitive estimates of the physical mass matrix [32,33,34,35].

All these works are restricted to undamped or proportionally-damped systems whose normal modes are real and the derived pseudo mass matrix is, therefore, real as well. However, when the system is nonproportionally-damped and its normal modes are complex, the pseudo mass matrix is complex and cannot be used as such for derivation of the undamped normal modes.

A simple numerical example illustrates this point: consider a nonproportionally-damped six degree of freedom simple system (Fig. 3-3).

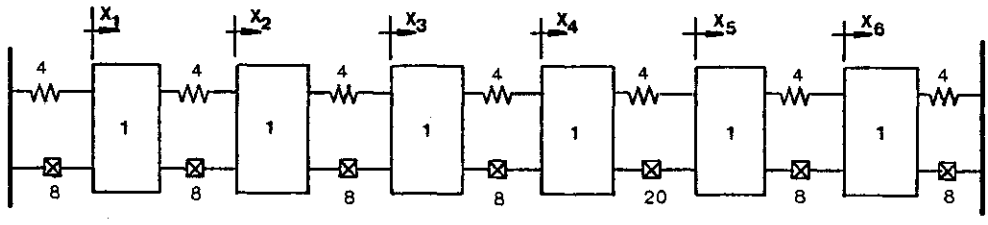

Fig. 3-3: Six degree of freedom nonproportional system

The complete mass matrix of this system is:

$$\begin{bmatrix} 1.00 & 0 & 0 & 0 & 0 & 0 \\ 0 & 1.00 & 0 & 0 & 0 & 0 \\ 0 & 0 & 1.00 & 0 & 0 & 0 \\ 0 & 0 & 0 & 1.00 & 0 & 0 \\ 0 & 0 & 0 & 0 & 1.00 & 0 \\ 0 & 0 & 0 & 0 & 0 & 1.00 \end{bmatrix}$$

The complete set of complex mass-normalized normal modes of it are (expressed by modulus and phase in degrees) is:

.2321	176.276	.4186	-178.858	.5210	-.325	.5211	.064	.2319	-.041	.4181	-178.581
.4182	-2.882	.5224	1.821	.2318	178.808	.2317	-1.586	.4179	-.051	.5213	-178.886
.5244	178.710	.2339	-174.508	.4178	178.608	.4182	-178.133	.5211	-.071	.2319	178.774
.5220	1.502	.2324	176.454	.4179	-.221	.4177	178.781	.5211	-.104	.2322	1.107
.4194	-178.885	.5214	-1.559	.2321	.742	.2319	-.874	.4180	.255	.5209	-.501
.2328	2.163	.4178	177.681	.5214	-178.392	.5215	.656	.2320	.265	.4178	-.386

The reduced (incomplete) set of modes which is created by ignoring mode six and removing coordinate x_1 is:

.5224	1.921	.2319	179.808	.2317	-1.566	.4179	-.051	.5213	-179.696
.2339	-174.508	.4178	179.609	.4182	-179.133	.5211	-.071	.2319	179.774
.2324	176.454	.4179	-.221	.4177	178.791	.5211	-.104	.2322	1.107
.5214	-1.559	.2321	.742	.2319	-.974	.4180	.255	.5209	-.501
.4178	177.661	.5214	-179.392	.5215	.656	.2320	.265	.4178	-.386

The pseudo-mass matrix derived according to (3-1) from this incomplete set is: (expressed by real and imaginary parts)

4.2446	.0954	-4.0410	-.2314	4.0290	.4284	-3.2271	-.4290	1.7945	.2117
-4.0410	-.2314	6.0290	.4284	-5.0072	-.6736	4.0076	.6465	-2.2294	-.3261
4.0290	.4284	-5.0072	-.6736	5.9734	.9176	-3.9754	-.8418	2.2131	.4348
-3.2271	-.4290	4.0076	.6465	-3.9754	-.8418	4.1753	.7599	-1.7684	-.3958
1.7945	.2117	-2.2294	-.3261	2.2131	.4348	-1.7684	-.3958	1.9847	.2052

It is clear that no physical meaning can be attributed to this complex 'mass' matrix and that there is no resemblance between this matrix and the original (complete) physical mass matrix.

For comparison purposes with theoretical studies the (real) proportional normal modes are needed. Experimental evidence (see chapters 5 and 7) suggests, however, that, if properly measured and analysed, typical lightly-damped systems do not exhibit high levels of complexity. We shall examine therefore, the relationship between the proportional normal modes and the complex normal modes to find how big is the difference between them and how sensitive is this difference to changes in the system's parameters. A theoretical and numerical study of a simple two degree of freedom system will enable us to draw some general conclusions regarding a multi-degree of freedom system and a numerical study of such a system will demonstrate these more general results.

As a first step in this study it was found necessary to define two new useful parameters: the 'nonproportionality factor' and the 'generalized loss factor'.

3.1.1 NONPROPORTIONALITY FACTOR

It is straightforward to decide whether a system is proportionally-damped or not by examining the relationship between the system's matrices. However, once we realize that

the system is not proportionally-damped, a parameter which expresses how nonproportional the system is may be defined as follows:

According to the general condition set by Caughey (2-38), it is sufficient for the damping matrix [H] to be proportional to either the stiffness matrix [K] or the mass matrix [M] so that the system will possess (real) proportional mode shapes.

We will restrict, therefore, our check of the degree of the nonproportionality of the system to the relationship between the stiffness matrix [K] and the damping matrix [H].

Let us denote each element in [H] by h_{ij} and each element in [K] by k_{ij} and plot h_{ij} vs. k_{ij} (Fig. 3-4). A straight line, h_{sl}, is fitted through these points so that the sum of the squares of the deviations from this line is minimized.

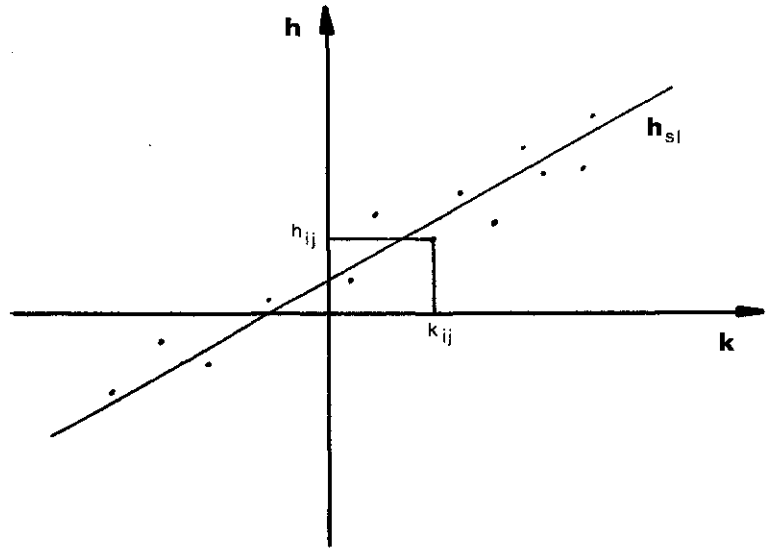

Fig.3-4: Stiffness elements vs. damping elements

The equation of this line is:

$$h_{sl}=a_0+a_1k \tag{3-6}$$

If the standard error of the fitted line is defined as:

$$S_{sl}^2=\frac{\sum_{i=1}^{n}\sum_{j=1}^{n}[h_{ij}-h_{sl}(k_{ij})]}{n^2} \tag{3-7}$$

and the standard deviation from the average $\bar{h}$ is

$$S_{\bar{h}}^2=\frac{\sum_{i=1}^{n}\sum_{j=1}^{n}(h_{ij}-\bar{h})^2}{n^2} \tag{3-8}$$

where

$$\bar{h}=\frac{\sum_{i=1}^{n}\sum_{j=1}^{n}h_{ij}}{n^2} \tag{3-9}$$

then the nonproportionality factor, J_n, is defined by,

$$J_n\equiv 1-\left(\frac{S_{sl}}{S_{\bar{h}}}\right)^2 \qquad (0\leqslant J_n\leqslant 1) \tag{3-10}$$

For a proportionally-damped system where

$$[H]=\alpha[K] \tag{3-11}$$

then

$$h_{ij}=\alpha k_{ij} \tag{3-12}$$

and

$$h_{sl}(k_{ij})=\alpha k_{ij} \tag{3-13}$$

therefore

$$S_{sl}^2=0 \qquad \text{and} \qquad J_n=1 \tag{3-14}$$

For a proprtionally-damped system, $J_n=1$, and as the nonproportionality of the system is increased (by changing one parameter in the damping matrix, for example)

J_n gets smaller and smaller.

For a given nonproportional system where

$$[H] \neq \alpha[K] \tag{3-15}$$

we may calculate a certain nonproportionality factor J_n. If the damping matrix [H] is changed to $[H_1]$ by multiplying it by a constant δ,

$$[H_1] = \delta[H] \tag{3-16}$$

then the standard error $\bar{s}_{s1}^2$ and the standard deviation $\bar{s}_{\bar{h}}$ are,

$$\bar{s}_{s1}^2 = \delta^2 s_{s1}^2 \tag{3-17}$$

$$\bar{s}_{\bar{h}}^2 = \delta^2 s_{\bar{h}}^2 \tag{3-18}$$

so that J_n maintains its previous value. We see that as long as the same form of nonproportionality is kept, J_n is independent of the actual values of damping or stiffness present in the system.

3.1.2 THE GENERALIZED LOSS FACTOR

Because the nonproportionality factor is independent of the amount of damping present in the system, an additional parameter, $\bar{\eta}$, which describes the overall magnitude of the damping is defined by

$$\bar{\eta} = \frac{\sum_{r=1}^{n} \omega_r^2 \, \eta_r}{\sum_{r=1}^{n} \omega_r^2} \tag{3-19}$$

and is referred to as the 'generalized loss factor' of the system.

It has been shown (par.2.2.1) that the diagonal matrix of the eigenvalues, $[\lambda_r^2]$, can be derived from the diagonal matrices of the modal masses and modal stiffnesses

$$[\lambda_r^2] = [\bar{M}]^{-1} [\bar{K}] \tag{3-20}$$

or using expressions (2-27) and (2-21)

$$[\lambda_r^2] = ([\Psi]^T [M] [\Psi])^{-1} ([\Psi]^T ([K]+i[H])[\Psi]) \tag{3-21}$$

or

$$[\lambda_r^2] = [\Psi]^{-1} [D] [\Psi] \tag{3-22}$$

where

$$[D] = [M]^{-1} ([K]+i[H]) \tag{3-23}$$

It can be shown that for any two matrices [A] and [B] the traces of the products [A][B] and [B][A] are equal, namely

$$\mathrm{tr}([A][B]) = \mathrm{tr}([B][A]) \tag{3-24}$$

Using property (3-24), we may write

$$\mathrm{tr}(([\Psi]^{-1} [D])[\Psi]) = \mathrm{tr}(([\Psi][\Psi]^{-1})[D]) = \mathrm{tr}([D]) \tag{3-25}$$

and because

$$\mathrm{tr}([D]) = \sum_{r=1}^{n} \lambda_r^2 \tag{3-26}$$

or

$$\mathrm{tr}([M]^{-1} ([K]+i[H])) = \sum_{r=1}^{n} (\omega_r^2 + i\omega_r^2 \eta_r) \tag{3-27}$$

from which then

$$\sum_{r=1}^{n} \omega_r^2 = \mathrm{tr}([M]^{-1}[K]) \tag{3-28}$$

$$\sum_{r=1}^{n} \eta_r \omega_r^2 = \mathrm{tr}([M]^{-1}[H]) \tag{3-29}$$

The generalized loss factor, $\bar{\eta}$, may be calculated, therefore, from

$$\bar{\eta} = \frac{\mathrm{tr}([M]^{-1}[H])}{\mathrm{tr}([M]^{-1}[K])} \tag{3-30}$$

3.2 COMPLEX NORMAL MODES OF A TWO-DEGREE-OF-FREEDOM-SYSTEM

Consider a general hysteretically-damped two-degree-of-freedom system (Fig. 3-5). Initially, the system is proportionally-damped thus having (real) proportional normal modes. In order to establish a relationship between the proportional normal modes and the (complex) normal modes, a nonproportional damping element, denoted by μ, is added to the left hand damper αk_1.

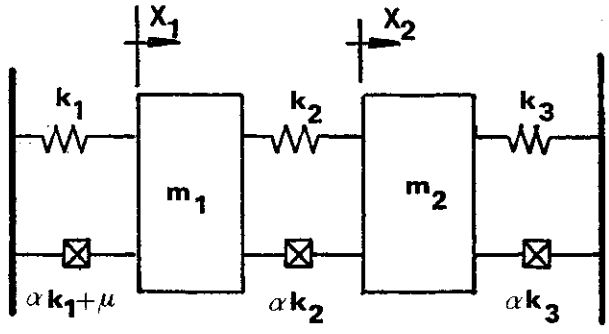

Fig. 3-5: General two-degree-of-freedom system

We may assume, without loss of generality, that

$$m_1=m_2=1 \tag{3-31}$$

and then the equation of motion for the system may be written as:

$$\begin{bmatrix}1 & 0\\ 0 & 1\end{bmatrix}\begin{Bmatrix}\ddot{x}_1\\ \ddot{x}_2\end{Bmatrix}+\left[\begin{bmatrix}k_1+k_2 & -k_2\\ -k_2 & k_2+k_3\end{bmatrix}+i\alpha\begin{bmatrix}k_1+k_2+\mu & -k_2\\ -k_2 & k_2+k_3\end{bmatrix}\right]\begin{Bmatrix}x_1\\ x_2\end{Bmatrix}=0 \tag{3-32}$$

or using a shorter notation

$$\begin{bmatrix} 1 & \emptyset \\ \emptyset & 1 \end{bmatrix} \begin{Bmatrix} \ddot{x}_1 \\ \ddot{x}_2 \end{Bmatrix} + \left[\begin{bmatrix} a & c \\ c & b \end{bmatrix} + i\alpha \begin{bmatrix} a+\mu & c \\ c & b \end{bmatrix} \right] \begin{Bmatrix} x_1 \\ x_2 \end{Bmatrix} = \emptyset \qquad (3\text{-}33)$$

The characteristic equation of the system is:

$$\begin{bmatrix} a(1+i\alpha)+i\alpha\mu-\lambda & c(1+i\alpha) \\ c(1+i\alpha) & b(1+i\alpha)-\lambda \end{bmatrix} = \emptyset \qquad (3\text{-}34)$$

If we denote

$$A=a+b \qquad (3\text{-}35)$$

$$D=ab-c^2 \qquad (3\text{-}36)$$

then the quadratic characteristic equation is

$$\lambda^2-B\lambda+C=\emptyset \qquad (3\text{-}37)$$

where

$$B=A(1+i\alpha)+i\alpha\mu \qquad (3\text{-}38)$$

$$C=D(1+i\alpha)^2+i\alpha\mu b(1+i\alpha) \qquad (3\text{-}39)$$

The eigenvalues, λ_r, are found by solving equation (3-37) i.e

$$\lambda_r=\frac{A(1+i\alpha)+i\alpha\mu \pm \sqrt{(A^2-4D)(1+i\alpha)^2+2i\alpha\mu(a-b)(1+i\alpha)-\alpha^2\mu^2}}{2} \qquad (3\text{-}40)$$

In order to derive the eigenvectors $\{x\}_r$, the following homogeneous set of linear equations is to be solved

$$\begin{bmatrix} a(1+i\alpha)+i\alpha\mu-\lambda_r & c(1+i\alpha) \\ c(1+i\alpha) & b(1+i\alpha)-\lambda_r \end{bmatrix} \begin{Bmatrix} x_1 \\ x_2 \end{Bmatrix} = \emptyset \qquad (3\text{-}41)$$

From this set it is possible to derive only the ratio of the elements in each eigenvector. We may assume, therefore, that

$$x_2=1 \tag{3-42}$$

and then

$$x_1=\frac{\lambda_r-b(1+i\alpha)}{c(1+i\alpha)} \tag{3-43}$$

or

$$x_1=\frac{\omega_r^2(1+i\eta_r)-b(1+i\alpha)}{c(1+i\alpha)} \tag{3-44}$$

The calculation of the complex number x_1 may be described by a vector diagram (Fig. 3-6) in which the angles are

$$\bar{\alpha}=tg^{-1}\alpha \quad ; \quad \bar{\eta}_r=tg^{-1}\eta_r \quad ; \quad \bar{\rho}_r=tg^{-1}\rho_r \tag{3-45}$$

and

$$s(1+i\rho_r)=\omega_r^2(1+i\eta_r)-b(1+i\alpha) \tag{3-46}$$

so that

$$x_1=\frac{s(1+i\rho_r)}{c(1+i\alpha)} \tag{3-47}$$

Examination of the vector diagram can give us some clues as to the 'complexity' of x_1 (the 'complexity' is measured by the angle $\bar{\rho}_r-\bar{\alpha}$; the larger $|\bar{\rho}_r-\bar{\alpha}|$, the more complex is the normal mode shape).

For a proportionally-damped system ($\mu=\emptyset$)

$$\eta_r=\alpha$$

and therefore

$$\rho_r=\alpha$$

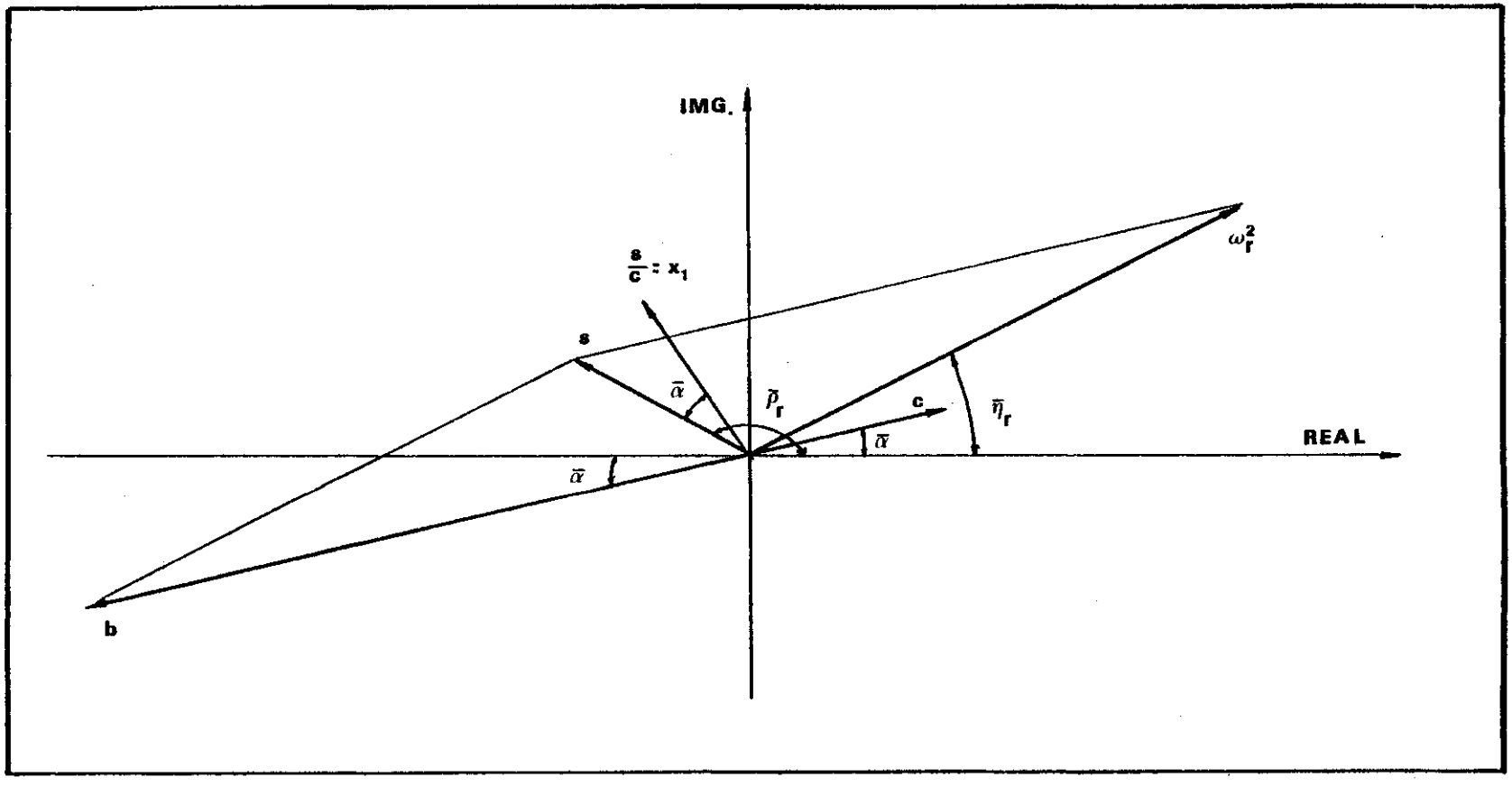

Fig. 3-6: Two degree of freedom system - vector diagram for calculation of the mode shape for close modes

and then the phase angle of x_1, $\bar{\rho}_r - \bar{\alpha}$, is zero and the mode shape is real. Once the system becomes nonproportional ($\mu > 0$), these simple relationships no longer apply and x_1 becomes complex.

When the two vectors b and ω_r^2 (whose resultant is s), are of the same order of magnitude i.e

$$|\omega_r^2 - b| \cong 0 \tag{3-48}$$

the phase angle of vector s, $\bar{\rho}_r$, is very sensitive to any small difference between $\bar{\alpha}$ and $\bar{\eta}_r$ and is

$$\bar{\rho}_r \cong \frac{\pi + (\bar{\alpha} - \bar{\eta}_r)}{2} \qquad (\bar{\alpha} \neq \bar{\eta}_r) \tag{3-49}$$

and the phase of x_1 is

$$\cong \frac{\pi - (\bar{\alpha} + \bar{\eta}_r)}{2} \qquad (\bar{\alpha} \neq \bar{\eta}_r) \tag{3-50}$$

From equation (3-40) we can derive the eigenvalues for the proportional system ($\mu = 0$) i.e

$$\lambda_r = \frac{a+b \pm \sqrt{(a-b)^2 + 4c^2}}{2}(1 + i\alpha) \tag{3-51}$$

It is clearly seen that for $a \cong b$ and $c \ll a$

$$\lambda_1 \cong a(1+i\alpha) \cong b(1+i\alpha) \tag{3-52}$$

The physical meaning of this is that the stiffness k_2 which couples the two masses is relatively small and each of them behaves, therefore, as a one-degree-of-freedom system with very close natural frequencies.

When this system is made nonproportional, the eigenvalues are

$$\lambda_1 \cong \lambda_2 \cong a(1+i\alpha) + \frac{i\alpha\mu}{2} \tag{3-53}$$

so that

$$\omega_1^2 \cong \omega_2^2 \cong a \cong b \tag{3-54}$$

From equation (3-46) it is clear that

$$\rho_r >> \alpha \tag{3-55}$$

from which we may conclude that the two elements in the eigenvector $\{x\}_r$ are of the same order of magnitude but with a relatively large phase difference (Fig. 3-6).

If the stiffness coupling element k_2 is increased we get a whole range of cases for which

$$|\omega_r^2 - b| \neq \emptyset \tag{3-56}$$

For these cases, $\bar{\rho}_r$ is less sensitive to the addition of nonproportional damping elements and as k_2 is increased the spectral distance between the natural frequencies is increased (Fig. 3-7) and

$$\bar{\alpha} - \bar{\rho}_r \rightarrow \emptyset \tag{3-57}$$

However, if the nonproportionality factor α is multiplied by a constant then it is clear from equation (3-53) that the loss factor is multiplied by the same value and the 'complexity' of the system is, therefore, approximately multiplied by the same constant. We may say, therefore, that the 'complexity' of the system is in direct proportion to the overall level of damping (indicated by the generalized loss factor). On the other hand, the real part of each eigenvalue, which describes the natural frequency, is hardly affected by changes in the damping of the system.

These results can be illustrated by numerical examples using a system with the following parameters:

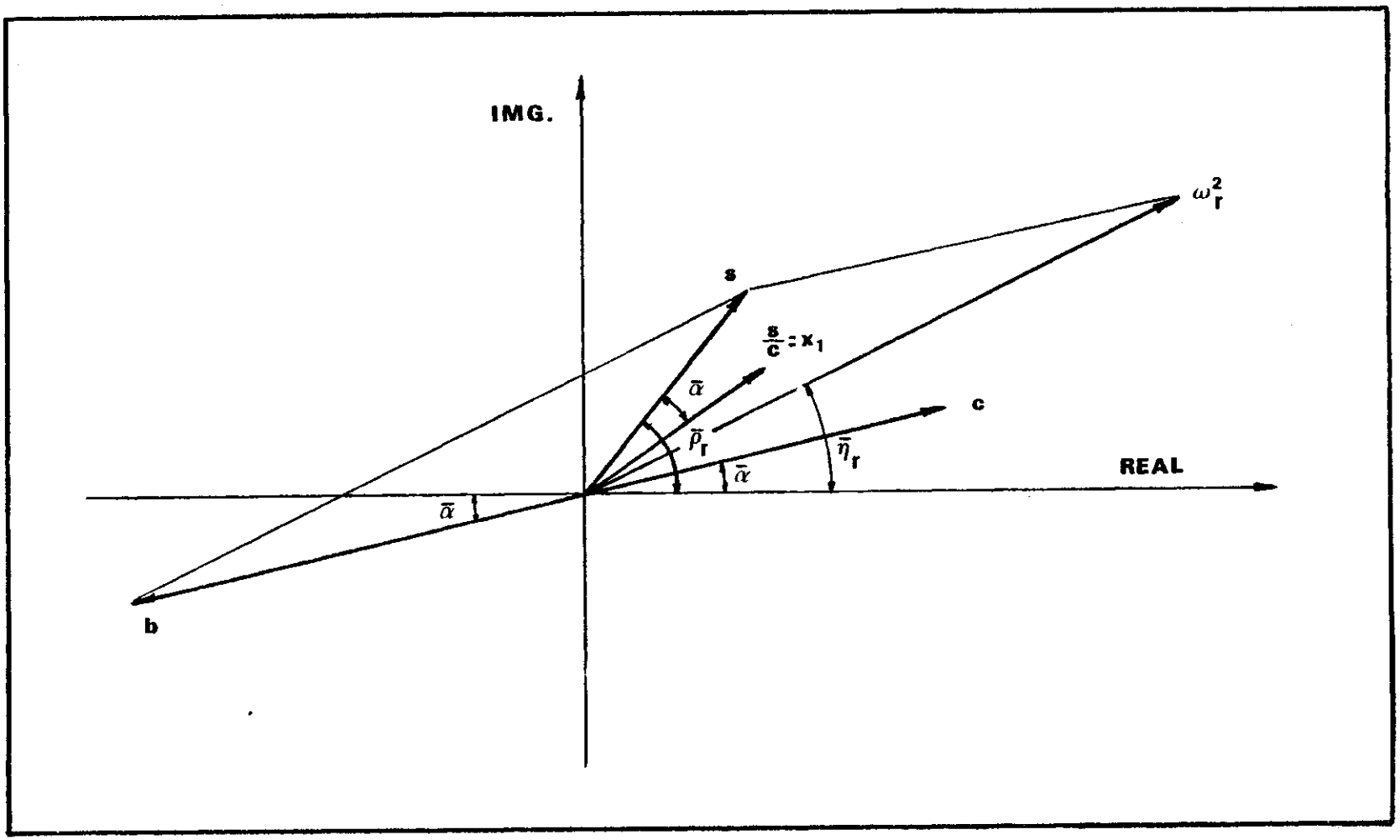

Fig.3-7: Two degree of freedom - vector diagram for calculation of the mode shape for separate modes

$k_1 = 3 \cdot 10^4$ N/m ; $k_2 = 10^3$ N/m ; $k_3 = 3.05 \cdot 10^4$ N/m ; $\alpha = .01$

This is a case where the coupling stiffness between the masses is relatively small and the natural frequencies of the two normal modes are, therefore, very close (small spectral distance).

The eigenproblem for this system was solved for different values of an added nonproportional damping element, μ, and the results are summarized in Table 3-1a.

Next, the coupling stiffness element was increased to

$$k_2 = 7 \cdot 10^3 \text{ N/m}$$

so that the spectral distance between the natural frequencies was increased. Table 3-1b summarizes the results of this eigenproblem as a function of μ/a ($a = k_1 + k_2$).

A graphical comparison of these two cases is given in Fig. 3-8 from which it is clear that:

(i) As the coupling stiffness is increased, the 'complexity' of the normal mode shapes becomes less sensitive to nonproportional damping.

(ii) The natural frequencies are insensitive to changes in the damping matrix but are sensitive to changes in the stiffness matrix.

(iii) The moduli of the normal mode shapes are changed as the system becomes more and more nonproportional but this change is relatively small for large values of nonproportionality.

(iv) The nonproportionality factor of a system is not by itself a sufficient indication as to the 'complexity' of the

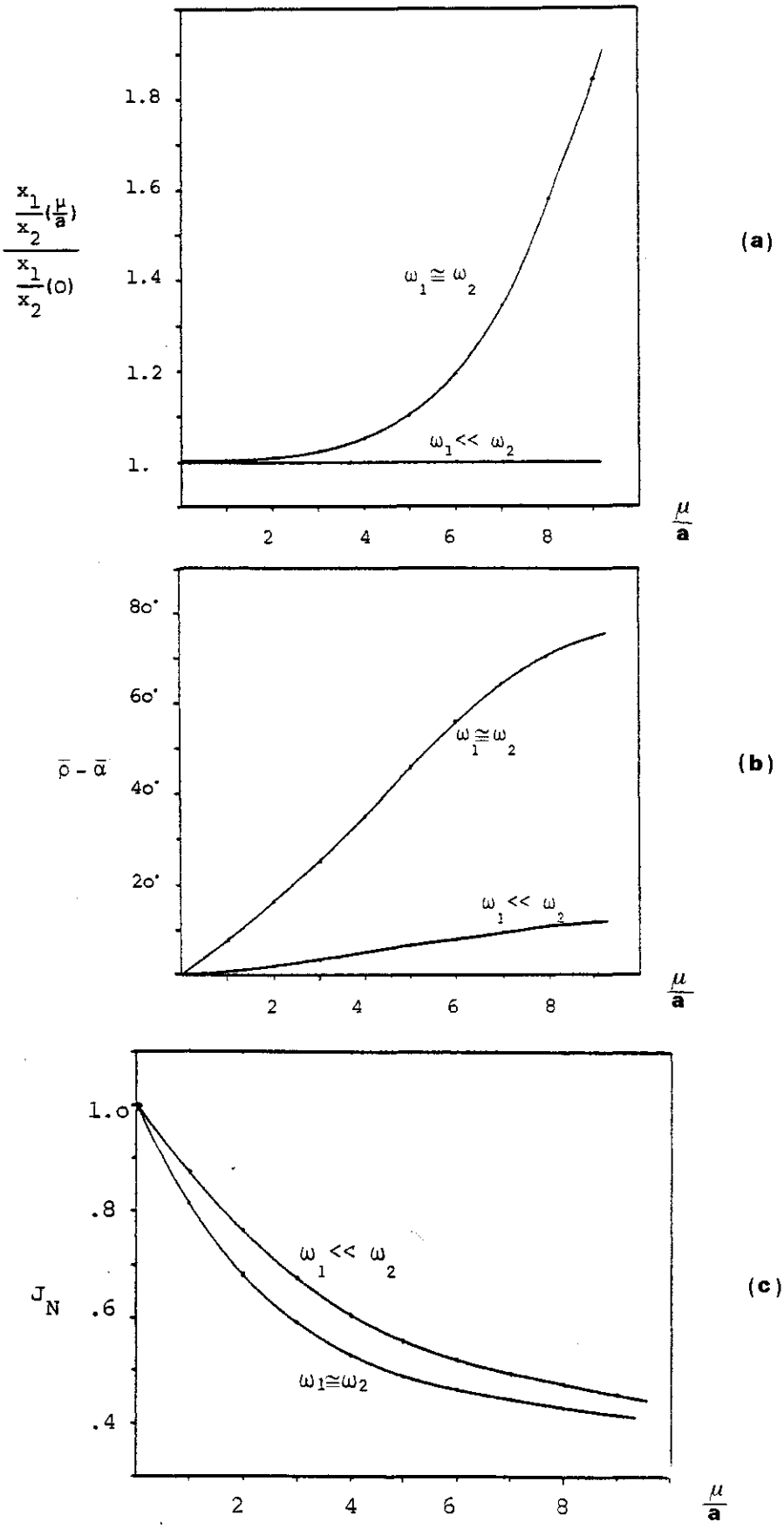

Fig. 3-8: Two degree of freedom system; close vs. separate modes as function of added nonproportional damping element. (a) relative change of moduli
(b) complexity of the modes
(c) nonproportionalty factor

mode shapes of that system as the spectral distance also has a big influence on the results.

These results relate to a simple system for which the addition of nonproportional damping was confined to one element. Nevertheless, the results obtained are general (for any two degrees of freedom system) and remain the same for any other form of nonproportionality (although the algebraic expressions involved become far more complicated).

In the following paragraphs they are extended to the general multi-degree of freedom system.

(b)

$\frac{\mu}{a}$	$\bar{\eta}$	J_n	ω_1 Hz	η_1	ω_2 Hz	η_2	$\bar{\rho} - \bar{\alpha}$ deg	$\frac{X_1}{X_2}$
0	.010	1.000	27.6790	.0100	33.4810	.0100	0.000	1.037
2	.018	.750	27.6820	.0203	33.4786	.0165	2.455	1.036
4	.0261	.596	27.6908	.0305	33.4713	.0231	4.914	1.036
6	.0342	.520	27.7055	.0407	33.4591	.0297	7.382	1.035
8	.0422	.477	27.7263	.0509	33.4419	.0362	9.864	1.035

(a)

$\frac{\mu}{a}$	$\bar{\eta}$	J_n	ω_1 Hz	η_1	ω_2 Hz	η_2	$\bar{\rho} - \bar{\alpha}$ deg	$\frac{X_1}{X_2}$
0	.010	1.0	27.6670	.010	28.5951	.01	0.0	1.280
2	.0196	.676	27.6861	.0244	28.5766	.0170	16.885	1.291
4	.0292	.533	27.7471	.0354	28.5174	.0233	35.094	1.342
6	.0388	.470	27.8566	.0510	28.4104	.0271	55.801	1.517
8	.0484	.436	27.9553	.0726	28.3133	.0248	71.981	2.031

Table 3-1: Two degree of freedom system - modal parameters for close modes (a) and for separate modes (b)

3.3 EIGENVALUES OF A NONPROPORTIONAL SYSTEM.

The complex eigenvalues of a damped system represent the natural frequency and the modal loss factor of each normal mode. It has been shown that for a proportionally-damped system the natural frequencies are equal to those of an undamped system and if $[H]=\alpha[K]$ then the modal loss factors are all identical and equal to α.

In this paragraph we shall investigate the effect of adding nonproportional damping elements to an otherwise proportionally-damped system on the derived eigenvalues (by comparison to those for the proportionally-damped system).

Definition of the problem:

Consider a proportionally-damped system described by:

$$[M]\{\ddot{x}\}+[K]\{x\}+i[H]\{x\}=\emptyset \qquad (3-58)$$

where

$$[H]=\alpha[K] \qquad (3-59)$$

the eigenvalues of which are

$$\bar{\lambda}_r^2=\varpi_r^2(1+i\alpha) \qquad (3-60)$$

Determine the eigenvalues of the modified system described by

$$[M]\{\ddot{x}\}+[K]\{x\}+i([H]+[\bar{H}])\{x\}=\emptyset \qquad (3-61)$$

where $[\bar{H}]$ is symmetric and at least semi-positive definite.

This problem was investigated extensively for the most general cases in connection with numerical algorithms used for the solution of eigenvalue problems [12].

These general studies were, however, restricted to small

perturbations, but because the matrices involved in our problem have some special features such as symmetry and at least semi-positive definiteness, it is possible to lift this restriction so that the magnitude of $[\bar{H}]$ is not limited. To this end, some general theorems are modified for our particular case and are given here without writing out the complete proofs, although they can found in references [14], [37] and [38].

Theorem 1:

If we denote the general complex eigenvalue of

$$[M]^{-1}([K]+i([H]+[\bar{H}])) \tag{3-62}$$

by

$$\lambda_r^2=u_r+iv_r \tag{3-63}$$

then the value of the real part, u_r, is bounded by the maximum and minimum values of the real positive eigenvalues of $[M]^{-1}[K]$ which are the natural frequencies of the undamped (or proportionally-damped) system. i.e

$$\emptyset<\varpi_1^2<u_r<\varpi_n^2 \tag{3-64}$$

The value of the imaginary part, v_r, is bounded by the non-negative eigenvalues of

$$[M]^{-1}([H]+[\bar{H}]) \tag{3-65}$$

If we denote the eigenvalues of (3-65) by ν_r then

$$0\leqslant\nu_{min}\leqslant v_r\leqslant\nu_{max} \tag{3-66}$$

The bounds of the complex eigenvalues can be illustrated by a plot in the complex plane (Fig. 3-9). The eigenvalues lie within the hatched area which is limited by the extreme natural frequencies of the undamped system, by

ν_{max} and ν_{min} and by part of the areas with radii $|\bar{\lambda}_n^2|$ and $|\bar{\lambda}_1^2|$. The two corners A and B of the hatched area represent the bounds of the modal loss factor, η_r,

$$\emptyset \leqslant tg(\bar{\rho}_o) \leqslant \eta_r \leqslant tg(\bar{\rho}_1) \qquad (3\text{-}67)$$

When the system is proportionally-damped ($[\bar{H}]=\emptyset$), the eigenvalues lie on the straight line AB which passes through the origin (Fig. 3-1Ø).

Theorem 2:

If the eigenvalues of $[M]^{-1}[H]$ are $\omega_r^2\alpha$ and the eigenvalues of $[M]^{-1}[\bar{H}]$ are $\bar{\nu}_r$, then the eigenvalues ν_r, of

$$[M]^{-1}([H]+[\bar{H}]) \qquad (3\text{-}68)$$

are the eigenvalues $\omega_r^2\alpha$ changed by an amount which lies between the smallest and greatest of the eigenvalues $\bar{\nu}_r$ i.e

$$\bar{\nu}_1 + \omega_s^2\alpha \leqslant \nu_s \leqslant \omega_s^2\alpha + \bar{\nu}_n \qquad (3\text{-}69)$$

Because [M] is symmetric and positive definite and $[\bar{H}]$ is symmetric and at least semi-positive definite, then

$$\bar{\nu}_r \geqslant \emptyset \qquad (3\text{-}7\emptyset)$$

and so

$$\nu_s \geqslant \omega_s^2\alpha \qquad (3\text{-}71)$$

Figure 3-11 shows bounds for the complex eigenvalues in relation to the proportional case (where they lie on the straight line AB). The extreme points A and C of the hatched area represent the bounds of the modal loss factor. i.e

$$tg^{-1}\alpha \leqslant \eta_r \leqslant tg\,\bar{\rho}_1 \qquad (3\text{-}72)$$

Any nonproportional system can be treated as a proportional one with an added nonproportional damping matrix $[\bar{H}]$

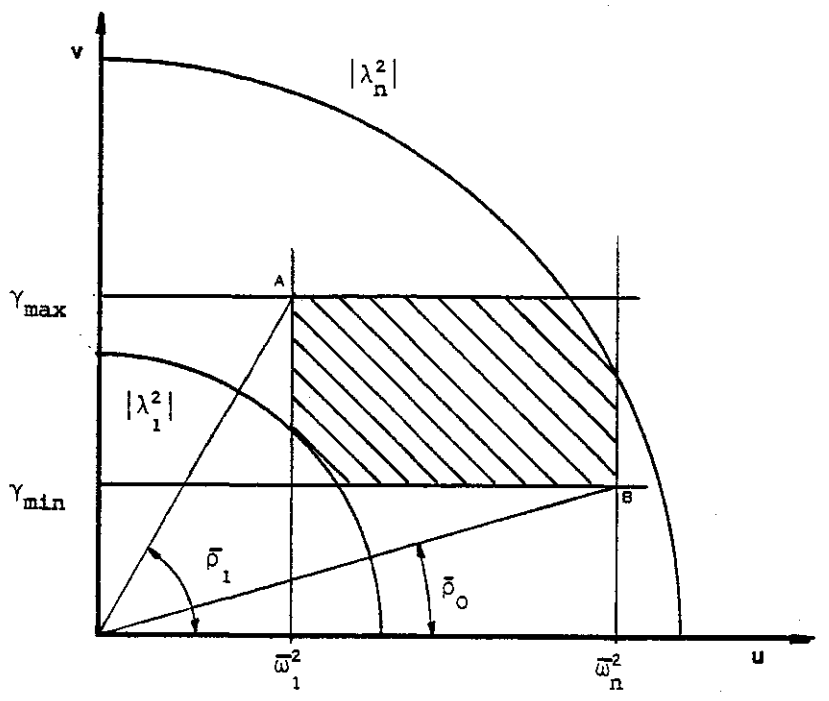

Fig. 3-9: Bounds of complex eigenvalues

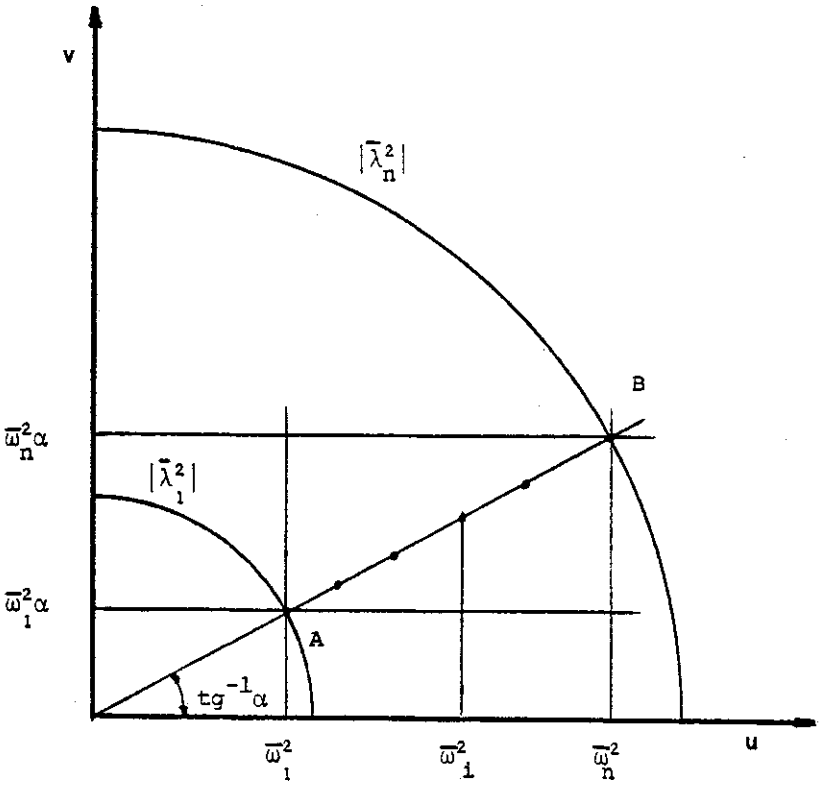

Fig. 3-10: Eigenvalues bounds for a proportionally-damped system

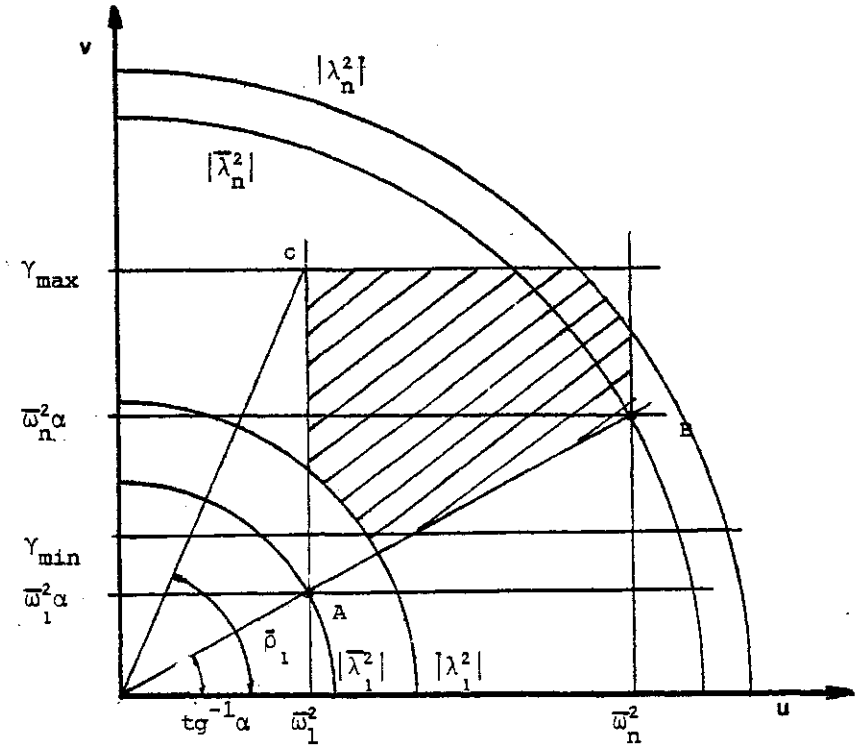

Fig. 3-11: Eigenvalues bounds for a nonproportionally damped system

which is at least semi-positive definite.

We may say, therefore, that the lowest bound of the loss factors is:

$$\eta_{min} = \left(\frac{h_{ij}}{k_{ij}}\right)_{min} \qquad (k_{ij} \neq 0) \qquad (3\text{-}73)$$

and the upper bound

$$\eta_{max} = \left(\frac{h_{ij}}{k_{ij}}\right)_{max} \qquad (k_{ij} \neq 0) \qquad (3\text{-}74)$$

where k_{ij} and h_{ij} are elements in the respective matrices [K] and [H].

The bounds of the imaginary parts of the eigenvalues change as morenonproportional damping is introduced into the

system. The bounds of the real parts, which represent the natural frequencies, are - according to theorem 1 - limited by the extreme natural frequencies of the undamped system and remain unchanged because [M] and [K] are unchanged. Nevertheless, the actual values of the natural frequencies within this range are changed slightly although it has been shown in the case of the two-degree-of-freedom system, this change is negligible in comparison with the change of the imaginary part of the eigenvalue.

3.4 COMPLEX EIGENVECTORS OF A MULTI-DEGREE OF FREEDOM SYSTEM

The relationship between the system matrices and the eigenvalues and eigenvectors of a multi-degree of freedom system are very complicated. We know that once the system is nonproportionally-damped, the eigenvectors become complex and that the level of complexity is dependent upon the particular numerical values of the elements in the system matrices and their relative magnitudes.

The main factor - the nonproportionality of the damping - cannot be defined in an explicit manner and it is, therefore, impossible to deduce a general theoretical relationship between the complexity of the normal mode shapes and the system matrices. However, we may generalize the theoretical results obtained for the two degrees of freedom system, combine them with the theoretical results derived for the bounds of the eigenvalues of a multi-degree of freedom system and draw some general conclusions regarding the complexity of the normal modes of a nonproportional multi-degree of freedom system.

Although it is not possible to support these conclusions with a rigorous theoretical proof, they can be demonstrated by numerical studies and supported by experimental results.

A numerical study was carried out on a six degree of freedom system (Fig. 3-12) and three different configurations were examined.

(i) The initial parameters of the proportional system were:

$$m_i = 1\,Kg \quad ; \quad k_1 = 4 \cdot 10^4\,N/m \quad : \quad h_1 = 400\,N/m$$
$$k_2 = 2 \cdot 10^4\,N/m \quad ; \quad h_2 = 200\,N/m$$
$$k_3 = 5 \cdot 10^3\,N/m \quad ; \quad h_3 = 50\,N/m$$
$$k_4 = 1 \cdot 10^3\,N/m \quad ; \quad h_4 = 10\,N/m$$
$$k_5 = 4.9 \cdot 10^3\,N/m \quad ; \quad h_3 = 49\,N/m$$
$$k_6 = 2.1 \cdot 10^4\,N/m \quad ; \quad h_6 = 210\,N/m$$
$$k_7 = 4.05 \cdot 10^4\,N/m \quad ; \quad h_7 = 405\,N/m$$

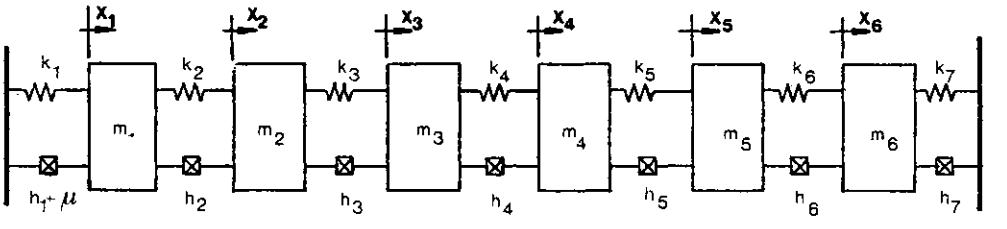

Fig.3-12: Six degree of freedom damped system

This system was tuned by low stiffness coupling between the masses m_3 and m_4 and by a slight asymmetry of the other stiffness elements so that it possessed close natural frequencies. It was expected, therefore, that the addition of small nonproportional damping elements anywhere in the system should produce very complex normal modes.

The eigenvalues and eigenvectors were computed for the proportional case and next, the value of of the damper h_1

was increased by adding to it more damping μ. The eigen-problem was then solved for various values of μ/h_1 and the results for the first four modes are summarized in Table 3-2.

The natural frequencies of the first and second modes are well-separated but those of the third and forth modes are very close. It is clear that as the system is made increasingly nonproportional, the two close mode shapes become more and more complex, whereas the complexity of the first two mode shapes is, and remains, very small.

Examination of the moduli of the mode shapes reveals a correlation between the complexity of the mode shape and the magnitude of the change in the moduli compared with the proportional case. The moduli of the first two mode shapes hardly change but the moduli of some elements in the two close modes change by a factor of almost two times. The natural frequencies of all these modes are hardly affected at all.

(ii) Next, the stiffness coupling between m_3 and m_4 was increased in order to separate the close modes. The stiffness k_4 and damping h_4 were increased by a factor of ten to

$$k_4=10^4 N/m \quad : \quad h_4=100N/m$$

The value of the damper h_1 was varied in the same manner as for the previous case with the results as summarized in Table 3-3.

We see that now the natural frequencies of all modes are

J_N	$\frac{\mu}{h_1}$	mode 1		mode 2		mode 3		mode 4	
1.00	0	ω =9.139		=11.303		=21.125		=21.295	
		η =.0100		=.0100		=.0100		=.0100	
		.0804	.000	.0932	180.000	.3421	.000	.2039	180.000
		.2280	.000	.2560	180.000	.7250	.000	.4291	180.000
		.6679	.000	.6491	180.000	.2982	180.000	.2063	.000
		.6650	.000	.6593	.000	.1604	180.000	.3104	180.000
		.2169	.000	.2477	.000	.4443	-.000	.7181	.000
		.0783	.000	.0921	.000	.2126	-.000	.3459	.000
.839	2	=9.139		=11.303		=21.133		=21.289	
		=.0196		=.0114		=.0154		=.0117	
		.0804	-1.308	.0931	-.996	.3593	-6.717	.2053	-160.777
		.2279	-.505	.2560	-.169	.7613	-5.765	.4323	-159.731
		.6679	-.138	.6492	.274	.3150	172.540	.2067	16.862
		.6651	.192	.6593	179.805	.1630	-157.054	.3245	174.778
		.2169	.214	.2476	179.840	.4466	19.177	.7552	-6.269
		.0783	.219	.0921	179.847	.2138	19.302	.3637	-6.228
.690	4	=9.140		=11.304		=21.152		=21.272	
		=.0131		=.0127		=.0217		=.0126	
		.0803	-2.613	.0931	178.009	.4038	-7.851	.1913	-136.096
		.2278	-1.008	.2559	179.662	.8555	-5.967	.4034	-133.986
		.6678	-.276	.6494	-179.453	.3597	171.219	.1905	38.646
		.6653	.383	.6591	-.389	.1558	-128.366	.3603	174.749
		.2170	.428	.2476	-.320	.4143	43.693	.8520	-6.833
		.0783	.438	.0921	-.305	.1985	43.963	.4100	-6.772
.602	6	=9.141		=11.304		=21.169		=21.260	
		=.0147		=.0141		=.0292		=.0122	
		.0802	-3.917	.0930	177.015	.4155	-4.532	.1420	-115.932
		.2276	-1.510	.2559	179.493	.8805	-1.747	.2999	-112.730
		.6677	-.414	.6498	-179.183	.3743	175.060	.1409	55.248
		.6656	.573	.6589	-.582	.1193	-103.799	.3672	178.591
		.2171	.639	.2475	-.479	.3063	63.530	.8794	-2.780
		.0783	.655	.0921	-.457	.1469	63.975	.4230	-2.727
.547	8	=9.142		=11.305		=21.180		=21.255	
		=.0162		=.0155		=.0368		=.0117	
		.0800	-5.217	.0929	176.022	.4100	-3.636	.1048	-107.056
		.2274	-2.009	.2559	179.323	.8694	.048	.2217	-102.761
		.6675	-.551	.6504	-178.915	.3707	176.528	.1047	60.581
		.6660	.761	.6586	-.775	.0908	-90.708	.3609	179.945
		.2172	.849	.2474	-.637	.2255	72.070	.8689	-1.132
		.0784	.869	.0920	-.609	.1081	72.692	.4179	-1.091

Table 3-2: Modes shapes (modulus and phase in degrees) for case (i) (close modes)

J_N	$\frac{\mu}{h_1}$	mode 1		mode 2		mode 3		mode 4	
1.00	0	ω =9.139		=18.935		=21.137		=26.028	
		η =.0100		=.0100		=.0100		=.0100	
		.0803	.000	.2688	.000	.2750	.000	.1427	.000
		.2276	.000	.6162	.000	.5824	.000	.2372	.000
		.6666	.000	.6613	.000	.2423	180.000	.6535	180.000
		.6663	.000	.2860	180.000	.2273	180.000	.6489	.000
		.2173	.000	.5767	180.000	.6215	.000	.2349	180.000
		.0784	.000	.2558	180.000	.2976	.000	.1420	180.000
.838	2	=9.139		=18.937		=21.137		=26.028	
		=.0116		=.0141		=.0134		=.0106	
		.0802	-1.160	.2687	-1.730	.2751	.134	.1427	-.236
		.2275	-.358	.6162	-.803	.5829	1.134	.2373	1.114
		.6666	.009	.2616	1.450	.2423	178.260	.6535	-179.997
		.6664	.042	.2860	179.326	.2275	-178.428	.6489	-.106
		.2173	.064	.5771	-179.044	.6214	-.804	.2349	179.800
		.0784	.069	.2560	-178.974	.2975	-.725	.1419	179.827
.686	4	=9.140		=18.940		=21.137		=26.028	
		=.0131		=.0181		=.0169		=.0112	
		.0802	-2.320	.2687	-3.463	.2755	.264	.1427	-.472
		.2274	-.714	.6163	-1.609	.5841	2.263	.2376	2.225
		.6666	.018	.2624	2.889	.2426	176.518	.6535	-179.994
		.6664	.084	.2860	178.650	.2281	-176.863	.6488	-.212
		.2173	.128	.5780	-178.091	.6213	-1.610	.2349	179.600
		.0784	.138	.2564	-177.951	.2975	-1.452	.1419	179.653
.594	6	=9.141		=18.946		=21.136		=26.028	
		=.0147		=.0222		=.0203		=.0118	
		.0801	-3.477	.2686	-5.203	.2762	.388	.1427	-.708
		.2273	-1.070	.6165	-2.422	.5861	3.383	.2380	3.333
		.6667	.026	.2637	4.308	.2430	174.770	.6535	-179.991
		.6665	.125	.2860	177.969	.2290	-175.309	.6488	-.319
		.2174	.191	.5795	-177.143	.6213	-2.422	.2349	179.399
		.0784	.206	.2572	-176.935	.2975	-2.184	.1419	179.480
.537	8	=9.142		=18.954		=21.136		=26.029	
		=.0162		=.0261		=.0238		=.0124	
		.0799	-4.631	.2685	-6.953	.2771	.502	.1427	-.945
		.2271	-1.423	.6168	-3.245	.5888	4.492	.2386	4.435
		.6667	.035	.2656	5.698	.2436	173.016	.6536	-179.988
		.6665	.166	.2861	177.282	.2303	-173.771	.6488	-.425
		.2174	.254	.5817	-176.204	.6212	-3.242	.2349	179.199
		.0784	.274	.2582	-175.927	.2974	-2.924	.1419	179.306

Table 3-3: Mode shapes (modulud and phase in degrees) for case (ii) (separate modes)

well-separated, and an increase in the nonproportionality of the damping has a very small effect, not only on the natural frequencies, but also on the complexity of the mode shapes.

(iii) The aim of the third study was to assess the influence of the overall level of damping on the complexity of the modes of a nonproportional system. To this end, a proportional system with well-separated modes was chosen, with the following parameters;

m_i=1Kg ; k_i=10^4N/m ; h_i=100N/m (i=1,6)

The natural frequencies and normal mode shapes for the proportional case are:

62.0576		57.3832		49.7732		39.6958		14.1664		27.6233	
.2578	.000	.4565	180.000	.5507	180.000	.5187	.000	.1327	.000	.3678	.000
.4565	180.000	.5187	.000	.1327	.000	.3678	.000	.2578	.000	.5507	.000
.5507	.000	.1327	180.000	.5187	.000	.2578	180.000	.3678	.000	.4565	.000
.5187	180.000	.3678	180.000	.2578	180.000	.5507	180.000	.4565	.000	.1327	.000
.3678	.000	.5507	.000	.4565	180.000	.1327	180.000	.5187	.000	.2578	180.000
.1327	180.000	.2578	180.000	.3678	.000	.4565	.000	.5507	.000	.5187	180.000

Next, the damping distributiuon in the system was changed by increasing gradually the damper h_6 and reducing the magnitudes of other dampers without changing the overall level of damping (the generalized loss factor was kept constant while the nonproportionality of the system was increased).

In this way, the damping was changed from the proportional case of uniform distribution to the maximum nonproportional case whereby all the damping was concentrated at one point (h_6). This process was repeated

for four different constant levels of generalized loss factor ($\bar{\eta}$=.Ø1 ÷ .Ø8).

To demonstrate the results of this process, we choose one typical normal mode (mode 4) and one element in this mode (No. 3). The changes, relative to the proportional normal mode, in the natural frequency, modulus and phase of $({}_4\Phi_3)$ as a function of the nonproportionality factor, J_n, and the generalized loss factor, $\bar{\eta}$, are plotted in Figures 3-13 ÷ 3-15.

The first indication from these plots is that the pattern of the change in each plot for different levels of generalized loss factor is very similar and we may conclude that for a given nonproportionality the level of complexity, the change in the modulus of the mode shape and the change of the natural frequency are in direct proportion to the level of damping present in the system. The higher is the value of the generalized loss factor, the bigger is the change in each of these parameters.

As the nonproportionality of the system is increased the mode shape becomes more and more complex and we see that the change of the modulus is in direct proportion to the complexity of the mode; the larger is the phase deviation of the mode from the proportional one, the larger is the change in the modulus relative to the modulus of the proportional mode. The same conclusions apply for the natural frequency, although the actual numerical change here is a very small percentage and for levels of $\bar{\eta}$ smaller then .Ø4 it is negligible.

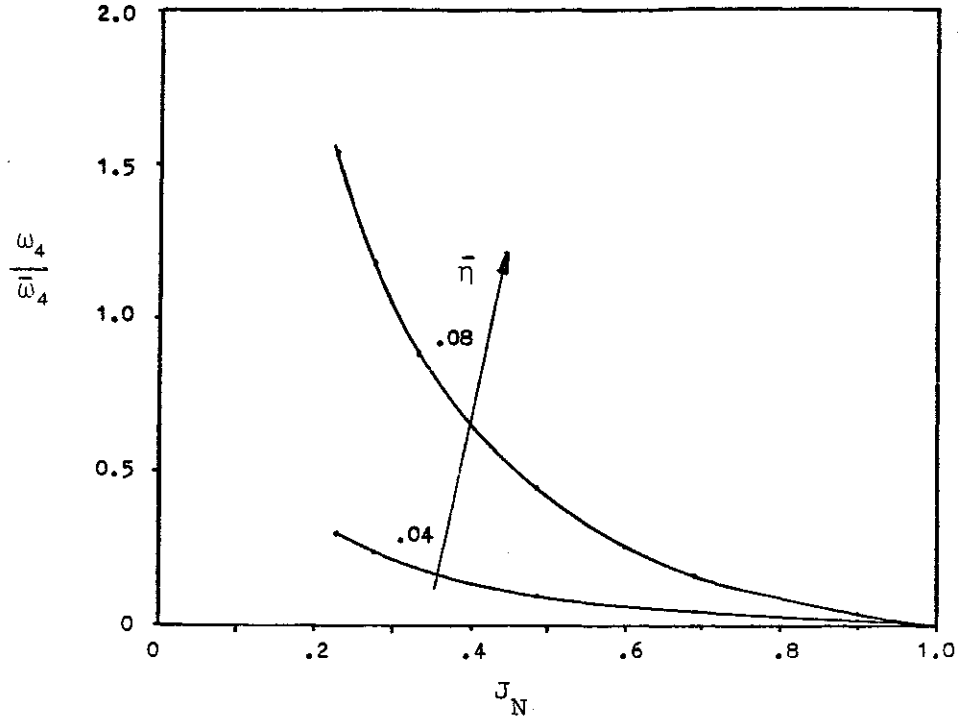

Fig. 3-13: Relative change of natural frequency of mode 4

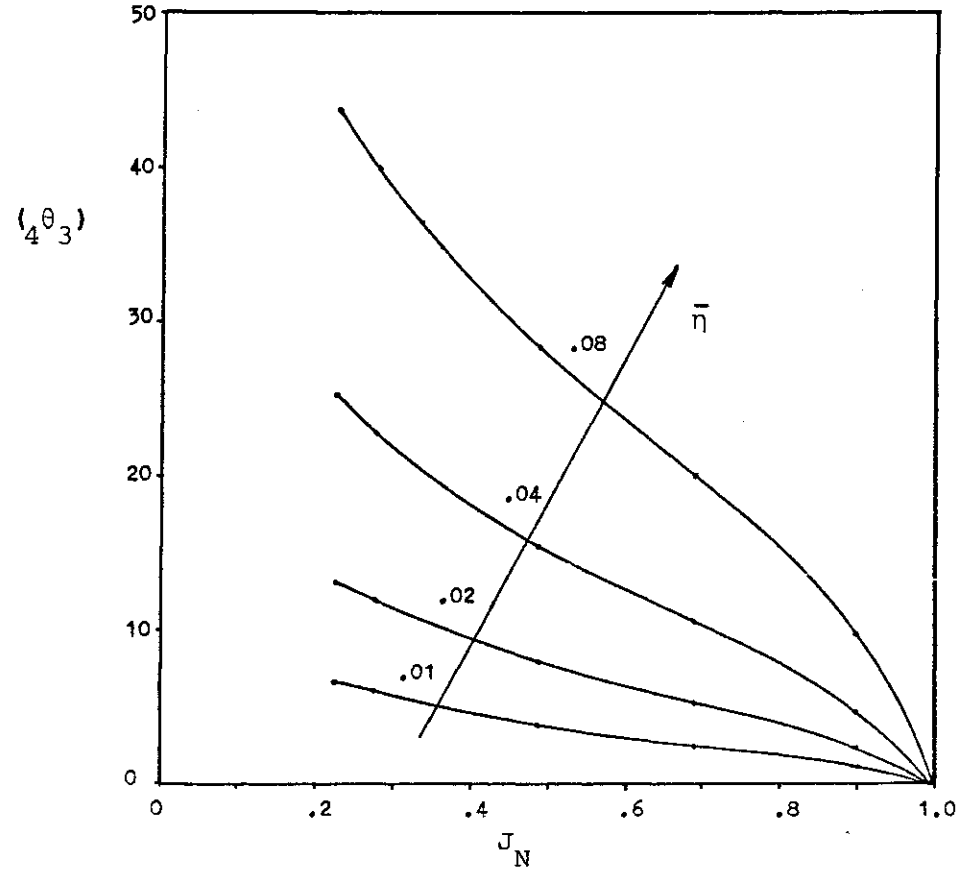

Fig. 3-14: Phase of $({}_4\Phi_3)$ as function of J_n and $\bar{\eta}$

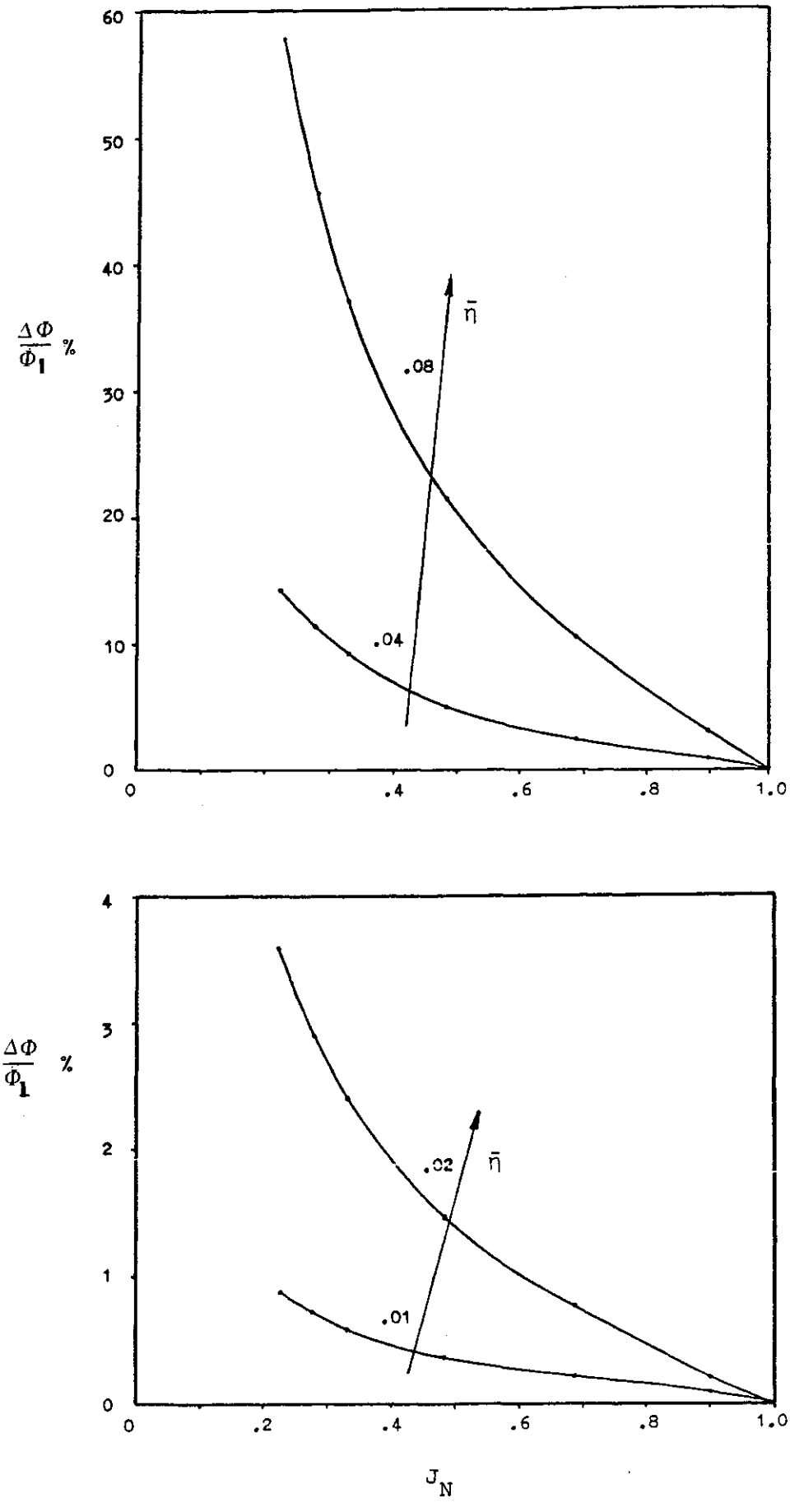

Fig. 3-15: Relative change of the modulus of $({}_4\Phi_3)$ as function of J_n and . (Φ_1 is the modulus of the proportional system and $\Delta\Phi = |\Phi - \Phi_1|$)

3.5 CONCLUSIONS.

It is appropriate here to draw some general conclusions regarding the (complex) normal modes of a nonproportionally damped system.

(i) Once a proportionally-damped system is changed into a nonproportionally-damped one, the real normal mode shapes change into complex normal mode shapes. The complexity of these modes depends on the level of the nonproportionality of the damping; the larger is the value of the nonproportionality factor, the more complex the mode shapes become. However, the complexity is also very sensitive to the closeness of the natural frequencies of neighbouring modes; the closer they are, the more complex the mode shapes are for the same level of nonproportionality.

(ii) The more complex the normal mode shape becomes, the bigger is the change in its modulus relative to the corresponding modulus derived for the proportionally damped system.

(iii) The natural frequencies are relatively insensitive to changes in the damping, but they are very sensitive to changes in the stiffness of the system.

(iv) The sensitivity of the normal mode shapes to changes in the damping is increased as the generalized loss factor of the system is increased.

The practical meaning of these conclusions is that for lightly-damped systems with well-separated natural

frequencies the moduli of the experimentally derived mode shapes can be regarded as a very good approximation to the undamped mode shapes of the system. However, in any situation where two modes are very close, they are more prone to be complex and, therefore, less confidence can be put in this approximation. In any case, practically it is usually more difficult to identify the modal parameters of close modes [39] and the identified normal mode shapes are expected to be less accurate than those for the well-separated modes.

As a rule of thumb, we may say that for values of modal loss factors which are smaller then .Ø3 and mode shape phase angles smaller then 3Ø°, the moduli of experimentally-determined complex normal mode shapes can be used as the undamped mode shapes in any further calculation.

The experimentally-derived natural frequencies can be used in any case, regardless of the level of damping or complexity of the mode shapes, as a very close approximation to the undamped natural frequencies of the system.

For a given system, addition to or change in the distribution of damping has no significant influence on the natural frequencies. However, addition or concentration of damping in a few points in the system reduces the level of response and makes the mode shapes more complex. On the other hand, reduction in the level of damping reduces the level of complexity and the response gets closer to the response of a proportionally-damped system.

4. MODAL IDENTIFICATION METHODS

4.1 INTRODUCTION

In a recent survey of modal vibration test and analysis techniques [41] conducted in the U.S.A, it was found that the single-point sine and the multi-point sine techniques are the most widely used (out of 16 different techniques) and that they provide the most accurate data and the largest number of valid modes

These two methods are well-established and have been used by investigators for quite a long time now. Of these two, the single-point sine is the simplest from the experimental point of view: the test piece is excited at a single point by a sine input force and the response is measured at various points on it. From these data the modal parameters may be derived using either the well known Kennedy and Pancu method [42] or a straight-forward curve fitting algorithm.

The multi-point sine method is theoretically very simple: by exciting the structure at several points with properly tuned force inputs, it can be made to vibrate in a mode which is identical to any one of its proportional normal modes. Experimentally, however, this method is more complicated because in order to find the correct force distribution a very sophisticated experimental procedure is needed.

There are thus two marked differences between the two

methods:

(i) The single-point excitation method requires relatively simple experimental equipment but needs a comprehensive analysis facility in order to derive satisfactory results. On the other hand, the multi-point excitation method requires complicated hardware but once the structure is forced to vibrate in a proportional forced mode, its mode shape and natural frequency are readily available with little further analysis.

(ii) The modal parameters derived by each of these two methods are not the same. For the generally-damped system, the single-point method derives the properties of the normal modes and the multi-point method the properties the system would possess if the damping were removed (undamped system). Only for the particular case where the system is proportionally damped do both methods derive the same modal parameters.

Each of these methods has its advantages and drawbacks and the decision as to which of them to use is dependent on the particular circumstances. However, probably the best choice (where money is no object) is to use both of them, like the MODLAB system [43].

For the experimental stages of this research, both techniques have been used;

(i) The single-point method using an automated mobility measuring routine MOB3 [44] and the two analysis programs POLAR5 [45] (which derives the modal parametrs from analysis

of the Nyquist plots) and SIM2 [46] (which derives them by simple curve fitting).

(ii) The multi-point excitation method using the MAMA system which was loaned to the Dynamics Section by the Royal Aircraft Establishment, Farnborough.

In this chapter these methods are described in some detail and a numerical study demonstrates the differences between the two identification methods used to analyse the data acquired by the single-point excitation method.

4.2 DERIVATION OF MODAL PARAMETERS FROM POLAR PLOTS

The identification of the system's modal parameters using a stepped-sine single excitation is based on equation (2-63), namely

$$\alpha_{jk}=\sum_{r=1}^{n}\frac{{}_{r}A_{jk}}{\omega_r^2(1-\beta_r^2+i\eta_r)}=\sum_{r=1}^{n}\frac{{}_{r}A_{jk}}{\omega_r^2}\delta_r \qquad (4-1)$$

where

$$\beta_r=\frac{\omega}{\omega_r} \qquad (4-2)$$

First, consider one element, δ_s, in the above summation

$$\delta_s=\frac{1}{1-\beta_s+i\eta_s}=\frac{(1-\beta_s^2)-i\eta_s}{(1-\beta_s^2)^2+\eta_s^2} \qquad (4-3)$$

It can be shown that

$$(\mathrm{Re}(\delta_s))^2+(\mathrm{Img}(\delta_s)+\frac{1}{2\eta_s})^2=(\frac{1}{2\eta_s})^2 \qquad (4-4)$$

When plotted in the complex plane this is the equation of a circle whose center is displaced downwards on the imaginary axis by a distance of $\frac{1}{2\eta_s}$ and whose diameter D_s is: (Fig. 4-1a)

$$D_s=\frac{1}{\eta_s} \qquad (4-5)$$

At the point where the circle intersects the imaginary axis $\beta_s=1$. Multiplying δ_s by the complex number $\frac{{}_{s}A_{jk}}{\omega_s^2}$ causes the circle to scale its diameter by $\frac{|{}_{s}A_{jk}|}{\omega_s^2}$ and to rotate about the origin by an angle of θ_s equal to the phase of ${}_{s}A_{jk}$; θ_s is referred to as 'the modal phase angle' (Fig. 4-1b)

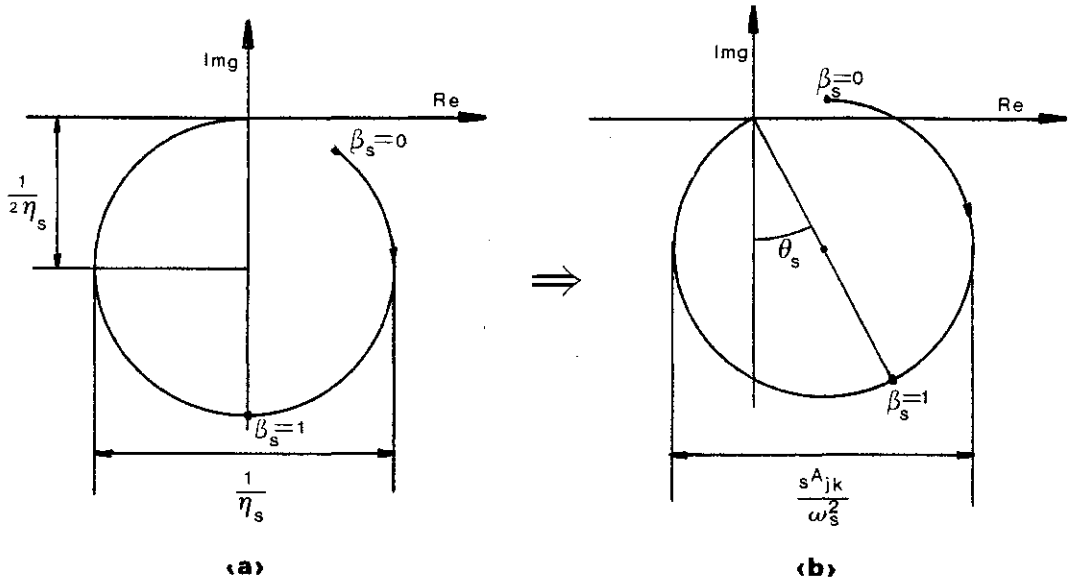

Fig.4-1: One degree of freedom - construction of the modal circle

4.2.1 NATURAL FREQUENCY

The phase angle, φ_s of δ_s is

$$\varphi_s = tg^{-1}\left(\frac{\eta_s}{1-\beta_s^2}\right) \tag{4-6}$$

Consider now the rate of change of φ_s as function of β_s^2,

$$\frac{d\varphi_s}{d\beta_s^2} = \frac{\eta_s}{(1-\beta_s^2)^2+\eta_s^2} \tag{4-7}$$

This quantity reaches a maximum (as a function of β_s) when

$$\frac{d}{d\beta_s}\left(\frac{d\varphi_s}{d\beta_s^2}\right) = \emptyset \tag{4-8}$$

i.e when

$$\frac{d}{d\beta_s}\left(\frac{d\varphi_s}{d\beta_s^2}\right)=\frac{4\eta_s\beta_s(\beta_s^2-1)}{((1-\beta_s^2)^2+\eta_s^2)^2}=\emptyset \qquad (4-9)$$

This occurs when

$$\beta_s=1 \qquad \text{or when} \qquad \omega=\omega_s \qquad (4-10)$$

Inserting into (4-7) we get:

$$\left(\frac{d\varphi_s}{d\beta_s^2}\right)_{\beta_s=1}=\frac{1}{\eta_s} \qquad \text{or} \qquad \left(\frac{d\varphi_s}{d\omega^2}\right)_{\omega=\omega_s}=\frac{1}{\omega_s^2\eta_s} \qquad (4-11)$$

The meaning of this result is that at the point where the rate of change of φ_s, as function of ω^2, reaches a maximum, as function of $\underline{\omega}$, the frequency is equal to the natural frequency, ω_s, of this mode.

Consider now the rate of change of φ_s as a function of β_s

$$\frac{d\varphi_s}{d\beta_s}=\frac{2\beta_s\eta_s}{(1-\beta_s^2)^2+\eta_s^2} \qquad (4-12)$$

The maximum rate of change of this quantity as a function of β_s occurs when

$$\frac{d}{d\beta_s}\left(\frac{d\varphi_s}{d\beta_s}\right)=\emptyset \qquad (4-13)$$

i.e when

$$\frac{d}{d\beta_S}\left(\frac{d\varphi_S}{d\beta_S}\right)=\frac{3\beta_S^4-2\beta_S^2-(1+\eta_S^2)}{((1-\beta_S^2)^2+\eta_S^2)^2}=0 \qquad (4\text{-}14)$$

By solving the quadratic equation in β_S^2 we get

$$\beta_S=\left[\frac{1+\sqrt{4+3\eta_S^2}}{3}\right]^{\frac{1}{2}} \qquad (4\text{-}15)$$

(only positive values of β_S are considered)

For values of η_S which are smaller than .1; the values of β_S at which the rate of change of φ_S is maximum, are

$$\beta_S<1.0012 \qquad (4\text{-}16)$$

We may write, therefore

$$\left(\frac{d\varphi_S}{d\beta_S}\right)_{\beta_S=1}\cong\frac{2}{\eta_s} \quad \text{or} \quad \left(\frac{d\varphi_S}{d\omega}\right)_{\omega=\omega_S}\cong\frac{2}{\eta_S\omega_S} \qquad (4\text{-}17)$$

The error incurred by this approximation is .06% for η_S=.1 and gets smaller as η_S gets smaller.

The practical meaning of this result is that the maximum rate, as a function of frequency ω, at which the locus sweeps around the periphery of the circle is obtained when $\omega\cong\omega_S$.

4.2.2 LOSS FACTOR

The modal loss factor, η_S, can be calculated from equation (4-17)

$$\eta_S = \frac{2}{\omega_S \left(\frac{d\varphi_S}{d\omega}\right)_{\omega=\omega_S}} \qquad (4\text{-}18)$$

or by the more general expression derived from the circle geometry (Fig. 4-2).[24]

$$\operatorname{tg}\tfrac{1}{2}\varphi_1 = \frac{\eta_S}{1-\omega_1^2}$$

$$\operatorname{tg}\tfrac{1}{2}\varphi_2 = \frac{\eta_S}{1-\omega_S^2}$$

from which we get

$$\eta_S = \frac{\omega_2^2 - \omega_1^2}{\omega_S^2} \cdot \frac{1}{\operatorname{tg}\tfrac{1}{2}\varphi_2 + \operatorname{tg}\tfrac{1}{2}\varphi_1} \qquad (4\text{-}19)$$

where ω_1 and ω_2 are two points on the circle ($\omega_1 \leqslant \omega_S$ and $\omega_2 \geqslant \omega_S$) and φ_1 and φ_2 are the corresponding angles measured from the diameter that passes through the natural frequency. (Throughout this work the first of these two loss factors will be referred to as the K loss factor and the latter as the M loss factor)

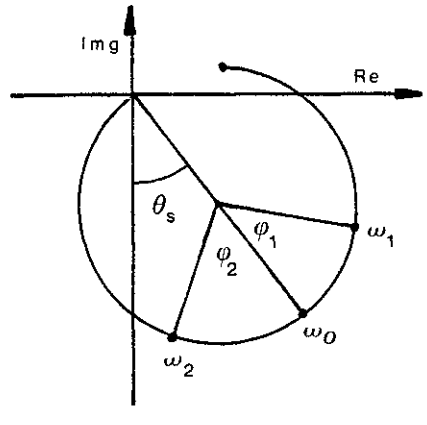

Fig. 4-2: Derivation of the loss factor

4.2.3 MODAL CONSTANT

The modulus of the complex modal constant ${}_sA_{jk}$ is calculated from the diameter of the circle D_s, the loss factor η_s and the natural frequency ω_s

$$|{}_sA_{jk}| = D_s \omega_s^2 \eta_s \qquad (4\text{-}20)$$

The phase of the modal constant, θ_s, is derived by observing the amount of rotation of the circle about the origin, this being determined by the location of the natural frequency.

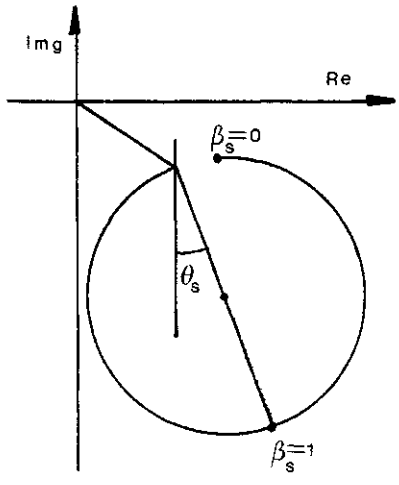

Fig. 4-3: Effect of neighbouring modes on the modal circle

Now, if we assume that the value of each term in the summation (4-1) for r≠s is unchanged as the frequency is changed in the vicinity of ω_s, then the whole circle is bodily displaced from the origin without affecting its shape (Fig. 4-3) and the modal parameters derived by examining the geometry of the circle are, therefore, unaffected.

The final plot, made of several modes, is illustrated in

Fig. 4-4 and shows how the response around each resonance approximates to that of a single mode, thus allowing the individual identification of each mode.

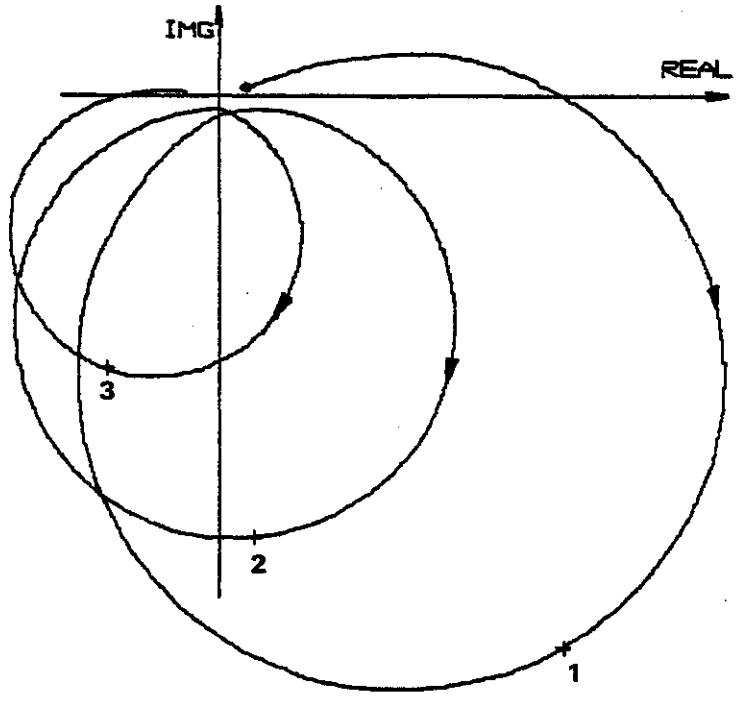

Fig. 4-4: Typical multi-degree of freedom polar plot

4.2.4 RESIDUAL TERMS

In practice, only a limited number of a structure's modes will be measured in a finite range of frequencies ('the range of interest'), the other modes which lie out of this range at lower and higher frequencies being unobserved. The assumption that the contribution to the response in the neighbourhood of a certain mode from all modes except the one under analysis is constant, may be extended to consider

the contribution of groups of modes, which are outside the range of interest, to the total response.

Expression (4-1) may be written as:

$$\alpha_{jk}=\sum_{r=1}^{l}\frac{{}_rA_{jk}}{\omega_r^2}\delta_r+\sum_{r=l+1}^{h}\frac{{}_rA_{jk}}{\omega_r^2}\delta_r+\sum_{r=h+1}^{n}\frac{{}_rA_{jk}}{\omega_r^2}\delta_r \qquad (4\text{-}21)$$

Where the range of interest includes the modes r=l+1 ÷ h. In this case, we may write for the summation of modes r=1÷l

$$\omega_r << \omega \qquad (4\text{-}22)$$

and therefore

$$\sum_{r=1}^{l}\frac{{}_rA_{jk}}{\omega_r^2}\cong\sum_{r=1}^{l}\frac{-{}_rA_{jk}}{\omega^2}=\frac{R_m}{\omega^2} \qquad (4\text{-}23)$$

For the summation of modes r=h+1 ÷ n we may write

$$\omega_r >> \omega \qquad (4\text{-}24)$$

and therefore

$$\sum_{r=h+1}^{n}\frac{{}_rA_{jk}}{\omega_r^2}\cong\sum_{r=h+1}^{n}\frac{{}_rA_{jk}}{i\omega_r^2\eta_r}=R_k \qquad (4\text{-}25)$$

The constants R_m and R_k are referred to as 'mass residual' and 'stiffness residual' respectively.

If we denote the total response calculated after identifying the modal parameters of all the modes in the range of interest by $\alpha_c(\omega)$ and the measured response due to all the modes of the system by $\alpha_m(\omega)$, then

$$\alpha_m(\omega)=\alpha_c(\omega)+\frac{R_m}{\omega^2}+R_k \qquad (4\text{-}26)$$

or

$$\alpha_m(\omega)-\alpha_c(\omega)=\frac{R_m}{\omega^2}+R_k \qquad (4\text{-}27)$$

In order to derive R_m and R_k, the responses at two

frequency points, at least, are needed (ω_1 and ω_2), thus

$$\alpha_m(\omega_1)-\alpha_c(\omega_1)=\frac{R_m}{\omega_1^2}+R_k$$
$$\alpha_m(\omega_2)-\alpha_c(\omega_2)=\frac{R_m}{\omega_2^2}+R_k \qquad (4\text{-}28)$$

or, using matrix notation

$$\begin{Bmatrix}\alpha_m(\omega_1)-\alpha_c(\omega_1)\\ \alpha_m(\omega_2)-\alpha_c(\omega_2)\end{Bmatrix}=\begin{bmatrix}\omega_1^{-2} & 1\\ \omega_2^{-2} & 1\end{bmatrix}\begin{Bmatrix}R_m\\ R_k\end{Bmatrix} \qquad (4\text{-}29)$$

from which

$$\begin{Bmatrix}R_m\\ R_k\end{Bmatrix}=\begin{bmatrix}\omega_1^{-2} & 1\\ \omega_2^{-2} & 1\end{bmatrix}^{-1}\begin{Bmatrix}\alpha_m(\omega_1)-\alpha_c(\omega_1)\\ \alpha_m(\omega_2)-\alpha_c(\omega_2)\end{Bmatrix} \qquad (4\text{-}30)$$

or

$$\{R\}_{2\times1}=[\Omega]^{-1}_{2\times2}\{\Delta\alpha\}_{2\times1} \qquad (4\text{-}31)$$

Theoretically, any two responses are sufficient for the derivation of {R}. However,as these responses are obtained experimentally, they contain errors which can affect seriously the values of {R} obtained by this simple method.

One way to overcome this problem is to increase the number of points (p for example) used for this process which is effectively a least-squares error estimation of the vector {R}.

Equation (4-29) is then

$$\{\Delta\alpha\}_{p\times1}=[\Omega]_{p\times2}\{R\}_{2\times1} \qquad (4\text{-}32)$$

In order to solve this system for {R} the pseudo-inverse approach is employed. Both sides of equation (4-32) are multiplied by $[\Omega]^T_{2\times p}$ thus,

$$[\Omega]^T_{2\times p}\{\Delta\alpha\}_{p\times1}=[\Omega]^T_{2\times p}[\Omega]_{p\times2}\{R\}_{2\times1} \qquad (4\text{-}33)$$

or

$$\{\Delta\}_{2\times1}=[\bar{\Omega}]_{2\times2}\{R\}_{2\times1} \tag{4-34}$$

from which

$$\{R\}_{2\times1}=[\bar{\Omega}]^{-1}_{2\times2}\{\Delta\}_{2\times1} \tag{4-35}$$

where

$$\{\Delta\}_{2\times1}=[\Omega]^{T}_{2\times p}\{\Delta\alpha\}_{p\times1} \tag{4-36}$$

$$[\bar{\Omega}]_{2\times2}=[\Omega]^{T}_{2\times p}[\Omega]_{p\times2} \tag{4-37}$$

It is then necessary to decide how many (and which) response points should be used in this calculation. As this is a statistical process, as many response points as possible should be used but in practice, this principle cannot be applied too literally.

Experience suggests that use of all available response points is unsatisfactory as the results are distorted by the numerically large data around the resonances. Conversely the anti-resonance regions are considerably affected by the residual terms and using only the anti-resonace points does improve the derived results. However, the anti-resonance response most often contain a high degree of error because the measured response signal is very low and is affected by the noise of the measuring system, and the derived results are thus, still liable to be unsatisfactory.

Between these two extremes there is an optimum set of response points which produces the best estimate of the residual terms; a maximum receptance level is set and only

those points below this level are included in the calculation. In this way, the influence of the near-resonance points can be reduced. If the results are still unsatisfactory, this level can be reset and a new estimate of {R} derived until satisfactory values are achieved.

Fig. 4-5 illustrates an experimentally-measured mobility curve together with two theoretically-derived curves; one of which is obtained using the modal constants plus the residual terms, while the other is generated omitting the residual terms. The straight line AB is the constant stiffness level which sets the maximum value of the points included in the calculation of the residual terms.

(All through this thesis the dotted curve represents the experimentally-measured data where each dot is the measured response at a certain frequency. The solid line represents the theoretically-regenerated curve.)

4.2.5 COMPUTER ALGORITHM POLAR5

Identification of the modal parameters of a single mode consists of the following steps:

(i) Calculation of the diameter and coordinates of the best fit circle through a number of experimentally-measured points near a resonance.

(ii) Location of the point on the modal circle where the angular spacing for equally-spaced frequency points is a maximum, giving the natural frequency and the modal phase

angle.

(iii) Calculation of the modal loss factor using either of the two methods described in par. 4.2.2.

(iv) Determination of the modulus of the complex modal constant from the diameter of the circle, the natural frequency and the loss factor.

This process is repeated for all the modes in the range of interest and once the modal parameters for all the modes are identified, the residual terms are calculated.

The above procedure was implemented in a computer algorithm (POLAR5) and is currently used in the Dynamics Section [45,44].

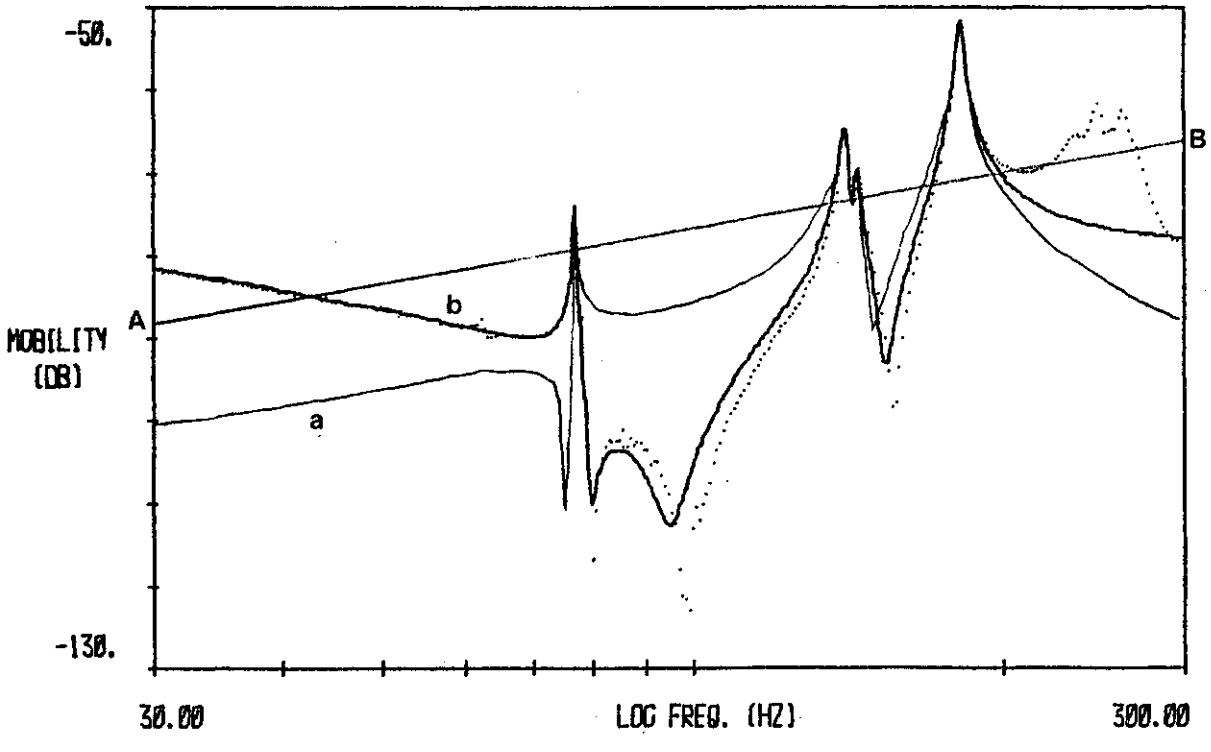

Fig. 4-5: Curve-fitting measured data; (a) without residual terms and (b) including residual terms

4.3 DERIVATION OF THE MODAL PARAMETERS BY CURVE-FITTING

The basic assumption on which the previous modal identification method is based is that over a small range of frequencies near each resonance, the contribution to the total response from all the other modes, except the one under consideration, is constant. This assumption is justified in the case of well separated modes, but when two adjacent modes are very close it may lead to significant errors and practically, the modes are insufficiently separated to permit the fitting of a simple circle to one mode at a time.

For cases of this latter kind a different approach is employed using a least squares error curve-fitting to the complete measured response. The concept of analysing one mode at a time is still kept, but instead of regarding the contribution from other modes as constant, it is treated as a function of the frequency and an iteration is made around all the modes to be analysed.

The algorithm for this simultaneous mode curve-fitting starts by making an initial guess of the modal parameters and the minimization of the fit error is done separately for each mode assuming at that time that the initial guess of the modal parameters for the other modes is correct.

If we denote the measured response by α_m, and the contribution of the s'th mode to the total response by $\bar{\alpha}_s$, then,

$$\bar{\alpha}_s(\omega) = \alpha_m(\omega) - \sum_{\substack{r=1 \\ r\neq s}}^{n} \frac{{}_rA_{jk}}{\omega_r^2(1-\beta_r^2+i\eta_r)} \tag{4-38}$$

and if α_s is its theoretical value, i.e

$$\alpha_s(\omega) = \frac{{}_sA_{jk}}{\omega_s^2(1-\beta_s^2+i\eta_s)} \tag{4-39}$$

the algorithm seeks to minimize the error E

$$E = \sum_{i=1}^{p} (\alpha_s - \bar{\alpha}_s)_i \tag{4-40}$$

By using a least squares error curve fitting process, taking into account p points around the natural frequency ω_s, the modal parameters for mode s which minimize expression (4-40) are derived. This process is repeated for the next mode but using the newly derived modal parameters for mode s.

The minimization process is done using the algorithm suggested by Gaukroger et.al [47] i.e

$$\frac{\partial E}{\partial k_i} + \sum_{j=1}^{4} \frac{\partial^2 E}{\partial k_i \partial k_j} \cdot \delta k_j = 0 \tag{4-41}$$

where k_i is the parameter to be determined and δk_j are the increments to be added to the initial estimate [46].

Because we do not take into account all the structure's modes, but only a finite number, N, we must resort, in this case, to the previous assumption and use the concept of residual terms which reflects the contribution of all the modes outside the range of measurement to the total response. Expression (4-38) takes, therefore, the form

$$\bar{\alpha}_s = \alpha_m - \sum_{\substack{r=1 \\ r\neq s}}^{N} \frac{{}_rA_{jk}}{\omega_r^2(1-\beta_r^2+i\eta_r)} + \frac{R_m}{\omega^2} + R_k \qquad (4\text{-}42)$$

Before starting the process of curve fitting the best estimate at that time for the residual terms is calculated, using the initial guess for the modal parameters. Then, these modal parameters are corrected mode by mode until satisfactory values are achieved.

A computer program (SIM2) using this algorithm was written and is currently used [44] in the Dynamics Section when the modal parameters derived by POLAR5 are unsatisfactory; these modal parameters are used as the initial estimates required at the beginning of SIM2.

A similar approach to the modal identification is employed by the computer program PAPA used at the RAE but assuming a viscously damped model [47].

4.4 NUMERICAL STUDY

It was expected that the modal parameters derived by the curve-fitting algorithm SIM2 would be more accurate then those derived by the Nyquist plot analysis algorithm POLAR5, especially for cases of close modes.

In order to assess the respective capabilities of the programs SIM2 and POLAR5, a comparative numerical study was made by analysing data where two of the modes were well separated and two were very close.

The synthesised data points were produced using the modal parameters listed in Table 4-1.

mode no.	ω_r (Hz)	η_r	A_r (1/Kg)	θ_r (deg)
1	77.20	0.007	6.27E-4	-179.2
2	141.3	0.016	7.83E-3	7.9
3	145.5	0.014	3.30E-3	1.0
4	182.6	0.016	0.0480	-10.0
Residual mass (1/Kg) = -0.016- i7.08E-1 Residual stiff.(m/N) = -3.45E-8 + i1.5E-8				

Table 4-1: Modal parameters for synthesised data

A further assessment of the sensitivity of the algorithms to random errors in the data was made when data were generated with the same modal parameters but with the introduction of random errors (4% and up to 8%)

The complete set of results is summarized in Table 4-2.

mode no.		resonance freq. (HZ)	%	loss factor	%	modal constant 1/Kg	%	phase (deg)	%
1	P	77.20	0.	0.0070	0.	6.302E-4	0.51	-179.21	0.01
	S	77.20	0.	0.0070	0.	6.270E-4	0.	-179.20	0.
2	P	141.3	0.	0.0156	2.5	7.324E-3	6.46	11.41	1.79
	S	141.3	0.	0.0160	0.	7.830E-3	0.	7.86	0.
3	P	145.6	0.07	0.0132	5.71	2.658E-3	19.45	-19.03	11.13
	S	145.5	0.	0.0140	0.	3.300E-3	0.	1.00	0.
4	P	182.6	0.	0.0160	0.	0.0479	0.21	-10.80	0.44
	S	182.6	0.	0.0160	0.	0.0480	0.	-10.00	0.

	Residual Mass (1/Kg) Real	%	Img.	%	Residual Stiffness (m/N) Real	%	Img.	%
P	-0.0157	1.88	-3.933E-4	44.45	-3.409E-8	1.99	1.510E-8	5.68
S	-0.0160	0.	-7.080E-4	0.	-3.450E-8	0.	1.590E-8	0.

a

mode no.		resonance freq. (Hz)	%	loss factor	%	modal constant 1/Kg	%	phase (deg)	%
1	P	77.20	0.	0.0068	1.71	5.955E-4	5.02	-179.06	0.08
	S	77.20	0.	0.0069	0.07	6.118E-4	2.42	-179.20	0.
2	P	141.2	0.08	0.0163	1.88	7.666E-3	2.09	20.53	7.4
	S	141.3	0.	0.0160	0.	7.723E-3	1.37	8.54	0.38
3	P	145.6	0.07	0.0124	11.43	2.319E-3	30.00	-13.23	7.91
	S	145.5	0.	0.0138	1.43	3.196E-3	3.15	0.54	0.24
4	P	182.7	0.05	0.0168	5.00	0.0520	8.33	-15.27	2.91
	S	182.6	0.	0.0159	0.63	0.0468	2.5	-10.26	0.14

	Residual Mass (1/Kg) Real	%	Img.	%	Residual Stiffness (m/N) Real	%	Img.	%
P	-0.0155	3.13	-4.390E-4	38.00	-3.587E-8	3.77	1.743E-8	9.26
S	-0.0154	3.75	-6.615E-4	6.75	-3.298E-8	4.41	1.508E-8	5.16

b

mode no.		resonance freq. (Hz)	%	loss factor	%	modal constant 1/Kg	%	phase (deg)	%
1	P	77.12	0.1	0.0067	3.53	5.748E-4	12.63	-145.69	18.62
	S	77.20	0.	0.0069	0.21	5.973E-4	4.74	-178.48	0.02
2	P	141.3	0.	0.0149	6.94	6.662E-3	14.92	5.84	1.12
	S	141.3	0.	0.0158	1.25	7.482E-3	4.44	7.47	0.22
3	P	145.6	0.03	0.0129	7.86	2.444E-3	25.94	-12.88	7.71
	S	145.5	0.	0.0138	1.43	3.150E-3	4.55	0.55	0.25
4	P	182.7	0.05	0.0160	0.	0.0463	3.54	-11.86	1.03
	S	182.6	0.	0.0160	0.	0.0463	3.54	-9.54	0.24

	Residual Mass (1/Kg) Real	%	Img.	%	Residual Stiffness (m/N) Real	%	Img.	%
P	-0.0150	6.25	3.994E-4	156.41	-2.911E-8	15.62	1.514E-8	4.78
S	-0.0154	3.75	-6.615E-4	6.75	-3.298E-8	4.41	1.507E-8	5.22

c

Table 4-2: Synthesised data - derived modal parameters and their relative errors for (a) 0%, (b) 4% and (c) 8% random errors in the data

A comparison of the modal parameters derived by the two programs clearly demonstrates the limitations of the single mode analysis method when the modes are very close. For all levels of random error, the error in the identification of the natural frequencies is negligible, regardless of the closeness of the modes. For all the other modal parameters, however, there is a considerable error in those identified by POLAR5 and a significant reduction in this error when the data are further analysed by SIM2. Furthermore, POLAR5 proves to be more sensitive to random errors in the data by comparison with SIM2.

The usual method of comparing measured data and the theoretically-regenerated curve is to draw both of them on the same plot and examine the closeness of the fit. This method, which is widely used, is very subjective and depends heavily on the format chosen for the plot. The visual comparison of the 'experimentally' generated data and the curves identified by the two programs demonstrates this point.

Presenting the measured data on a log mobility vs. log frequency plot is convenient and very informative for the engineer who is interested in the resonances and the anti-resonances as well. However, this presentation does not provide any information about the phase shift and because the resonance peaks are somewhat 'compressed' the quality of the data in these important areas is not readily obvious. The comparison with the identified curve emphasises,

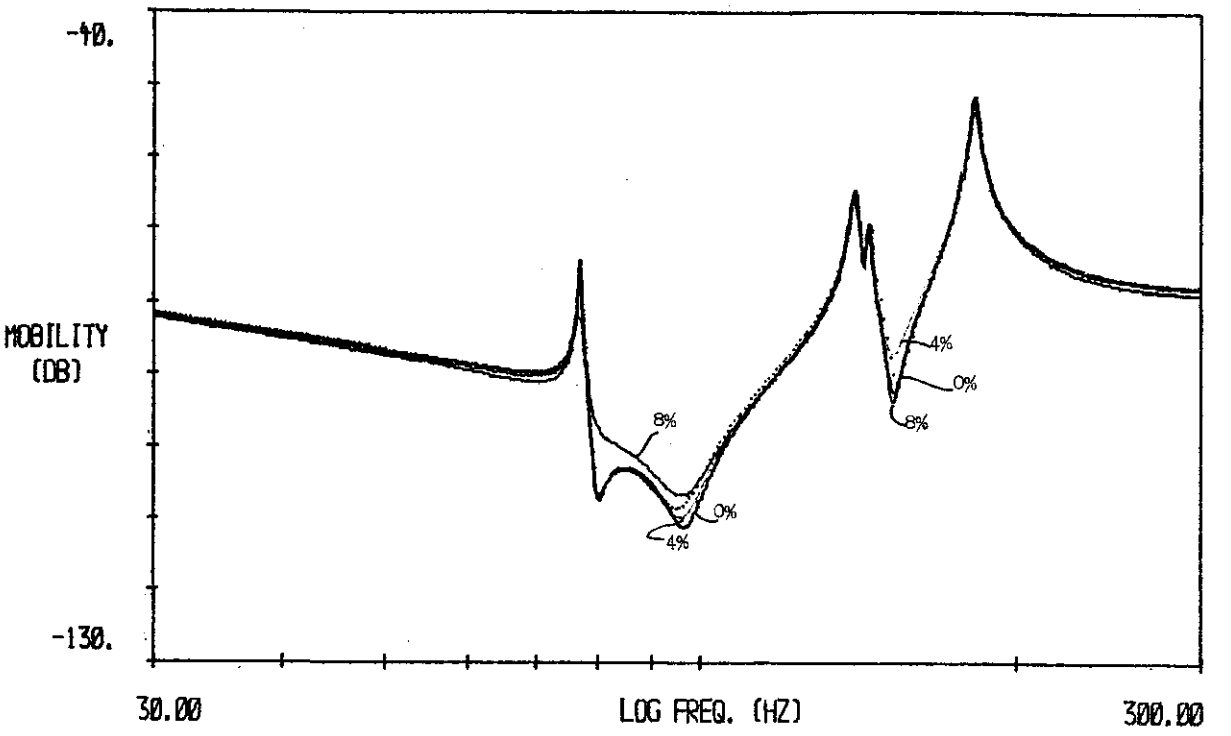

Fig. 4-6: Curve-fitting for the three levels of random error on a log mobility scale

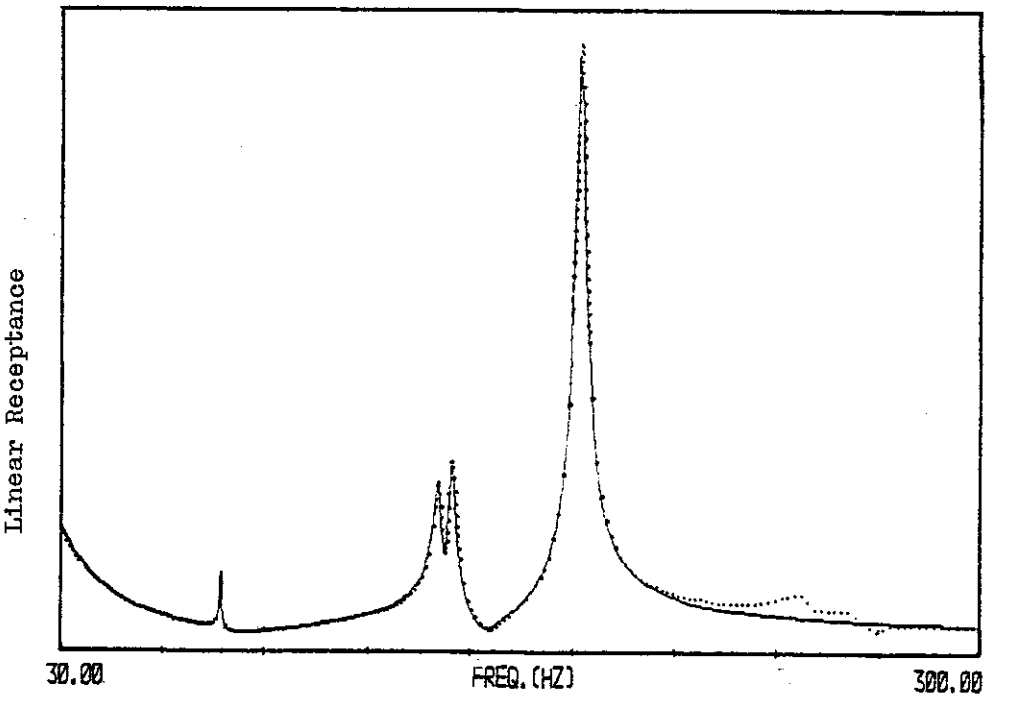

Fig. 4-7: Curve-fitting on a linear receptance scale

therefore, the quality of the fit at off resonance areas where the actual numerical values are relatively small and they tend to minimize, visually, the numerically larger errors at the resonances. Checking Fig. 4-6, it seems, therefore, that all three derived curves fit equally well the four resonances.

Presenting the data on a linear receptance scale (Fig. 4-7) emphasises the resonances but completely attenuates the anti-resonances; but the phase information is still unavailable.

The third option for presentation of the data is the polar plot of receptance; this presentation is very informative as to the quality of the data around resonances and gives some idea as to the degree of influence between two close modes (and, as will be shown later, to the linearity properties of the data). Presenting the results in the polar plane shows more clearly the quality of the fit at resonances and the difference between the POLAR5 and SIM2 derived parameters is evident (Figures 4-8 ÷ 4-12).

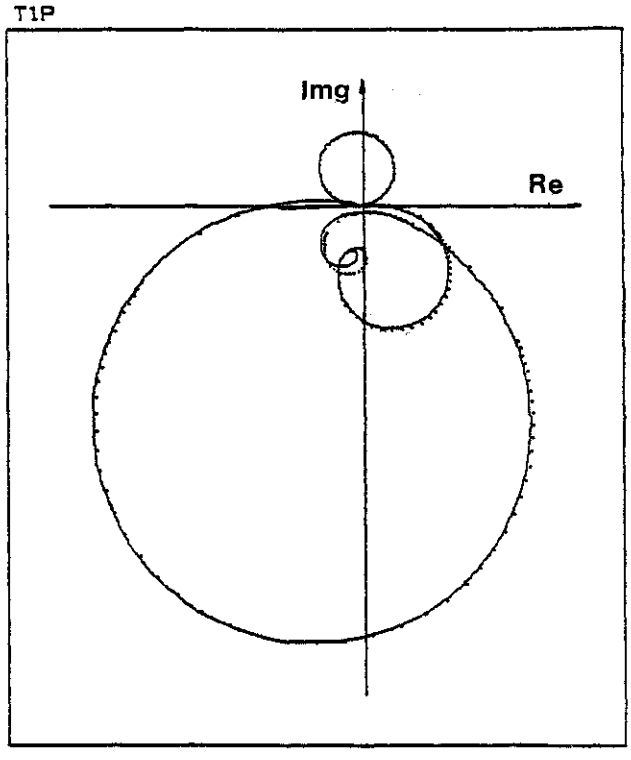

Fig. 4-8: 0% random error - curve fit by POLAR5

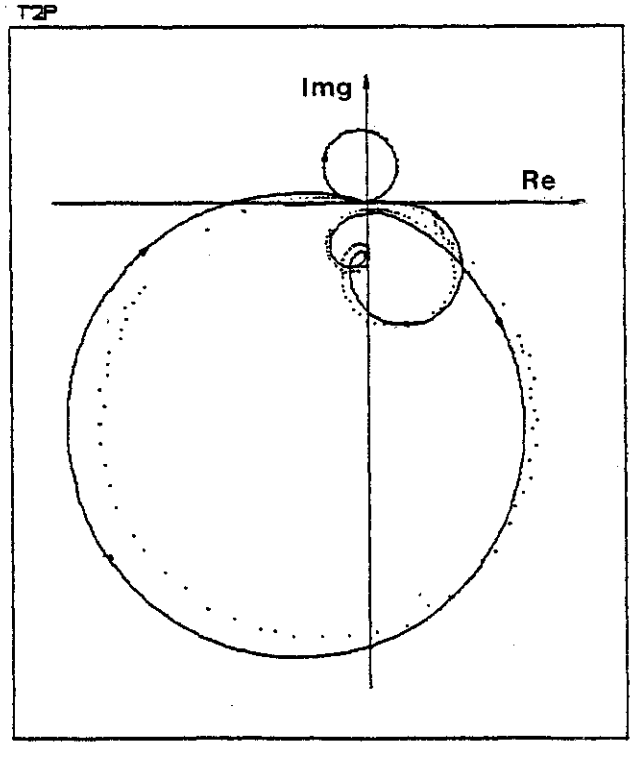

Fig. 4-9: 4% random error - curve fit by POLAR5

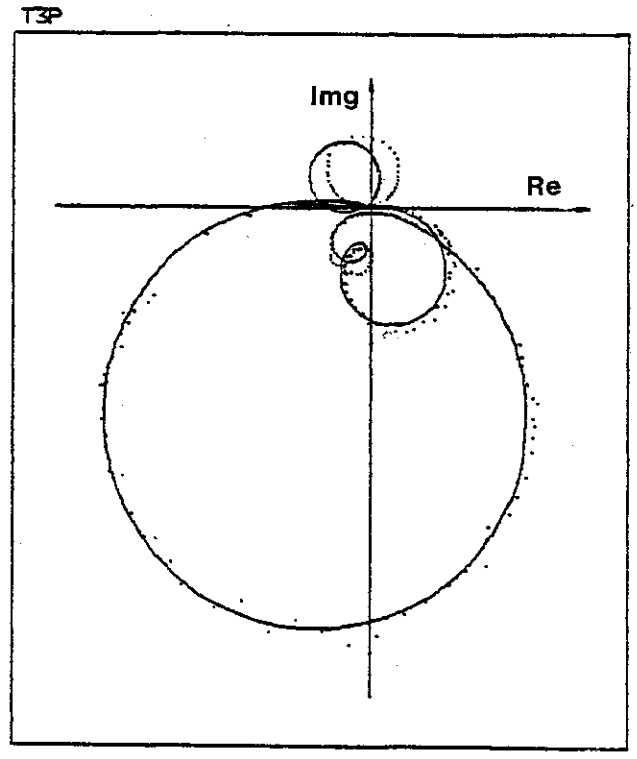

Fig. 4-10: 8% random error - curve fit by POLAR5

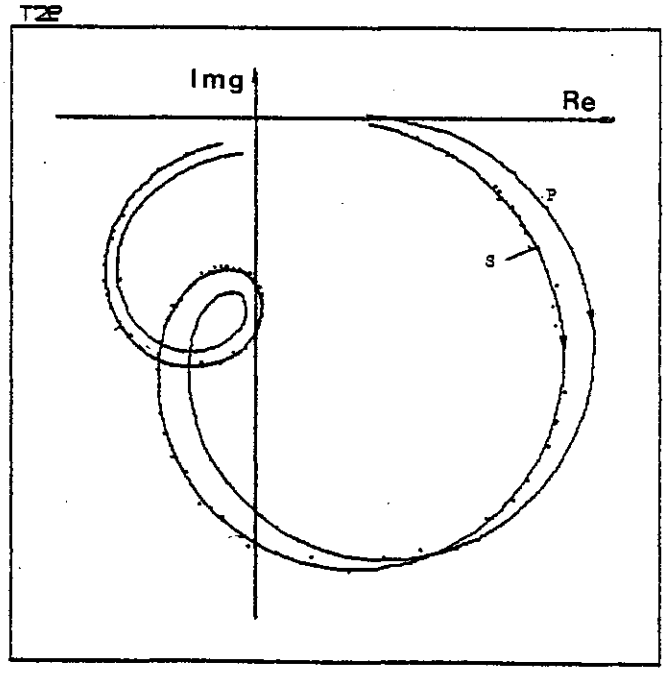

Fig. 4-11: 4% random error - curve fit by POLAR5 and SIM2 of second and third modes

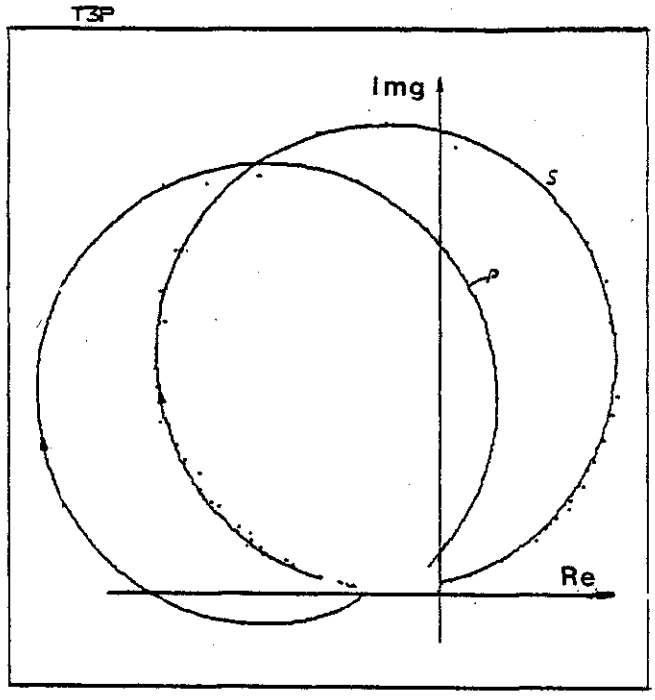

Fig. 4-12: 8% random error - curve fit by POLAR5 and SIM2 of the forth mode

4.5 MULTI-POINT EXCITATION METHOD

A widely used modal identification technique, especially in the fixed wing aircraft industry, is the multi-point excitation method. The theoretical basis for this method was laid by Fraeijs de Veubeke [19] (see chapter 2) who showed that a system with a finite number of degrees of freedom and with either viscous or hysteretic damping can be excited by a set of properly tuned mono-phased forces at a natural frequency of the undamped system to vibrate in a mode which is identical to the undamped normal mode of the system (a forced proportional mode).

The practical implementation of this method is rather complicated; the two main problems which confront the user are the need to find the required number of shakers and how to find most efficiently the correct levels of force distribution to excite a 'pure' mode.

These problems were discussed theoretically by many investigators [48,49] and there are some different practical methods for the implementation of this theoretically simple technique [43,50,51].

It should be pointed out, however, that unless the system is proportionally damped (or, more generally, the damping matrix does not couple the undamped normal modes) the natural frequencies and the (real) mode shapes measured by this method are not identically the natural frequencies and normal (complex) mode shapes of the actual system but rather the modal parameters of a fictitious undamped system.

The common technique for deriving the loss factor is to switch off the exciters and record the transient response from which it can be simply calculated. (This method is sometimes referred to as 'purity check of excited mode'). A proportionally-damped system will vibrate in the natural frequency of this mode but in a generally-damped system, 'beating' occurs in the transient response which means that the excited (real) mode is not a true normal mode of the system. In this case, there is no unique loss factor which can be associated with the excited mode. In practice, most of the investigators using this technique assume a priori that the system is proportionally-damped: an assumption which may not always be justified.

In the experimental part of this research a multi-point excitation system was used: the Manual Multi-point Apparatus (MAMA) developed and built at the RAE [52]. This system is able to control up to five shakers which apply sinusoidal mono-phased force inputs to the structure. The excitation frequency is controlled automatically so that a quadrature relationship exists between the force input of one exciter and the displacement response at a point on the structure. The force distribution is tuned manually so as to obtain a quadrature relationship between the force inputs of the remaining four exciters and the displacement response at four points on the structure. Once this condition is reached, the mode shape is simply measured on the structure.

5. THE EFFECT OF NONLINEARITIES

5.1 INTRODUCTION

The fundamental assumption on which our mathematical model is based is that the system under consideration behaves in a linear way.

It is expected that real systems will be to a lesser or greater extent nonlinear, but practical experience suggests that given the right conditions, their nonlinear component is generally negligible. However, as more accurate and more powerful equipment for measurement and analysis is available, and consequently there is a demand for better and more accurate results from modal surveys, it is realized that often the nonlinear component is no longer negligible and must be accounted for.

This may be done in two ways: (i) by identifying the sources of the nonlinearity in the system and trying to eliminate or minimize their effect or (ii) by changing the test conditions so as to minimize the nonlinear behaviour of the system

In any case, analysing a system for which the linearity assumption cannot be fully justified leads to inaccurate and misleading results. Using these results in further computations can give rise to even greater errors and result in a final model which does not describe the system adequately.

The mathematical modelling of nonlinear vibrations

encountered in practice requires the solution of nonlinear differential equations. The most common types of nonlinearities are cubic stiffness and dry (coulomb) friction damping. The equations of these system are well known and have been studied by many investigators and the theoretical techniques for analysing them are well established [53,54,55,56]. Far less investigation has been devoted to the problem of identifying real nonlinear systems, probably for the obvious reason that actual nonlinearity of real systems is much more complicated than the relatively simple mathematical models available [57,61].

The influence of cubic stiffness on the Nyquist plot was examined by Newman [59] and White [58] and both showed that the angular spacing of the points is distorted. White identified the system's parameters using transient techniques and compared his theoretical predictions with experimental results from a simple structure. More recently, Tomlinson [60,62] has investigated the effect of dry friction on the Nyquist plot and presented a method, based on the in-phase and quadrature power dissipated when a normal mode is excited, by which the nonlinear friction force and the hysteretic damping are identified. The experimental validation of this technique is restricted to a very simple laboratory device designed to behave according to the theoretical model.

The approach employed in this research towards the problem of nonlinearities in the measured response is

similar to that exercised towards the problem of noise pollution of the measured signal. Accordingly, we shall treat the effect of nonlinearities as a measurement error superimposed on the 'true' linear response attempting to identify its existence rather than its type and thus to minimize its effect.

It seems unlikely that analysis of simple nonlinear systems will ever cover the real nonlinear response of a multi-degree of freedom system. However, in order to understand how a weakly nonlinear system behaves and to gain some insight into the sensitivity of the linear modal identification technique, a simple one-degree-of-freedom weak nonlinear oscillator is investigated in some detail. The behaviour of a real system is rather complicated and it seems impossible to describe it precisely by an analytical model. To get nearer to this goal a mathematically-simple nonlinear component is assumed and added to the linear equation of motion. The underlying assumption in this process is that the nonlinear component is small enough that the new equation can be solved analytically by an approximate method.

The nonlinearity of the system demonstrates its presence when excitation conditions are changed by producing a disproportionate change in the measured response. A parameter which gives some measure as to the magnitude of the nonlinearity relative to a linear system - the nonlinearity factor - is first defined. Then, the influence

of small nonlinearities on the shape of the polar plot and on the subsequent linear modal identification process are investigated. To this end four different types of nonlinearity are examined: (i) dry friction, (ii) cubic stiffness, (iii) quadratic viscous damping and (iv) a combination of dry friction and quadratic viscous damping.

Theoretical data for different conditions are generated and then subjected to analysis by a linear modal identification algorithm (POLAR 5). The derived modal parameters are presented and as the exact linear parameters of the system are known a priori, the influence of the nonlinearity present in the system on the identification process can be evaluated in detail.

Finally, an experimental study which demonstrates the practical problem created by real nonlinearities is presented.

5.2 THE NONLINEARITY FACTOR.

Measured mobility data from real systems are polluted by many errors resulting in bad estimates of the system parameters. These errors may be grouped into two categories: variance and bias.

The variance part of the error is due to random deviations from the 'true' value and is essentially Gaussian in distribution. Statistically, therefore, if sufficient samples are evaluated, such random errors will be averaged out and the measured estimate will closely approximate the 'true' value with a high degree of confidence.

The bias error, on the other hand, does not usually diminish as a result of taking more samples, as it is due to a system characteristic or measurement procedure which results in an incorrect estimate. With this type of error it is vital to know its form or source in order to be able to reduce its effect on the measured data.

Nonlinearity of the system produces a bias error. Nonlinearities will generally shift energy from one frequency to many new frequencies in a very complicated way. The result will be a deviation of the measured response at the excitation frequency from the 'true' linear response at this frequency.

For the random excitation method of measuring mobility data, there exists a value which serves as a measure of the degree of noise contamination in the measurement - the

coherence function. This describes the division of output power into coherent and incoherent parts with respect to the input. If the measurement contains bias error due to nonlinearities of the system then the coherence function does not improve and will reach, as the number of samples is increased, a maximum of less then 1 at each frequency.

A factor similar to the coherence function may be defined for the steady-state harmonic excitation method with single input and output. It is referred to as the 'nonlinearity factor'.

Let us assume, for the sake of this theoretical discusion, that we know the 'true' linear response of the system and can denote it by $\alpha_l(\omega)$. Furthermore, suppose that we manage to measure the exact linear response of the system $\alpha_m(\omega)$. If we plot this 'measured' response vs. the 'true' response at various (but corresponding) frequencies, the points will all lie on a straight line which passes through the origin and which has an inclination of 45° (Fig. 5-1).

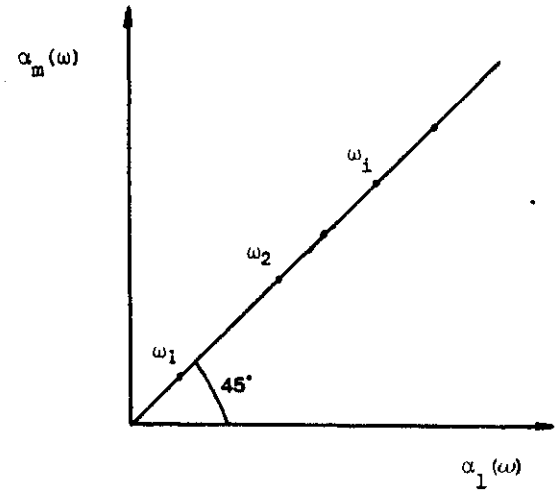

Fig. 5-1: 'True' vs. 'measured' linear response.

In practice, however, the measured response, α_m, will not be identical to the 'true' linear response, α_l. Their deviation, due to nonlinearities may be described by two bias errors, namely the constant linear error, V, and the constant logarithmic error, U. i.e

$$\alpha_m(\omega) = U\alpha_l(\omega) + V \qquad (5\text{-}1)$$

If we assume that the logarithmic error is equal to zero (i.e. log(U)=Ø, U=1) and if we plot on a linear scale α_m and α_l vs. frequency ω (Fig. 5-2a) then the deviation of α_m from α_l has a constant width V. If we plot α_m vs. α_l (Fig. 5-2b) then the points will lie on a straight line which has an inclination of 45° but which does not pass through the origin.

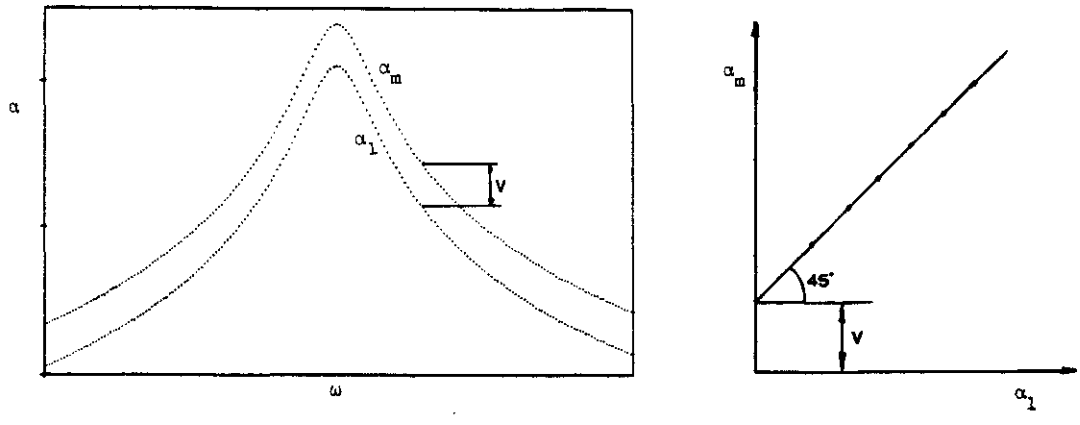

(a) (b)

Fig. 5-2: α_m vs. α_l for a constant linear bias.

If we next assume that the linear error, V, is zero and if we plot on a logarithmic scale α_m and α_l vs. frequency (Fig. 5-3a) then the deviation of $\log(\alpha_m)$ from $\log(\alpha_l)$ has a constant width, log(U). If we now plot α_m vs. α_l (Fig. 5-3b)

then the points will lie on a straight line which passes through the origin but with an inclination which is equal to $tg^{-1}(U)$.

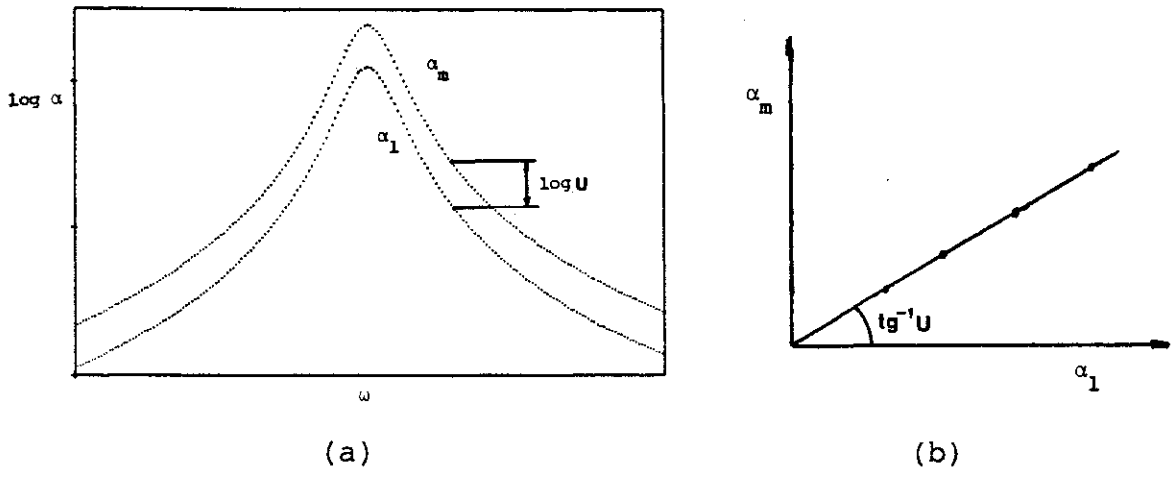

(a) (b)

Fig. 5-3: α_m vs. α_l for a constant logarithmic bias.

The combined effect of these two errors when displayed as α_m vs. α_l is a set of points which lie on a straight line. This line, y_{sl}, has an inclination of $tg^{-1}(U)$ and intersects the α_m axis at V (Fig. 5-4).

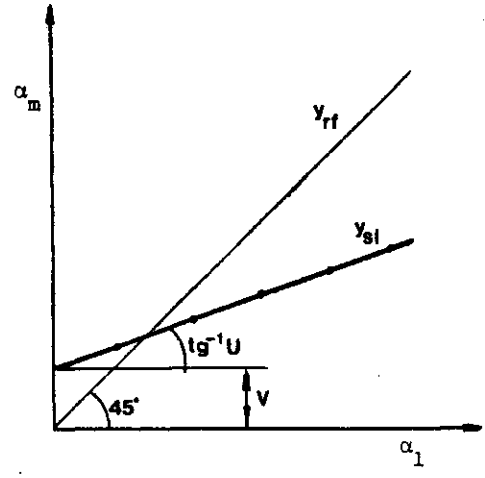

Fig. 5-4; α_m vs. α_l for both bias errors.

The degree of deviation of this line, y_{sl}, from the straight line which passes through the origin and has a 45° inclination, y_{rf}, (the reference line) gives an indication to the amount of bias error present in the system.

In fact, the nonlinearity bias errors are functions of the amplitude, P, and frequency, ω, of the excitation. Thus

$$\alpha_m(\omega)=U(P,\omega)\alpha_l(\omega)+V(P,\omega) \qquad (5-2)$$

which means that the deviation of the measured response, α_m, from the 'true' linear one is more complex than we have assumed so far. In this case, if we plot α_m vs. α_l the points will not lie, any longer, on a straight line.

A theoretical nonlinear response (cubic stiffness) to a constant level of harmonic excitation is given in Fig. 5-5. When this response, α_m, is plotted vs. the true linear response, α_l, it is obvious that the points do not lie on a straight line (Fig. 5-5b).

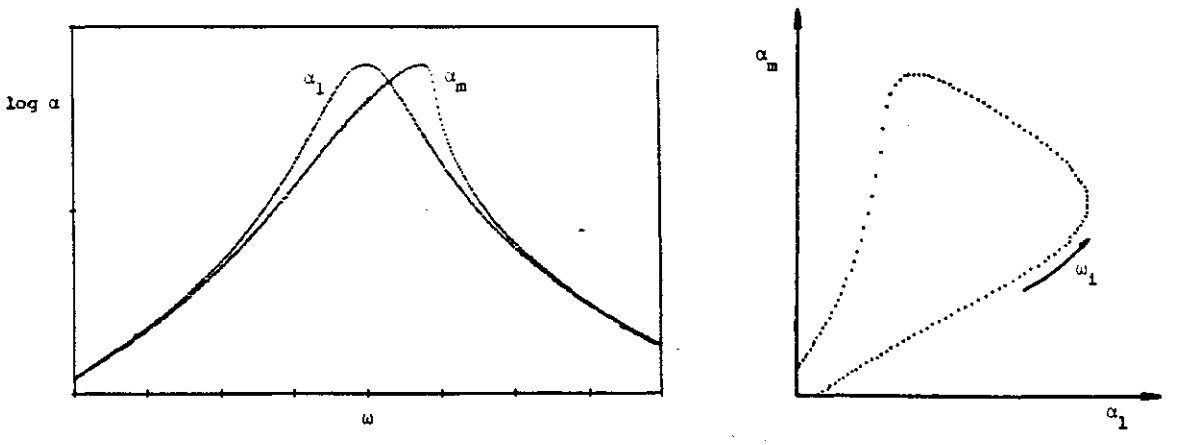

(a) (b)

Fig. 5-5: α_m vs. α_l for a theoretical nonlinear response.

In this case the degree of deviation of these points from the reference line y_{rf} gives an indication to the amount of nonlinearity present in the system. This can be quantified in the following way:

Let the 'true' response be written as $x(\omega_i)$ and the nonlinear response as $y(\omega_i)$ (or as x_i and y_i)

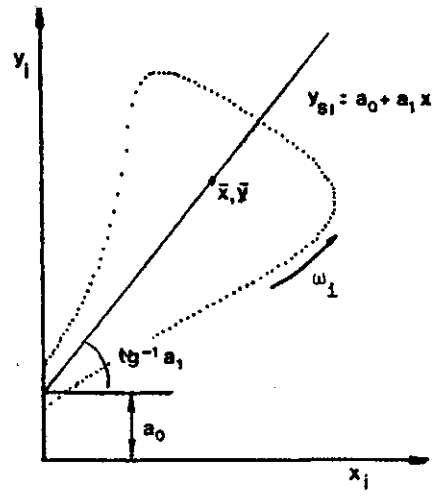

Fig. 5-6: Calculation of the nonlinearity factor.

A plot of y_i vs. x_i for corresponding frequency points (n points) is shown in Fig. 5-6. A straight line, y_{sl}, is fitted through these points such that the sum of the squares of the deviations from it shall be a minimum. Because x_i represents the 'exact' response the deviations are measured along the y_i axis.

The equation of the straight line y_{sl} is

$$y_{sl} = a_0 + a_1 x \qquad (5-3)$$

where

$$a_0=\left[\sum_{i=1}^{n} x_i^2 \sum_{i=1}^{n} y_i - \sum_{i=1}^{n} x_i \sum_{i=1}^{n} x_i y_i\right] D \qquad (5\text{-}4)$$

$$a_1=\left[-\sum_{i=1}^{n} x_i \sum_{i=1}^{n} y_i + n \sum_{i=1}^{n} x_i y_i\right] D \qquad (5\text{-}5)$$

$$D=\left[n\sum_{i=1}^{n} x_i^2 - \left(\sum_{i=1}^{n} x_i\right)^2\right]^{-1} \qquad (5\text{-}6)$$

By definition, the straight line y_{sl} always passes through the 'center of gravity' of the points $(\bar{x},\bar{y})$ where

$$\bar{y}=\frac{1}{n}\sum_{i=1}^{n} y_i \quad \text{and} \quad \bar{x}=\frac{1}{n}\sum_{i=1}^{n} x_i \qquad (5\text{-}7)$$

The standard error of the fitted line is defined as;

$$s_{sl}^2=\frac{1}{n}\sum_{i=1}^{n} (y_i-y_{sl})^2=\frac{1}{n}\sum_{i=1}^{n} [y_i-(a_0+a_1 x_i)]^2 \qquad (5\text{-}8)$$

and the standard deviation from the average $\bar{y}$ is

$$s_{\bar{y}}^2=\frac{1}{n}\sum_{i=1}^{n} (y_i-\bar{y})^2 \qquad (5\text{-}9)$$

The 'nonlinearity factor' - which is a measure of the deviation of y_{sl} from the reference line y_{rf} - is a combination of three values, namely (i) the general linear bias, (ii) the general logarithmic bias and (iii) the degree of correlation of the points to the straight line y_{sl}.

(i) The general linear bias is denoted by a_0 and the dimensionless factor J_1 which expresses its relative

magnitude is defined as:

$$J_1 \equiv 1 - \frac{a_0}{\bar{y}} \qquad \text{for } a_0 \geq \emptyset \tag{5-10}$$

or

$$J_1 \equiv 1 + \frac{a_0}{a_1 \bar{x}} \qquad \text{for } a_0 \leq \emptyset \tag{5-11}$$

for $a_1 \geq \emptyset$ the range of J_1 is

$$\emptyset \leq J_1 \leq 1 \tag{5-12}$$

For zero linear bias error ($a_0 = \emptyset$) $J_1 = 1$ and as the error gets larger, J_1 gets smaller and smaller.

(ii) The general logarithmic bias is denoted by a_1 and the dimensionless factor J_2 which expresses its relative deviation from 1 is defined as:

$$J_2 \equiv 1 - \frac{\left|\varphi - \frac{\pi}{4}\right|}{\frac{\pi}{4}} \tag{5-13}$$

where

$$\varphi = tg^{-1}(a_1) \tag{5-14}$$

for $a_1 \geq \emptyset$ the range of J_2 is

$$\emptyset \leq J_2 \leq 1 \tag{5-15}$$

For zero logarithmic bias error ($a_1 = 1$) $J_2 = 1$ and as the error gets larger, J_2 gets smaller and smaller.

(iii) The degree of correlation of the points to a straight line is expressed by the dimensionless factor J_3 which is defined as:

$$J_3 \equiv 1 - \left(\frac{S_{s1}}{S_{\bar{y}}}\right)^2 \tag{5-16}$$

The range of J_3 is always

$$\emptyset \leqslant J_3 \leqslant 1 \qquad (5\text{-}17)$$

For perfect correlation $J_3=1$ which means that the bias errors are not a function of the frequency ω and the excitation P (or that P is kept constant). J_3 gets smaller as there is less and less correlation between the points and the fitted line y_{sl}. (see appendix)

The nonlinearity factor is defined as

$$J \equiv J_1 \cdot J_2 \cdot J_3 \qquad (5\text{-}18)$$

As the responses, α, are complex numbers, this procedure must be applied twice; once when x_i and y_i are the moduli of the response and once when they are the corresponding phases. For each case a nonlinearity factor is calculated, J_m for the moduli and J_p for the phases. An overall nonlinearity factor may be defined as:

$$J \equiv (J_m \cdot J_p)^{\frac{1}{2}} \qquad (5\text{-}19)$$

and its range is (Fig. 5-7)

$$\emptyset \leqslant J \leqslant 1 \qquad (5\text{-}20)$$

When J=1, the measured response is purely linear and as J gets smaller, the data are less and less linear.

The plot of y_i vs. x_i is referred to as the 'J plot' and the nonlinearity factor as the 'J factor'.

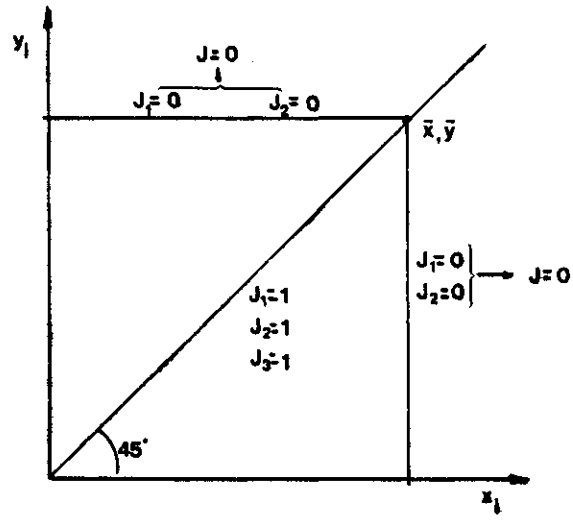

Fig. 5-7: The range of the J factor (for $a_1 \geq 0$)

The preceding analysis assumes bias errors only and that they are due to nonlinearities within the system. However, this method can be applied in order to detect the level of random errors as well. This can be done by calculating the J factor for two sets of data measured twice over the same frequency range while maintaining the same level of excitation and integration time (which is special to the sine excitation method). The effect of integration time on the level of random errors in the measurements can also be checked by calculating the J factor for the same measurement taken at different integration times.

An additional linearity check can be made by calculating the J factor for two corresponding transfer measurements which should, theoretically, be identical

For those cases where none of the sets of data used in the process of the calculation of the J factor can be assumed as 'exact' the deviation used in the derivation of

y_{sl} should be calculated perpendicular to the straight line, but as the arithmetic involved is rather complicated we choose either the x or y direction for the deviation, realizing that the price paid for the simpler mathematics is a sacrifice in the accuracy of the best fit of the line. The choice between the x and y directions is made in favour of that direction in which the larger standard deviation is found. Actually, this procedure is employed for the calculation of the 'nonlinearity factor' as, practically, the 'true' linear response, α_l, is not available to us. Instead we decide which of the measured responses may serve as the 'best' 'true' linear response. (The way in which this response is chosen will be described in a later stage.)

5.2.1 LINEARITY CHECK VIA CALCULATION OF THE M LOSS FACTOR.

In order to calculate the J factor, a reference set of data is needed. However, in many practical cases only one single measurement is available so that it is impossible to calculate the J factor.

A different, though less powerful, check for identifying the existence of nonlinear behaviour from a single set of data may be made by examining different calculated values of the M loss factor.

The expression for the M loss factor is derived from the geometry of the Nyquist plot (Fig. 5-8) i.e

$$\eta_M = \frac{\omega_2^2 - \omega_1^2}{\omega_o^2} \cdot \frac{1}{tg\frac{1}{2}\varphi_1 + tg\frac{1}{2}\varphi_2} \qquad (5\text{-}21)$$

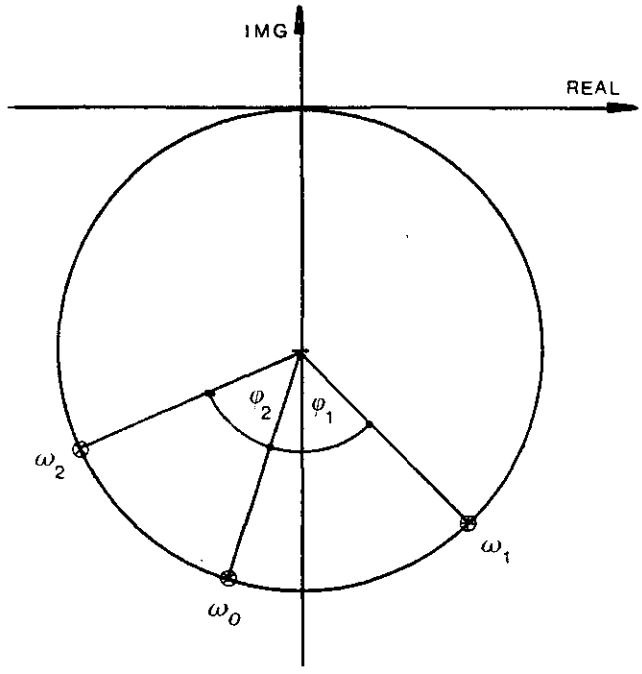

Fig. 5-8: Calculation of the M loss factor.

For a linear set of data the derived loss factor for any two frequency points ω_1 and ω_2 will be the same as long as $\omega_2 \geqslant \omega_o$ and $\omega_1 \leqslant \omega_o$

However, as the presence of small nonlinearities in the system must cause some change in the geometry of the Nyquist plot, then the M loss factor derived using different combinations of frequency points will be different for each combination. Checking the values derived for the M loss factor as a function of $\Delta\omega = (\omega_2 - \omega_1)$ where $\omega_2 - \omega_o = \omega_o - \omega_1$ may, at most, give some indication as to the nature of the nonlinearity or, at least, to its existence.

5.3 GENERAL EQUATION OF A WEAKLY NONLINEAR SYSTEM

In order to get some better insight as to the influence of small nonlinearities on the linear modal identification process, a theoretical one-degree-of-freedom nonlinear system is examined in detail.

The general equation which may describe such a system subjected to harmonic excitation is,

$$\ddot{x}+2h\dot{x}+c\dot{x}|\dot{x}|+R\frac{\dot{x}}{|\dot{x}|}+\omega_o^2 x(1+bx^2)=P\cos\omega t \qquad (5\text{-}22)$$

where

x - harmonic displacement. [m]

P - amplitude of harmonic exciting force. [N/Kg]

ω - frequency of exciting force. [sec^{-1}]

h - linear viscous damping coefficient. [sec^{-1}]

c - quadratic viscous damping coefficient. [m^{-1}]

R - constant dry friction force. [N/Kg]

ω_o - natural frequency of linear system. [sec^{-1}]

b - cubic stiffness coeffecient. [m^{-2}]

This equation is solved for some particular cases of nonlinearity using the method of equivalent linearization.

5.3.1 THE METHOD OF EQUIVALENT LINEARIZATION.

A convenient method for deriving a satisfactory approximate solution to equation (5-22) is the method of equivalent linearization [55] which states:

The amplitude and phase of the periodic vibration of a weakly nonlinear oscillator i.e

$$\ddot{x}+\epsilon f(\dot{x})+\omega_0 x+\epsilon g(x)=P\cos\omega t \qquad (5-23)$$

where $f(\dot{x})$ and $g(x)$ are odd functions, in the neighbourhood of the resonance, are equal to the amplitude and phase of the steady state vibration of the linear oscillator with the governing equation

$$\ddot{x}+2\bar{h}(a)x+\varpi_0^2(a)x=P\cos\omega t \qquad (5-24)$$

whose coefficients $\bar{h}(a)$ and $\varpi_0(a)$ are chosen in such a way that the solution of these two equations differ by terms of second or higher order in ϵ.

As a first approximation, we assume that the solution to equation (5-23) is

$$x=a\cdot\cos(\omega t+\theta) \qquad (5-25)$$

where a and θ are 'slightly varying' amplitude and phase respectively. This solution is the first harmonic which is actually measured on a real system.

The expression that describes the system's response (or the 'resonance curve') is,

$$a^2(\omega^2-\varpi_0^2)+(2\omega a\bar{h})^2=P^2 \qquad (5-26)$$

Solving this equation gives the value of a as a function of the driving frequency ω. The phase is then determined from

$$\sin\theta=\frac{-2\omega a\bar{h}(a)}{P} \quad ; \quad \cos\theta=\frac{a[\varpi_0^2(a)-\omega^2]}{P} \qquad (5-27)$$

where,

$$\bar{h}(a)=\frac{1}{2\pi\omega_o a}\int_0^{2\pi} f(\omega_o a\sin\sigma)\sin\sigma\, d\sigma \qquad (5\text{-}28)$$

$$\bar{\omega}_o^2(a)=\omega_o+\frac{1}{\pi a}\int_0^{2\pi}\epsilon g(a\cos\sigma)\cos\sigma d\sigma \qquad (5\text{-}29)$$

where σ is an integration variable.

5.4 NUMERICAL STUDY

The equation of motion of a nonlinear oscillator does not lend itself easily to analytical study. Therefore, a numerical study of some particular cases of equation (5-22) was carried out.

A program was first used (NL1) to generate synthesised data for a given set of system parameters. In order to detect the effect of the nonlinear component, different sets of data were generated while only one parameter was changed at a time. The influence of two parameters was examined; the level of nonlinearity and the magnitude of the exciting force.

The generated data were displayed in three formats, (i) log modulus (mobility) vs. frequency, (ii) phase vs. frequency and (iii) response locus in the polar plane (the Nyquist plot). Thus, a visual check enabled us to identify the way in which the small nonlinearity affects the response of the linear system.

Next, the data were analysed using a linear modal identification program (POLAR5). The variation in the derived modal parameters gave us some quantitative measure as to the sensitivity of the linear modal identification algorithm to small nonlinearities in the analysed data.

Finally, the change in the derived M loss factor as function of $\omega_2-\omega_1$ was examined.

5.4.1 DRY FRICTION

The equation of motion of an oscillator with both dry friction and linear viscous damping is,

$$\ddot{x}+2h\dot{x}+R\frac{\dot{x}}{|\dot{x}|}+\omega_o^2 x=P\cos\omega t \qquad (5\text{-}30)$$

By applying the method of equivalent linearization, an equation is derived* for the resonance curve, i.e

$$\left(\frac{\omega^2-\omega_o^2}{P}\right)^2 a^2+\left(\frac{2\omega ha}{P}+\frac{\omega}{\omega_0}d\right)^2=1 \qquad (5\text{-}31)$$

The phase is obtained from

$$\sin\theta=\frac{-2\omega ah}{P}-d\frac{\omega}{\omega_o} \quad ; \quad \cos\theta=\frac{a}{P}(\omega^2-\omega_o^2) \qquad (5\text{-}32)$$

where

$$d=\frac{4R}{\pi P} \quad \geq 0 \qquad (5\text{-}33)$$

This an approximate solution which is sufficiently accurate only in the neighbourhood of the resonance. The underlying simplifying hypothesis is that R is small enough for the motion to proceed without pauses. The maximum magnitude of R at any frequency is limited by:

$$R<a\omega^2 \qquad (5\text{-}34)$$

Sets of data were generated for two cases; (i) maintaining a constant excitation force and changing the

---

*See ref 75 for detailed analysis of each nonlinear case.

amount of friction force R, (ii) keeping the friction force constant and changing the level of excitation.

Plots of mobility and phase for case (i) are shown in Fig. 5-9. It is clearly seen that an increase in the level of friction reduces the level of the response, as expected, and increases the phase difference between the real and imaginary parts of it.

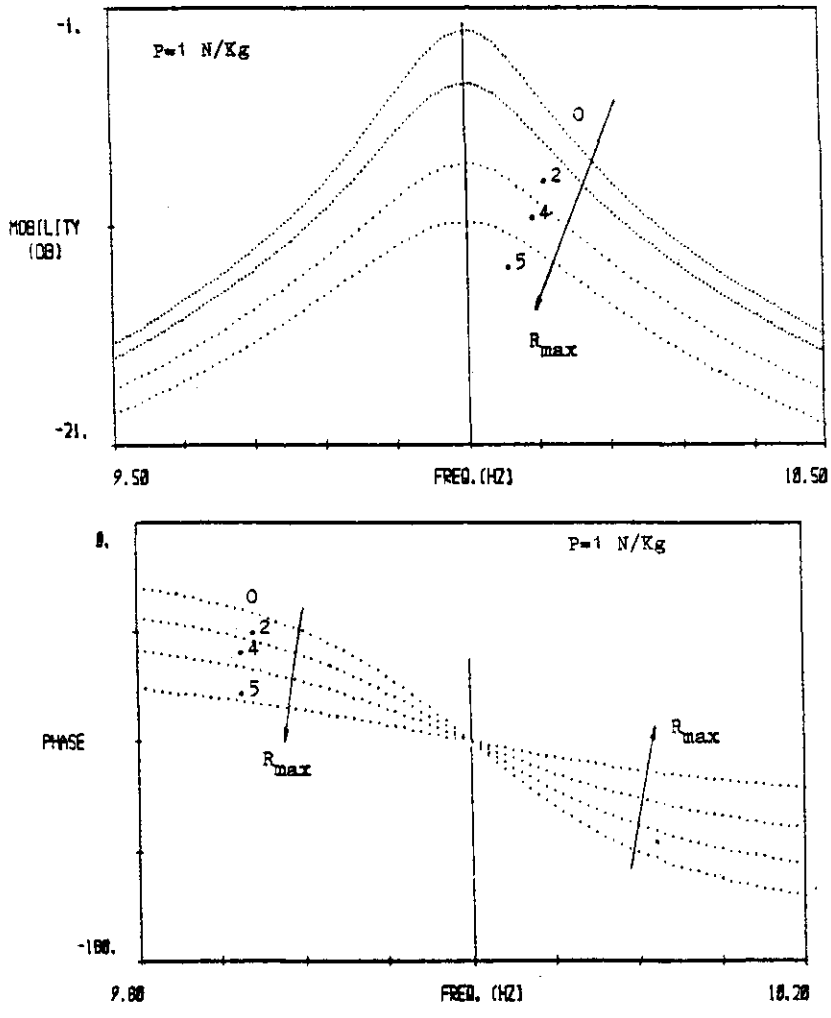

Fig. 5-9: mobility (a) and phase (b) for varying levels of dry friction.

However, the shape of each individual curve, when examined separately, does not reflect the presence of dry friction.

The corresponding Nyquist plots (Fig. 5-1Ø) reveal immediately the existence of the nonlinearity; it is very clear that the circular shape of the plot for the linear case (R=Ø) is gradually transformed into an 'egg shape' as friction in the system is increased. A visual examination of these 'egg shaped' plots shows that there is no distortion in the angular spacing of equally-spaced frequency points and that the natural frequency of the system is still at the point where the angular spacing is maximum and the real part of the response is zero.

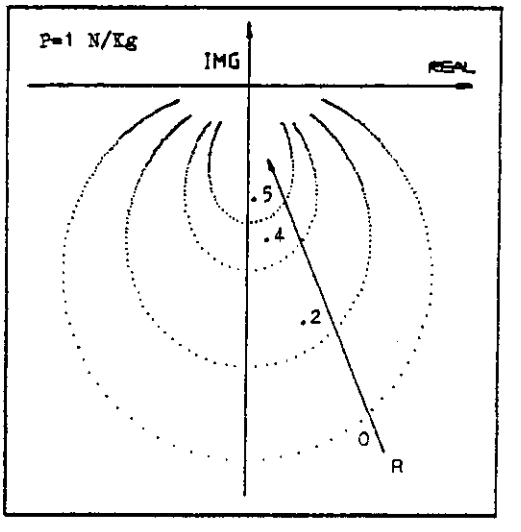

Fig. 5-1Ø: Nyquist plots for varying levels of dry friction.

The results of a linear modal identification of these data is summarized in Table 5-1.

Because dry friction has only an effect on the modulus and the phase of the response and does not affect the

angular spacing of the response points, the natural frequency and the modal phase angle are identified correctly regardless of the level of damping. On the other hand, the modal constant and the modal loss factor are distorted severely and for low levels of damping (R=Ø.2 N/Kg), the error in the modal constant is about 25%. The identified modal loss factor does not reflect the linear loss factor because dry friction acts as an additional damping in the system.

R N/Kg	ω Hz	η	A m/N	θ deg	J
.2	9.9993	(K) .0230 (M) .0229	.7424 .7411	.03	.603
.4	9.9995	(K) .0275 (M) .0267	.4555 .4425	-1.33	.313
.5	10.0115	(K) .0320 (M) .0303	.3391 .3210	-11.25	.199
linear	10.0	.020	1.0	0.0	1.0

Table 5-1: Dry friction - modal parameters for varying levels of friction.

The M loss factor, η_M, was calculated for different combinations of frequency points and Fig. 5-11 shows the variation in the derived results as a function of $\Delta\omega$ ($\Delta\omega=\omega_2-\omega_1$ where $\omega_2-\omega_o=\omega_o-\omega_1$). It is seen that the variation is very small for low levels of friction and as the friction is increased there is a decrease in the calculated M loss factor as $\Delta\omega$ is increased.

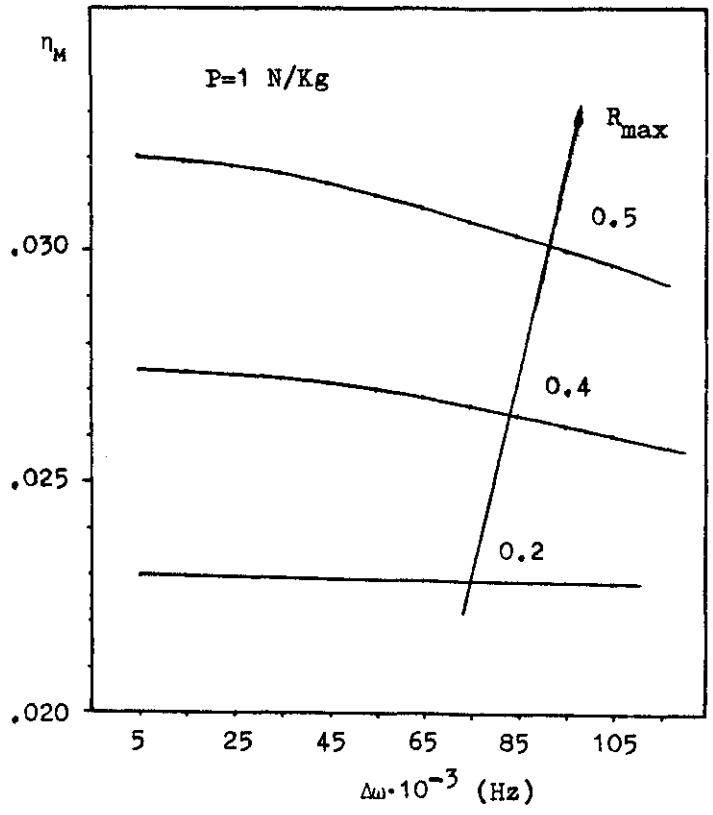

Fig. 5-11: Variation of the M loss factor as function of $\Delta\omega$ for varying levels of dry friction.

(ii) A second set of frequency responses was generated for a constant level of friction and varying levels of excitation.

Figures 5-12 and 5-13 describe the mobility, phase and Nyquist plots for these sets. It is seen that the general shape of all the curves is similar to those of the previous case. It is also noticed that as the level of excitation is increased the response gets closer to the linear one. The linearity check by calculating different M loss factors (Fig. 5-14) produces the same pattern. A full set of results of a linear modal identification algorithm is summarized in Table 5-2.

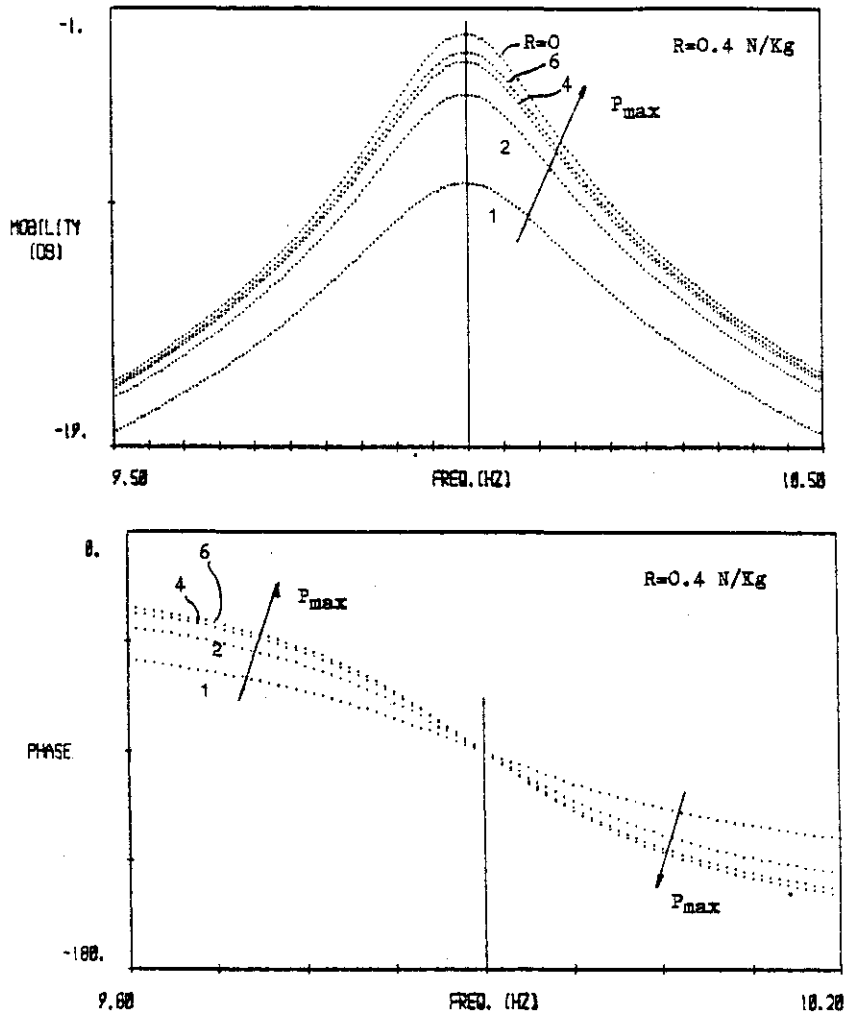

Fig. 5-12: Mobility & phase plots for varying levels of excitation.

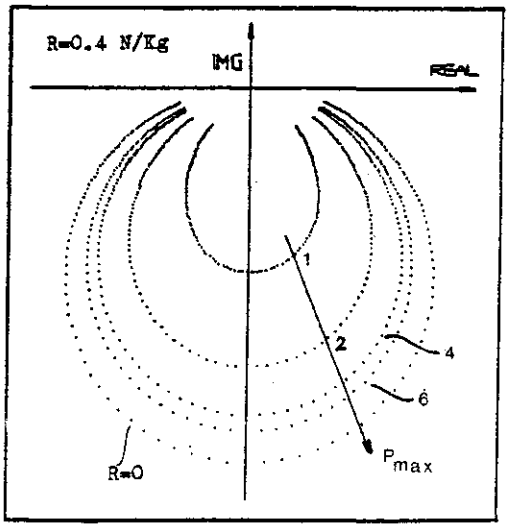

Fig. 5-13: Nyquist plots for varying levels of excitation

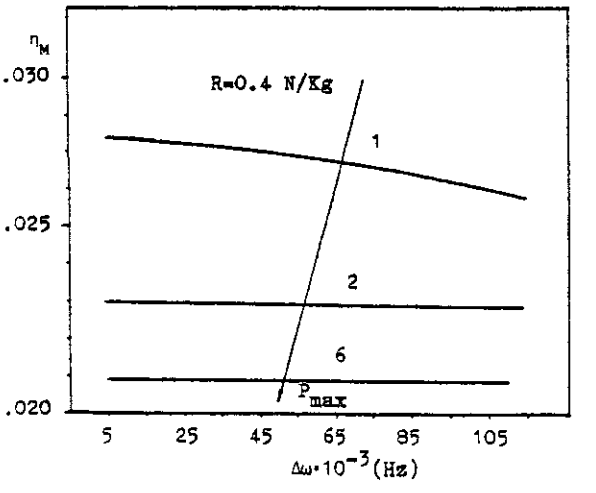

Fig. 5-14: η_M as function of $\Delta\omega$ for varying levels of excitation

P N/Kg	ω Hz	η	A m/N	θ deg	J
1	9.9955	(K) .0274 (M) .0271	.4518 .4469	1.72	.313
2	9.9980	(K) .0230 (M) .0229	.7345 .7323	1.22	.598
4	9.9993	(K) .0217 (M) .0217	.8949 .8949	.43	.779
6	9.9990	(K) .0209 (M) .0209	.9157 .9157	.68	.847
linear	10.0	.020	1.0	0.0	1.0

Table 5-2: Dry friction - modal parameters for varying levels of excitation.

We may conclude that the effect of an increase in the excitation level is equivalent to reduction in the level of dry friction and in practical cases, when it is suspected that dry friction may affect the measured results, it is possible to reduce its effect by raising the level of excitation.

When only one set of measured data is available, the only form of display which might indicate the presence of dry friction is the Nyquist plot - the expected circular shape is then distorted into 'egg shape'. As the M loss factor is relatively insensitive to changes in $\Delta\omega$ it cannot serve as a good indication for the existence of dry friction nonlinearity.

5.4.2 CUBIC STIFFNESS

The forced vibration of an oscillator with linear viscous damping and cubic stiffness is governed by the equation:

$$\ddot{x}+2h\dot{x}+\omega_o^2 x(1+bx^2)=P\cos\omega t \qquad (5\text{-}35)$$

which is also known as the generalized Duffing's equation with damping. This equation has been studied by many investigators (i.e [54]) but so far exact solutions are known only for particular values of ω_o, b and P.

By applying the method of equivalent linearization, we can derive an equation for the resonance curve:

$$(\omega_o^2-\omega^2+\frac{3}{4}b\omega_o^2a^2)^2+4h^2\omega^2=\left(\frac{P}{a}\right)^2 \qquad (5\text{-}36)$$

and the corresponding phases,

$$\sin\theta=\frac{-2\omega ha}{P} \quad ; \quad \cos\theta=\frac{a}{P}(\omega_o^2-\omega^2+\frac{3}{4}b\omega_o^2a^2) \qquad (5\text{-}37)$$

The resonance curve described by equation (5-36) exhibits a well-known phenomenon: for small levels of cubic stiffness and constant excitation force the curve (Fig. 5-15) tends to lean slightly (curve a). Above a certain level of cubic stiffness there seems to exist (curve b) three simultaneous different levels of response amplitudes within a certain region of excitation frequencies. Practically, this multiple response cannot exist and in a real system when the exciting frequency is increased gradually the response curve follows path OAC and

then 'jumps' to point D. If the frequency is decreased gradually the response follows path FDB and then 'jumps' to point A. We see clearly that the branch CB is practically

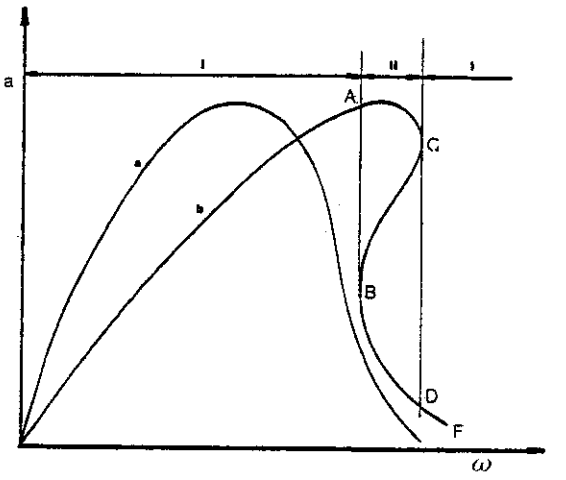

Fig. 5-15: Typical response of a system with cubic stiffness.

unattainable. The behaviour just described applies for positive value of b and is referred to as 'cubic hardening stiffness'. When $b<0$, the system behaves in a similar manner but then the curve leans backwards. This system is referred to as having 'cubic softening stiffness'.

Sets of synthesised data were generated for three cases:
(i) Constant level of excitation and varying levels of hardening cubic stiffness.
(ii) constant level of excitation and varying levels of softening cubic stiffness.
(iii) Constant hardening cubic stiffness and varying levels of excitation.

The mobility and phase plots for case (i) are given in Fig. 5-16. It is clearly noticed that as cubic stiffness in

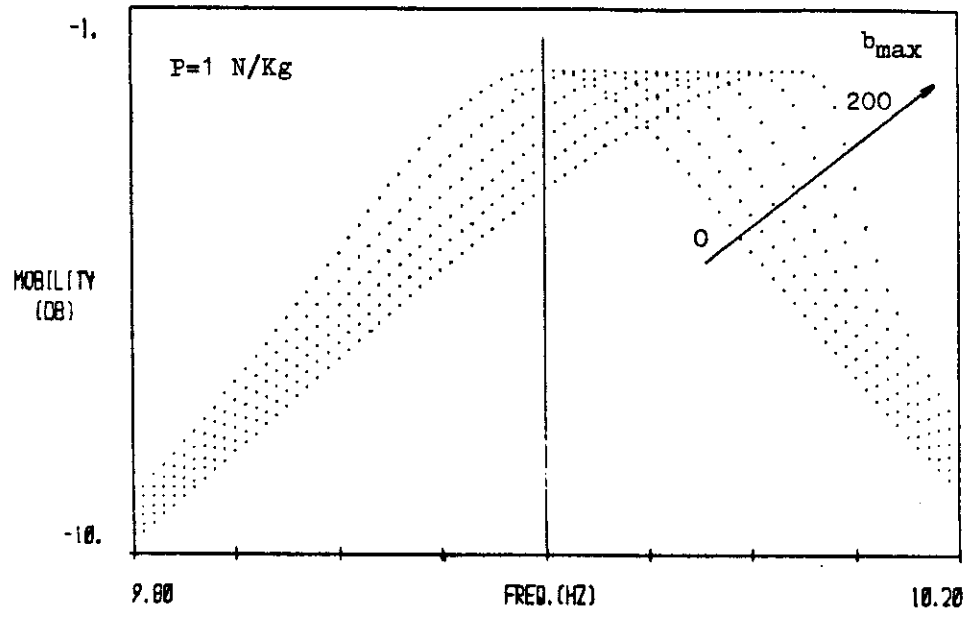

(a)

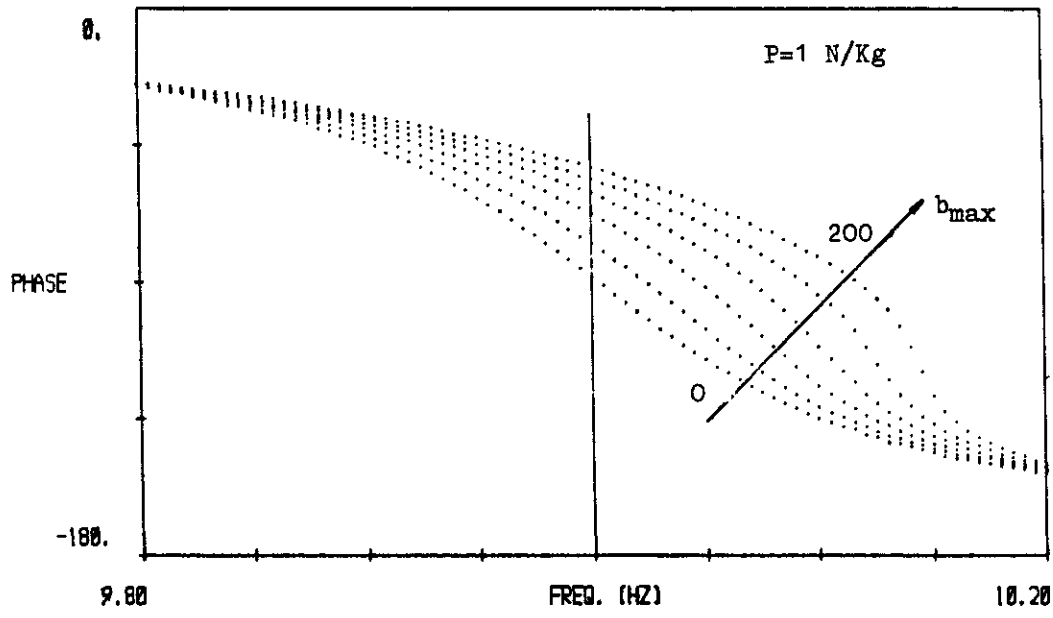

(b)

Fig. 5-16: Mobility (a) and phase (b) plots for varying levels of hardening cubic stiffness.

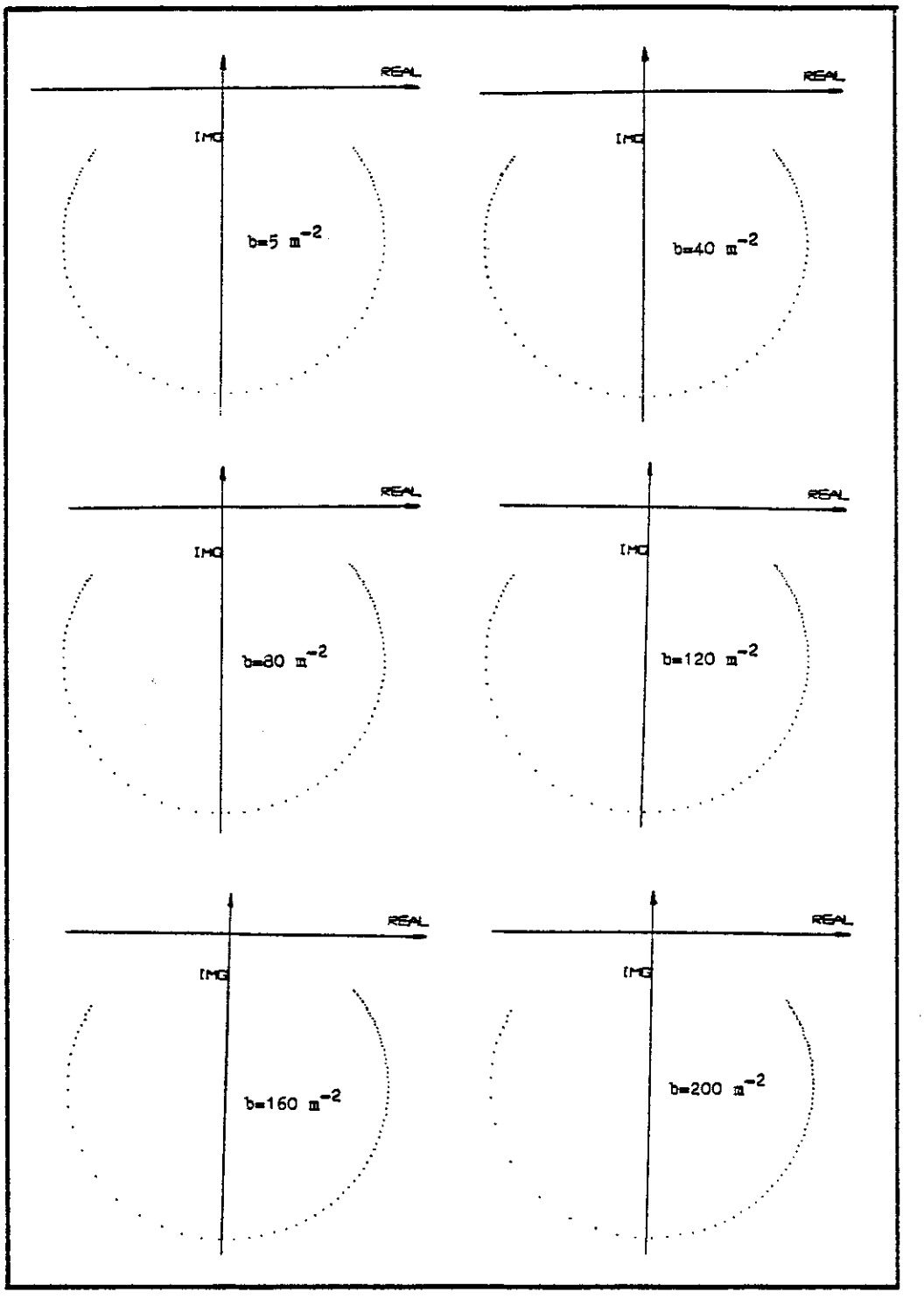

Fig. 5-17: Nyquist plots for varying levels of hardening cubic stiffness

the system is increased the mobility curve leans forward without changing the level of the response. There is also a distinct change in the phase plot which is no longer symmetrical as for the linear system. Examination of the corresponding family of Nyquist plots (Fig. 5-17) indicates that there is no apparent change in the circular shape of the plot and, as also noticed in the mobility curve, no change in the magnitude of the response. A closer look, however, reveals that the angular spacing of the points is changed: as the cubic stiffness is increased, the maximum spacing moves in a clockwise direction.

Despite these clear changes in the plots, when one examines a single plot, especially as part of a multi-degree of freedom system, the existence of nonlinear stiffness is not so immediately obvious, because there is no way to distinguish it from a response of anonproportionally-damped system. This fact is demonstrated when these sets of data are analysed by a linear identification algorithm (Table 5-3).

b m^{-2}	ω Hz	η	A m/N	θ deg	J
5	10.0060	(K) .0200 (M) .0200	.9990 .9979	-3.74	.995
40	10.0433	(K) .0189 (M) .0193	.9524 .9712	-23.22	.863
80	10.0755	(K) .0165 (M) .0176	.8350 .8918	-36.29	.577
120	10.1018	(K) .0134 (M) .0155	.6827 .7921	-44.92	.306
160	10.1238	(K) .0100 (M) .0132	.5110 .6728	-50.02	.125
200	10.1433	(K) .0065 (M) .0116	.3355 .5940	-52.53	.036
0.0	10.0	.020	1.0	0.0	1.0

Table 5-3: Hardening cubic stiffness - modal parameters for varying b and constant excitation force.

Because the angular spacing of the points is distorted the identified modal phase angle is greatly in error and as a consequence, all the other modal parameters are wrongly identified. When a single set of data is analysed in this manner, there is no clear indication of the nonlinearity and the final conclusion may as well be that the analysed mode is a complex one. However, calculation of the M loss factor, η_M, for different values of $\Delta\omega$ (Fig. 5-18) exhibits a distinct pattern; as the cubic stiffness is increased the value of η_M becomes increasingly sensitive to changes in $\Delta\omega$. The calculated value for any level of cubic stiffness is always lower then the correct one. We may say that the only means of checking for cubic stiffness nonlinearity in a single curve is by calculation of the M loss factor as function of $\Delta\omega$.

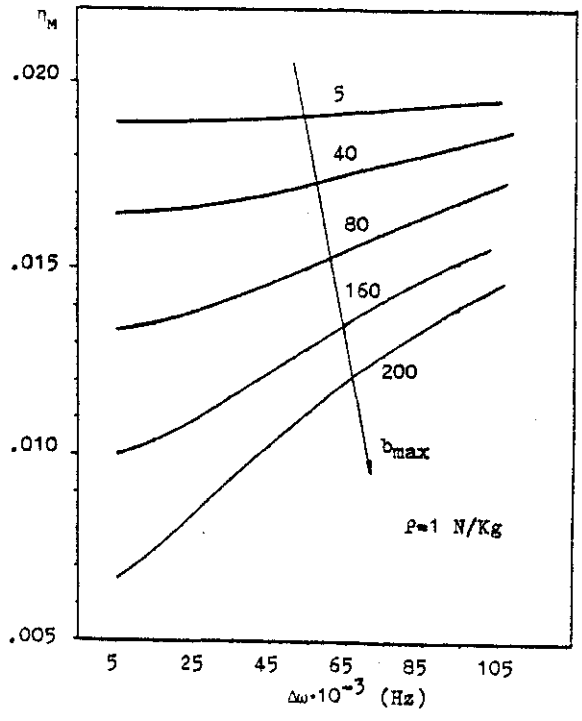

Fig. 5-18: Variation in M loss factor as function of $\Delta\omega$ for varying levels of hardening cubic stiffness

Figure 5-19 shows the mobility, phase and Nyquist plots for a softening cubic stiffness system. It is noticed clearly that this case is an exact mirror image of the corresponding hardening cubic stiffness case. As the softening cubic stiffness is increased, the mobility curve leans further and further backwards and the maximum angular spacing moves in an anticlockwise direction.

The linearly-identified modal parameters (Table 5-4) are also distorted; the values of the natural frequencies are lower then for the linear case and the modal phase angle is changed in the opposite direction to that of the hardening cubic stiffness case.

b m^{-1}	ω Hz	η	A m/N	θ deg	J
-40	9.9548	(K) .0190 (M) .0193	.9431 .9589	24.68	.856
-80	9.9215	(K) .0165 (M) .0175	.8109 .8641	38.39	.555
-160	9.8715	(K) .0092 (M) .0131	.4465 .6367	51.93	.097
linear	10.0	.020	1.0	0.0	1.0

Table 5-4: Softening cubic stiffness - modal parameters for varying b and constantexcitation force.

The variation in the M loss factor as function of $\Delta\omega$, however, does not change its direction; as the softening cubic stiffness is increased, its value becomes more and more sensitive to changes in $\Delta\omega$.

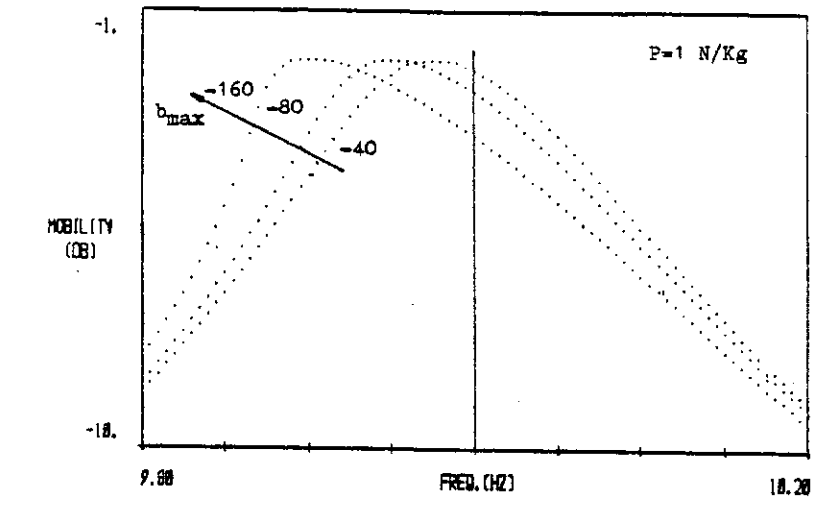

(a)

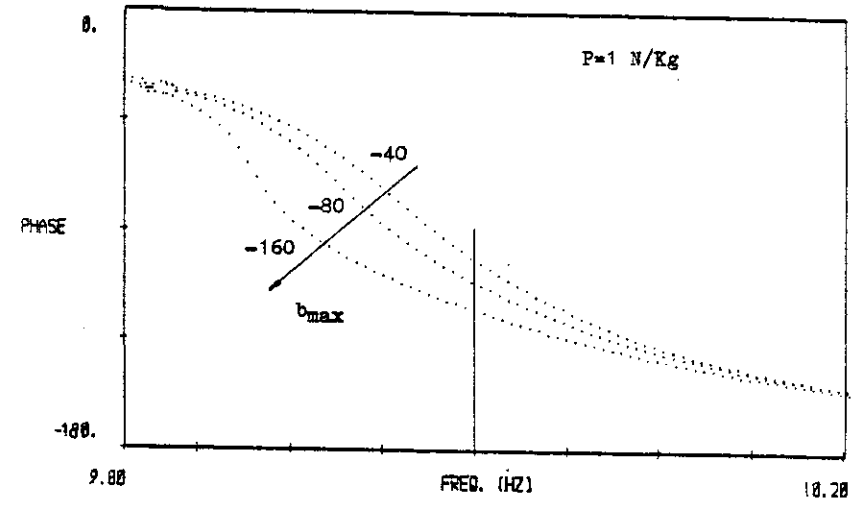

(b)

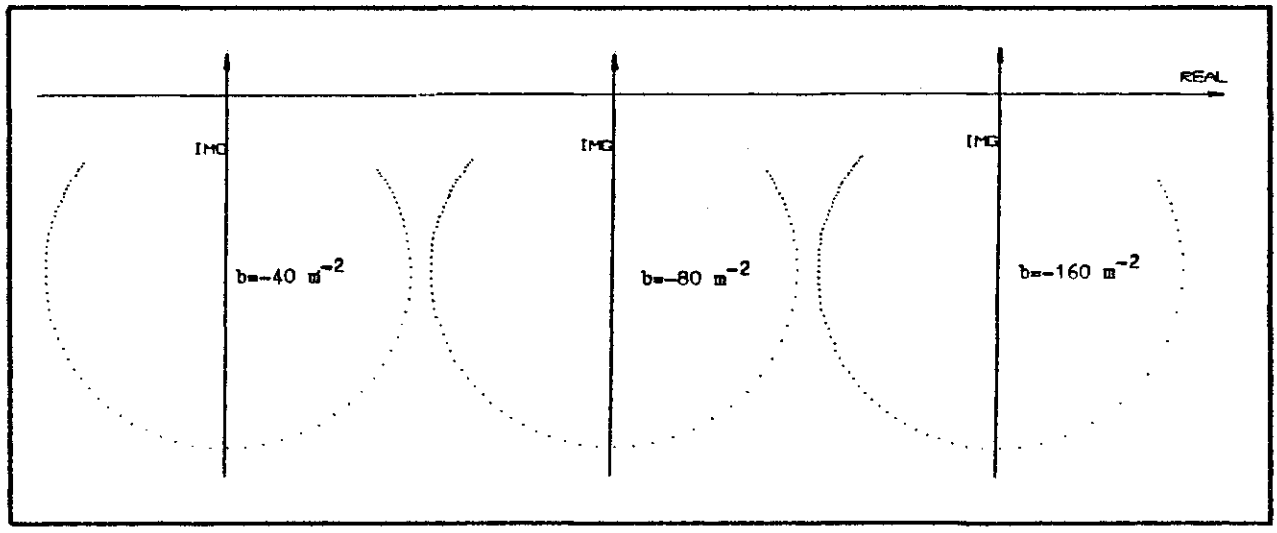

(c)

Fig. 5-19; Mobility (a), phase (b) and Nyquist (c) plots for varying levels of softening cubic stiffness

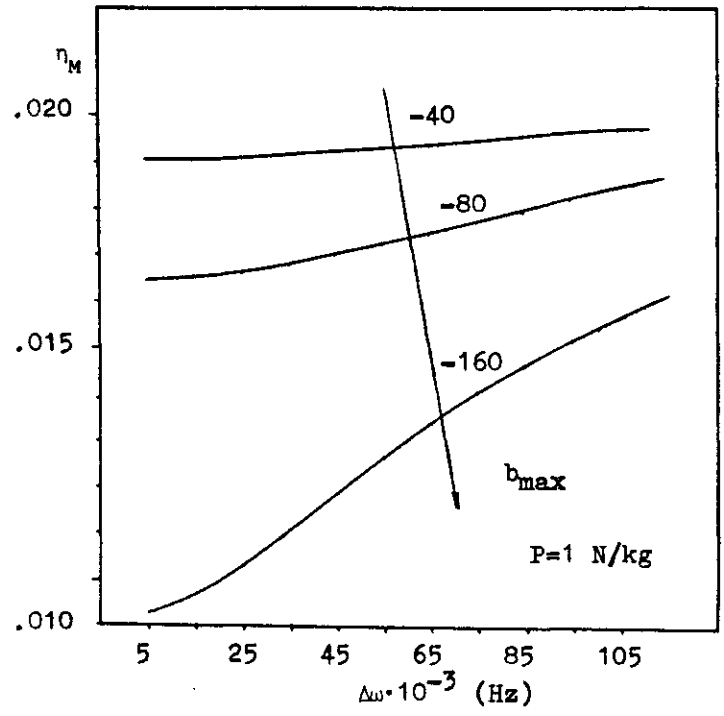

Fig. 5-20: Variation of the M loss factor as function of $\Delta\omega$ for varying levels of softening cubic stiffness.

For the third case, where the hardening cubic stiffness is kept constant and the level of excitation force is increased, the behaviour of the system (Fig. 5-21) has the same pattern as for the case of increase in the level of the hardening cubic stiffnes. The distortion of the linearly identified modal parameters is similar (Table 5-5) and the sensitivity of the M loss factor to changes in $\Delta\omega$ is increased as the excitation level is increased (Fig. 5-22)

It has been clearly shown that addition of a small cubic stiffness nonlinearity severely affects the linear response of the system in the vicinity of a resonance and,

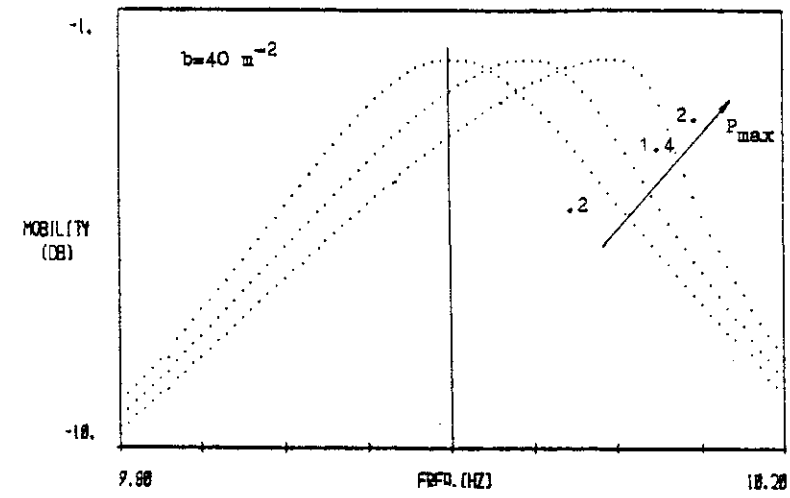

(a)

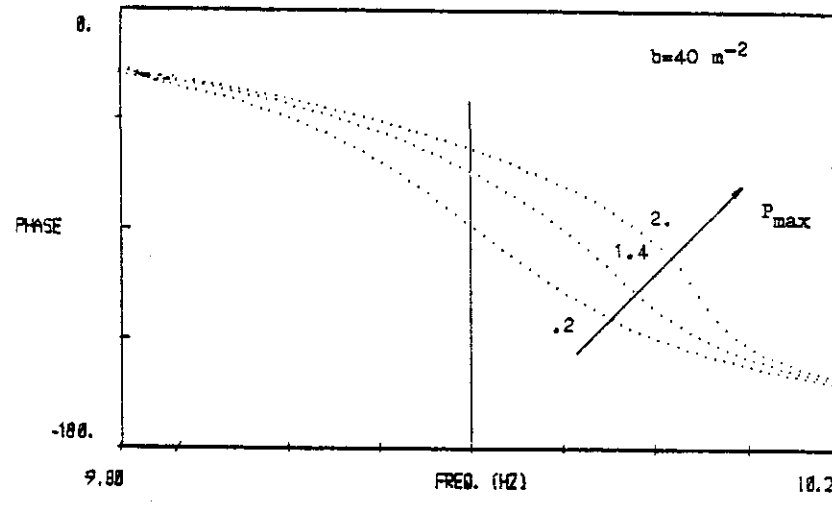

(b)

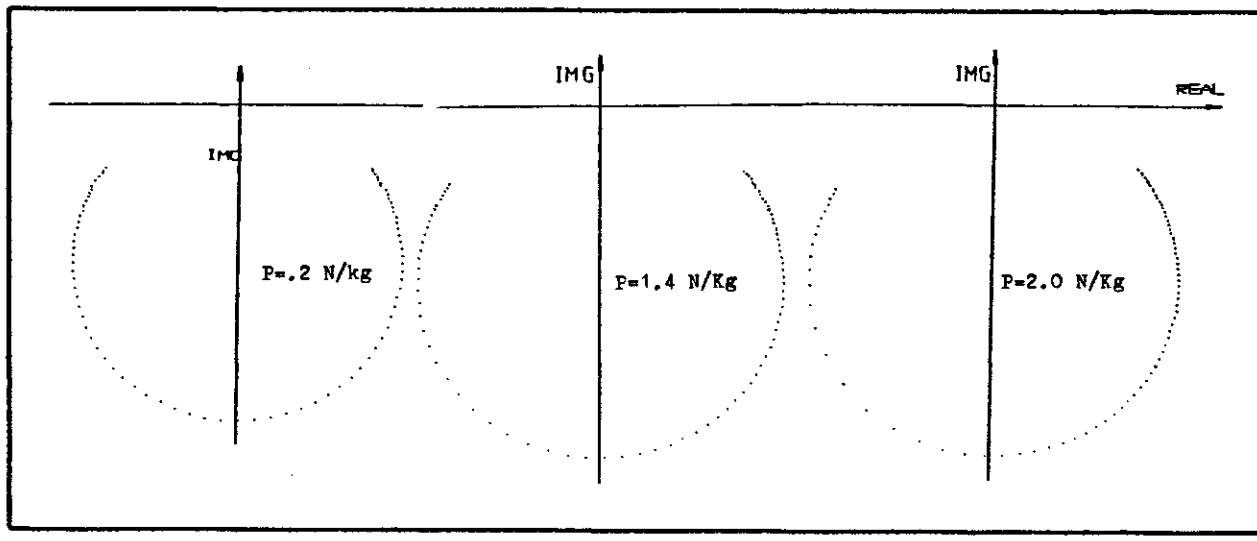

(c)

Fig. 5-21: Mobility (a), phase (b) and Nyquist (c) plots for varying levels of excitation

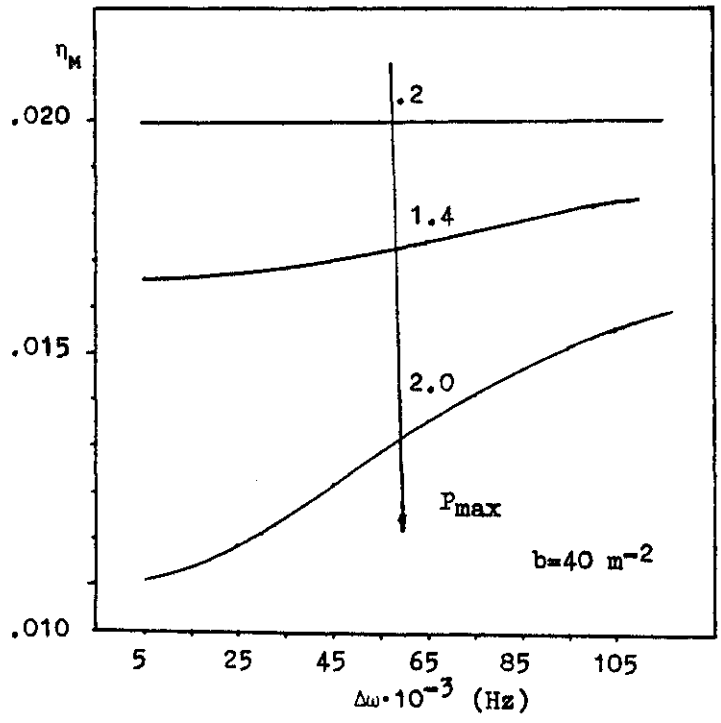

Fig. 5-22: Variation of M loss factor as function of $\Delta\omega$ for varying levels of excitation

P N/Kg	ω Hz	η	A m/N	θ deg	J
.2	10.0015	(K) .0201 (M) .0201	1.007 1.007	-.93	.988
1.4	10.0748	(K) .0166 (M) .0175	.8411 .8893	-36.43	.589
2.0	10.1238	(K) .0100 (M) .0133	.5126 .6819	-49.98	.125
linear	10.0	.020	1.0	0.0	1.0

Table 5-5: Hardening cubic stiffness - modal parameters for varying levels of excitation force

consequently, all the identified modal parameters are distorted, the modal phase angle suffering the most.

We see that, for a given system, the effect of an increase in the level of excitation is equivalent to an increase of the level of cubic stiffness. The practical conclusion that we may draw from this result is that in order to minimize the effect of cubic stiffness nonlinearities we should drive the test structure at the lowest possible level of excitation which can still provide acceptable measured data.

When only one set of measured data is available it is impossible to detect the presence of cubic stiffness nonlinearity by visual examination of any of the conventional plots; the only means to this end is the calculation of the M loss factor as a function of $\Delta\omega$, as this changes very rapidly when the level of cubic stiffness is increased.

5.4.3 QUADRATIC VISCOUS DAMPING

When the flow of the liquid in a viscous hydraulic damper is turbulent rather then laminar, the damping of the component may be described by quadratic viscous damping. The equation of motion for such a system under the action of a simple harmonic excitation is:

$$\ddot{x}+c\dot{x}|\dot{x}|+\omega_o^2 x=P\cos\omega t \qquad (5-38)$$

The resonance curve and phase are derived by the application of the method of equivalent linearization i.e

$$(\omega_o^2-\omega^2)^2+\left(\frac{8c\omega_o\omega a^2}{3\pi}\right)=\left(\frac{P}{a}\right)^2 \qquad (5-39)$$

$$\sin\theta=\frac{-8c\omega_o\omega a^2}{3\pi P} \quad ; \quad \cos\theta=\frac{a}{P}(\omega_o^2-\omega^2) \qquad (5-40)$$

If we remove the nonlinear component from equation (5-38) the linear equation is undamped and the comparison between the cases is not simple. Nevertheless, by changing the quadratic damping coeffecient and the force level we are able to demonstrate the influence of the nonlinearity on the analysis process.

The mobility, phase and Nyquist plots for these two cases are shown in Figures 5-23 and 5-24. It is noticed that as the level of quadratic viscous damping is increased, the amplitude of the response is decreased without affecting the position of the resonance point. The Nyquist plot, however, is severely distorted into an 'apple shape' but, still, without significantly affecting the angular spacing of the points.

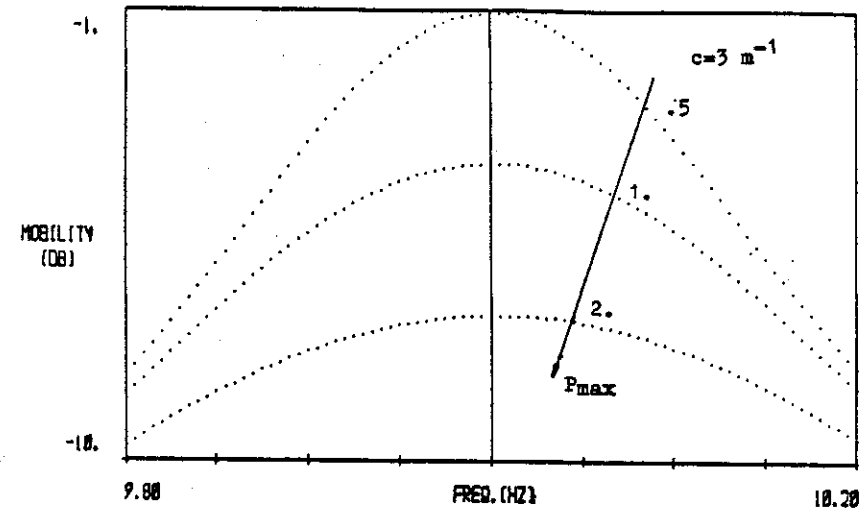

(a)

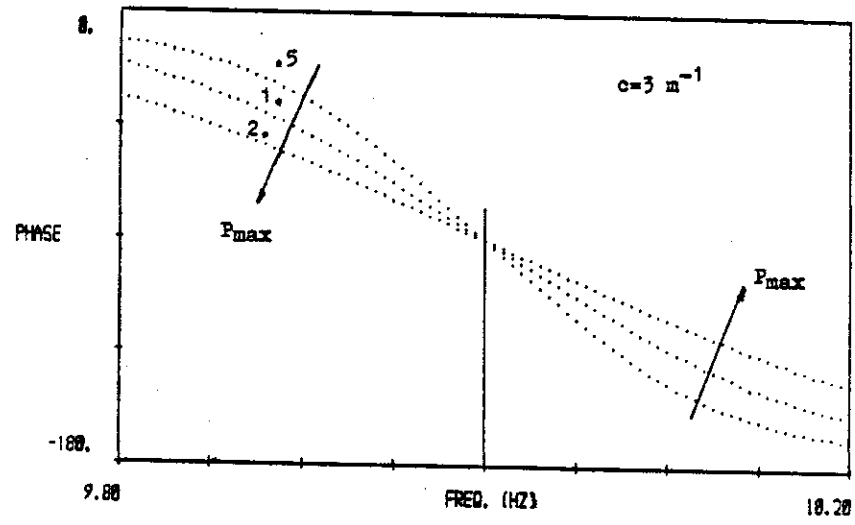

(b)

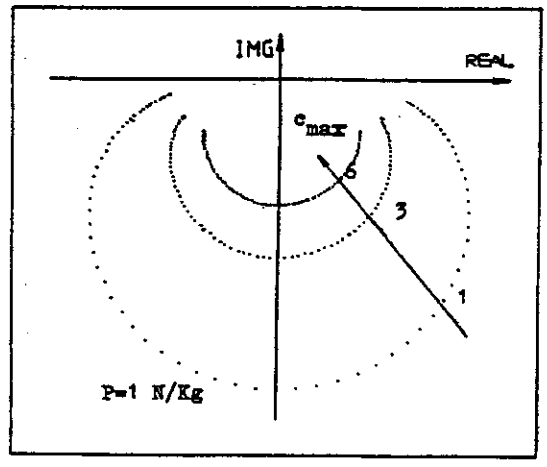

(c)

Fig. 5-23: Mobility (a), phase (b) and Nyquist (c) plots for varying levels of quadratic viscous damping

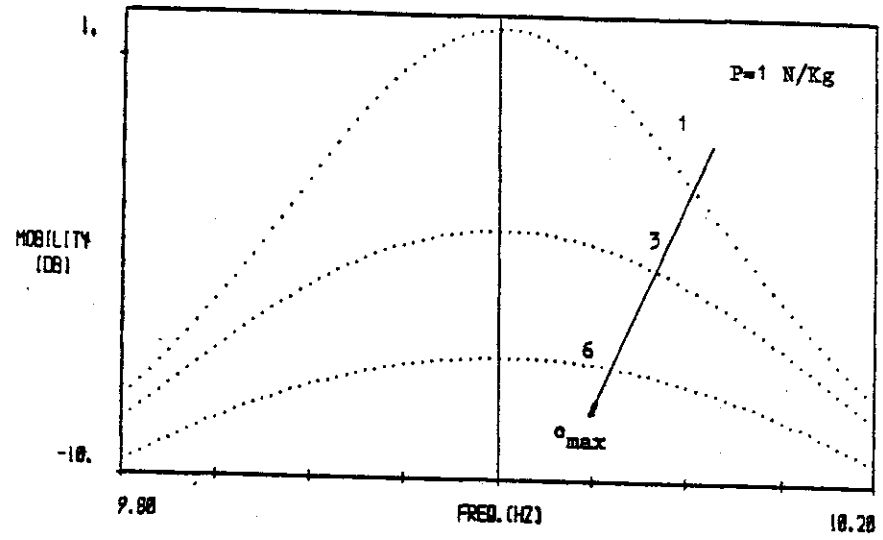

(a)

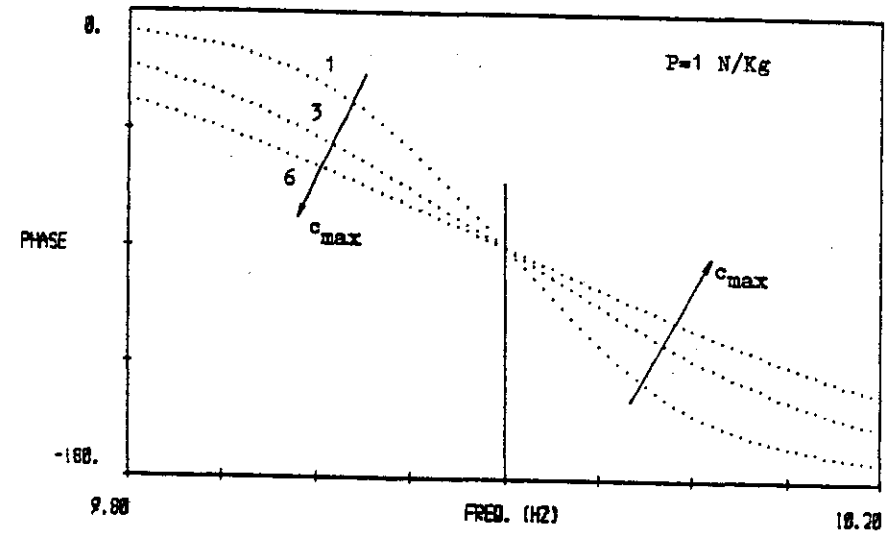

(b)

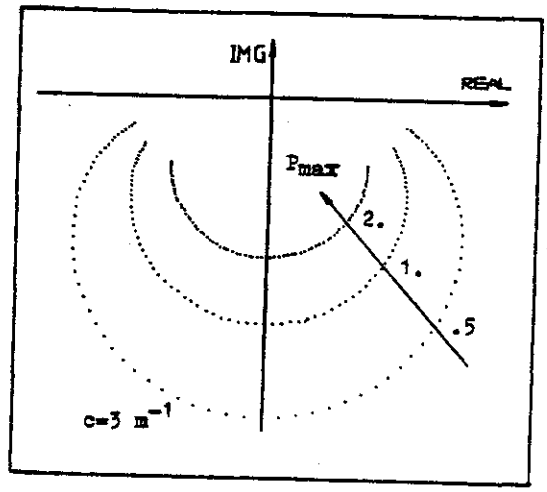

(c)

Fig. 5-24: Mobility (a), phase (b) and Nyquist (c) plots for varying levels of excitation and constant quadratic viscous damping

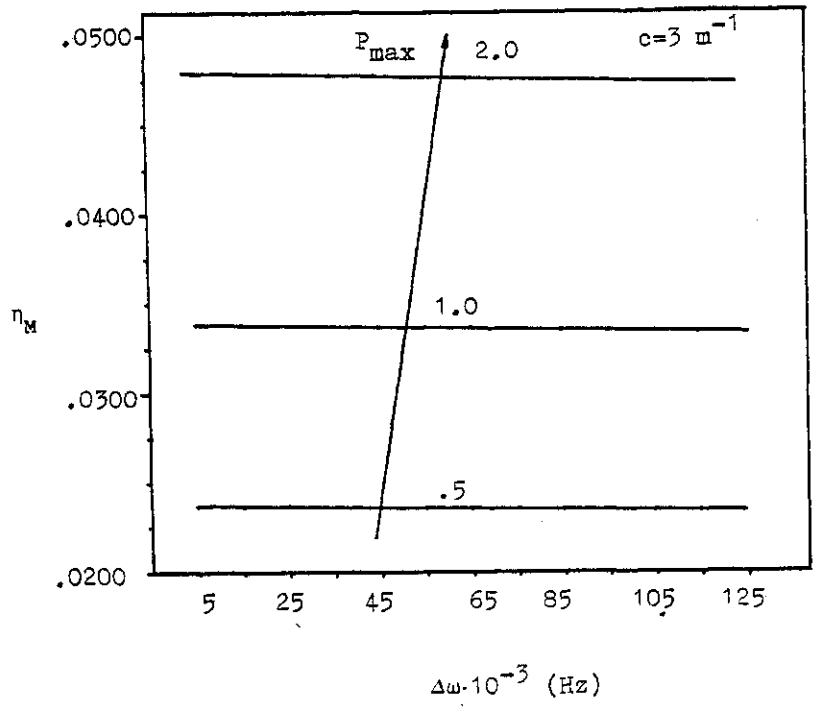

(a)

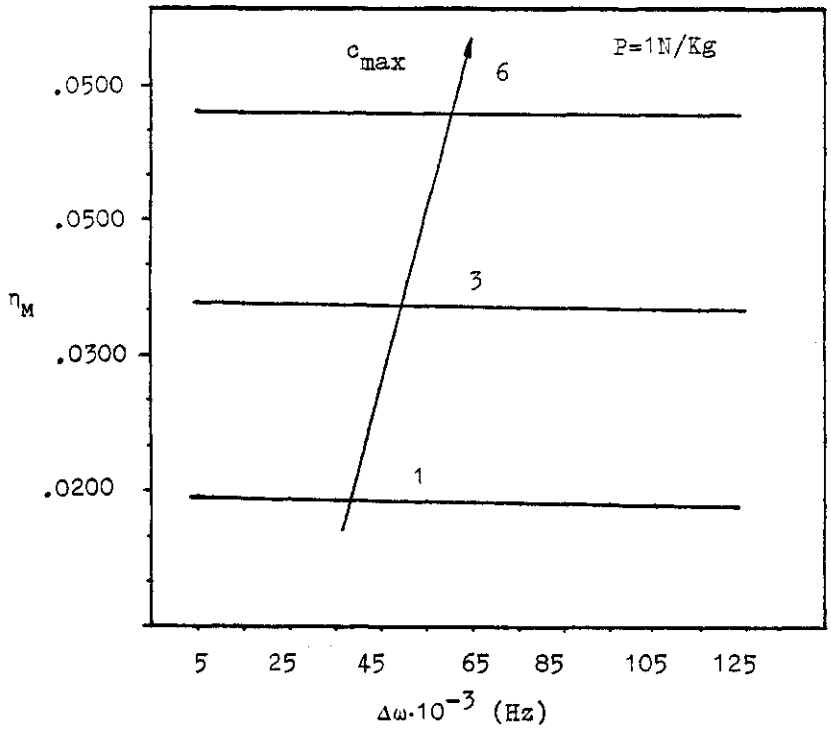

(b)

Fig. 5-25: Quadratic viscous damping - variation in M loss factor for varying levels of excitation (a) and for varying levels of damping (b)

It is clear from these plots that an increase in the level of excitation is equivalent to an increase in the level of quadratic damping which means in practice that by maintaining a low level of excitation, the measured data of a real system are least affected by the nonlinearity.

When only a single curve is available the nonlinearity is readily detected from the distortion of the Nyquist plot. The check for nonlinearity by calculating the M loss factor as function of $\Delta\omega$ is not informative in this respect (Fig. 5-25).

5.4.3.1 QUADRATIC VISCOUS DAMPING PLUS DRY FRICTION.

When dry friction is added to the previous system the governing equation is:

$$\ddot{x}+c\dot{x}|\dot{x}|+R\frac{\dot{x}}{|\dot{x}|}+\omega_o^2 x=P\cos\omega t \qquad (5-41)$$

The resonance curve and the phase are derived by usage of the method of equivalent linearization, i.e

$$(\frac{a}{P})^2(\omega_o^2-\omega^2)^2+(\frac{8c\omega_o\omega a^2}{3\pi P}+d\frac{\omega}{\omega_o})^2-1=\emptyset \qquad (5-42)$$

$$\sin\theta=\frac{-8c\omega_o\omega a^2}{3\pi P}-d\frac{\omega}{\omega_o}$$

$$\cos\theta=\frac{a}{P}(\omega_o^2-\omega^2) \qquad (5-43)$$

where,

$$d=\frac{4R}{\pi P}>\emptyset \qquad (5-44)$$

This system was examined for two cases: (i) varying levels of dry friction and (ii) varying levels of excitation force. The mobility, phase and Nyquist plots for these are

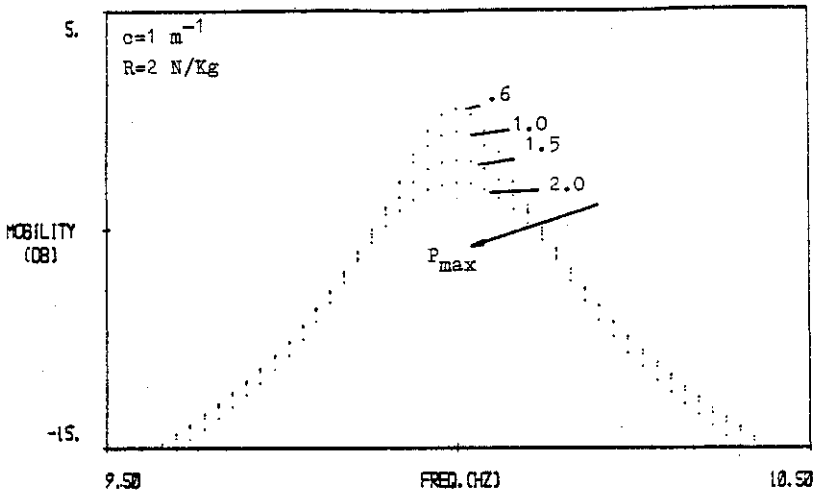

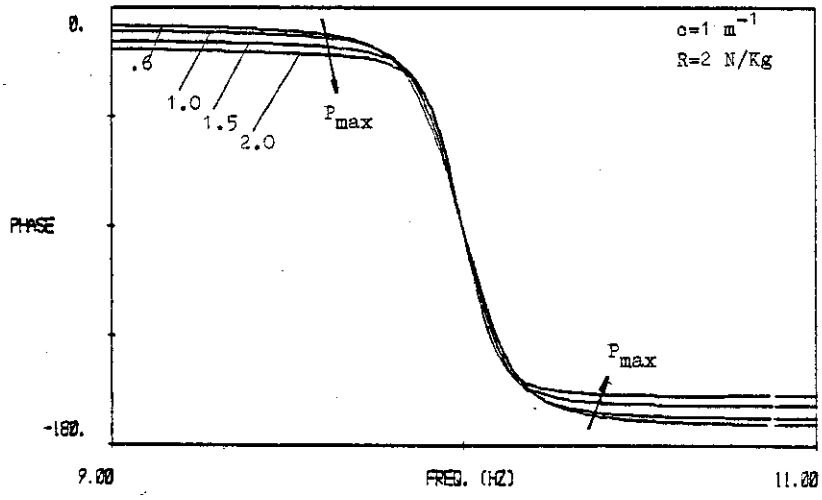

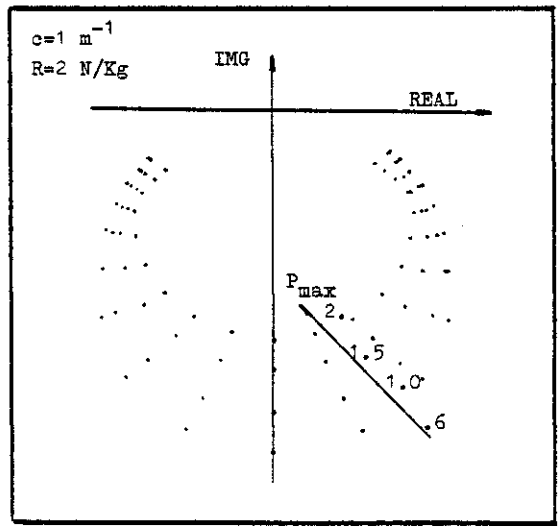

Fig. 5-26: Quadratic viscous damping + dry friction - modulus, phase and Nyquist plots for varying levels of excitation

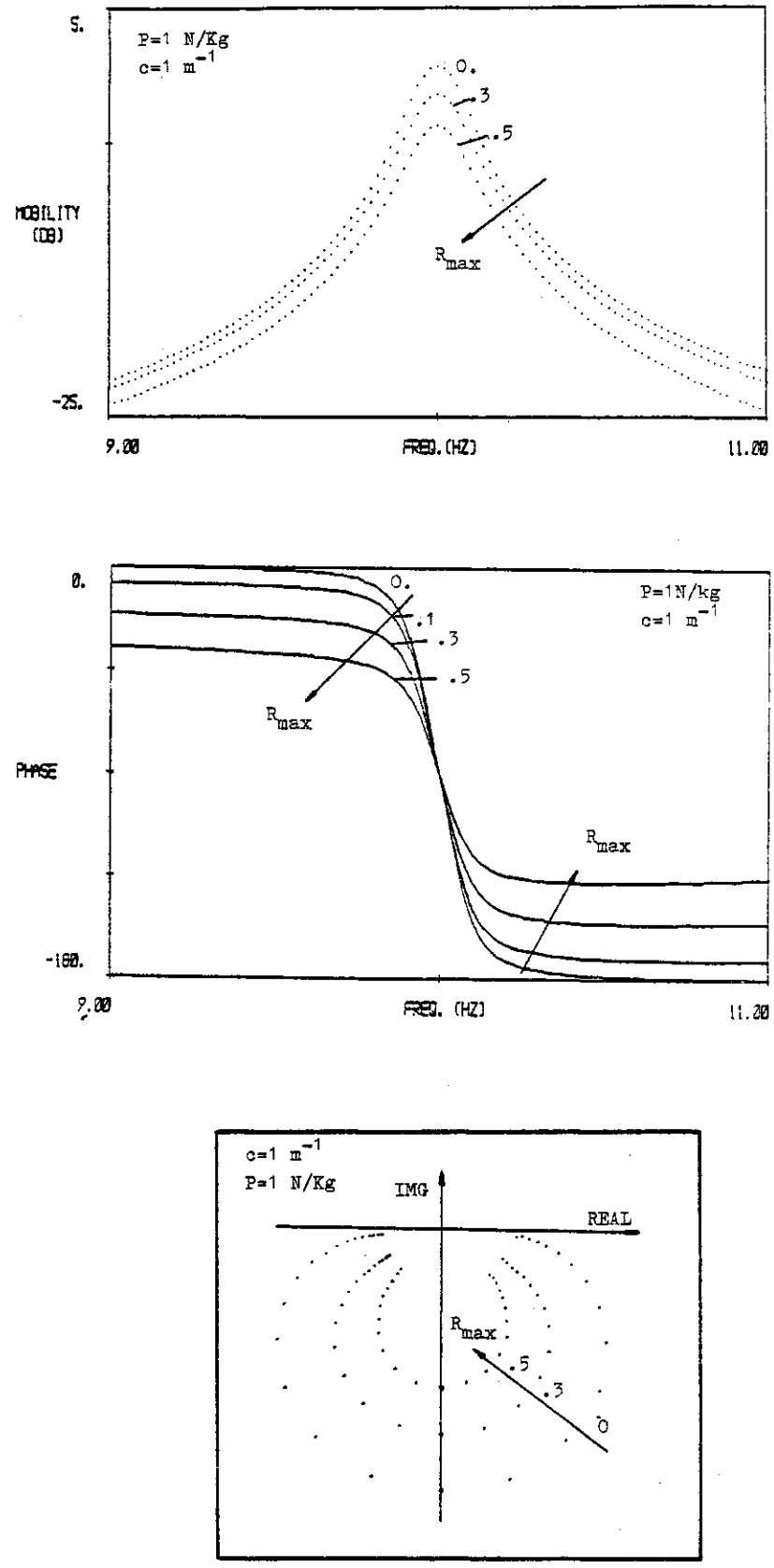

Fig. 5-27: Quadratic viscous damping + dry friction - modulus, phase and Nyquist plots for varying levels of dry friction

given in Figures 5-26 and 5-27. The changes in the mobility and phase plots are similar to those of the previous system. The Nyquist plot, however, is distorted in a somewhat different way; as the level of dry friction is increased, the 'apple-shaped' polar plot changes gradually into an 'egg-shaped' form or, as the level of excitation is increased, it changes from 'egg-shaped' to 'apple-shaped'. In both cases, this change passes through a perfect circular shape and in any case, when examining a single curve, distortion from the circular shape is not easily detected.

In practice, minimizing the nonlinear influence is very difficult to achieve because of the opposing demands on the forcing level; in order to minimize the effect of dry friction, the excitation level has to be increased: on the other hand, the effect of the quadratic viscous damping is then increased.

5.5 EXPERIMENTAL STUDY.

It is accepted that these simple types of nonlinearity cannot fully represent the behaviour of real structures. The nonlinearity of a practical structure is more complicated and at most can be described as some combination of these simple types.

However, examination of its measured responses can give us some indication as to the types or the dominant type of its nonlinearity and by application of the conclusions derived from the previous numerical study, we can minimize their effect on the measured results and the modal data extracted from them.

To this end, a mini modal survey was performed on a real structure where special attention was paid to the nonlinear aspects of its behaviour, its effect on the derived results and on ways to reduce its influence.

The structure tested was designed to contain many of the features common in helicopter construction which give rise to problems and uncertainties in the theoretical modelling stage, such as rivetted joints , asymmetry, stiffening ribs, honeycomb sandwich panels, heavy masses mounted on relatively flexible components etc. The complete structure is shown in Fig. 5-28. It is made of a 1x1m stiffened base plate, attached at eight points to the 'rigid' floor base of the laboratory, supporting a square-sectioned (although not symmetrical) tower some 1.3m tall. On top of this tower was mounted a heavy mass on three point pin-supported mounts.

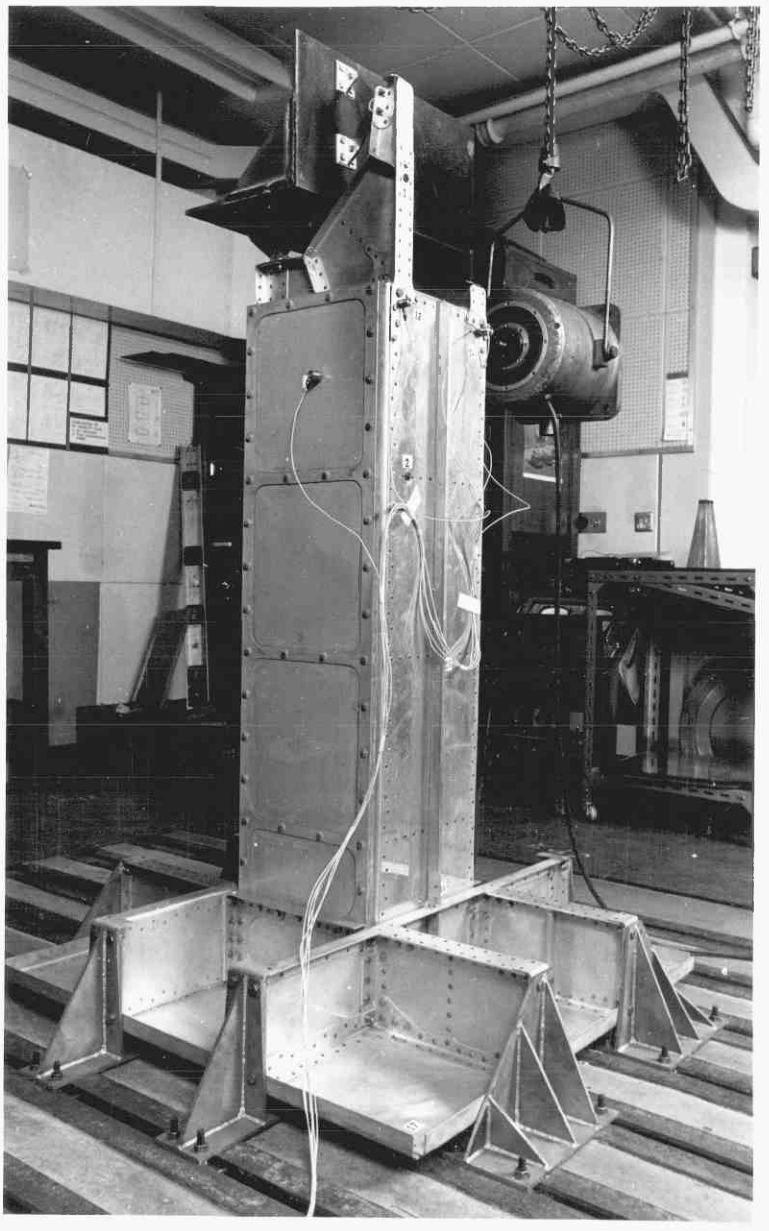

Fig. 5-28: The structure used for the studies of nonlinearities

One complete side of the tower section consisted of a light-weight honeycomb sandwich panel. The tower is described schematically in Fig. 5-29 showing the point where the excitation force was applied (point 12 direction x). The acceleration was measured at all the five points indicated and in the same direction.

The first step in this survey was a standard mobility measurement where force and acceleration levels were allowed to vary throughout the frequency range (optimal level control). The data were then analysed by SIM2 but the results were unsatisfactory; although presenting no apparent difficulty, the identified modal phase angles implied that the normal mode shapes of the tower were very complex but the complete curve fit showed large discrepencies between measured mobility and regenerated curve (Fig. 5-30).

This discrepency between analysis and measurement was attributed to nonlinear behaviour of the structure and a set of detailed measurements were made to verify this conclusion. To this end, all the mobility measurements were made whilst maintaining a constant level of excitation force (force level control). Typical results for mode 1 and 3 for point mobility Y_{12} are shown in Figures 5-31 and 5-32. The nonlinear behaviour of the tower is very clear: as the excitation level is increased, the mobility curves tend to lean backwards and there is a drop in the level of response amplitude. From the Nyquist plots we see that there is no significant distortion in the circular shape of the plot but

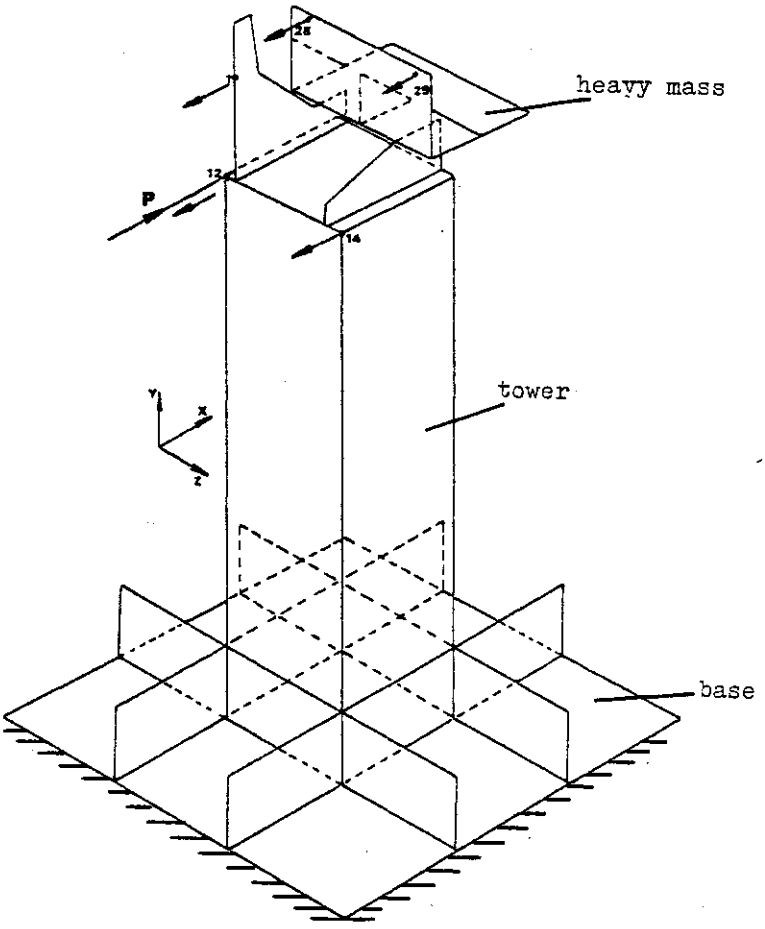

Fig. 5-29: Schematic view of the measured tower

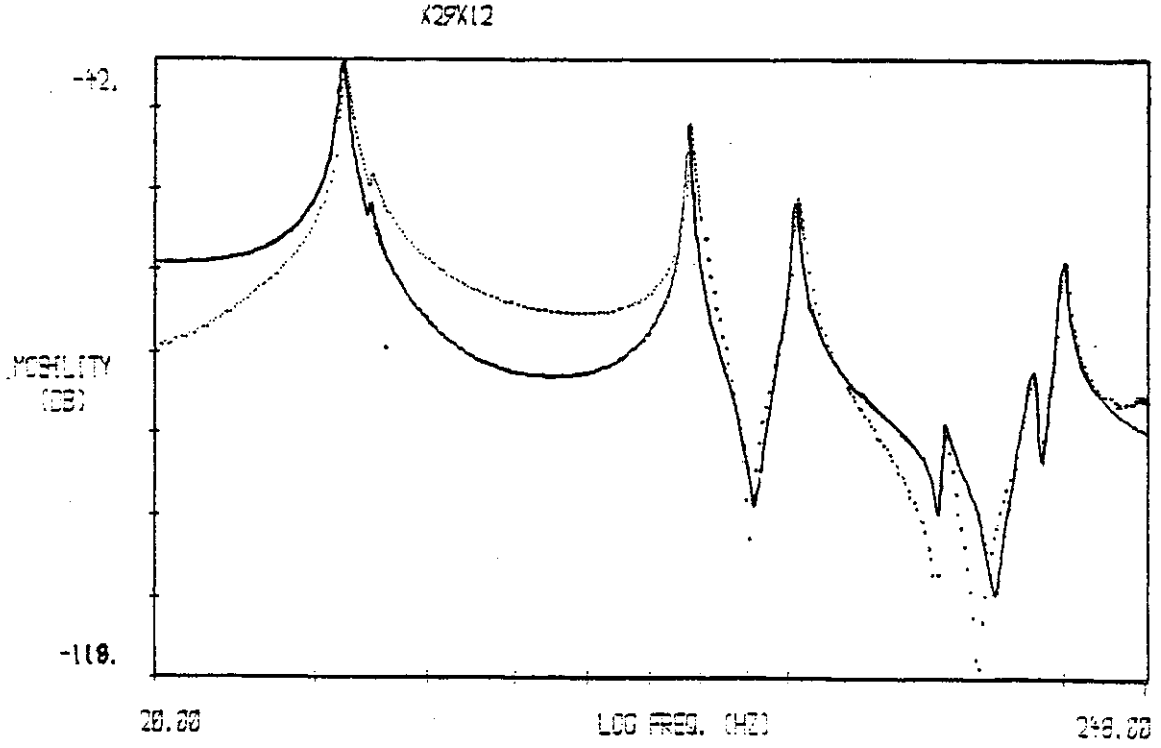

Fig. 5-30: Measured (optimal control) vs. identified curve for mobility $Y_{29,12}$

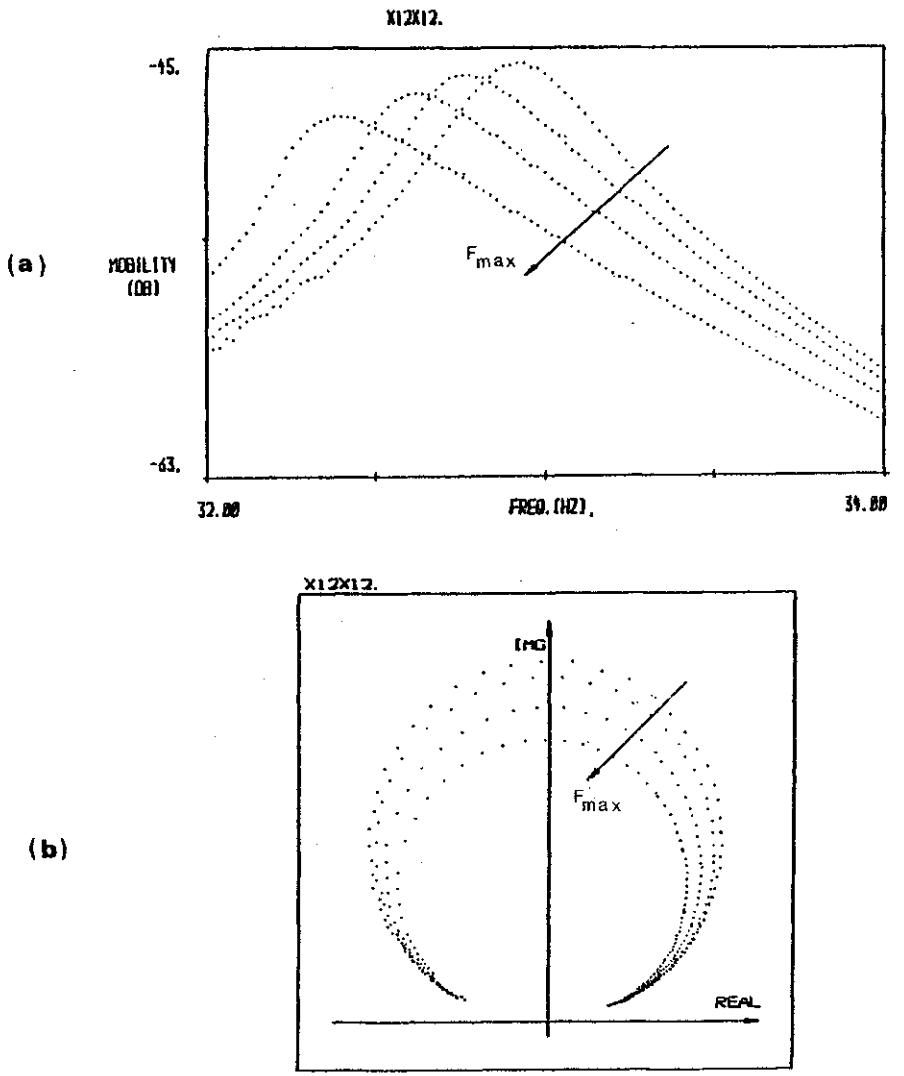

Fig. 5-31: Mobility (a) and Nyquist (b) plots for point measurement Y_{12} under constant levels of excitation (mode 1)

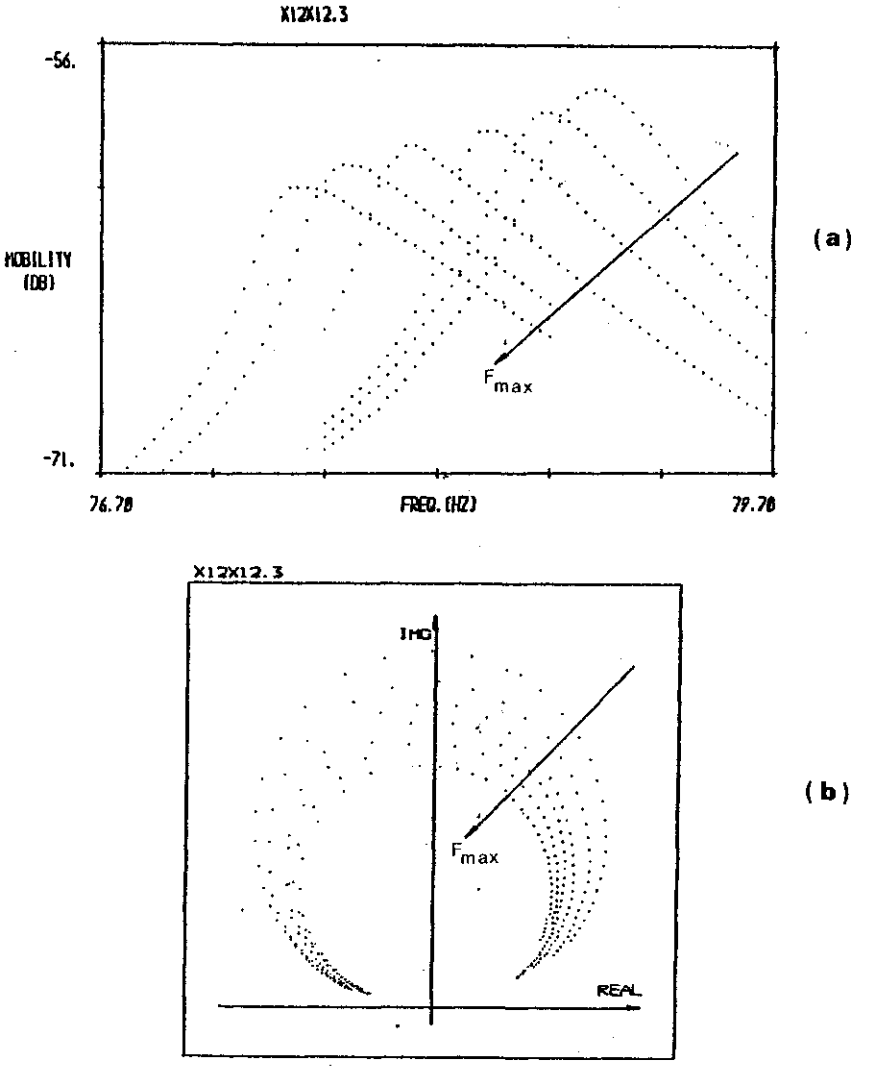

Fig.5-32: Mobility (a) and Nyquist (b) plots for point measurement Y_{12} under constant levels of excitation (mode 3)

the angular spacing of the points is changed and the maximum spacing tends to move in a counterclockwise direction. From these curves we may say, at this stage, that the dominant type of nonlinearity of the tower may be represented by a softening cubic stiffness.

Each curve in these two sets of data was analysed by POLAR5 and the identified modal parameters are given in Table 5-7. (For calculation of the nonlinearity factor, J_n, the mobility of the lowest excitation level was taken as the datum response.)

Examination of these results reveals some very clear trends; as the excitation level is increased:

(i) The identified natural frequency decreases.

(ii) The variation of the modal loss factor is relatively small and appears to be random.

(iii) There is a reduction in the modulus of the modal constant and hence a corresponding reduction in the modulus of the mode shape.

(iv) The most significant change is in the modal phase angle and consequently the identified normal mode shape becomes increasingly complex.

An example of the circle-fitting process and the location of the natural frequency for two excitation levels is shown in Fig. 5-33. The change of the angular spacing and hence derivation of a greater modal phase angle as the excitation level is increased is very clear.

At this stage we are able to conclude that in order to

P volts	ω_1 Hz	η_1	$_1A_{12,12}$ 1/Kg	$_1\theta_{12,12}$ deg	J_1	$_1\Phi_{12}$
.05	32.92	.0139	.0150	-177.69°	-	.1225 ⌊1.15°
.1	32.75	.0142	.0145	-168.08°	.617	.1204 ⌊5.96°
.2	32.57	.0143	.0136	-154.89°	.167	.1166 ⌊12.55°
.4	32.25	.0135	.0115	-110.83°	.001	.1072 ⌊34.58°

P volts	ω_3 Hz	η_3	$_3A_{12,12}$ 1/Kg 10^{-3}	$_3\theta_{12,12}$ deg	J_3	$_3\Phi_{12}$
.05	78.82	.0077	5.167	-150.87°	-	.0719 ⌊14.56°
.1	78.60	.0070	4.286	-141.08°	.559	.0655 ⌊19.46°
.2	78.32	.0062	3.399	-128.17°	.237	.0583 ⌊25.91°
.4	77.98	.0064	3.295	-135.77°	.060	.0574 ⌊22.11°
.6	77.69	.0070	3.382	-134.26°	.000	.0582 ⌊22.87°
.8	77.51	.0068	3.058	-140.00°	.000	.0553 ⌊20.00°

Table 5-7: Identified modal parameters of modes 1 and 3 for point mobility Y_{12} as fuction of excitation

r	$_1\Phi_r$	$_2\Phi_r$	$_3\Phi_r$	$_4\Phi_r$
12	.122 ⌊.53°	.0384 ⌊8.24°	.0673 ⌊-1.12°	.0206 ⌊7.19°
14	.145 ⌊-1.93°	.0412 ⌊13.72°	.0415 ⌊-1.42°	.1445 ⌊174.02°
01	.189 ⌊.35°	.0341 ⌊-6.11°	.0722 ⌊-1.43°	.223 ⌊-7.96°
29	.243 ⌊.55°	.0594 ⌊2.64°	.257 ⌊-177.18°	.585 ⌊172.33°
28	.209 ⌊.80°	.0592 ⌊11.60°	.179 ⌊-1.55°	.674 ⌊-7.03°

Table 5-9: Complete set of identified normal mode shapes of the tower

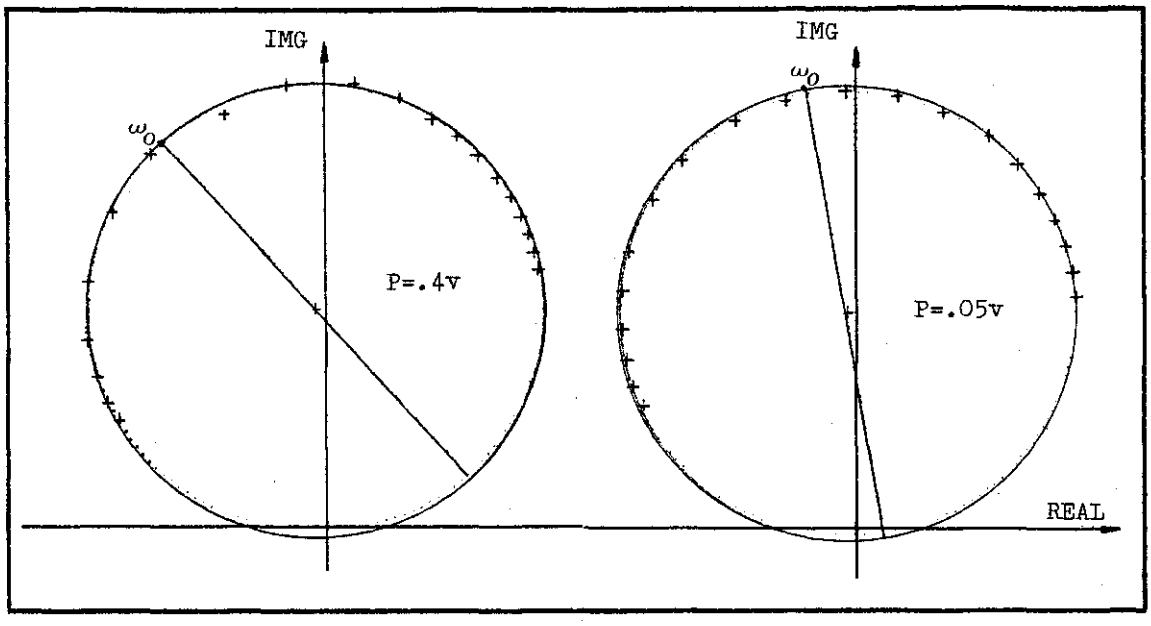

Fig. 5-33: Modal circles for mode 3 of point mobility Y_{12} for different levels of excitation

mode	ω_r Hz	η_r	$r^A_{29,12}$ 1/Kg	$r^\theta_{29,12}$ deg	$r^S_{29,12}$ %
1	32.88	.0136	.0296	-181.08	4.2
2	34.94	.0120	$2.28 \cdot 10^{-3}$	169.12	15.8
3	78.72	.0074	.0173	1.69	8.0
4	103.36	.0141	.0120	-.482	1.5

Residues	R_m (1/Kg)	I_m (1/Kg)	R_k (m/N)	I_k (m/N)
	$3.38 \cdot 10^{-3}$	$-1.89 \cdot 10^{-3}$	$-1.77 \cdot 10^{-8}$	$1.72 \cdot 10^{-8}$

Table 5-8: Identified modal parameters for mobility $Y_{29,12}$

minimize the influence of the nonlinearity of the tower on the measurement it must be treated as having a softening cubic stiffness nonlinearity. Thus, reduction of the excitation force to the minimum practical level was expected to produce the 'best' linear response and so the tower was measured at the lowest excitation level possible and the mobility curves were again analysed by SIM2. A typical result is shown in Fig. 5-34 and Table 5-8 and compared with the initial curve fit (Fig. 5-30) the improvement is remarkable.

A set of normal mode shapes resulting from this analysis is given in Table 5-9 where it is clearly noticed that the normal mode shapes have a very small phase angle and we may attribute this to measurement and analysis errors rather then to a nonproportional damping of the tower.

Finally, The M loss factor for different levels of excitation as a function of $\Delta\omega$ was calculated. (Fig. 5-35). Examination of each curve identifies clearly the existence of the cubic stiffness nonlinearity of the tower and we see that even at the lowest level of excitation there is still a small nonlinear influence.

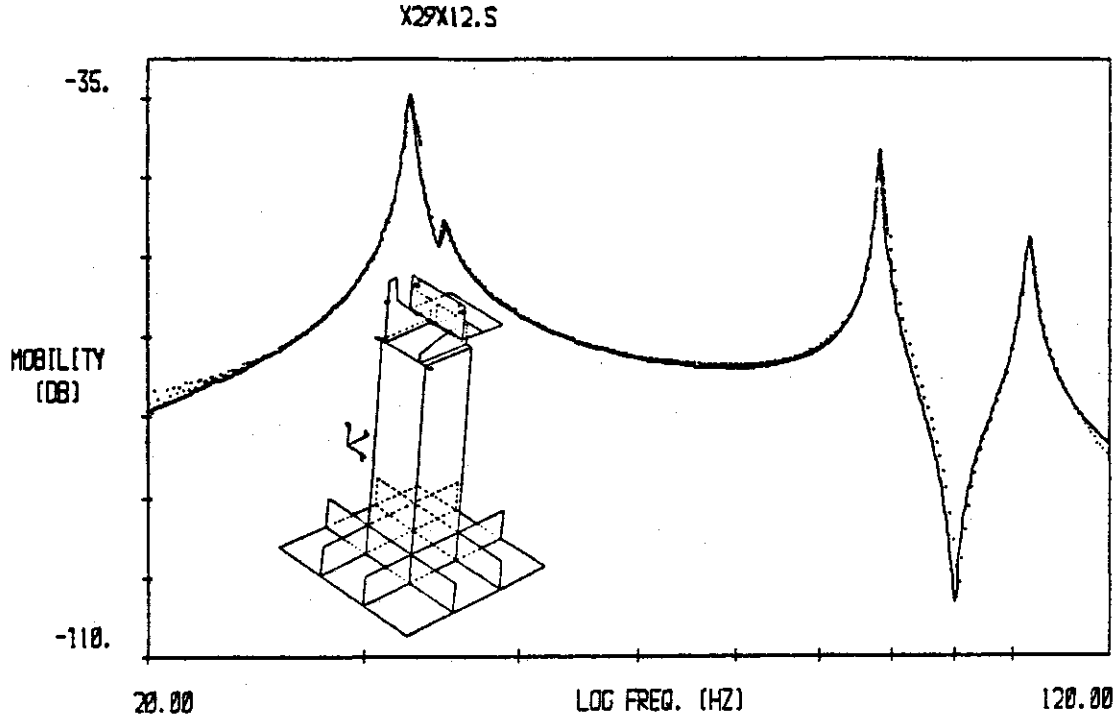

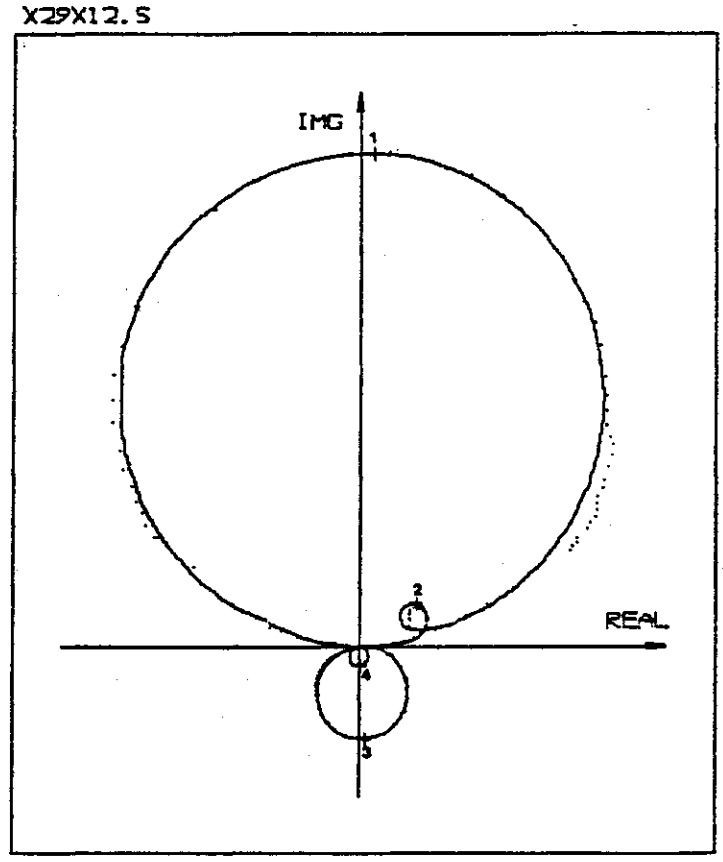

Fig. 5-34: Measured vs. identified curves for mobility $Y_{29,12}$ for optimal level of excitation

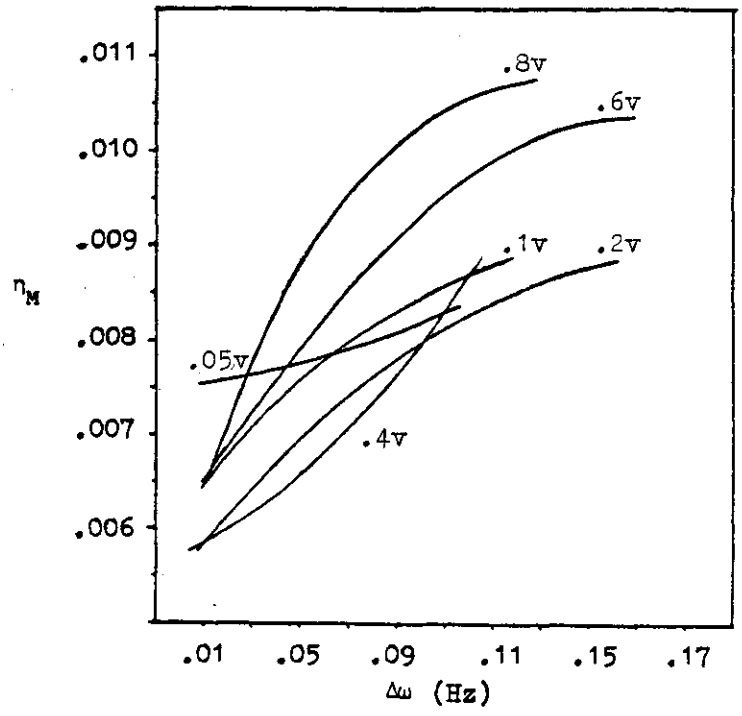

Fig. 5-35: Variation of M loss factor as function of $\Delta\omega$ for varying levels of excitation for point mobility $Y_{12,12}$ (mode 3)

5.6 CONCLUSIONS.

It has been shown that small nonlinearities can affect the modal identification analysis of measured mobility data if the analysis algorithm assumes a linear behaviour in the resonance regions.

Some simple types of theoretical nonlinearities were examined and from these we are able to draw some practical conclusions:

(i) The existence of each type of nonlinearity may be detected by a different form; some cause a distortion in the circular shape of the Nyquist plot around resonance while another distorts the angular spacing without affecting the circular shape or the diameter of the circle. In any case, a set of measurements taken at different but constant excitation levels immediately reveals the exsitance of nonlinearity.

(ii) In order to minimize the influence of the nonlinearity on the measured mobility, the excitation level must either be increased or decreased according to the dominant type of the nonlinearity. In order to reduce the influence of cubic stiffness, the force level has to be reduced, on the other hand, for dry friction it has to be increased. When a system posseses these two types it may be difficult to minimize their effect on the measurement because of these opposing influences.

(iii) The nonlinearity factor gives a very good indication of the level of nonlinearity. (i.e in cases of

synthesised data). For practical cases we must choose one set of data as the 'best' linear and use it as a basis for calculation of the nonlinearity factor of other measurements.

(iv) When only one set of measurements is available for a system with cubic stiffness nonlinearity, the presence of it cannot be detected by examining the standard plots. However, it is possible to identify such an effect by examination of the variation of the M loss factor as function of $\Delta\omega$. This check is only practical for cubic stiffness nonlinearity because for other types (e.g dry friction) the variation is negligible. A constant M loss factor as function of $\Delta\omega$ does not, therefore, necessarily mean that the system is linear. However, some types of nonlinearity are not detectable from any form of plot nor from examination of the M loss factor check. The only way to reveal their existence is by a set of different constant force excitation tests.

6. DERIVATION OF CONSISTENT MODAL PARAMETERS FROM SEVERAL SINGLE POINT EXCITATION TESTS.

6.1 INTRODUCTION.

It has been shown (chapter 2) that the modal constant of the r'th mode of receptance α_{ij}, ${}_rA_{ij}$, is defined as the product of the two mass-normalized eigenvector elements ${}_r\Phi_j$ and ${}_r\Phi_i$ i.e

$$ {}_rA_{ij} = ({}_r\Phi_i)\,({}_r\Phi_j) \tag{6-1} $$

For each mode, a modal constant matrix $[A]_r$ can be constructed from

$$ [A]_r = \{\Phi\}_r \{\Phi\}_r^T \tag{6-2} $$

From expression (6-1) it is clear that

$$ {}_rA_{ij} = {}_rA_{ji} \tag{6-3} $$

which means that the modal constant matrix of mode r is symmetric. This property is referred to as 'reciprocity' and it derives directly from the assumption of linear behaviour of the system. However, experience has shown that for most practical cases this reciprocity condition is not met precisely, for a number of reasons.

The accuracy of the modal constants derived from experimental data depends heavily upon the quality of the measurements made and upon the particular character of the frequency response function analysed. One of the key factors which influences the results is the choice of the response and excitation points. If either the excitation or the response point happens to lie on (or very close to) a nodal

point of a particular mode, then the response of that mode will barely appear in the measured frequency response function, if at all. Similarly, it may be impossible to excite certain modes adequately from a single point, especially on large structures.

A second factor to influence the analysis results is the character of the measured frequency response function. High modal density (many modes present within a certain analysis bandwidth), close modes, or the local dominance of a single mode which obscures or affects the measurement all make the identification of certain modes difficult and inaccurate when analysed by a single-mode-at-a-time identification method (POLAR5 for example). They also affect the more complete identification procedure undertaken by a simultaneous mode fitting method (SIM2 for example).

It has been shown that the presence of small nonlinearities in the system may, under certain conditions, seriously affect the identified results. It has also been shown by Tomlinson [64] that when exciting a structure using an electro-dynamic shaker, the input force is distorted, especially in the resonance regions, due to nonlinearities in the shaker.

The cumulative effect of all these factors is a distortion of the symmetric form of the identified modal constant matrices and, as a result, the reciprocity condition is not fulfilled. Thus when measuring several columns of the frequency response matrix and deriving the

complete eigenvector matrix from each column, it is usually found that these derived matrices are not identical, as they should be according to theory. Furthermore, the natural frequencies and the modal loss factors of the various modes are generally not found to be identical when derived from two frequency responses of a given system.

In this chapter, a systematic method is presented for an assessment of the quality of measured data and, once the modal parameters are derived, a quantity which describes the quality of these results is devised. Finally, a method for deriving a consistent set of modal parameters is developed.

6.2 METHODS FOR EVALUATING MODAL TEST RESULTS.

As the accuracy of the experimentally-identified modal parameters depends heavily on the quality of the frequency response data analysed, it is desirable to have some quantitative means of evaluating the quality of the data and of examining the modal character of the particular function in question before starting the process of modal identification.

Once the modal analysis of a frequency response function is completed, it is useful to measure the confidence that can be placed in each of the derived modal parameters. The usual method for this process is to plot the measured data and the theoretically-generated curve and to assess visually the closeness of the two. Such a method is very subjective and depends on the scale and the format of the plot. This question of confidence becomes especially important when we have more than one set of parameters for the same mode. Simple averaging may lead us to significant errors as some of the results will have been derived using 'poor' data and consequently they are likely to be 'poor' as well. Thus there is a need for an objective weighting or quality factor to be assigned to each identified set of modal parameters.

6.2.1 ASSESSMENT OF THE QUALITY OF MEASURED DATA.

The quality of the experimentally-derived modal parameters is directly related to the quality of the

measured data. The analysis program assumes a linear behaviour and a certain model for the damping, both of which are only convenient approximations to the 'true' behaviour of the structure. Furthermore, an inherent feature in any experimental process is the pollution of the measured data by random errors. It is important, therefore, to check the data at the acquisition stage for significant deviations from the assumed model and, where possible, to improve their quality.

Standard procedures for correct measurement routines are well established and described by Ewins [65,66], Silva [67], Caruzo [68], Gleeson [69] and many others. However, there are some fine details which may seriously influence the quality of the data and the following systematic approach provides a tool for checking the experimental layout, the structure and the measuring system and for identifying sources of pollution to the measured data.

(i) Initial selection of excitation and response points on the structure. These points are chosen according to engineering judgement and accessibility to the necessary instrumentation.

For a point measurement, the accelerometer and force gauge are supposed to be located at the same point on the structure. Usually, this is achieved by mounting them on the opposite sides of a panel, but very often this arrangement is not practical and they are then mounted as close as possible to each other on the same side of the structure.

From a strict point of view, this arrangement records a transfer response, α_{ij}, but the practical approach assumes that its deviation from the exact point measurement is negligible, i.e

$$\alpha_{ij} \cong \alpha_{ii} \cong \alpha_{jj}$$

It is worthwhile checking the validity of this assumption by measuring the transfer response to point k from point i and j and comparing α_{ik} and α_{jk}. If this assumption is valid then these two transfer measurements should be practically identical, i.e

$$\alpha_{ik} \cong \alpha_{jk}$$

(ii) Initially, a coarse sweep of the frequency range of interest is performed and the main modes in this range are identified. At this point it is possible to identify excitation and response points which are poorly located (i.e close to a node of a certain mode), and where possible, to change their position. Noise generated by loose parts in the structure (e.g cables, pipes, hinges, gear, etc.) can be detected and eliminated too. It is sometimes possible to improve the quality of the data acquired at this stage quite considerably, just by moving a measurement point by a small amount.

(iii) Once all the excitation and response points on the structure have been chosen and the operator has some general idea of the dynamic behaviour of the structure, a fine sweep around the resonances in the frequency range of interest is performed.

(iv) Plotting these measurements on a polar plot usually reveals the quality of the data in the resonance regions. A distortion of the basically-circular shape of the plot or a distortion in the angular spacing of the points may give some early indication to the nonlinear behaviour of the structure and enable the operator to decide which mode to check very thoroughly, or to remeasure.

(v) In order to establish the degree of nonlinearity of the structure, several measurements over the same frequency range should be performed at different levels of constant excitation force. The level of excitation force starts at the lowest practical level possible (where the level of noise is still acceptable) and increases to the maximum which can be maintained by the instrumentation (where the signals are not clipped) or the structure. A set of nonlinearity factors may be calculated where the data collected at the lowest excitation level are taken as the 'linear' response. The rate of change of the nonlinearity factor as a function of the increase in the excitation level gives the operator an indication of the extent of the nonlinearity of the whole system (structure and measuring instrumentation). A set of polar plots of these measurements can often give an indication as to the dominant form of nonlinearity.

Calculation of the nonlinearity factor of α_{ij} relative to α_{ji} produces more information which enables the operator to assess the quality of the data collected.

(vi) At this stage the operator should make his decision regarding the quality of the data, bearing in mind the accuracy he demands from the identified modal parameters. In extreme cases, where the data prove to be very bad, the operator may decide not to proceed with the analysis, choosing instead to try to locate the causes for the poor quality of these data and to repeat the whole process of measurement. In any case, the interpretation of the nonlinearity factors is ultimately left to the experience and judgement of the operator.

6.2.2 ASSESSMENT OF THE QUALITY OF IDENTIFIED MODAL PARAMETERS.

Once a set of modal parameters for a certain mode have been identified, the quality of this identification can be assessed by calculating the normalized standard error of the fit between measured points and the theoretical curve (Fig. 6-1).

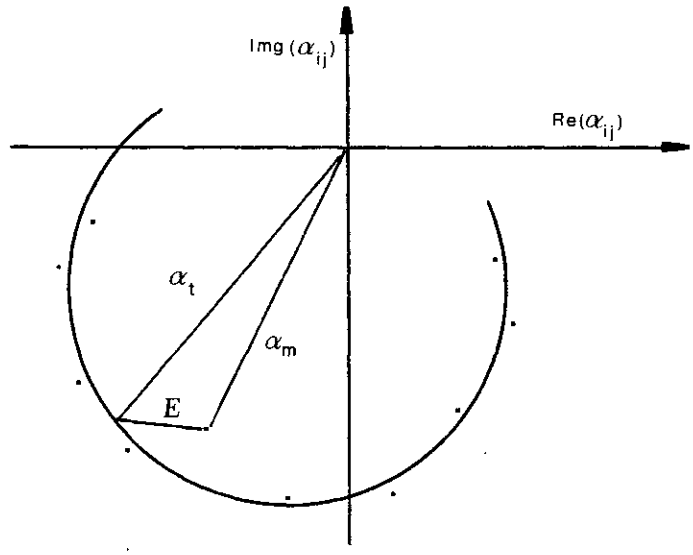

Fig. 6-1: Error of the fitted curve

The standard error is calculated for each mode over the frequency range used for identification of this mode. If we denote the measured response by $\alpha_m(\omega)$ and the fitted response by $\alpha_t(\omega)$ i.e

$$\alpha_t(\omega) = \sum_{r=1}^{m} \frac{{}_rA_{ij}}{\omega_r^2\left[1-(\frac{\omega}{\omega_r})^2+i\eta_r\right]} + \frac{R_m}{\omega^2} + R_k \qquad (6\text{-}4)$$

where R_m and R_k are the residual mass and residual stiffness respectively and m is the number of modes analysed for this particular frequency response function.

The error of the fit, $E(\omega)$, at any individual frequency is defined as:

$$E(\omega) = |\alpha_t(\omega) - \alpha_m(\omega)| \qquad (6\text{-}5)$$

and the quality factor, ${}_rS_{ij}$, for the mode r of receptance α_{ij} is defined as:

$${}_rS_{ij} = \frac{\left[\frac{1}{p}\sum_{k=1}^{p}[E(\omega_k)]^2\right]^{\frac{1}{2}}}{\frac{|{}_rA_{ij}|}{\omega_r^2\,\eta_r}} \qquad (6\text{-}6)$$

where p is the number of points used for identification of this mode. The normalizing factor, $|{}_rA_{ij}|/(\omega_r^2\eta_r)$, is the diameter of the circle that fits best through these points on a Nyquist plot.

When several attempts to identify the modal parameters of a certain mode are made, either with the same identification program or by different methods, the quality of these attempts can be evaluated by comparing the quality factors calculated for each derived set of modal parameters.

The smaller is the value of $_{r}S_{ij}$, the better is the quality of the fit and, hence, the greater is the confidence which can be placed in this set of results.

6.3 CALCULATION OF THE OPTIMAL MODAL PARAMETERS.

By measuring one column or row in the frequency response function matrix using the single-point excitation technique, it is possible to derive the complete matrix of the normal mode shapes, $[\Phi]_{n\times m}$, where n is the number of coordinates used to define the motion of the system and m is the number of modes in the measured frequency range. (usually n>m)

By definition (equation 6-1), the modal constant of the point measurement is

$$ {}_rA_{ii} = ({}_r\Phi_i)^2 \tag{6-7} $$

from which we may derive

$$ {}_r\Phi_i = ({}_rA_{ii})^{\frac{1}{2}} \tag{6-8} $$

and then all the other elements in the normal mode matrix are obtained using

$$ {}_r\Phi_j = \frac{{}_rA_{ij}}{\sqrt{{}_rA_{ii}}} \tag{6-9} $$

It is usually found that the normal mode shape matrices derived from different measured columns of the frequency response function are not identical and in many cases it is not possible to identify all the terms because some elements in the modal constant matrix column are missing due to low signals, often as a result of poor choice of excitation or response points. If the missing element is the modal constant of the point measurement ${}_rA_{ii}$ then it is impossible to identify the mass-normalized mode shape elements ${}_r\Phi_j$ even though the modal constants of the transfer measurements, ${}_rA_{ij}$, are available, because the process hinges on knowledge

of $_{r}A_{ii}$.

The above method has been shown for the hysteretic damping model only but it was shown by Gaukroger and Copley [36] that the same procedure applies for the viscously damped system.

For each column identified, different estimates of the natural frequency and loss factor are derived for each mode (n estimates for each mode). These two modal parameters derived by analysing each receptance α_{ij} are denoted by $_{r}\omega_{ij}$ for the natural frequency and $_{r}\eta_{ij}$ for the loss factor, and for each mode they comprise two matrices $[\omega]_r$ and $[\eta]_r$ the size of which is nxN where N is the number of measured columns in the receptance matrix .

6.3.1 DERIVATION OF THE 'BEST' ESTIMATE OF THE NATURAL FREQUENCY AND LOSS FACTOR.

The 'best' estimates of natural frequency and loss factor for each mode are obtained by a process of averaging, using the quality factor, $_{r}S_{ij}$, as a weighting parameter.

The variable to be manipulated is denoted by $_{r}X_{ij}$ (representing either $_{r}\omega_{ij}$ or $_{r}\eta_{ij}$) and the weighting attached to it by $_{r}g_{ij}$ where

$$_{r}g_{ij}=\left(\frac{1}{_{r}S_{ij}}\right)^{2} \qquad (6\text{-}10)$$

First, the weighted mean, $_{r}X^{*}_{j}$, of the elements of column j is calculated

$$ {}_rX_j^* = \frac{\sum_{i=1}^{n} ({}_rg_{ij})\,({}_rX_{ij})}{\sum_{i=1}^{n} ({}_rg_{ij})} \tag{6-11} $$

and the weighted standard deviation of ${}_rX_j^*$, ${}_rS_j^*$ is defined by

$$ {}_rS_j^* = \left[\frac{\sum_{i=1}^{n} ({}_rg_{ij})\,[{}_rX_{ij} - {}_rX_j^*]^2}{\sum_{i=1}^{n} ({}_rg_{ij})} \right]^{\frac{1}{2}} \tag{6-12} $$

The final estimate is calculated by averaging all the N derived means ${}_rX_j^*$.

The full weighted mean, $\bar{X}_r$, is

$$ \bar{X}_r = \frac{\sum_{j=1}^{N} ({}_rg_j^*)\,({}_rX_j^*)}{\sum_{j=1}^{N} ({}_rg_j^*)} \tag{6-13} $$

where the weighting factor is defined as

$$ {}_rg_j^* = \left(\frac{1}{{}_rS_j^*} \right)^2 \tag{6-14} $$

The standard deviation, $\bar{S}_r$, of the full mean is

$$ \bar{S}_r = \left[\frac{\sum_{j=1}^{N} ({}_rg_j^*)\,[{}_rX_j^* - \bar{X}_r]^2}{\sum_{j=1}^{N} ({}_rg_j^*)} \right]^{\frac{1}{2}} \tag{6-15} $$

6.3.2 DERIVATION OF THE OPTIMIZED NORMAL MODE SHAPES.

When more than one column of the frequency response matrix is available, an improved estimate of the normal mode shapes can be obtained. Richardson and Kniskern [70] suggested an algorithm for this purpose - it contains some

arbitrary rules and is based on the authors experience and intuition without setting any criteria for the derived results. Goyder [71,72] developed an algorithm which fits simultaneously all the measured frequency response functions and thus derives one consistent set of modal parameters.

By using the following algorithm, it is possible to obtain a consistent normal mode matrix, to derive values in this matrix which are not always available by the one column at a time method and to reduce the overall error in the estimate of the modal parameters.

At the previous stage the 'best' estimates for the natural frequencies, ϖ_r, and loss factors, $\bar{\eta}_r$, have been derived and since the diameter of the fitted modal circle, $|{}_rA_{ij}|/(\omega_r^2\eta_r)$, is a constant geometrical property, there is no justification to accept an adjustment in its value and a proper adjustment in the modal constant ${}_rA_{ij}$ must be made. Thus, in order to make the modal constant estimates consistent with the 'best' values of the natural frequency and loss factor, a new adjusted value, ${}_r\bar{A}_{ij}$, is calculated from

$$ {}_r\bar{A}_{ij} = {}_rA_{ij}\left(\frac{\varpi_r^2\bar{\eta}_r}{\omega_r^2\eta_r}\right) \qquad (6\text{-}16) $$

Then, mode by mode, the algorithm searches for the values of the elements in the normal mode shape $\{\Phi\}_r$ which minimize the error function, E_r, given by

$$ E_r = \sum_{i=1}^{n}\sum_{j=1}^{n} \left| {}_r\bar{A}_{ij} - ({}_r\Phi_i)({}_r\Phi_j) \right|^2 ({}_rg_{ij}) \quad ; \quad (r=1,2..m) \qquad (6\text{-}17) $$

This error function is minimized for each mode separately using all the adjusted modal constants available. For missing elementsin the modal constant matrix the weighting factor ${}_r g_{ij}$ is taken as equal to zero, so that they are excluded from the process. In order to start this algorithm, an initial guess of the values of the elements of the vector $\{\Phi\}_r$ must be provided and these initial values are obtained using the weaker algorithm suggested by Richardson et.al.[70].

As the modal constants ${}_r\bar{A}_{ij}$ and the normal mode shapes ${}_r\Phi_j$, are complex terms, the optimization process has to evaluate 2xn variables. This is undertaken in two stages: (i) the values of the phases are kept constant and the moduli of ${}_r\Phi_j$ to minimize E_r are found, (ii) these moduli are kept constant and the phases to minimize E_r are found, and so on until the change in the value of E_r from one iteration to the next is less then a prescribed value.

It should be appreciated, however, that the optimized modal parameters derived by this method are only a result of a statistical process and as more redundant data are available the better is the estimate of these parameters. In any case, by this method, an enormous amount of measured and analysed information is reduced into a single consistent set of parameters which describe the measured structure 'best' and can be conveniently used in any further theoretical calculations.

7. EXPERIMENTAL STUDY

A comprehensive experimental study of a typical aerospace structure was performed as part of this research, the aims of which were:

(i) to investigate the problems commonly encountered in practice when using the single-point excitation method.

(ii) to demonstrate the use of the methods described in the previous chapters;

(iii) to compare different methods of modal identification when used on real structures.

7.1 TESTPIECE AND MEASUREMENT SYSTEM

The structure used for this study was a tailcone of a helicopter (Westland Lynx) (Fig. 7-1). This tailcone, which has a mass of about 80 Kg and is about 2.6m long, is a bare structural frame containing some electrical cables and hydraulic pipes. The tailcone was suspended by two nylon ropes attached to its two ends. Various types of suspension systems were tried including steel cables, rubber straps, nylon ropes, etc and the system which showed the minimum influence on the measured data in our range of interest (30-300 Hz) - i.e nylon ropes - was chosen.

The measurements on the tailcone were performed using the 1191 computer-controlled system of the Dynamics Section at the Imperial College. The components of this system are described in Fig. 7-2. The system is controlled by a

PDP11/34 mini-computer and the measurements were made using the program MOB3, developed for this project.

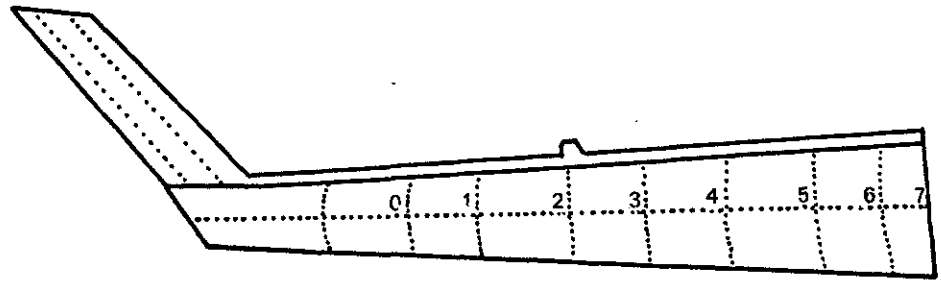

Fig. 7-1: Tailcone and response points

At first, the tailcone was excited at a single point and the response was measured at eight points along the tail (points Ø-7 in Fig. 7-1). This process was repeated four times, each time using a different excitation point, so that a total of 32 frequency response functions were obtained (Table 7-1). The modal parameters were extracted from each of these measured response functions using the modal identification programs POLAR5, SIM2 and PAPA.

In addition, the tailcone was measured using the multi-point excitation system MAMA, where the appropriate modal parameters are directly read from the system once proper tuning of the exciting forces is achieved.

The vibration characteristics of the tailcone were measured over a one decade frequency range (30-300 Hz) and within this range interest was focused on the first four modes. This group of modes provides a good example of typical problems encountered in practice. The first mode

(around 77 Hz) is lightly damped and well-separated from the next two modes (around 141 and 145 Hz), which, in turn, are moderately damped and very close to each other. The last mode (around 183 Hz) is moderately damped and well-separated from its neighbouring modes.

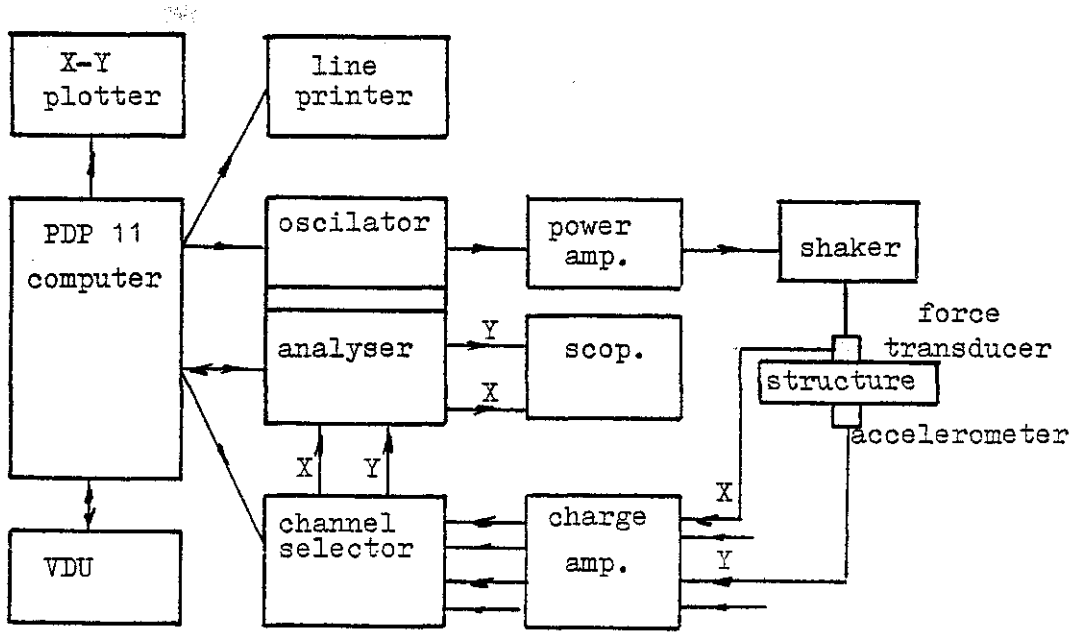

Fig. 7-2: The measurement system

Because four columns of the mobility matrix were measured and because some of our excitation and response points were located close to nodal points of certain modes, the measured data collected contain many of the problems common to the single point excitation method.

Figures 7-3 ÷ 7-5 show typical examples of the nature of the measured data; in experimental mobility plot Y_{24} , the

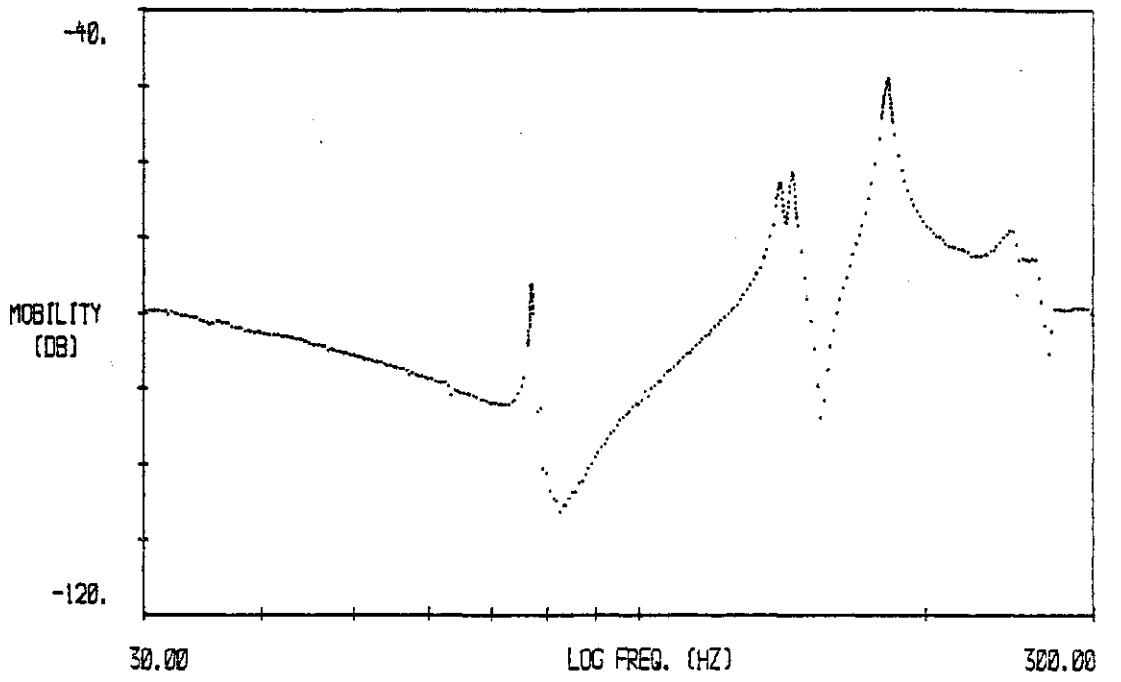

Fig: 7-3: Mobility plot of Y_{24}

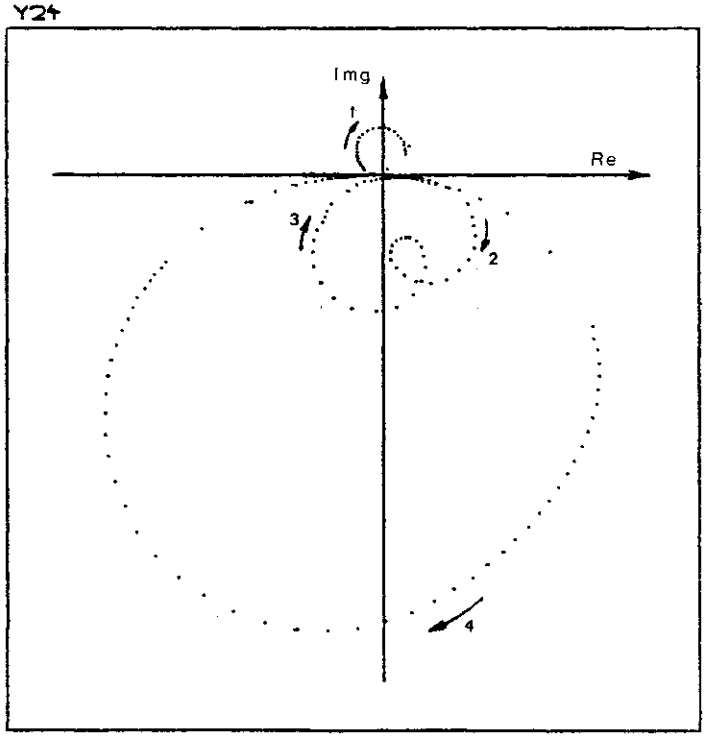

Fig. 7-4: Polar plot of α_{24}

Y_{77}	Y_{76}	Y_{74}	Y_{72}
Y_{67}	Y_{66}	Y_{64}	Y_{62}
Y_{57}	Y_{56}	Y_{54}	Y_{52}
Y_{47}	Y_{46}	Y_{44}	Y_{42}
Y_{37}	Y_{36}	Y_{34}	Y_{32}
Y_{27}	Y_{26}	Y_{24}	Y_{22}
Y_{17}	Y_{16}	Y_{14}	Y_{12}
Y_{07}	Y_{06}	Y_{04}	Y_{02}

Table 7-1: The measured mobility matrix

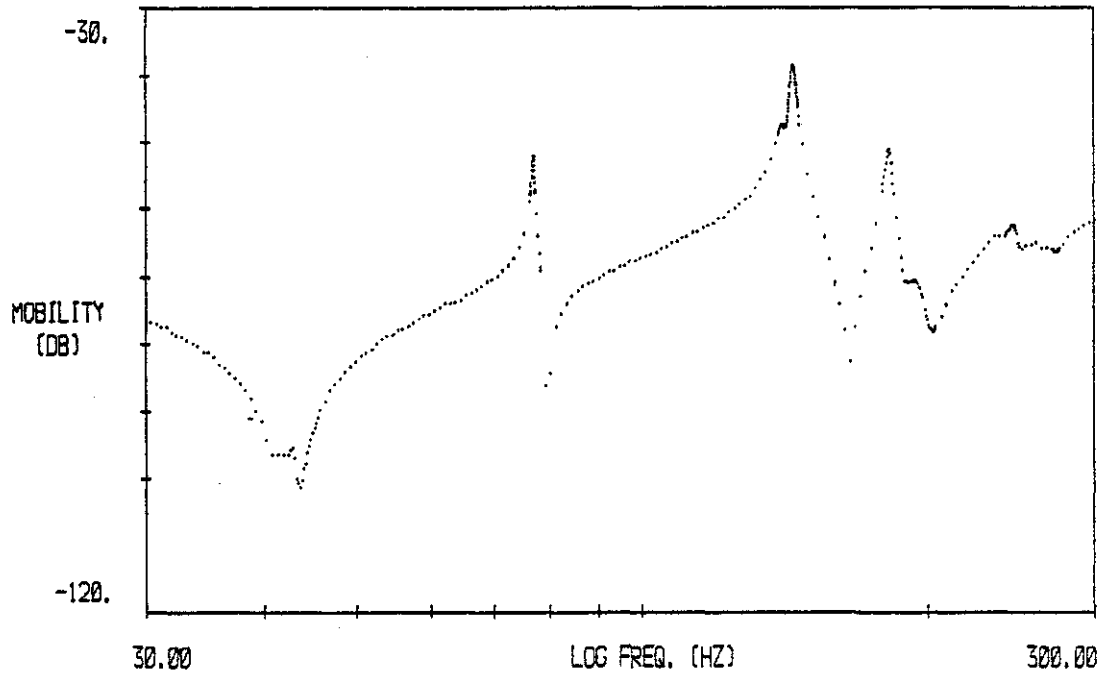

Fig. 7-5: Mobility plot of Y_{77}

two close modes and the low response of the first mode are clearly seen, this latter because point 4 is close to a node of this mode. In experimental mobility plot Y_{77}, one of the close modes is dominant and the other one is hardly noticed. In both cases the very small modes above 200 Hz are mainly due to pipes and cables left in the tailcone. A careful check of this range indicated that these modes are highly nonlinear and depend heavily on the level of excitation. However, they are not genuine modes of the structure and their influence on the overall response is minimal.

7.1.1 ASSESSMENT OF LINEARITY

Before starting the modal identification process, the measured mobility data were tested for nonlinearity according to the procedure outlined in 6.2.1. The tailcone was excited at a certain mode, maintaining the lowest constant amplitude of excitation force possible (F_{min}). Then the measurement was repeated for the same frequency range but under the highest constant amplitude of excitation force practicable (F_{max}). Using the first set of data as the 'best' linear response of the tailcone, the nonlinearity factor was calculated. Figures 7-6 and 7-7 illustrate two typical nonlinearity checks for mode 1 and mode 4 using mobility Y_{42}. In these two cases the structure was also measured at some intermediate amplitudes of constant forcing levels. The nonlinearity factor for these checks are summarized in Tables 7-2 and 7-3 and a typical J plot for

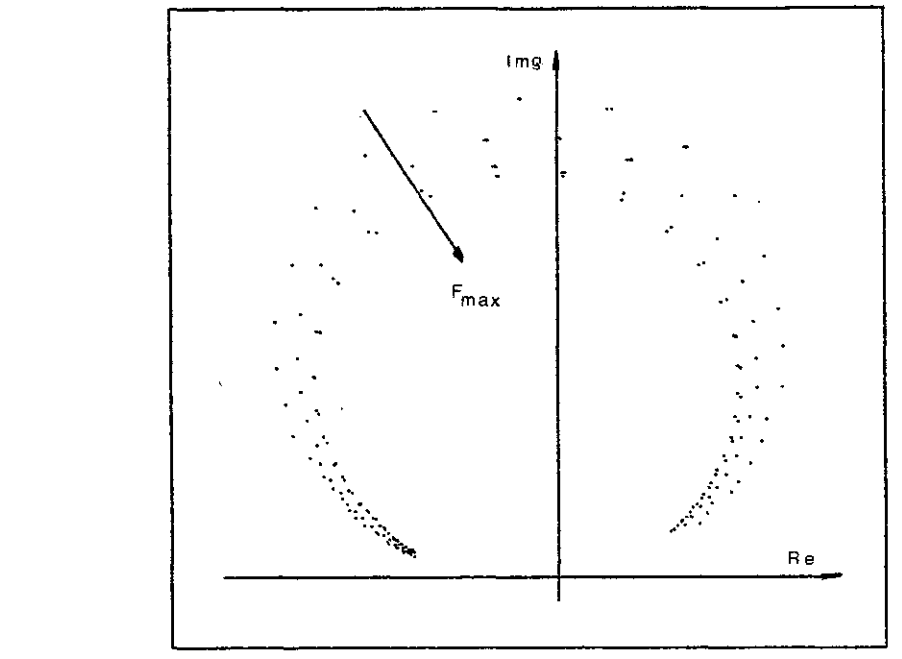

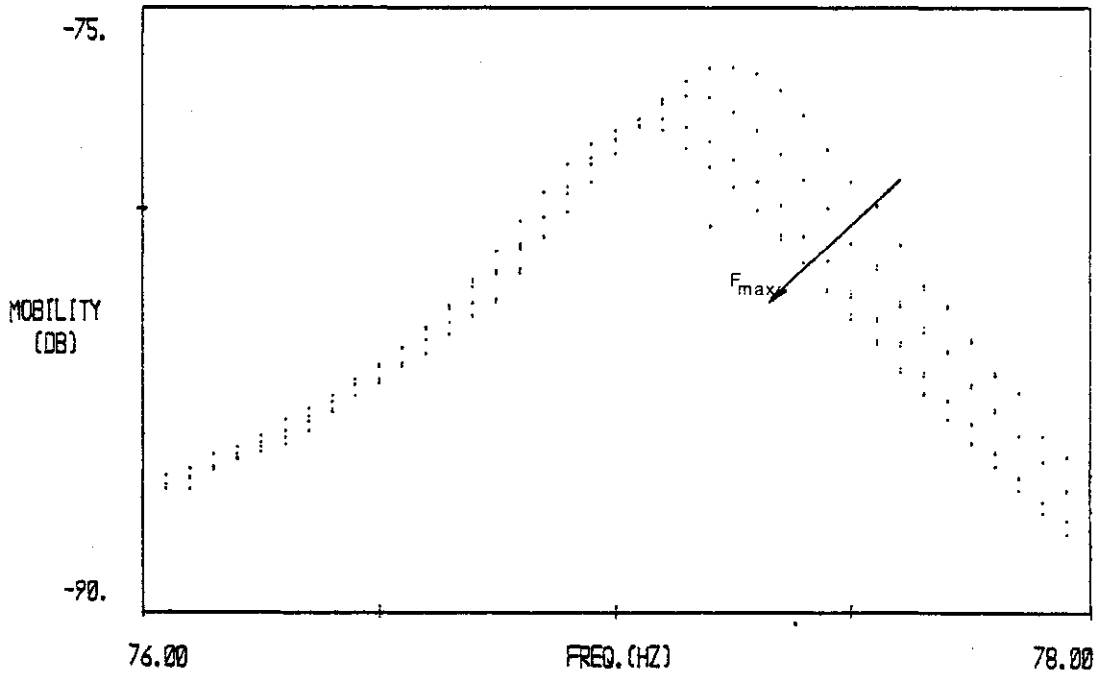

Fig.7-6: Polar and mobility plots of first mode of α_{42} for several levels of constant excitation

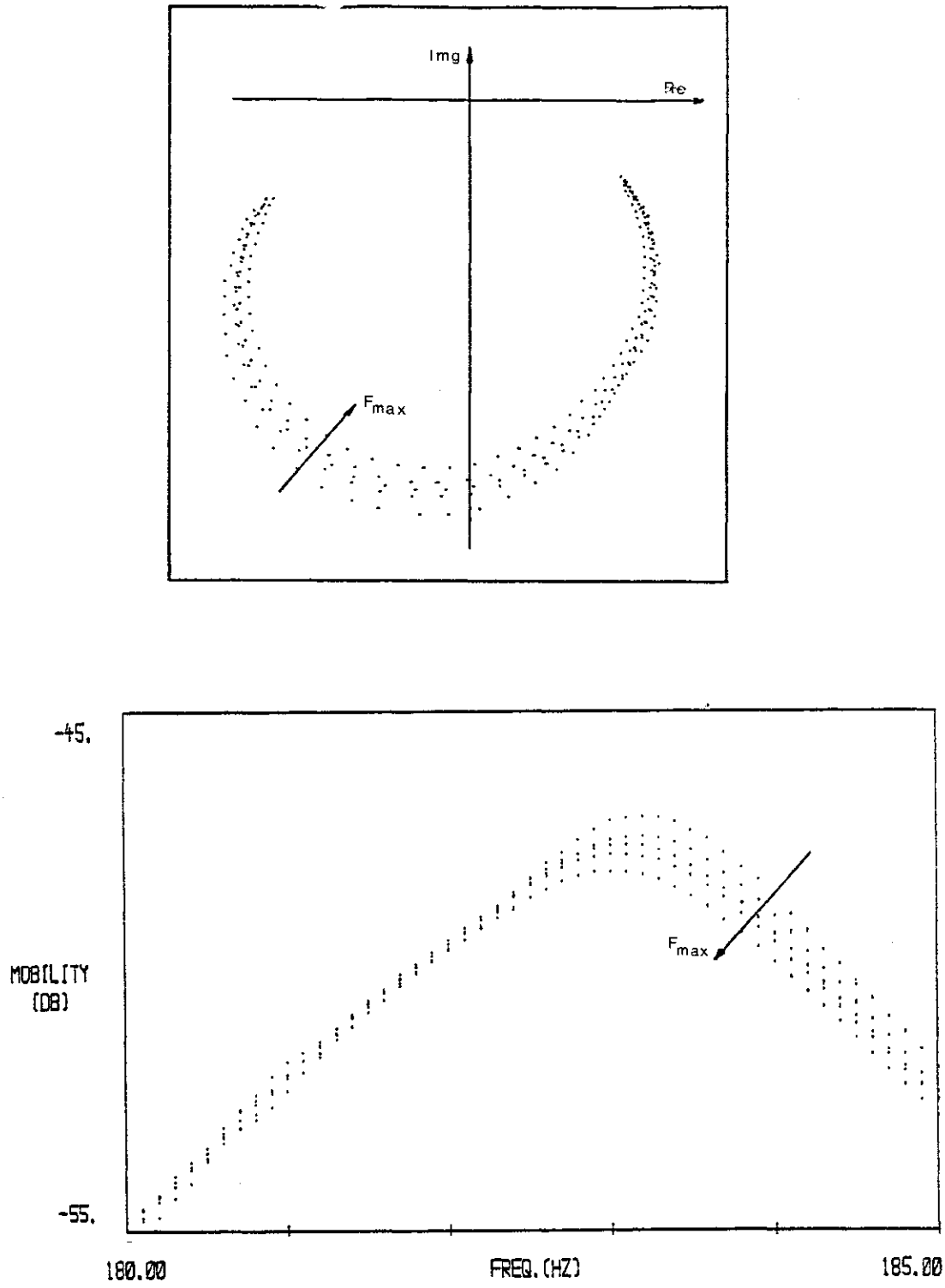

Fig. 7-7: Polar and mobility plots of forth mode of α_{42} for several levels of constant excitation

excitation level (v)	J_m	J_p	J
0.6	0.831	0.832	0.831
1.0	0.776	0.774	0.775
1.4	0.641	0.537	0.606

Table 7-2: Nonlinearity factor for mode 1 of α_{42} (reference level is F_{min}=.2v)

excitation level (v)	J_m	J_p	J
0.05	.945	.964	.954
0.07	.859	0.971	0.913
0.10	0.798	0.956	.873
0.20	0.733	0.863	0.795

Table 7-3: Nonlinearity factor for mode 4 of α_{42} (reference level is F_{min}=.02v)

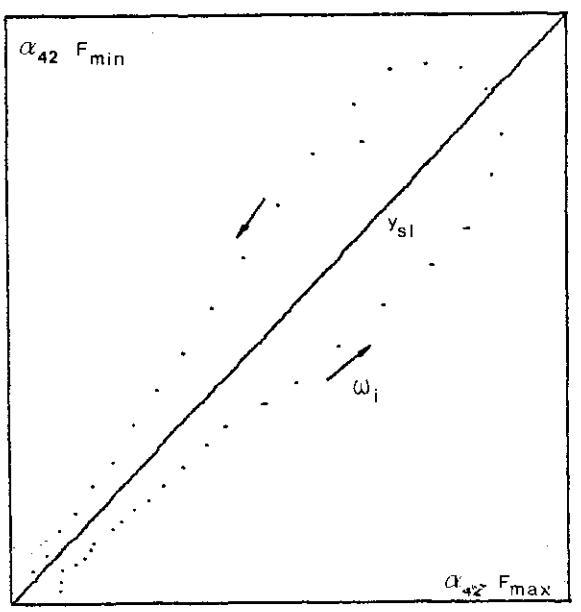

Fig. 7-8: Linearity check (J plot) of mode 1 for α_{42}

the first mode of Y_{42} is showen in Fig. 7-8.

An additional linearity check was made by comparing two reciprocal transfer mobilities (Y_{42} and Y_{24}) over the whole frequency range (Fig 7-9).

Examination of the nonlinearity factors for these checks shows that the degree of nonlinearity of the tailcone in the range of interest is not significant and that if the excitation levels are kept below the maximum level which is practicable with our equipment, the measured data can be treated as linear. The main reason for the good linear behaviour of the tailcone may be attributed to the way it was suspended; with 'free free' suspension high levels of forcing are needed in order to induce large deflections in the structure (which are usually responsible for marked nonlinear behaviour). These required levels were beyond the range our equipment could maintain.

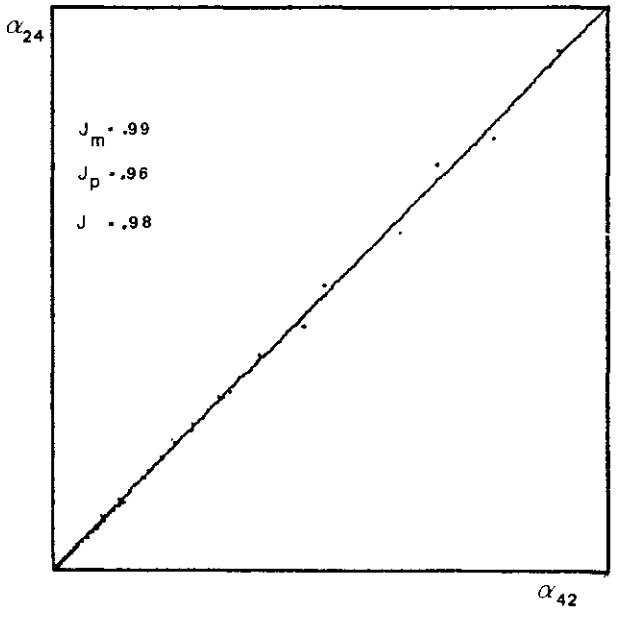

Fig. 7-9: Linearity check of α_{42} and α_{24}

7.2 SINGLE-POINT EXCITATION MODAL IDENTIFICATION

The modal parameters for the 32 measured frequency response functions were identified using three different identification programs:

(i) POLAR5 (P) - a one-mode-at-a-time identification routine.

(ii) SIM2 (S) - a simultaneous modal identification routine.

(iii) PAPA (PP) - a simultaneous mode identification routine.

The first two routines assume a hysteretic damping model and the last one assumes a viscous damping model (see appendix).

Two typical sets of results are summarized in Tables 7-4 and 7-5. Because the second and the third modes are very close, and in some measurements one of them was dominant, it was sometimes impossible to identify the other mode (mode 3, for example, in Table 7-5). The results provided by PAPA did not include residual terms or quality factor. In general, it is noticed that the quality of SIM's results is better than POLAR's, especially for the two close modes. (A complete set of results is given in ref[73])

When presenting the results on a log mobility vs frequency plot, the difference between the results obtained by the three programs is effectively indistinguishable (only true around resonances in this case, as there are no residual terms included for PAPA's results).

Y22

Mode		ω_r (Hz)	η_r	A_r (1/Kg)	θ_r (deg)	ζ_r %
1	P	77.16	.0075	.393E-02	-6.3	10.5
	S	77.09	.0077	.415E-02	-1.0	1.5
	PP	77.12	.0074	.407E-02	-7.6	
2	P	141.30	.0155	.282E-01	5.0	2.4
	S	141.30	.0148	.270E-01	3.5	1.0
	PP	141.40	.0150	.275E-01	-3.3	
3	P					
	S					
	PP	145.50	.0156	.330E-02	-22.5	
4	P	182.40	.0164	.103E+00	-8.5	5.0
	S	182.50	.0165	.102E+00	-9.2	4.6
	PP	182.50	.0168	.105E+00	-8.7	

	R_m (1/Kg)	I_m (1/Kg)	R_k (m/N)	I_k (m/N)
P	-.0213	1.857E-3	3.323E-7	-3.590E-8
S	-.0210	2.878E-3	3.277E-7	-6.012E-8

Table 7-4: Derived modal parameters for mobility Y_{22}

Y32

Mode		ω_r (Hz)	η_r	A_r (1/Kg)	θ_r (deg)	ζ_r %
1	P	77.28	.0074	.209E-02	-16.9	16.0
	S	77.19	.0065	.211E-02	-2.3	10.9
	PP	77.23	.0063	.206E-02	-11.8	
2	P	141.30	.0143	.190E-01	4.5	3.1
	S	141.30	.0155	.203E-01	3.6	.9
	PP	141.40	.0160	.213E-01	-2.5	
3	P	145.40	.0139	.590E-02	-10.7	7.4
	S	145.30	.0116	.495E-02	-.2	2.9
	PP	145.30	.0129	.603E-02	-3.6	
4	P	182.40	.0151	.984E-01	-5.4	5.0
	S	182.50	.0152	.975E-01	-8.1	3.9
	PP	182.50	.0155	.101E+00	-7.4	

	R_m (1/Kg)	I_m (1/Kg)	R_k (m/N)	I_k (m/N)
P	-.0216	1.134E-3	3.151E-8	-1.718E-9
S	-.0228	1.352E-3	3.784E-8	3.188E-11

Table 7-5: Derived modal parameters for mobility Y_{32}

A typical example of a fitted curve as derived by SIM2 both in logarithmic and polar formats is given in Fig. 7-10. (taken from the complete set reported in ref. [73]).

However, when these results are presented on a nyquist plot, the differences between them are much clearer and in many cases a visual check can tell which set of results fits the experimental data best. An example to illustrate this point is given in Fig. 7-11; when presenting the results in this format, it was noticed that the modal parameters of small modes were identified relatively poorly by PAPA (Fig. 7-12).

Examination of the complete set of results indicates that as the quality of the identification improves, the values of the modal phase angles are reduced thus indicating

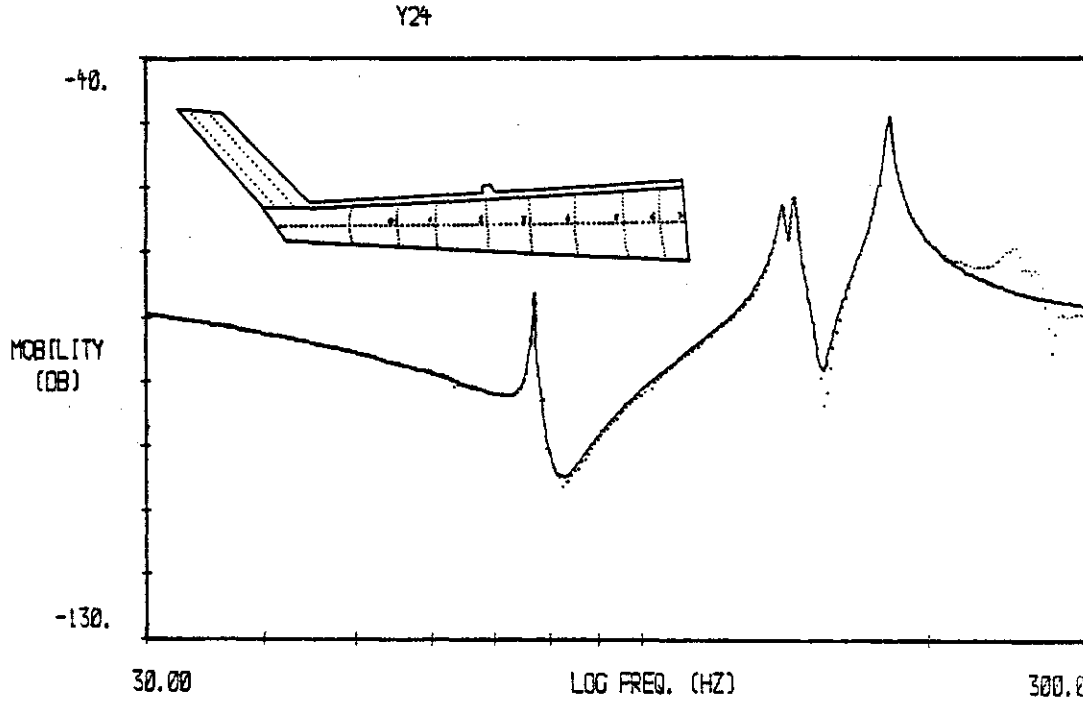

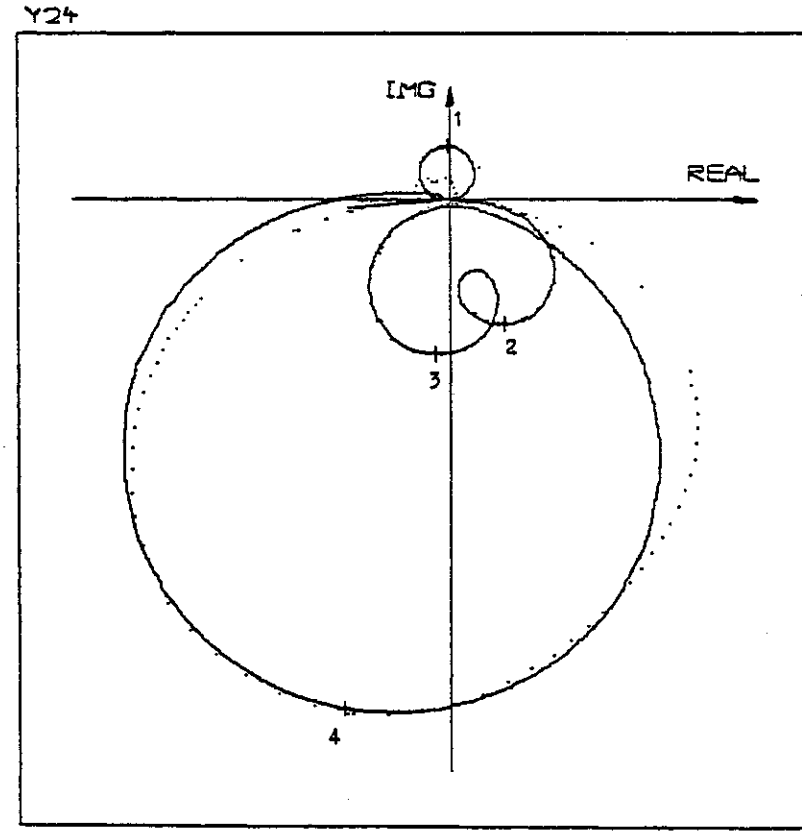

Fig. 7-10: Mobility and polar plots of measured and fitted curve (SIM2) of receptance α_{24}

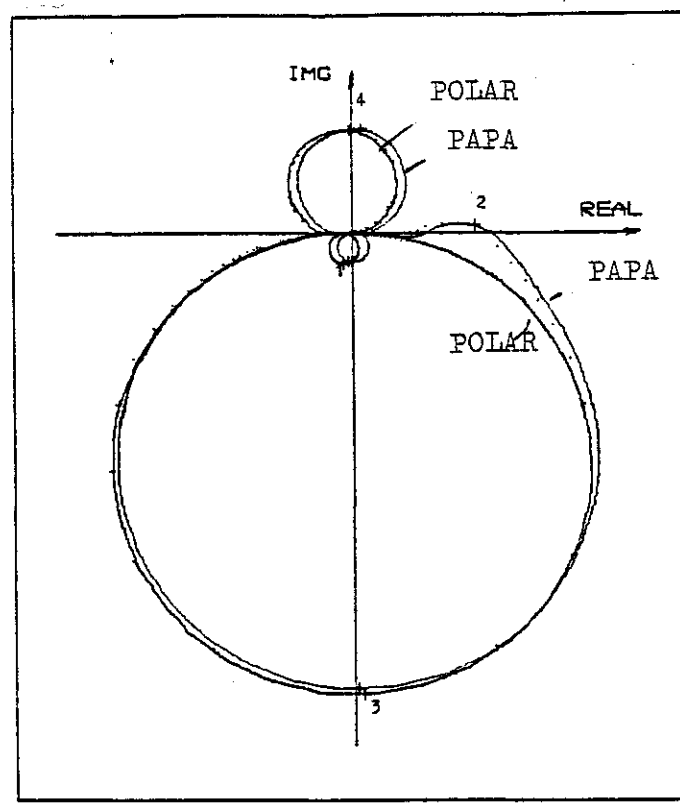

Fig. 7-11: Polar plot of α_{46} and the theoretical curves derived by POLAR5 and PAPA

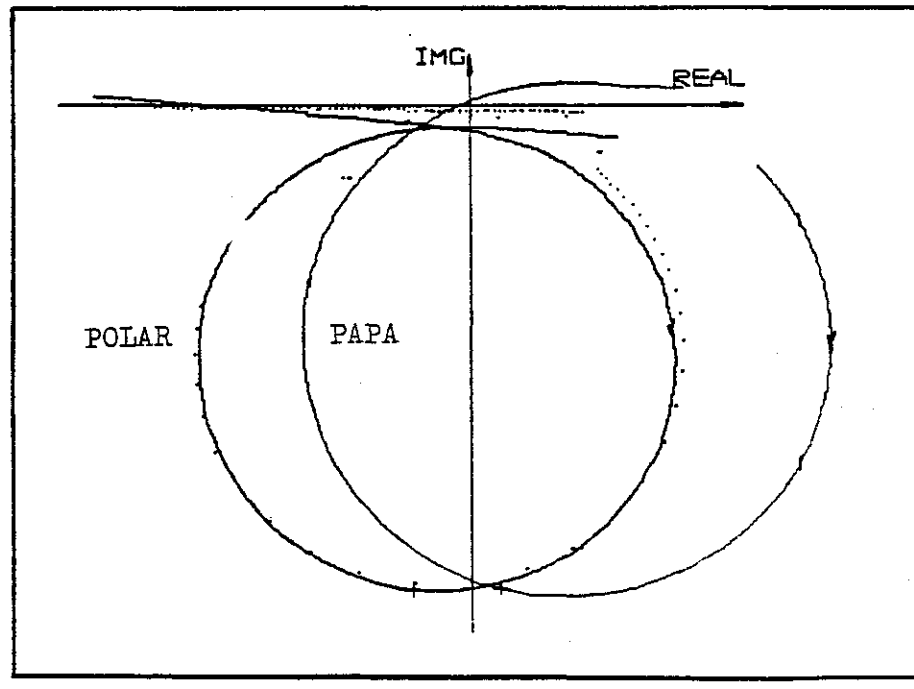

Fig. 7-12: Theoretically derived curves for mode 1 of α_{46} by POLAR5 and PAPA (detail from Fig. 7-11)

that the true 'complexity' of the normal mode shapes of the tailcone is very small and indeed, is smaller than is first indicated by the preliminary modal analysis.

7.2.1 DERIVATION OF NORMAL MODE SHAPES

As the four columns in the frequency response function matrix were measured and identified, it was possible to derive four estimates for the normal mode shape (eigenvector) matrix, one estimate derived from each column in the modal constant matrix.

A set of modal constant matrices for the four modes (one matrix for each mode) as derived by SIM2 is given in Table 7-6. It is clear that the matrices are not symmetric and, therefore, that the normal mode shapes derived from each column are not identical (as they should be according to theory). An example of the four different normal mode shapes of mode 1 are given in Table 7-7 and a modulus plot of these shapes is given in Fig. 7-13 (The complete set is given in ref. [73]).

It should be noted that the normal mode shapes are mass normalized and are thus scaled absolute quantities the unit of which is $(1/Kg)^{-\frac{1}{2}}$.

It may also be noticed that the phase angles of the normal mode shape elements are either very close to 0° or to 180°. It is expected, therefore, that the moduli of the (complex) normal mode shapes are practically equal to the moduli of the (real) mode shapes of the hypothetical

EXCITATION AT POINT NO.							
2		4		6		7	

Mode 1

.00584	-.27	.00067	176.37	.00736	178.77	.00829	178.70
.00567	-.07	.00062	178.44	.00694	-178.32	.00750	-179.78
.00415	-1.00	.00052	179.85	.00524	179.20	.00577	-178.89
.00211	-2.35	.00027	176.65	.00232	177.97	.00260	-178.73
.00053	-177.99	.00009	23.54	.00068	-.69	.00097	-7.33
.00377	179.09	.00045	-6.01	.00424	-1.19	.00486	-.19
.00584	179.69	.00078	-10.82	.00632	-.24	.00778	-.51
.00596	179.94	.00087	-.45	.00739	-1.34	.00853	.75

Mode 2

.01160	2.98	.00351	3.65	.00869	-177.89	.01090	156.61
.02640	3.29	.00810	.42	.01910	166.43	.02280	173.55
.02700	3.52	.00834	.32	.01850	-178.40	.02570	-173.40
.02030	3.60	.00542	.38	—	—	—	—
.00859	1.31	—	—	—	—	—	—
—	—	—	—	—	—	—	—
.01988	-176.58	—	—	.00829	1.07	—	—
.02780	-176.30	—	—	.02070	-1.75	—	—

Mode 3

—	—	—	—	—	—	—	—
—	—	.00330	1.27	—	—	—	—
—	—	.01040	-.01	.01820	.49	.02360	3.70
.00495	-.23	.02080	-1.34	.03660	14.08	.04440	18.75
.00960	2.62	.03200	-2.24	.06110	2.32	.06320	4.16
.01360	15.38	.05120	.27	.09430	-5.47	.10680	-3.15
.01880	1.63	.06210	1.24	.11240	-8.72	.13830	-6.77
.02240	1.12	.06740	2.61	.12780	-1.59	.14390	-11.49

Mode 4

.02260	-9.95	.01550	-12.39	.00858	173.74	.01470	170.03
.07310	-9.14	.04830	-9.66	.02700	174.48	.04990	173.04
.10200	-9.23	.06600	-10.35	.03760	175.26	.06480	171.34
.09750	-8.05	.06560	-7.41	.03620	172.49	.06560	173.17
.06620	-8.42	.04570	-8.64	.02520	173.60	.04120	173.47
.01050	-4.11	.00629	-9.07	.00477	168.63	.00693	-167.10
.03540	175.05	.02410	174.65	.01520	.23	.02850	7.23
.06290	174.18	.03960	173.30	.02490	-3.37	.04360	-2.28

Table 7-6; Modal constant matrices derived by SIM2 (modulus (1/Kg) and phase in degrees)

Excitation at point:

2		4		6		7	
.09069	.23	.07085	164.60	.09259	178.80	.08977	178.32
.08805	.43	.06543	166.67	.08737	-178.20	.08119	179.84
.06438	-.50	.05498	168.08	.06595	179.32	.06244	-179.27
.03280	-1.85	.02809	164.88	.02925	178.09	.02818	-179.11
.00819	-177.49	.00947	11.77	.00851	-.57	.01046	-7.70
.05853	179.59	.04761	-17.78	.05333	-1.07	.05263	-.56
.09068	-179.81	.08235	-22.59	.07948	-.12	.08421	-.88
.09265	-179.56	.09168	-12.22	.09295	-1.22	.09237	.38

Table 7-7; Mode shapes (modulus $(1/Kg)^{-\frac{1}{2}}$ and phase in degrees) of mode 1 as derived from each column of the modal constant matrix (SIM2)

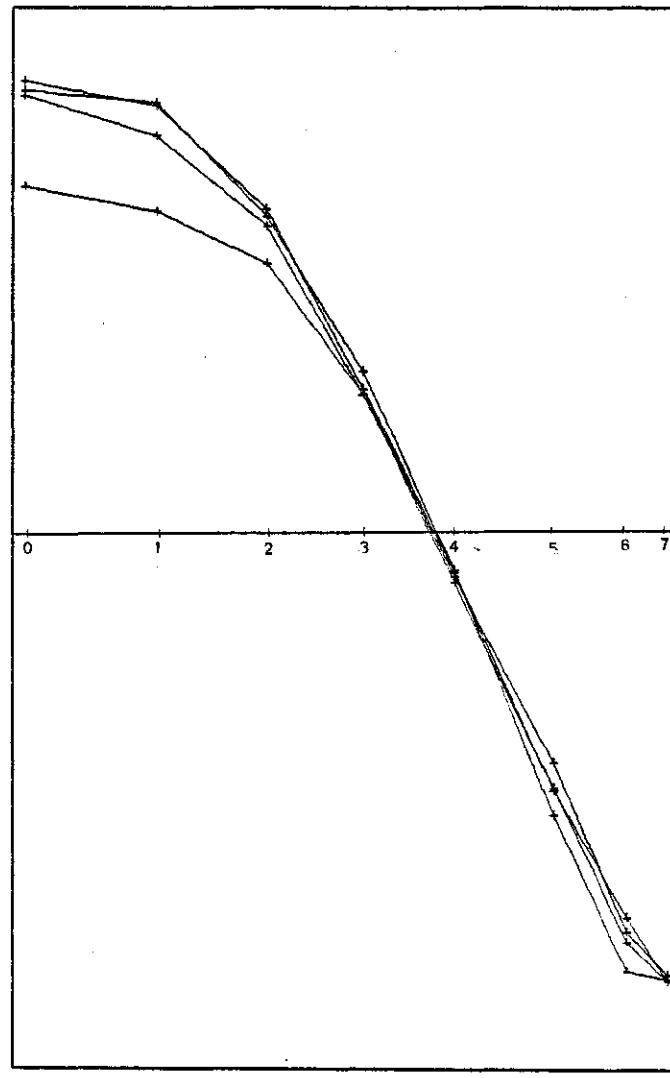

Fig. 7-13: Mode 1 - four estimates for the normal mode shape derived by SIM2

undamped system.

7.2.2 DERIVATION OF THE OPTIMAL MODAL PARAMETERS

The estimates of the modal parameters obtained from each column of the mobility matrix were not consistent; in other words, excitation at point i produced slightly different modes to excitation at point j. In order to derive a 'best' set of consistent modal parameters, the method described in 6.3 was applied to the measured data.

The 'best' values for the natural frequencies and modal loss factors were deduced by a process of weighted averaging and the results are given in Table 7-8 for each identification program. It is noticed that the differences between the best estimates from each identification program are very small and, practically, it does not matter which set of values is used in further calculation.

The 'best' normal mode shapes were derived by a specially developed optimization program (OPMOD) [74] and are given in Table 7-9 for each of the three analysis programs. It is, once again, noticed that the complexity of the derived consistent set of mode shapes is very small. A graphical representation of one of these sets of results (mode 1, modulus only) is also illustrated in Fig. 7-14, again taken from the complete set included in ref. [74].

mode no.		$\bar{\omega}_r$ [Hz]	$\pm \epsilon$	$\bar{\eta}_r$	$\pm \epsilon$
POLAR	1	77.20	.021	.0067	.00024
	2	141.33	.023	.0162	.00019
	3	145.04	.042	.0133	.00010
	4	182.77	.051	.0137	.00025
SIM	1	77.12	.026	.0076	.00014
	2	141.38	.021	.0158	.00015
	3	144.90	.025	.0133	.00026
	4	182.68	.029	.0145	.00016
PAPA	1	77.15	.011	.0076	.00004
	2	141.42	.031	.0153	.00012
	3	145.04	.031	.0132	.00023
	4	182.63	.030	.0158	.00024

Table 7-8: Weighted average and tolerance of natural frequencies and loss factors for the three analysis programs

mode	SIM		POLAR		PAPA	
1	.09020	178.805	.09096	-179.083	.08911	180.000
	.08553	-178.609	.08413	-173.388	.08502	180.000
	.06517	-180.000	.06229	-179.963	.06462	-179.746
	.02866	179.270	.02836	178.481	.03026	179.606
	.00859	-1.298	.00742	-4.515	.00887	15.677
	.05414	-.834	.05329	-.091	.05149	-2.717
	.08117	-.302	.08467	-.329	.08045	-1.798
	.09218	.230	.09426	-.118	.09382	-.370
2	.07099	.911	.07115	1.141	.07171	-173.617
	.15893	.427	.15587	1.911	.15763	-176.172
	.16466	2.321	.16820	2.170	.16474	-180.000
	.12316	1.283	.11296	2.350	0	-82.203
	.05151	-.826	.04963	.667	.04286	-180.000
	0	89.966	0	89.986	.04053	4.039
	.11858	-179.440	.12821	-175.733	.11772	-1.698
	.16481	-177.898	.18289	172.505	.16333	-.286
3	0	0.0	0	0.0	0	0.0
	.01868	-.803	.01150	-32.790	.02176	9.061
	.05692	2.443	.05607	5.801	.05584	2.245
	.11680	-2.850	.11267	9.680	.10926	2.466
	.17667	3.196	.18364	-.064	.17744	1.699
	.28521	-2.758	.27622	-2.046	.27720	1.302
	.34108	-.984	.33058	-4.420	.33686	-2.772
	.37452	-1.156	.37954	-.245	.38260	-2.305
4	.07213	-7.222	.06216	-15.547	.07531	-1.968
	.23355	-4.841	.20410	-9.730	.23260	-4.232
	.31331	-6.630	.31609	-4.092	.32224	-4.534
	.30936	-5.147	.30978	-4.870	.31356	-4.807
	.20464	-4.967	.20113	-6.338	.21271	-5.391
	.03273	1.439	.02803	-10.733	.03594	3.316
	.12158	-179.413	.11451	-180.000	.11669	-180.000
	.20731	-180.000	.19737	-180.000	.21518	-180.000

Table 7-9: Optimized normal mode shapes (modulus $(1/Kg)^{-\frac{1}{2}}$ and phase in degrees) for the three analysis programs

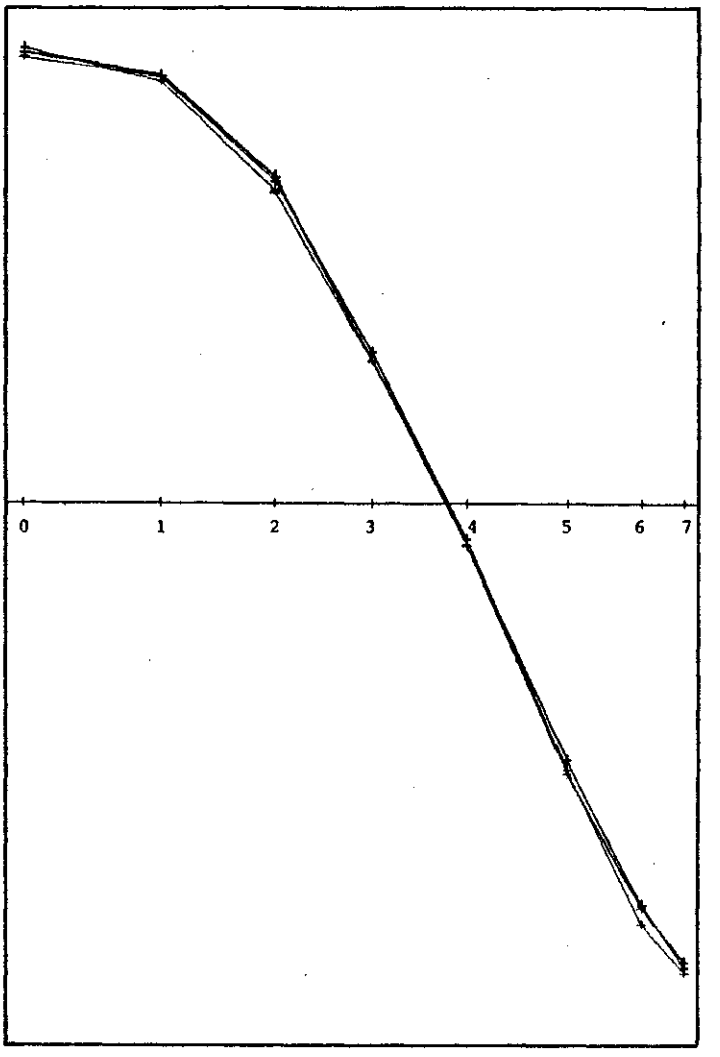

Fig. 7-14: Optimized normal mode shapes of mode1 for the three analysis programs

7.3 MULTI-POINT EXCITATION MODAL IDENTIFICATION

In addition to the single-point excitation tests, a modal identification of the tailcone was made using a multi-point excitation approach.

By this method the tailcone was excited simultaneously with four shakers at different points on the structure (at positions 2,4,6, and 7; Fig. 7-1), while the acceleration response was measured at all eight points of interest. At each natural frequency the shakers were tuned so that the input forces and the responses of the tailcone were in quadrature. When this condition was reached, the level of the acceleration at each point was measured thus providing the forced proportional mode shape corresponding to this mode. Table 7-1Ø summarizes these mode shapes for the first four modes. The 'natural frequency' (corresponding to the natural frequency of the undamped system) is read directly from the control unit.

If the system is assumed to be nonproportionally-damped, then there is no unique modal loss factor associated with each forced proportional mode. However, because we knew a priori that the complexity of the normal mode shapes was very small, it was reasonable to assume that the tailcone was proportionally damped and thus possessing one modal loss factor for each forced proportional mode.

This loss factor was calculated by the half-power method whereby the tailcone was excited at two frequencies (ω_1 and ω_2) one below and one above the natural frequency (ω_r) where

mode	ω_r (Hz)	η_r
1	77.16 (77.12)	.0077 (.0076)
2	141.24 (141.38)	.0144 (.0158)
3	144.30 (144.90)	.0152 (.0133)
4	181.40 (182.68)	.0166 (.0145)

Table 7-11: Natural frequencies and loss factors derived by the multi-point excitation method.
(In brackets, the optimized values derived by SIM2)

MODE

POINT	1	2	3	4
0	.0938	.0642	.0093	.0719
1	.0873	.1419	.0339	.2396
2	.0566	.1526	.0722	.2875
3	.0291	.1071	.1292	.3234
4	-.0091	.0385	.1959	.2156
5	-.0556	-.0589	.2761	.0335
6	-.0760	-.1392	.3296	-.1198
7	-.0957	-.1820	.3741	-.2060

Table 7-10: The forced proportional modes as derived by the multi-point excitation method (unscaled)

the phase differences between input and response was 45° and then using

$$\eta_r = \frac{|\omega_2 - \omega_1|}{\omega_r}$$

Table 7-11 summarizes the first four natural frequencies and the corresponding modal loss factors derived by this method.

We see that the differences between the results obtained by this method and those from the single-point excitation method are negligible. A graphical representation (Fig. 7-15) of the mode shapes in comparison to those derived by SIM2 indicates that, practically, both results are identical.

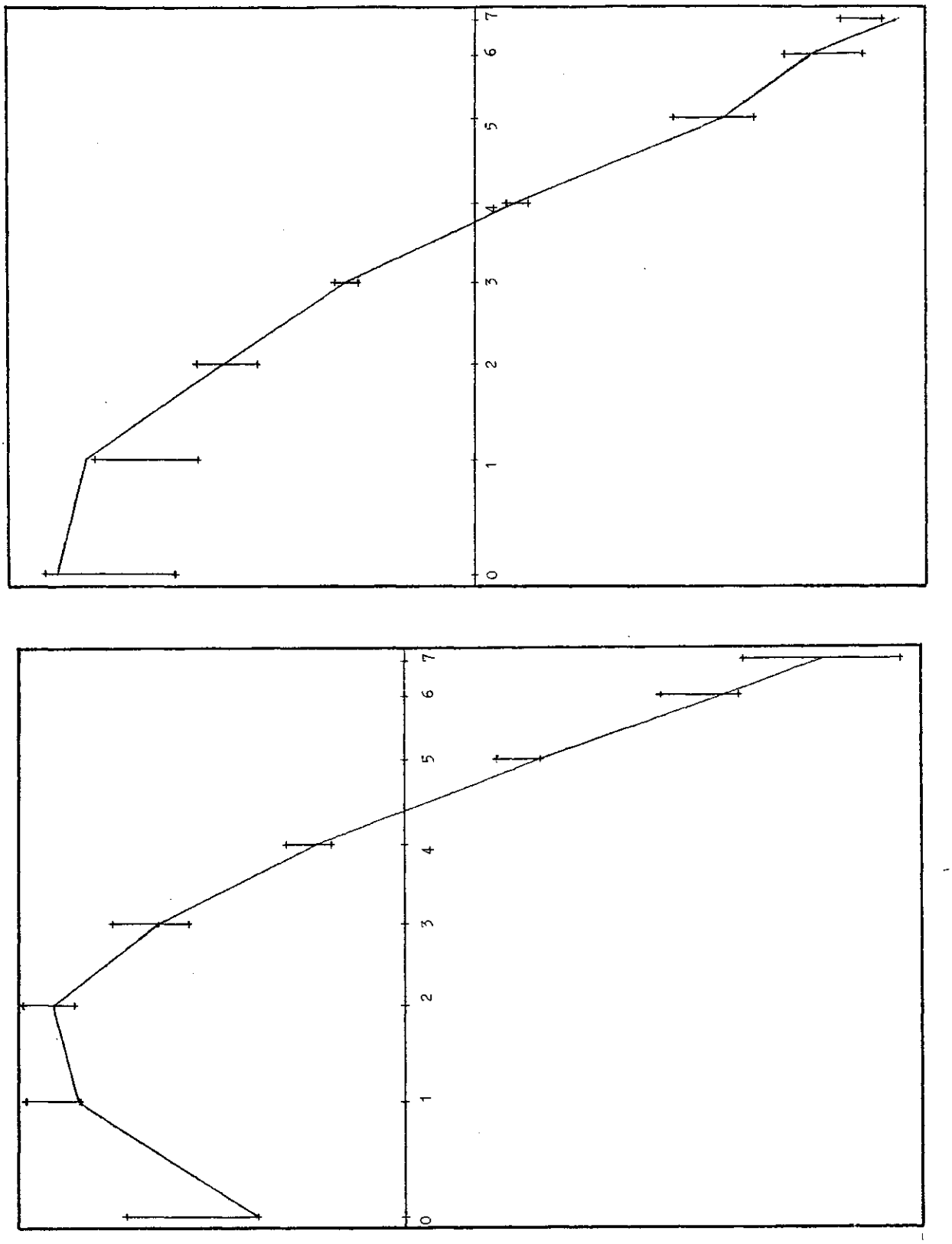

Fig. 7-15: Forced proportional mode shapes vs. normal mode shapes derived by SIM2 (the bar represents the spread of the estimates derived by SIM2) for (a) mode 1, (b) mode 2, (c) mode 3 and (d) mode 4.

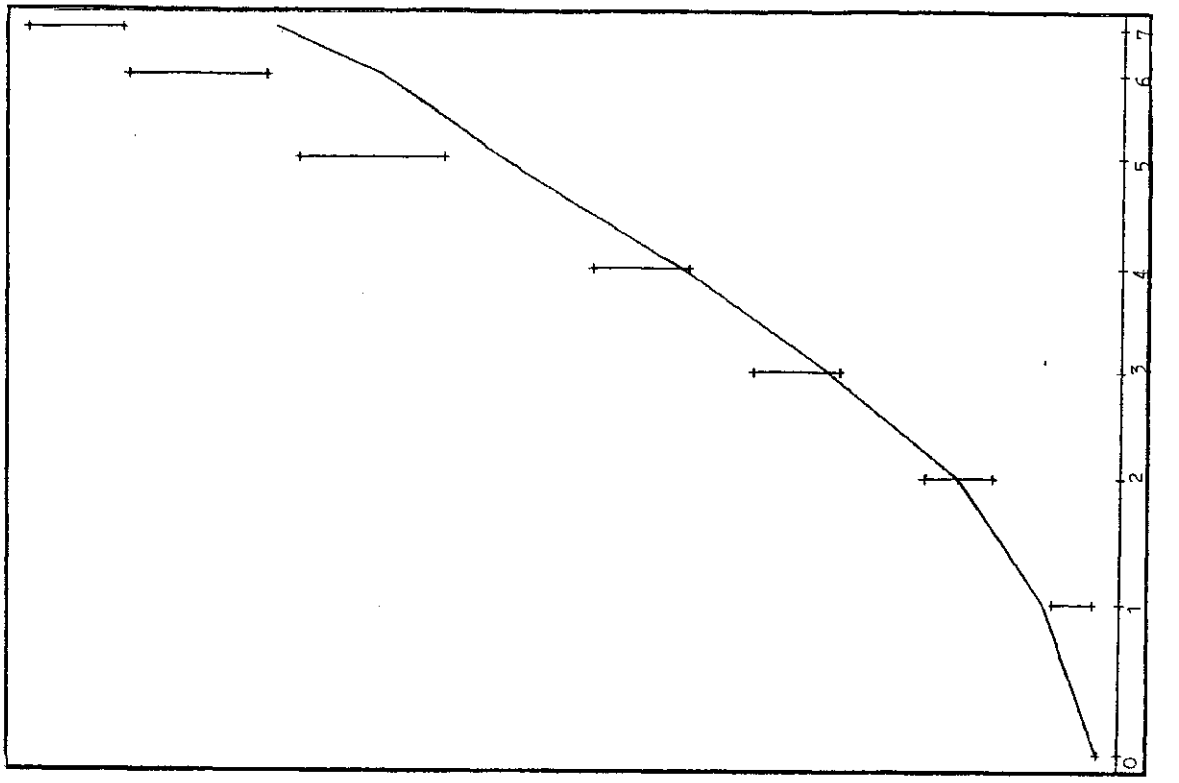

c

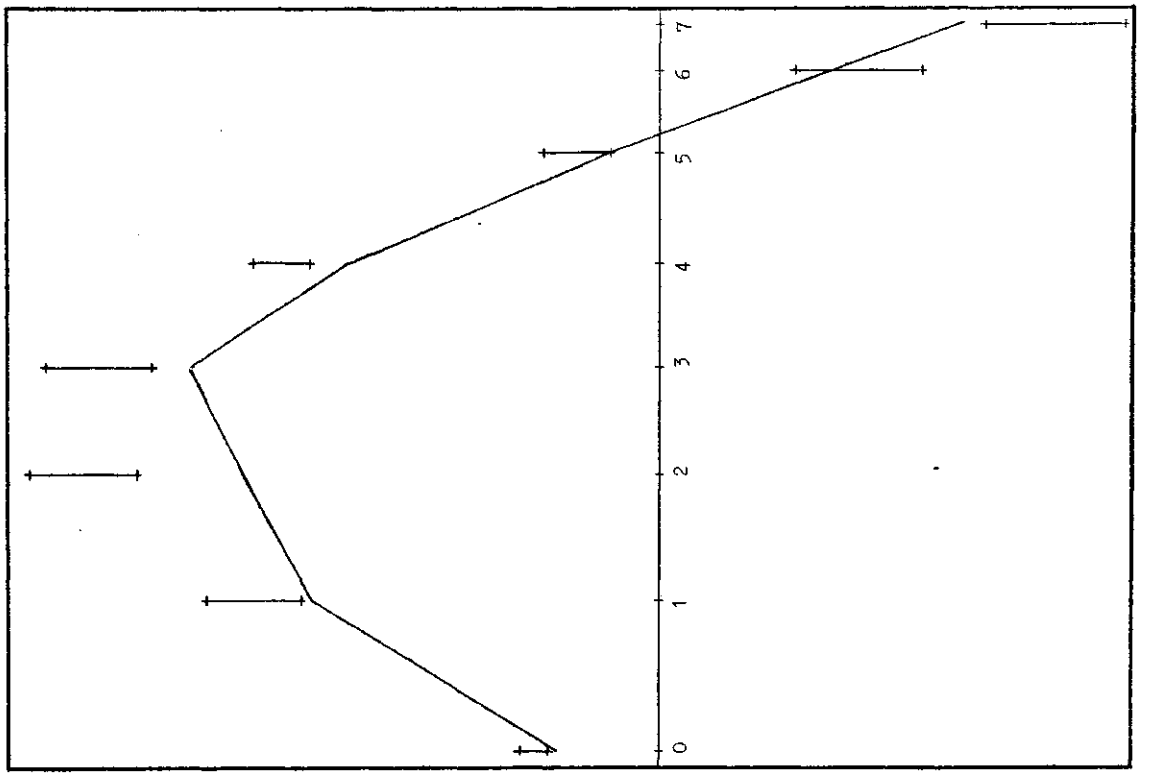

d

7.4 CONCLUSIONS

This experimental study served as a valuable example for evaluation of the methods developed in this work. Examination of the results derived at the various stages of this study leads us to the following conclusions:

(i) When using the single-point excitation method it is possible (and desirable with complete engineering structures) to check the testpiece for nonlinear behaviour and it is usually possible to change the testing conditions so that the nonlinear influence on the measured data is removed or minimized. The systematic method developed in this work facilitates this process and enables us to acquire a 'best' linear model of the structure.

With the multi-point excitation method it is not feasible to detect nonlinear behaviour and in severe cases of nonlinearity it is impossible to reach the quadrature relationship between input and response.

(ii) When an identification program is developed its performance is usually checked by analysing synthesised 'experimental' data (i.e data from a linear system polluted with random errors). It is found that when the algorithm is improved, the results obtained using synthesised data improve as well. However, such a marked improvement is not observed when analysing real experimental data. This is because real data contain systematic errors due to nonlinearities of the structure as well as random errors from measurement. Thus, there is often little point in

trying to improve the analysis program by developing more refined linear algorithms as the results do no justify it. Furthermore, the optimized mode shapes derived from the modal constant matrices obtained using different analysis programs in this study were very close, further supporting the previous conclusion that there is no reason to improve the linear identification algorithm.

(iii) The modal phase angle is the parameter which is usually the most severly distorted when the analysed data is nonlinear or when the modes are very close. This distortion tends to indicate that the normal mode shapes are significantly complex, but when the data are acquired in a very careful manner (i.e minimizing the influence of the nonlinearities) or when more precise algorithms are used to analyse close modes, we usually find that the derived normal mode shapes are almost real.

A comparison with the (real) forced proportional mode shapes derived by the multi-point excitation method suggestd that, practically, the complex normal modes derived by the single-point method may be regarded as the undamped normal modes of the structure and can be used as such in any further computation.

However, when a complete structure like a helicopter is measured it is harder to minimize the nonlinear influences and to reduce the level of random errors and the general quality of the acquired data is , therefore, not as good as for the tailcone. In this case, some caution should be taken

when assuming that the derived complex normal modes are equal to the undamped ones.

8. CONCLUDING REMARKS

The results obtained throughout this work have already been discussed and detailed conclusions given at the end of each chapter. A brief summary of these conclusions is now made as a review of the entire project.

8.1 THEORETICAL BASIS

Analysis of measured data in order to extract modal parameters is effectively a process of 'linearization' in which a simple linear model is constructed to represent an actual structure which will, in general, be far more complex.

A widely-used theoretical linear model is the lumped mass system with constant mass, stiffness and damping elements. The solution of the eigenproblem for this type of system is relatively simple; for a proportionally damped system the derived eigenvectors for either the hysteretically-or the viscously-damped system are identical and are expressed in real terms. Generally, however, the eigenvectors are expressed in complex terms and then the analysis of the hysteretic model is simpler than that for the viscous one and is more amenable to analysis of experimental data.

Because there seems to be some confusion in the definition of the term 'normal mode shape', this has been defined in a consistent manner and some of its special forms

have been pointed out. It has also been shown that the mode shapes derived by the multi-point excitation method are always real and are identical to the normal modes of the proportionally-damped system regardless of the form or type of the damping present in the structure.

Experimental observations have shown that quite often the derived normal modes are complex. On the other hand, the mode shapes needed for comparison with theoretical predictions or with multi-point excitation results are the real proportional normal modes. A theoretical and numerical study indicates that for moderately-damped systems with separated natural frequencies, the (real) proportional normal modes and the (complex) normal modes are approximately identical, but as the level of damping is increased or as two natural frequencies get closer, the normal modes become more complex and then this approximation must be applied with greater caution.

As the complexity of the normal modes hinges on the relationship between the damping and stiffness matrices a statistical parameter - 'the nonproportionality factor'-has been devised in order to quantify the level of the nonproportionality of a theoretical model and thus to enable a comparison to be made between differently damped theoretical systems.

8.2 PRACTICAL BASIS

8.2.1 IDENTIFICATION ALGORITHMS

In order to extract the modal parameters from measured data, two identification algorithms have been developed:

(i) a relatively simple one which assumes that the response at each resonance is dominated by that of a one-degree-of-freedom system and derives the modal parameters from analysis of the polar plot; and

(ii) a more advanced one which takes into account the response of the structure at all the measured resonances and curve-fits the experimental data simultaneously for all the modes.

The second algorithm proved to be superior when assessed with theoretically-generated data, especially for difficult cases of close natural frequencies which were poorly identified by the first algorithm.

8.2.2 EFFECT OF NONLINEARITIES

Experimental evidence has suggested that many of the derived normal modes of practical structures are more complex than expected by theory, even for cases of well-separated modes. As this trend could not be simulated theoretically it was felt that the cause for the discrepency might lay in inadequate measurement or analysis procedures which could be affected by slight nonlinearities of the

structure. A theoretical study of several synthesised one-degree-of-freedom nonlinear systems has proved that when analysed with linear modal identification algorithms, the derived modal parameters are poorly identified, even for small amounts of nonlinearity. An experimental study on a real structure supported these conclusions.

8.2.3 FINAL DATA REDUCTION

The latter results indicate that in order to derive the linear properties of a real system much more attention should be given to the data acquisition process. A systematic method for this process has been outlined and several useful tools have been devised in order to facilitate its application.

(i) A 'nonlinearity factor', which enables the investigator to assess the level of nonlinearity of the measured data, and once the data are analysed;

(ii) the 'quality factor' which describes the accuracy of the identification of each set of the derived modal parameters and finally,

(iii) the 'generalized loss factor' which gives an overall measure of the amount of damping present in the system.

Although it is theoretically possible to derive the complete mobility matrix (as well as the natural frequency and mode shape matrices) from measurement of one column of this matrix, it is found in practice that measurement of

more columns is usually necessary. The redundant data thus obtained are used to improve the quality of the derived modal parameters by applying a newly-developed optimization technique which employs the quality factor as a weighting parameter. The end result of this process is the reduction of a very large amount of data to produce a single consistent set of modal parameters which describe the system 'best'.

8.3 EXPERIMENTAL STUDY

Finally, a comprehensive experimental study on a typical aerospace structure demonstrated some of the common problems encountered and the methods developed in this research in order to derive a satisfactory modal identification of a real structure. It has been found that when real data are analysed, the difference between the final results derived by the various identification algorithms is negligible and the marked superiority of the more sophisticated curve-fitting methods when checked with synthesised data is not achieved with real data. This is probably due to the fact that real data are never entirely linear; they are polluted with measurement errors to which the identification algorithms are sensitive.

Derivation of the undamped mode shapes by the multi-point excitation method has proved that practically they are equal to the moduli of the complex normal mode

shapes derived by the single-point excitation method. This result supports the theoretical conclusion that for separated modes the complexity of the normal modes is very small and is practically negligible.

The derivation of the real proportional normal modes from the experimentally-identified complex normal modes could not be done exactly because the modal parameters derived from experimental data always comprise an incomplete set. However, in the light of the theoretical and experimental work described in this thesis we may say that for most practical cases of separated modes the moduli of the complex normal modes may be used as a very good approximation to the real proportional modes.

8.4 SUGGESTIONS FOR FURTHER RESEARCH

The theoretical part of the modal identification method is well-established; the practical aspects of it, however, provide a fertile field for further topices for research.

As it has been shown that one of the main causes for badly identified modal parameters is the deviation of real system from linear behaviour, it is suggested that further research should be devoted to this aspect, mainly in developing methods for identification of the type of nonlinearity. Some work in this direction has been done by Tomlinson [62] for simple cases of dry friction, but more comprehensive research to include more types of nonlinearity

is needed. As a first step in this direction, an algorithm to generate synthesised multi-degree-of-freedom nonlinear data has to be developed. Such data may serve as an additional tool to check the sensitivity of linear modal identification algorithms to nonlinearities.

In parallel, effort should be devoted to improve measuring techniques to enable the investigator to acquire error-free data and to have more control on the nonlinear component measured.

Finally, further research is needed for cases of close modes at higher frequencies where the modal density is high and the existing identification algorithms prove to be inadequate.

9. REFERENCES

1. HAMMA G.H, SMITH S and STROUD R.C.
   An evaluation of excitation and analysis methods for modal testing
   SAE paper No. 760872

2. WALGRAVE S.C. and EHLBECK J.M.
   Understanding modal analysis
   SAE paper No. 780695

3. SNOEYS R, ROESEMS D, VANDEURZEN U and VANHONACKER
   Survey of modal analysis application
   Annals of the CIRP Vol. 28/2/1979

4. KORTUM W and NIEDBAL N
   Application of modern control theory to modal survey techniques
   Euromech 131 June 1980

5. EWINS D.J , SILVA J.M.M and MALECI G
   Vibration analysis of a helicopter plus an externally attached structure
   The Shock and Vibration Bulletin
   No. 50, part 2, September 1980

6. FLANNELLY W.G
   Modal analysis for managers
   Sound and Vibration, Nov. 1979

7. EWINS D.J
   A classified bibliography of mechanical impedence measurement
   A Solartron publication (1972)

8. RADES M
   Analysis techniques of experimental frequency response data
   Shock and Vibration Digest Vol. 11, No. 2 Feb. 1979

9. RADES M
   Methods for the analysis of structural frequency response measurement data
   Shock and Vibration Digest, Vol. 8, No. 2, Feb. 1976

10. RADES M
    Metode dinamice pentru identifcarea sistemelor mecanica
    (Identification of vibrating systems)
    Editura academiei republicii socialiaste Romania 1979

11. BISHOP R.E.D and GLADWELL G.M.L
An investigation into the theory of resonance testing
Philosophical Transactions of The Royal Society of London
Vol. 255, Jan. 1963

12. WILKINSON J.H
The algebraic eigenvalue problem
Clarendon Press Oxford, 1965

13. BISHOP R.E.D
The general theory of hysteretic damping
Aeronautical Quarterly, Feb. 1956

14. LANCASTER P
Lamda matrices and vibrating systems
Pergamon Press, 1966

15. CAUGHEY T.K and O'KELLY M.E.J
Classical normal modes in damped linear dynamic systems
Journal of Applied Mechanics, Sept. 1965

16. SLOANE E and McKEEVER B
Modal survey techniques and theory
SAE paper no. 751067

17. CRANDALLL S.H and McCALLEY Jr.
Shock and Vibration Handbook - Chapter 28
Matrix methods of analysis
McGraw Hill, New York, 1976

18. FOSS K.H
Coordinates which uncouple the equation of motion of damped linear dynamic system
Journal of Applied Mechanics 25 (361), 1958

19. FRAEIJS deVEUBEKE B.M
Bull. Acad. Belg. Sci. 34, 1948

20. ALLEMANG R.J
Experimental modal analysis
Ph.D dissertation, University of Cincinnati (1980)

21. BISHOP R.E.D and JOHNSON D.C
The mechanics of vibration
Cambridge University Press, 1960

22. KLOSTERMAN A.L and PETERSON E.L
Evaluating the accuracy of an experimental modal survey
Paper presented at a symposium on signal processing for vibration shock and noise at Imperial College London 1977

23. MEAD D.J
The exsistance of normal modes of linear systems with arbitrary damping
Symposium on structural dynamics
Loughborough University of Tecnology. March 1970

24. EWINS D.J
Whys and wherefores of modal testing
SEE Journal, September 1979

25. BERMAN A and FLANNELLY W.G
The theory of incomplete models of dynamic structures
AIAA Journal Vol. 9 No. 8,1971

26. ROSS R.G Jr.
Synthesis of stiffness and mass matrices from experimental vibration modes
S.A.E paper No. 710787

27. THOREN A.R
Derivation of mass and stiffness matrices from dynamic test data
AIAA Journal, April 1972

28. FLANNELLY W.G, McGARVEY and BERMAN A
A theory of identification of the parameters in the equation of motion of a structure through dynamic testing
Symposium on structural dynamics
Loughborough University of Technology, March 1970

29. KELLER C.L
Methods for determining modal parameters and mass, stiffness and damping matrices
Air Force Flight Dynamics Laboratory
Technical report 78-59, June 1978

30.IMREGUN M
Dynamic condensation: theory and application
M.Sc thesis, Imperial College, Dynamics Section, Sept. 1980

31. LINCOLN A.P
Modelling of structural behaviour from frequency response data
ISVR Report No. 83, Sept. 1977

32. TARGOFF W.P
Orthogonality check and correection of measured modes
AIAA Journal Vol. 14, No. 2, Jan. 1976

33. BERMAN A
Mass matrix correction using an incomplete set of measured modes
AIAA Journal Vol. 17, No. 10, Oct. 1979

34. CHEN J.C and GARBA
Analytical model improvement using modal test results
AIAA Journal Vol. 18, No. 6, June 1980

35. BARUCH M
Proportional optimal orthogonalization of measured modes
AIAA Journal Vol. 18, No. 10, July 1980

36. GAUKROGER D.R and COPLEY J.C
Methods for determining undamped normal modes and transfer functions from receptance measurements
RAE Technical report 79071, June 1979

37. PIPES L.A
Matrix methods for engineering
Prentice-Hall Inc. 1963

38. CRANDALL S.H
Engineering analysis
McGraw Hill 1956

39.
PENDERED J.W
Theoretical investigation into the effects of close natural frequencies in resonance testing
Journal of Mechanical Engineering Science 7 (1965)

40.
GLEESON P.T
Identification of spatial models
Ph.D thesis, Imperial College, Dynamics Section, 1979

41. MUSTAIN R,W
Survey of modal vibration test/analysis techniques
SAE paper No. 760870

42. KENNEDY C.C and PANCU C.D.P
Use of vectors in vibration measurement and analysis
Journal of the Aeronautical Science, Vol. 14, Nov. 1947

43. STROUD R.C, SMITH S and HAMMA G.H
MODLAB- A new system for structural dynamic testing
The Shock and VIbration Bulletin
Vol. 46, part 5, August 1976

44. KIRSHENBOIM J
User's guide for the mobility measurement and analysis programs on the 1191 computer
Imperial College, Mechanical engineering Dept.
Dynamics Section Report No. 80007, Oct. 1980

45. KIRSHENBOIM J
POLAR - Computer aided graphical method for modal identification
Imperial College, Mechanical Engineering Dept.
Dynamics Section Report No. 79003, May 1979

46. KIRSHENBOIM J
SIM - Modal identification by simultaneous mode fitting
Imperial College, Mechanical Engineering Dept.
Dynamics Section Report No. 7914, August 1979

47. GAUKROGER D.R, SKINGLE C.W AND HERON K.H
Numerical analysis of vector response loci
Journal of Sound and Vibration (1973) 29(3)

48. CRAIG R.R Jr. and SU Y.W.T
On multiple-shaker resonance testing
AIAA Journal Vol. 12, No. 7, July 1974

49. IBANEZ P
Force appropriation by extended Asher's method
SAE paper No. 760873

50. HALLAUER W.L and STAFFORD J.F
On the distribution of shaker forces in multiple shaker modal testing
The Shock and Vibration Bulletin
No. 48, part 1, Sept. 1978

51. GABRI B.S and MATTHEWS J.T
Normal mode testing using multiple exciters under digital control
Paper presented at the symposium of the Society of Enviromental Engineers London May 1979

52. TAYLOR G.A, GAUKROGER D.R and SKINGLE C.W
MAMA- A semi-automatic technique for exciting the modes of vibration of complex structures
RAE Technical Report No. 67211

53. McLACLAN N.W
Ordinary nonlinear differential equations in engineering and physical science
2nd. edition, Oxford University Press 1956

54. STOKER J.J
Nonlinear vibrations
Interscience Publishers Inc. New-York 1950

55. DINCA F. and TEODOSIU C
Nonlinear and random vibration
Academic Press Inc. New-York, London 1973

56. CLAUSER F.H
The behaviour of nonlinear systems
Journal of the Aeronautical Sciences
Vol. 23, No. 5, May 1956

57. TONDEL A
The application of skeleton curves and limit envelops to the analysis of nonlinear vibrations
Shock and Vibration Digest 7, 1975

58. WHITE R.G
Use of transient excitation in the measurement of the frequency response of systems with nonlinearities arising from large deflections
ISVR Technical report No. 27, Feb. 1970

59. NEWMAN K.W
The effect of stiffness nonlinearity on vector response loci
RAE Technical report No. 71119

60. TOMLINSON G.R
An analysis of the distortion effects of colomb damping on the vector plots of lightly damped systems
Journal of Sound and Vibration (1980) 71(1)

61. YEH

Forced vibrations of a two degree of freedom system with combined coulomb and viscous damping
Journal of the Acoustical Society of America 39, 1966

62. TOMLINSON G.R and HIBBERT J.H
Identification of the dynamic characteristics of a structure with colomb friction
Journal of Sound and Vibration (1979) 64(2)

63. TOMLINSON G.R
Determination of the modal properties of complex structures including nonlinear effects
Ph.D Thesis, University of Salford May 1979

64. TOMLINSON G.R
Force distortion in resonance testing of structures with electro-dynamic vibration exciters
Journal of Sound and Vibration (1979) 63(3)

65. EWINS D.J
Measurement and application of mechanical mobility data
Solartron publication

66. EWINS D.J
Measurement and application of mechanical impedence data
Journal of the Society of Environmental Engineers
Part 1: Introduction and ground rules. Vol 14-4, Dec 75
Part 2: Measurement techniques. Vol. 15-1, March 76
Part 3: Interpretation and application of measured impedence data. Vol. 15-2, June 76

67. SILVA J.M.M
On the influence of the push-rod in mechanical impedence testing
Imperial College, Dynamics Section Report Oct. 75

68. CARUSO H
An introduction to the application of modal analysis surveys in the test laboratory
The Shock and Vibration Bulletin
*

69. GLEESON P.T
Factors affecting the accuracy of the modal identification process
Imperial College, Dynamics Section Report, March 79

70. RICHARDSON M and KNISKERN J
Identifying modes of large structures from multiple input and response measurements
SAE paper No. 760875 (1976)

71. GOYDER H.G.D
Structural modelling by the curve fitting of measured frequency response data
ISVR Technical Report 87 (1976)

72. GOYDER H.G.D and WHITE R.G
The analysis of measured data for the determination of the fundamental dynamic properties and vibration transmission characteristics of structures
Paper presented at a symposium of the Society of Environmental Engineers at the Imperial College, London April 1977

73. KIRSHENBOIM J
Modal identification from measured frequency response data
Imperial College, Mechanical Engineering Dept.
Dynamics Section Report No. 8005 Feb. 1980

74. KIRSHENBOIM J
A method for the derivation of consistent modal parameters from several single-point excitation tests
Imperial College, Mechanical Engineering Dept.
Dynamics Section Report No. 8010, May 1980

75. KIRSHENBOIM J
The effect of small nonlinearities on the shape and modal analysis of polar response loci
Imperial College, Mechanical Engineering Dept.
Dynamics Section Report No. 7914, August 1979

76. SILVA J M M
Measurement and application of structural mobility data for the vibration analysis of complex structures
Ph.D Thesis, Imperial College, March 1978

10. APPENDICES.

APPENDIX 10.1

A NOTE ON 'FORCED PROPORTIONAL MODE' VS. 'NORMAL MODE'

"Therefore, with single-frequency, in-phase drive and response, it is not possible to excite a pure mode of a nonproportionally damped system. The experimenter who is required to run a modal survey on a nonproportionally damped system but who is limited to any of the techniques based on in-phase drive and response in quadrature for identification of a natural mode is being asked to do the impossible." (E. Sloane and B. McKeever; Modal Survey Techniques and Theory. SAE paper no. 751067, page 2979)

This categorical statement taken from this very long paper is a good example of the confusion which can arise from the ambiguity in the definition of the term 'mode'. The authors of this paper failed to recognize the difference between the 'forced proportional mode' and the 'normal mode' of the system. This led them to an unnecessary numerical example of a two degrees of freedom system in order to demonstrate that the normal modes of a nonproportionally damped system are complex and not identical to the (real) undamped or proportional normal modes.

They assumed that the 'forced proportional modes' and the 'normal modes' are identical (they refer to them as 'pure modes') and justifiably proved that they were not. They also failed to understand that the multi-point

excitation method excites the system in a real mode (forced proportional mode) which is always identical to the (real) undamped normal mode regardless of the model assumed for damping (If the damping is proportional this can be done at any frequency. For nonproportionally damped systems this mode can be excited at the natural frequency of the undamped system.)

Following their analysis they developed a complicated method identical to the multi-point excitation method but which has the capability of tuning the phase of the force as well as the amplitude and thus excite the system in a (complex) normal mode, which is not the goal of the 'traditional' multi-point excitation method.

10.2 VISCOUS AND HYSTERETIC DAMPING APPROXIMATE RELATION

The basic equation of motion for the harmonic forced vibration of a viscously damped system is:

$$[M]\{\ddot{q}\}+[C]\{\dot{q}\}+[K]\{q\}=\{F\}e^{i\omega t} \tag{10-1}$$

The general term derived for receptance α_{jk} is:

$$\alpha_{jk} = \sum_{r=1}^{n} \frac{({}_rR_{jk})+i\left(\frac{\omega}{\Omega_r}\right)({}_rS_{jk})}{\Omega_r^2\left[1-\left(\frac{\omega}{\Omega_r}\right)^2+2i\left(\frac{\omega}{\Omega_r}\right)\xi_r\right]} \tag{10-2}$$

where ξ_r is the modal critical damping ratio for the r'th mode.

This term differs from the corresponding hysteretic damping case in the frequency dependence of the numerator. However, when performing a modal analysis, this expression may be approximated to:

$$\alpha_{jk} = \sum_{r=1}^{n} \frac{{}_rA_{jk}}{\Omega_r^2\left[1-\left(\frac{\omega}{\Omega_r}\right)^2+2i\left(\frac{\omega}{\Omega_r}\right)\xi_r\right]} \tag{10-3}$$

where ${}_rA_{jk}$ is the modal constant, as in the hysteretic case:

$$\left|{}_rA_{jk}\right|^2 \cong \left|{}_rR_{jk}\right|^2 + \left|{}_rS_{jk}\right|^2 \tag{10-4}$$

and its phase is:

$${}_r\theta_{jk}=tg^{-1}\left(\frac{{}_rS_{jk}}{{}_rR_{jk}}\right) \tag{10-5}$$

The critical damping ratio ξ_r may be related to the hysteretic loss factor η_r,

$$\eta_r=2\xi_r \tag{10-6}$$

10.3 THE RANGE OF THE NONLINEARITY FACTOR

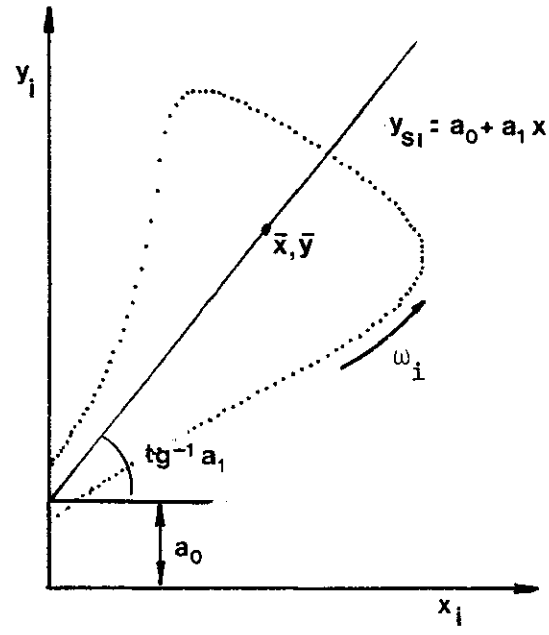

Fig 10-1: Calculation of the nonproportionality factor

(i) Range of J_1

If $a_1=0$ then we get from (5-4) and (5-5) that

$$a_0=\bar{y} \tag{10-7}$$

and therefore

$$J_1=0 \tag{10-8}$$

If $a_0=0$ then from (5-10) we obtain that

$$J_1=1 \tag{10-9}$$

The range of J_1 for $a_1 \geq 0$ is therefore

$$0 \leq J_1 \leq 1 \tag{10-10}$$

(ii) Range of J_2

For $a_1 \geq 0$ we get from (5-14) that

$$0 \leq \varphi \leq \pi/2 \tag{10-11}$$

and therefore

$$0 \leq J_2 \leq 1 \tag{10-12}$$

(iii) Range of J_3

In order to show that $0 \leq J_3 \leq 1$ we shall prove that

$$S_{sl}^2 \leq S_{\bar{y}}^2 \tag{10-13}$$

y_{sl} was derived for the minimum sum of deviations along the y axis, E_{min}

$$E_{min} = \sum_{i=1}^{n} (y_i - a_0 - a_1 x_i)^2 \tag{10-14}$$

S_{sl}^2 is by definition (5-8)

$$nS_{sl}^2 = E_{min} \tag{10-15}$$

from which follows that for any other straight line, $\bar{y}$

$$nS_{\bar{y}}^2 \geq E_{min} \tag{10-16}$$

and therefore

$$S_{\bar{y}}^2 \geq S_{sl}^2 \tag{10-17}$$

from which follows that J_3 is always

$$0 \leq J_3 \leq 1 \tag{10-18}$$

The range of the nonproportionality factor J where

$$J = J_1 \cdot J_2 \cdot J_3 \tag{10-19}$$

is therefore (Fig, 10-2)

$$0 \leq J \leq 1 \tag{10-19}$$

for $a_1 \geq 0$.

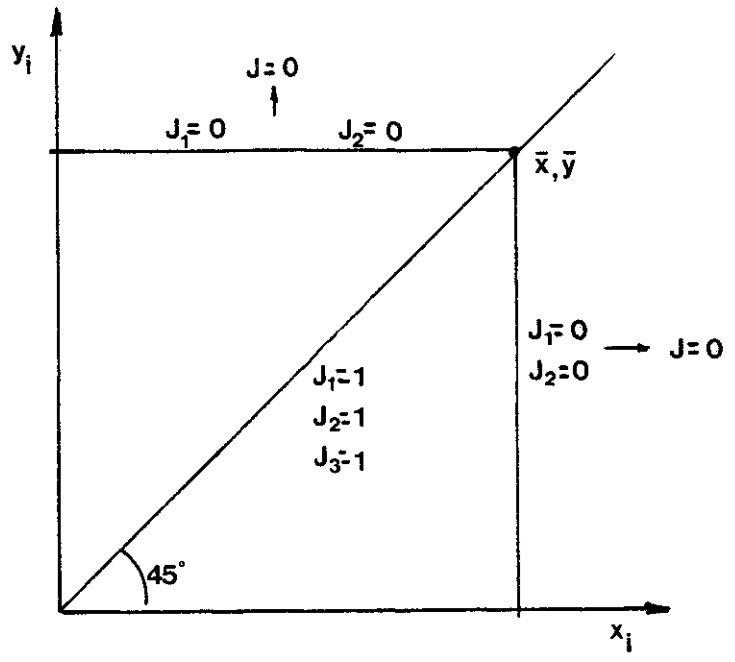

Fig. 10-2: The range of the J factor (for $a_1 \geq 0$)